Framework for Assessing Stability Challenges in Future Converter-Dominated Power Networks

Mengran Yu

A thesis submitted for the degree of Doctor of Philosophy to Department of Electronic and Electrical Engineering

University of Strathclyde

September 2018

This thesis is the result of the author's original research. It has been composed by the author and has not been previously submitted for examination which has led to the award of a degree.

Abstract

With requirements to deal with ageing infrastructure and to meet environmental targets, the installed capacity of converters, including converter-interfaced generation and back-to-back converters, is expected to experience a continued growth. In traditional power networks, synchronous generators provided the overwhelming majority of electrical power, with some induction generators providing the remaining electrical power. The dynamics of operation of both machines are well understood, including potential stability issues. With the introduction of converter-interfaced generation, power networks are becoming diverse systems, associated with which is an increased number of stability issues to consider.

The majority of modern converters employ *dq*-axis current injection control (or vector current control) in which a phase-locked loop is used to synchronise with the voltage at the point of common coupling where the converter is connected with the network. In recent years, potential issues with performance of PLL when the AC network it is connected to is weak have been reported. Poor performance of PLL under such circumstances will lead to a cascade of errors in the control system, culminating in an unstable system.

This thesis investigates the stability of the power system when large quantities of converter-based generation are present. The stability thresholds, termed as system tipping points in this work, are evaluated for both small and large disturbances. A time-domain analytical method to assess the tipping points, the tipping point search method, is introduced. This can be applied to any network model. Additionally, a network frequency perturbation tool, which can also be applied in time-domain model, is introduced to visualise the response of individual generators to network frequency fluctuation and predict potential interactions among the generators.

Following the identification of the limitations of vector current control, alternative control strategies which emulate synchronous generators, some more so than others, are investigated. Based on these studies, recommendations for power system engineers are made to ensure that the transition from a generator-dominated network to a converter-dominated network is as smooth as possible.

Acknowledgements

It is through the kind support and help of many individuals that this thesis could be achieved. I would like to extend my sincere thanks to all of them.

First of all, I would like to express my gratitude to my first supervisor, Dr Adam Dyśko, for his continuous support throughout the research and writing of this thesis. His patience, enthusiasm, encouragement and immense knowledge was contagious and motivational for me; more importantly, the Dyśko-style humour has enlightened many of my days.

I would like to thank my second supervisor, Dr Andrew J. Roscoe, who has been extremely helpful and supportive all this time. His enthusiasm and innovations in research have greatly motivated me and got me through all those tough times.

I would also like to thank Prof Campbell D. Booth from whom I have learnt a great deal. His kindness, constructive suggestions, encouragement, and optimism have been of great value to me during the research as well as for future life.

My gratitude extends to National Grid for the financial and technical support to this research. In particular, I would like to thank Helge Urdal, Jiebei Zhu and Richard Ierna for their valuable contribution to my work with their extensive experience and knowledge.

Completing this work would have been more difficult without the support from my colleagues and friends. They have been there through good times and bad, and they know who they are. I would especially thank Alexander D. Giles for his proof reading of this thesis.

Last but not the least, I would like to thank my parents, Changyou and Jiangyan, for their unconditional and faithful love, support and encouragement. This thesis is dedicated to them.

Contents

Chapter 1 Introduction 19

1.1 Motivation and scope 20

1.2 Principal research contributions 22

1.3 Thesis Outline 24

1.4 Publications 25

References 26

Chapter 2 Future Energy Scenarios and generating technologies 28

2.1 Introduction 29

2.2 Driving forces behind power system changes 29

2.3 Operational challenges 34

2.3.1 Frequency stability 35

2.3.2 Voltage stability 38

2.3.3 Sub-synchronous resonance 39

2.4 Grid code requirements for non-synchronous devices 41

2.4.1 Synthetic inertia 41

2.4.2 Frequency and voltage control 41

2.5 Synchronous generator 42

2.5.1 Principles of operation 42

2.5.2 Motion mechanics 43

2.5.3 Controllers 45

2.6 Power system stability 47

2.7 Power converters 50

2.7.1 HVDC transmission systems 51

2.7.2 LCC-HVDC 52

2.7.3 VSC-HVDC 53

2.7.4 Comparisons between LCC-HVDC and VSC- HVDC systems 54
2.8 Operation principles of VSC-HVDC and its control system 57
2.8.1 Models of VSC 57
2.8.2 Configuration of a VSC-HVDC 59
2.8.3 DQCI control 60
2.8.4 Active and reactive power capability 65
2.9 Alternative converter control techniques to assist system stability under high penetration of converters 66
2.9.1 Stability enhancing solutions based on DQCI control 67
2.9.2 Stability improvement solutions without DQCI control 72
2.10 Summary 79
References 81
Chapter 3 Methodology, Models and Analytical Tools 91
3.1 Introduction 92
3.2 Tipping point search method 92
3.3 Simulation models 94
3.3.1 RGBT model in PowerFactory 95
3.3.2 APS model in MATLAB 99
3.4 NFP method 102
3.4.1 Linearised model of a SG 103
3.4.2 Key trendlines 106
3.5 Summary 109
References 111
Chapter 4 Instability and Tipping Points with DQCI Converters 113
4.1 Introduction 114
4.2 Instability introduced by converters 114
4.2.1 RGBT model in DIgSILENT PowerFactory 114

4.2.2 APS model in MATLAB SimPowerSystems 118
4.2.3 NPF analysis 127
4.3 Investigation of possible reasons for instability 131
4.3.1 System inertia 131
4.3.2 System impedance 133
4.3.3 Converter capacity factor 136
4.3.4 NLL 140
4.4 Summary 147
References 148
Chapter 5 Effectiveness of Alternative Converter Control Methods in Enhancing System Tipping Points 149
5.1 Introduction 150
5.2 Frequency and voltage droop controllers on DQCI converter 150
5.3 SEBIR control in DQCI converter 153
5.4 VSM0H converter control 159
5.4.1 VSM0H dynamic response 159
5.4.2 Tipping point studies 166
5.4.3 NFP analysis 168
5.5 VSM-type control 170
5.5.1 VSM-type converter dynamic response 170
5.5.2 Tipping point studies 177
5.5.3 NFP analysis 178
5.5.4 Test of VSM-type control algorithm in PowerFactory 181
5.6 Benefits of grid forming converters 182
5.7 Summary 183
References 185
Chapter 6 Conclusions and Future Work 186

6.1 Conclusions 187
6.2 Future work 195
Appendices 197
Appendix A Settings for APS model in MATLAB 197
Appendix B Park and Clarke transformation 199
Appendix C Operation of VSC 201
References 204

Figures

Figure 2-1. Expected values for maximum penetration levels of renewable energy resources (based on power output from renewable generation over the hourly system demand power) by countries for 2016, 2020 and 2025 (data from ENTSO-E [6] published by 2015) 31

Figure 2-2. Forecast electricity demand in GB power network [7] 31

Figure 2-3. Installed capacity of generation by type under Two Degrees scenario for GB power system [7] 32

Figure 2-4. GB hourly instantaneous penetration level of NSG (%) to demand in 2030 under Two Degree scenario [11] 33

Figure 2-5. Illustrative frequency management requirement with respect to time [14] 34

Figure 2-6. Generator with a synchronous coupling to the network (e.g. conventional SGs) [14] 35

Figure 2-7. Generator without a synchronous coupling to the network (e.g. converter-interfaced generation) [14] 35

Figure 2-8. Classification of sub-synchronous interaction in power networks [15] ..39

Figure 2-9. (a) Illustration of operation in a single phase of a SG; and (b) its equivalent circuit when connected to a grid [42] 42

Figure 2-10. Main controllers of a SG including turbine-governor and voltage controller [43] 45

Figure 2-11. Example block diagram representation with AVR and PSS [23] 46

Figure 2-12. Classification of power system stability [45] 46

Figure 2-13. Illustrated structure of modern power networks and applications of power electronics [48] 49

Figure 2-14. Average-value model (AVM) of VSC in single line diagram 57

Figure 2-15. Generic configuration of a symmetrical mono-polar VSC-HVDC link 58

Figure 2-16. VSC-HVDC configuration with its vector current control system, i.e. DQCI control (* represents reference value) 59

Figure 2-17. Schematic of a SRF PLL 61

Figure 2-18. Illustration of the inner current controller in the DQCI control algorithm 63
Figure 2-19. Active and reactive power capability for VSC-HVDC transmission system 65
Figure 2-20. Configuration of SEBIR control applied as additional loop to DQCI control 67
Figure 2-21. Droop characteristics for (a) active power-frequency and (b) reactive power-voltage 69
Figure 2-22. Implementation of active power-frequency and reactive power-voltage droop controllers as additional control loop on outer controllers of DQCI converter control 70
Figure 2-23. VSM0H converter control algorithm and single-line diagram of switching bridge and line filter 74
Figure 2-24. High-level control diagram for a 'true' VSM converter controller with virtual rotor angle measured from active power output at the converter PCC 76
Figure 3-1. Reduced GB 36-bus/substation transmission model under 2030 Two Degrees Scenario in DIgSILENT Power Factory with UK map outline from [9] 96
Figure 3-2. General layout of each substation in the RGBT model (HVDC interconnectors and static compensators are not shown) 97
Figure 3-3. Example section of the spreadsheet for dispatching the generation in the RGBT model to achieve various instantaneous penetration levels 97
Figure 3-4. Configuration of the APS model in MATLAB SimPowerSystems 99
Figure 3-5. Model of DQCI converter in the APS model in MATLAB SimPowerSystems 99
Figure 3-6. Illustrative schematic of NFP method where network frequency is perturbed and amplitude and phase of the active power change is measured 102
Figure 3-7. Diagram of the IEEEG1 steam turbine and governor model [11] 103
Figure 3-8. Schematic of the SG model in this thesis 103
Figure 3-9. Illustration of the key featured responses *R* introduced by the NFP method based on linear analysis method 107
Figure 4-1. Active power, reactive power and terminal voltage for a Scottish SG in the RGBT model under a stable case with converter penetration level slightly below tipping point 115

Figure 4-2. Active power, reactive power and terminal voltage for a Scottish SG in the RGBT model under an unstable case with converter penetration level slightly above tipping point....115

Figure 4-3. Active power, reactive power and terminal voltage for a Scottish SG in the RGBT model under an unstable case with converter penetration level significantly above tipping point....115

Figure 4-4. System performance for an example under a stable case with converter penetration level below tipping point for small signal stability (60% instantaneous penetration level based on generation VA ratings) 118

Figure 4-5. System performance for an example under a stable case with converter penetration level slightly below tipping point for small signal stability (71% instantaneous penetration level based on generation VA ratings) 119

Figure 4-6. System performance for an example under an unstable case with converter penetration level slightly above tipping point for small signal stability (72% instantaneous penetration level based on generation VA ratings) 120

Figure 4-7. System performance for an example under a stable case with converter penetration level below tipping point for transient stability (60% instantaneous penetration level based on generation VA ratings) 122

Figure 4-8. System performance for an example under a stable case with converter penetration level slightly below tipping point for transient stability (65% instantaneous penetration level based on generation VA ratings) 122

Figure 4-9. System performance for an example under an unstable case with converter penetration level slightly above tipping point for transient stability (66% instantaneous penetration level based on generation VA ratings) 123

Figure 4-10. Responses of *dq*-axis currents for small signal stability 124

Figure 4-11. Responses of *dq*-axis currents for transient stability 125

Figure 4-12. Effects of penetration level of converters on the SSAD in APS model 126

Figure 4-13. Comparisons of NFP responses for SG obtained based on classical linear analysis and numerical simulation....128

Figure 4-14. NFP charts for SG (R_{SG}) and DQCI converter (R_{DQCI}) obtained by time-domain simulation along with the three key trend-lines R_{Droop}, R_H, R_{HD} predicated by classical linear analysis 129

Figure 4-15. Effects of system inertia on tipping points in terms of small signal stability and transient stability based on the APS model in MATLAB 132
Figure 4-16. Effect of system inertia on SSAD in the APS model 132
Figure 4-17. Effects of system impedance on tipping points in terms of small signal stability and transient stability based on the APS model in MATLAB 134
Figure 4-18. Effects of system impedance on SSAD in the APS model.....134
Figure 4-19. Relationship between tipping points in terms of small signal stability and SSAD with effects of system impedance 135
Figure 4-20. Range of recent capacity factor estimates in 2017 for utility-scale renewable energy technologies in the U.S. [12] 136
Figure 4-21. Effects of DQCI converter capacity factor on tipping points in terms of small signal stability and transient stability based on the APS model in MATLAB.....138
Figure 4-22. Effects of DQCI converter capacity factor on SSAD in the APS model 138
Figure 4-23. Relationship between tipping points in terms of small signal stability and SSAD with effects of DQCI converter capacity factor.....139
Figure 4-24. Configuration of three parallel single-phase rectifier (with resistor and capacitor connected in parallel at the DC side) forming as the NLL.....140
Figure 4-25. Model configuration for testing the single-phase rectifier NLL 142
Figure 4-26. Fourier analysis of harmonic distortion of phase A of the network PCC currents when NLL is not connected 142
Figure 4-27. Fourier analysis of harmonic distortion of phase A of the load PCC voltages when NLL is connected.....143
Figure 4-28. Fourier analysis of harmonic distortion of phase A of the load PCC currents when NLL is connected.....143
Figure 4-29. Fourier analysis of harmonic distortion of phase A of the network PCC voltages when NLL is connected.....144
Figure 4-30. Fourier analysis of harmonic distortion of phase A of the network PCC currents when NLL is connected.....144
Figure 4-31. Voltage THD measured at the SG PCC with various percentages of NLL in the APS model 145

Figure 4-32. Effects of various percentages of NLL out of total system load on tipping points in terms of small signal stability and transient stability based on the APS model in MATLAB 145

Figure 5-1. Effects of frequency droop slope D_f in DQCI converter and its LPF time constant $\tau_{\_Df}$ on system tipping points for small signal stability.....150

Figure 5-2. Effects of frequency droop slope D_f in DQCI converter and its LPF time constant $\tau_{\_Df}$ on system tipping points for transient stability.....150

Figure 5-3. Effects of voltage droop slope D_v in DQCI converter and its LPF time constant τ_{L_Dv} on system tipping points for small signal stability 151

Figure 5-4. Effects of voltage droop slope D_v in DQCI converter and its LPF time constant τ_{L_Dv} on system tipping points for transient stability 151

Figure 5-5. Implementation of SEBIR control in addition to the active power controller for DQCI converter in the APS model.....153

Figure 5-6. Tipping points in terms of steady state stability in APS model with SEBIR control implemented on DQCI converter using M class PMU to measure the RoCoF 154

Figure 5-7. Tipping points in terms of steady state stability in APS model with SEBIR control implemented on DQCI converter using P class PMU to measure the RoCoF 154

Figure 5-8. Effects of SEBIR control with various delay in the control loop in the RGBT model shown from frequency measured at a Scottish nuclear station in GB network.....156

Figure 5-9. NFP charts for SG, DQCI and SEBIR-equipped DQCI obtained by time-domain simulation along with the key trend-lines R_{Droop} and R_H predicated by classical linear analysis 157

Figure 5-10. Network model for comparison studies of SG and VSM0H-type converter.....158

Figure 5-11. Responses of SG and VSM0H converter under the event of a load step 160

Figure 5-12. Responses of SG under a balanced three-phase fault.....162

Figure 5-13. Responses of VSM0H converter under a balanced three-phase fault.162

Figure 5-14. Responses of SG and VSM0H converter under the event of a balanced three-phase fault 163

Figure 5-15. Responses of SG under the event of an unbalanced phase A to phase B fault....164
Figure 5-16. Responses of VSM0H converter under the event of an unbalanced phase A to phase B fault....165
Figure 5-17. APS model in MATLAB Simulink with implementation of VSM0H converter in parallel with SG and DQCI converter for tipping point studies....166
Figure 5-18. Tipping points in terms of steady state stability and transient stability in APS model with VSM0H converter implemented....166
Figure 5-19. NFP charts for SG and VSM0H converter obtained by time-domain simulation along with VSM0H trend and the key trend-lines R_{Droop}, R_H and R_{HD} predicated by classical linear analysis....168
Figure 5-20. Network model for comparison studies of SG and VSM-type converter....169
Figure 5-21. Responses of SG and VSM-type converter under the event of a load step....171
Figure 5-22. Effects of various damping factor zeta in VSM-type converter on its active power output measured at the PCC....172
Figure 5-23. Responses of SG under the event of a balanced three-phase fault....173
Figure 5-24. Responses of VSM-type converter under the event of a balanced three-phase fault....173
Figure 5-25. Responses of SG and VSM-type converter under the event of a balanced three-phase fault....174
Figure 5-26. Responses of SG under the event of an unbalanced phase A to phase B fault....175
Figure 5-27. Responses of VSM-type under the event of an unbalanced phase A to phase B fault....176
Figure 5-28. Tipping points in terms of steady state stability and transient stability in APS model with VSM-type converter implemented....177
Figure 5-29. NFP charts for SG and VSM-type converter obtained by time-domain simulation along with VSM trend and the key trend-lines $\boldsymbol{R_{Droop}}$, $\boldsymbol{R_H}$ and $\boldsymbol{R_{HD}}$ predicated by classical linear analysis....178
Figure 5-30. Effects of damping factor Zeta in the VSM-type control on the NFP charts (obtained by time-domain simulation)....179

Figure 5-31. Summary of maximum achievable system tipping points in terms of both transient stability and small signal stability with various converter control technologies 183

Glossary of Terms

AC	Alternating Current
APS	Aggregated Power System
AVR	Automatic Voltage Regulator
CHIL	Converter Hardware-In-Loop
DC	Direct Current
DQCI	*dq*-axis Current Injection
EMT	Electro Magnetic Transient
EU	European Union
EV	Electric Vehicle
GB	Great Britain
HVAC	High Voltage Alternating Current
HVDC	High Voltage Direct Current
IGBT	Insulated-Gate Bipolar Transistor
LCC	Line-Commutated Converter
LOM	Loss Of Main
LPF	Low-Pass Filter
MTDC	Multi-Terminal Direct Current
NFP	Network Frequency Perturbation
NLL	Non-Linear Load
NSG	Non-Synchronous Generation
NVP	Network Voltage Perturbation

PCC	Point of Common Coupling
PI	Proportional and Integral
PLL	Phase-Locked Loop
PMU	Phasor Measurement Unit
PSS	Power System Stabiliser
PV	Photovoltaic
PWM	Pulse Width Modulation
RES	Renewable Energy Source
RMS	Root Mean Square
RoCoF	Rate of Change of Frequency
RGBT	Reduced GB Transmission
SEBIR	Swing Equation Based Inertial Response
SG	Synchronous Generator
SOGI	Second-Order Generalised Integrator
SPF	Synchronous Reference Frame
STATCOM	Static Synchronous Compensators
SVC	Static VAr Compensators
SSAD	Steady-State Angle Difference
THD	Total Harmonic Distortion
TPS	Tipping Point Searching
UK	United Kingdom
US	United States

VSC	Voltage Source Converter
VSM	Virtual Synchronous Machine
VSM0H	Virtual Synchronous Machine with Zero Inertia

Chapter 1

Introduction

1.1 Motivation and scope

Owing to various government policies concerning the reduction of CO_2 emissions, future power systems will be predominantly powered by renewable energy sources, the bulk of which connect to a power system through converters. Thus, conventional, directly-coupled synchronous generation will have a smaller contribution to the dynamics of a future power system; that is, the contribution to voltage stability from directly-coupled synchronous generation will be reduced, but so too will the overall system inertia be, by which frequency stability is also affected [1]. Accordingly, a complete understanding of the dynamics of the converters in a power system where there is a small amount of directly-coupled synchronous generation, covering all possible operating conditions, becomes paramount.

Modern-converters are typically controlled using the vector current control approach, referred to as *dq*-axis current injection (DQCI) control in this work, which operates in a rotating frame, known as the *dq* frame, which is, in principle, synchronised with the voltage at the point of common coupling (PCC); the grid synchronisation is achieved with a phase-locked loop (PLL) [2]. Under the assumption of satisfying synchronisation of the PLL, i.e. *q*-axis voltage is zero, control over active power output is then achieved through regulation of the direct (*d*-axis) component of the current flowing through the filter impedance; reactive power output, or AC voltage control, is achieved through regulation of the quadrature (*q*-axis) component of the current flowing through the filter impedance. The performance of the PLL is dependent on the voltage stability of the grid to which the converter is supplying power. The lack of a strong voltage source, which will characterise future power systems with high penetration of converters, manifests itself in poor grid synchronisation by the PLL [3]. Thus, what is originally an angle synchronisation issue causes, through a cascade of errors in the converter control system, other issues, such as frequency instability.

There is an existing body of research exploring the effects of converters on system performance, covering network frequency stability [4, 5], angular stability [6, 7] and voltage stability [6, 8]. However, there are limited studies on the stability issues for converter-dominated systems. The penetration level at which the instability phenomenon is first observed is defined as system "tipping point". For example, the authors of [9] investigate system performance when power generated from non-synchronous

distribution generation, including wind and photovoltaic (PV) units, is up to 30% of the system demand. Helge et al. [10] studied the stability of the Great Britain (GB) power system under a small, predefined set of operating points penetration ranges of non-synchronous generation (NSG) including high voltage direct current (HVDC) transmission systems, using a phasor based simulation.

A state-space approach to small signal stability analysis involves deriving linearised models of each component in the system, before amalgamating the component models into a single, large model. The electrical part of a synchronous generator (SG) is a single component in a power system, as is the electrical part of the converter; additional components are the control systems associated with each source of generation. Accordingly, since the number of states associated with models of each component can be quite large, the combined model of the power system may comprise a multitude of state variables. Moreover, due to the highly non-linear blocks in the PLL such as voltage controlled oscillator and phase detector, developing theoretically robust linearised models of the PLL particularly when the inertia is low, can be challenging. As a result, a state-space model which would include adequate representation of inverter connected sources with their controllers can be very difficult and thus impractical to develop.

Instead, in this thesis, a time domain approach is proposed to assess the system tipping points, the method which will henceforth be referred to as the tipping point searching (TPS). In the TPS method, a set of combined viability criteria has been defined to detect instability, which includes the PLL locking status in DQCI controller, system frequency, rate of change of frequency (RoCoF), voltage magnitude and voltage total harmonic distortion (THD) level, with the operating limits chosen according to the existing network grid codes. This method can be used in any time-domain power system model. In this thesis, system tipping points, both in terms of small signal stability and transient stability, for systems which feature conventional DQCI converters are investigated using two network models: a reduced GB transmission (RGBT) model in DIgSILENT PowerFactory (RMS-simulation), and an aggregated power system (APS) model in MATLAB SimPowerSystems (EMT-simulation). The effects of various critical parameters including overall system inertia, system impedance, converter capacity factor and existence of non-linear load (NLL), on the system tipping points are systematically studied.

Along with the TPS method, a network frequency perturbation (NFP) tool is introduced to visualise the response of individual generators to a periodic fluctuation in network frequency. This way potential interactions between different generators can be identified. With a generator exposed to perturbed network frequency, its active power output is analysed using the Fourier Transform and the NFP response are obtained. Similar to the traditional frequency domain analysis of control systems, the NFP analysis can be carried out based on the linearised model of the generator and its controller; it can also be applied to the generator model in time-domain with network perturbed by a sweep of frequency.

In the last two decades, the displacement of conventional generation by renewable energy sources led transmission system operators to be concerned with the reduction in the system inertia [1, 11]. Consequently, attention was primarily given to investigating control algorithms which circumvent associated frequency stability issues. That is, control algorithms which contained the RoCoF equation, were embedded into conventional DQCI controller [12]. For frequency events, droop control algorithms were also considered. Relatively little attention was paid to voltage stability; indeed, it had been assumed that any voltage stability issues could be handled by incorporating droop control. In the last five years, the issue of voltage stability has become significantly more important. Given that the consensus now is that DQCI control has fundamental issues in weak systems, alternative algorithms have been developed, typically emulating, to one extent or another, the dynamics of a synchronous machine [3]. In such control algorithms, synchronisation is achieved through power flow considerations. The resulting converter systems (including the controller) are referred to as grid-forming converters by system operators (e.g. published by GB National Grid [13] and ENTSO-E [14]) or virtual synchronous machine (VSM) techniques. In this thesis, having explored the stability thresholds of DQCI converter, the stability implications of adopting the aforementioned variations on DQCI control and alternative control approaches are studied in this work.

1.2 Principal research contributions

The main contribution of the thesis are summarised as follows:

- A novel time-domain analysis method for investigation of power system stability threshold associated with the voltage instability issue under high penetration of converters is proposed. A set of combined viability criteria to detect the instability has been defined, which includes the PLL locking signal in DQCI controller, system frequency, RoCoF, voltage magnitude and voltage total harmonic distortion level. The operating ranges for those parameters are chosen based on the existing network grid codes. Awareness of the instability phenomenon and system tipping points is important to assist system operators and manufacturers with future system planning and operation. This method can be applied to any time-domain power system model for tipping point assessment. This is distinct from traditional stability assessment methods, such as small signal stability analysis, which involves linearisation of the system and can become very complex (and thus not practical) when dealing with power systems with high penetration of converters.
- A novel tool for visualisation of the responses of individual generators to a periodic fluctuation in network frequency herein referred to as the NFP method. It can be used to compare responses of converters' different control algorithms with traditional SGs. The analysis can be conveniently performed using time-domain model only. With a rapidly increasing penetration of converters, the NFP analysis tool could be particularly useful in the future power networks where a variety of control algorithms may be operating at any instant in time. The NFP analysis tool combined with the TPS method forms a powerful analytical framework to study network stability under high penetration of converters.
- Assessment of the impact of various converter control techniques on system stability thresholds to provide guidance to system operators on network planning and regulation. While different types of converter control techniques have been widely reviewed under high penetration of converters, uncertainty of their effects on system stability and potential interactions remain. With utilisation of the TPS method and NFP analysis tool, such effects can be studied; the results have been of great interest to manufacturers and system operators. For example, GB

National Grid [13] and ENTSO-E [14] have considered the outcome of this research in their next-stage review.

1.3 Thesis Outline

Chapter 2 reviews future energy scenarios and power system challenges associated with increasing penetration of converters. This chapter also gives an overview of operation principles for traditional SGs and power electronic converters, as well as their control systems. The converter-related literature review includes both line-commutated converters (LCC)-HVDC and voltage source converters (VSC)-HVDC. The principles of operation of VSC-HVDC and its conventional DQCI control are included. Alternative converter control techniques that could contribute to the resolution of stability issues in converter-dominated systems are also to be reviewed and discussed. Two algorithms which emulate characteristics of synchronous machines, namely the Virtual Synchronous Machine with zero inertia (VSM0H) and VSM-type, are described in detail.

Chapter 3 presents methodology used in this thesis, including simulation models for power networks, the TPS method and its detection criteria, as well as NFP tool for frequency response visualisation.

Chapter 4 demonstrates and quantifies the power system instability phenomenon using the simulation models, which contain synchronous generation and DQCI converters. The tipping points are systematically assessed for small-signal and transient stability. NFP responses of conventional converter controlled by DQCI controller are studied and compared with SGs. Effects of various system model parameters including, but not limited to, system inertia, system impedance, generation loading level and existence of NLL are also explored.

Chapter 5 explores performance of various converter control techniques reviewed in Chapter 5 compared to the conventional DQCI converter, and their potential enhancing effects on the tipping points. NFP charts for the various converter controllers are also compared in terms of their effects on system dynamics and potential interactions.

Chapter 6 concludes this thesis by summarising the contributions of the research, as well as future work that can be built upon the finding and outcomes of this work.

1.4 Publications

Journal papers:

- M. Yu, A. J. Roscoe, A. Dysko, C. D. Booth, R. Ierna, J. Zhu and H. Urdal, "Instantaneous Penetration Level Limits of Non-Synchronous Generation in the British Power System," *IET Journal on Renewable Power Generation,* 2016.

Conference papers:

- A. J. Roscoe, M. Yu, R. Ierna, H. Urdal, A. Dysko, H. Urdal and C. D. Booth, "A VSM (Virtual Synchronous Machine) Convertor Control Model Suitable for RMS Studies for Resolving System Operator/Owner Challenges," in *15th Wind Integration Workshop*, Vienna, Austria, 2016.
- R. Ierna, J. Zhu, A. Roscoe, M. Yu, H. Urdal, A. Dyśko and C. D. Booth, "Effects of VSM Convertor Control on Penetration Limits of Non-Synchronous Generation in the GB Power Sytstem," in *15th Wind Integration Workshop*, Vienna, 2016.
- M. Yu, A. J. Roscoe, C. D. Booth, A. Dysko, R. Ierna, J. Zhu and H. Urdal, "Use of an Inertia-less Virtual Synchronous Machine to Stabilise Networks with High Penetrations of Converters," in *Power Systems Computation Conference (PSCC)*, Genoa, Italy, 2016.
- M. Yu, A. Dysko, A. J. Roscoe, C. D. Booth, R. Ierna, H. Urdal and J. Zhu, "Effects of Swing Equation-Based Inertial Response (SEBIR) Control on Penetration Limits of Non-Synchronous Generation in the GB Power System," in *IET Renewable Power Generation Conference*, Beijing, China, 2015.
- M. Yu, A. Dysko, C. D. Booth, A. J. Roscoe, J. Zhu, and H. Urdal, "Investigations of the constraints relating to penetration of non-synchronous generation (NSG) in future power systems," in *PACWorld Conference*, Glasgow, UK, 2015.
- M. Yu, A. Dysko, C. D. Booth, A. J. Roscoe, and J. Zhu, "A review of control methods for providing frequency response in VSC-HVDC transmission systems," in *Power Engineering Conference (UPEC), 2014 49th International Universities*, 2014, pp. 1-6.

References

[1] National Grid (GB), "System Operability Framework," 2016. Available: http://www2.nationalgrid.com/UK/Industry-information/Future-of-Energy/System-Operability-Framework/, accessed in 2017/2/10.

[2] N. Ray Chaudhuri, B. Chaudhuri, R. Majumder, and A. Yazdani, "The Voltage-Sourced Converter (VSC)," in *Multi-Terminal Direct-Current Grids*, ISBN 9781118960486: John Wiley & Sons, Inc, 2014, pp. 23-75. Available: http://dx.doi.org/10.1002/9781118960486.ch2, accessed in 2017/5/19.

[3] National Grid (GB), "Performance of Phase-Locked Loop Based Converters," Sep 2017. Available: https://www.nationalgrid.com/sites/default/files/documents/Phase%20locked%20loop%20FINAL.pdf, accessed in 2018/1/8.

[4] J. O'Sullivan, A. Rogers, D. Flynn, P. Smith, A. Mullane, and M. O'Malley, "Studying the Maximum Instantaneous Non-Synchronous Generation in an Island System: Frequency Stability Challenges in Ireland," *IEEE Transactions on Power Systems,* vol. 29, pp. 2943-2951, 2014.

[5] M. Nahid Al, Y. Ruifeng, T. K. Saha, and N. Modi, "Frequency response and its enhancement using synchronous condensers in presence of high wind penetration," in *Power & Energy Society General Meeting, 2015 IEEE*, 2015, pp. 1-5.

[6] L. Meegahapola and T. Littler, "Characterisation of large disturbance rotor angle and voltage stability in interconnected power networks with distributed wind generation," *IET Journal on Renewable Power Generation,* vol. 9, pp. 272-283, 2015.

[7] M. Edrah, K. L. Lo, and O. Anaya-Lara, "Impacts of High Penetration of DFIG Wind Turbines on Rotor Angle Stability of Power Systems," *IEEE Transactions on Sustainable Energy,* vol. 6, pp. 759-766, 2015.

[8] E. Vittal, M. O'Malley, and A. Keane, "A Steady-State Voltage Stability Analysis of Power Systems With High Penetrations of Wind," *IEEE Transactions on Power Systems,* vol. 25, pp. 433-442, 2010.

[9] P. N. Papadopoulos and J. V. Milanovic, "Impact of penetration of non-synchronous generators on power system dynamics," in *2015 IEEE PowerTech*, Eindhoven, 2015, pp. 1-6.

[10] H. Urdal, R. Ierna, Z. Jiebei, C. Ivanov, A. Dahresobh, and D. Rostom, "System strength considerations in a converter dominated power system," *IET Journal on Renewable Power Generation,* vol. 9, pp. 10-17, 2015.

[11] National Grid (GB), "Future Energy Scenario," 2017. Available: http://fes.nationalgrid.com/, accessed in 2017/11/23.

[12] National Grid (GB), "System Operability Framework," 2015. Available: http://www2.nationalgrid.com/UK/Industry-information/Future-of-Energy/System-Operability-Framework/, accessed in 2017/2/10.

[13] "Effects of VSM/Option 1 (Grid Forming) Converter Control on Penetration Limits of Non-Synchronous Generation (NSG) in the GB Power System," June 2017. Available: https://www.nationalgrid.com/sites/default/files/documents/GC0100%20Annex%206%20FFCI%20supporting%20documents.pdf, accessed in 2017/12/15.

[14] "Implementation Guidance Document (IGD) on High Penetration of Power Electronic Interfaced Power Sources (HPoPEIPS)," 2017 Available: https://www.entsoe.eu/Documents/Network%20codes%20documents/Implementation/CNC/170322_IGD25_HPoPEIPS.pdf, accessed in 2017/8/15.

Chapter 2

Future Energy Scenarios and generating technologies

2.1 Introduction

In this chapter, key motivating factors for the large scale implementation of non-synchronous devices, as well as various challenges associated with that will be discussed. Besides, working principles of main existing generating technologies and their controllers will be covered. This includes conventional synchronous generation and HVDC based systems as it is expected that a significant amount of power will be transferred via HVDC links in future interconnected systems. Additionally, the conventional vector current control technique for the VSC-HVDC system based on PLL to synchronise with the AC grid, i.e. the DQCI controller, will be described.

The principles of operation of the DQCI controller are based on the assumption of a perfect PLL; that is, one which perfectly tracks the grid voltage at the point of common coupling. The departure from perfect phase tracking, as would occur with any real PLL (particularly in weak systems) leads to a cross-coupling phenomenon in the inner current control loop which could lead to converter and system instability issues. Therefore, various converter control techniques that have the potential of resolving system stability issues under high penetration of converters, which are categorised based on whether DQCI control and PLL are used or not, will be reviewed and discussed. VSM concepts, also termed as grid-forming converters, which have been the most popular topic in this field, mimic the behaviour and characteristics of a real synchronous machine based on the converter interface. Two representative models of VSM are covered in detail in this thesis: the VSM0H and VSM-type converter. Both are considered helpful for system stability studies and promising to assist the high penetration of converters.

2.2 Driving forces behind power system changes

The combination of an increasing global population and the industrialisation/modernisation of nations has led, and will continue to lead, to an increased demand for energy. Indeed, according to [1], the total world energy consumption may increase by 48% between 2012 and 2040.

At the same time in Asian countries such as China, Japan and Korea, energy demand can increase by as much as 72% [1]. In particular, the partial liberalisation of Chinese

markets which begun under Deng Xiaoping led to and continues to drive a massive increase in industrialisation and wealth of many Chinese citizens. Combined with the continued population growth of China, this is yielding a huge increase in energy demand. With the Chinese government focusing primarily on economic growth in recent decades, it mainly used conventional, fossil fuel based, energy sources such as coal to power the economic transformation. However, in more recent times, the Chinese government has pushed for a massive increase in the deployment of renewable energy devices, culminating in the Chinese government's participation in the Manila-Paris deal. This stipulates that full decarbonisation should be achieved by 2050 with the peaking of global emissions occurring no later than 2020. More immediately, the Chinese government has pledged that 15% of its energy generation will be contributed from renewable energy resources by 2020 as stated in [2]. Presently, China has the largest absolute value of installed capacity of renewable energy devices (though this was largely due to numerous massive hydropower plants such as the Three Gorges Dam). Even when hydropower is not included, China still led the world in wind and solar generation during 2015 [1].

The next largest contributor to CO_2 emissions (as measured in 2015) is the US [1]. Due to the significantly smaller population, the US does actually have a higher emission per capita. Renewable energy sources accounted for about 16.7% of the total installed capacity in the United States, and 13.8% of the total electricity generation by 2015, with wind and solar to be the fastest-growing renewable technologies [3]. Approximately 15GW of coal-fired generation was retired in 2015, which was the highest achieved rate in a single year to date.

Whilst the US has recently withdrawn from the Paris deal, all recent administrations (including the current administration) acknowledge the threat posed by climate change. As a result, whilst the policy of the US is currently unclear, it is expected that the US will also move towards more renewable energy systems and more converter-based technologies.

In Europe, the situation is somewhat different. Due to the modernisation of European countries not being a recent phenomenon and net population growth being moderate in comparison to nations such as China or India, most European countries have not experienced the same level of growth in electricity demand. However, being industrialised for more than a century meant that the emissions per capita were already

high. Indeed, as a unit, the EU contributes 9% of global emissions [1]. In an effort to curb emissions, the EU and nation states of Europe have set themselves targets for deriving increasing amounts of energy from renewables. The EU has set itself up targets for reducing the greenhouse gas emission progressively by 2050, i.e. the "20-20-20" targets [4], where a 20% cut in greenhouse gas emissions is expected by 2020 compared to levels in 1990, at least 40% by 2030 and 80% by 2050. By 2014, the greenhouse gas emissions in EU have dropped by 24% below the 1990 levels [4].

With the majority of the Member States advancing towards the 2020 target, the gross electricity power generated from renewables in EU has reached to almost 26% in 2014, up from 15% in 2012 [5]. Figure 2-1 indicates the forecast maximum hourly penetration level of renewable energy sources relative to system load in the EU countries published by ENTSO-E in 2015 [6] for 2016, 2020 and 2025, where the penetration level of renewable energy source (RES) is defined by the power output from RES contributing to the system demand. Of the thirty-three countries in the EU, eight countries (Germany, Denmark, GB, Greece, Ireland, Northern Ireland, Netherlands and Portugal) are expected to encounter periods during which all power is provide by converter-connected sources; twenty-two countries (including the aforementioned countries) will reach penetration levels over 50% by 2025. Note that the 100% penetration levels do not mean that they occur simultaneously for the eight countries mentioned above on the same hour. Among the different types of renewable energy resources, the most popular ones in EU areas have been the wind and solar, whose installed capacity are forecast to increase by 80% and 60%, respectively according to [6].

The UK government has agreed to EU targets which stipulate that renewable energy sources account for 15% of total energy consumption by 2020. Since renewable energy sources are more easily integrated into the electricity system, it is expected that the main impact of renewables will occur in this sector; accordingly, 40% of electricity power is projected to be derived from renewable energy sources by 2022 under Two Degrees scenario [7]. Note that the Two Degree scenario defines the scenario where the environmental sustainability is the top priority, i.e. optimal development of low carbon energy and high penetration levels of converters. In 2008, UK government adopted a new Climate Change Act [8] where it is specified that the UK should reduce its greenhouse gas emissions by at least 80% below 1990 levels by 2050. In spite of the deindustrialisation

of GB, which caused (and is projected to cause) a short term fall in electricity demand as shown in Figure 2-2, the electricity demand in GB will increase in the medium to long term. This is for the following reasons: a growing population, increased deployment of electric vehicles (EVs), and the proliferation of electric heating systems.

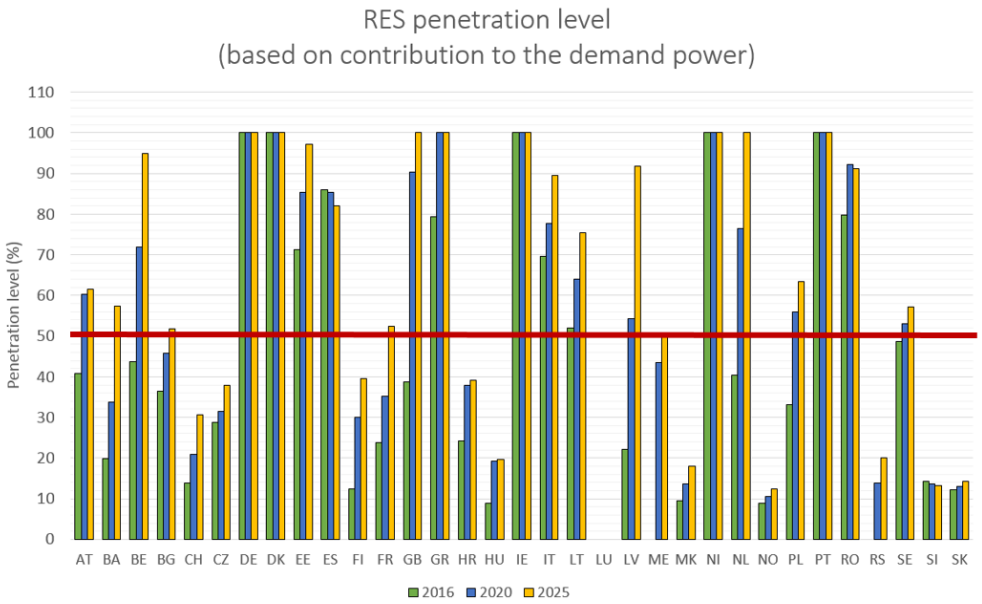

Figure 2-1. Expected values for maximum penetration levels of renewable energy resources (based on power output from renewable generation over the hourly system demand power) by countries for 2016, 2020 and 2025 (data from ENTSO-E [6] published by 2015)

Figure 2-2. Forecast electricity demand in GB power network [7] [1]

[1] This image has been removed by the author of this thesis for copyright reasons.

Figure 2-3. Installed capacity of generation by type under Two Degrees scenario for GB power system [7] [2]

With a substantial increase of the renewable electricity sources, UK generated 7% of energy from renewable energy resources in 2014 [9] and 12% of energy is expected to come from renewable energy resources by 2020 under Two Degrees scenario [7]. The renewable target in GB power network will be achieved by 2022 under Two Degrees scenario which falls slightly beyond the targeted time due to relatively slow decarbonisation in the heating and transport sectors [7]. Between 2016 and 2020, as shown in Figure 2-3, fossil fuel including coal-fired plant and some old gas-fired power stations will be closed due to difficult market conditions and environmental legislation while the last coal-fired power station will be decommissioned by 2025. Gas generation will make a valuable contribution to security of the supply. New technologies led by renewable energy resources, mainly wind and solar, will experience further increases out of the total generation capacity. Due to more investment being made by introduction of Ofgem's Cap and Floor Regime [10], a rapid increase of interconnectors can be seen as well, with installed capacity expected to ramp up by about 20 GW between 2015 and 2040 [7]. Electricity storage technology has been evolving rapidly to support system security and reliability under increasing penetration of NSG, such as balancing and ancillary services.

In all of the aforementioned regions, the transition to renewable-based energy will result in power systems that were once dominated by synchronous machines being dominated by converters. Even when synchronous machines are employed, for example

[2] This image has been removed by the author of this thesis for copyright reasons.

in hydropower stations, the location of the plant can be far from the demand centres, especially in large countries such as China. To minimise transmission losses, HVDC systems are employed, decoupling the SGs of the hydropower station from the grid in which the demand centre is located. Indeed, HVDC interconnectors are already commonplace in China as a result of the large distances between generation and load.

Moreover, as shown in Figure 2-4, the hourly instantaneous penetration level of NSG in 2030, i.e. mainly wind and PV, in the GB power network is expected to vary dramatically from 0% in August (moderate wind and high demand) to 165% in December (strong wind and low demand), which could potentially pose great challenges on system operation and security.

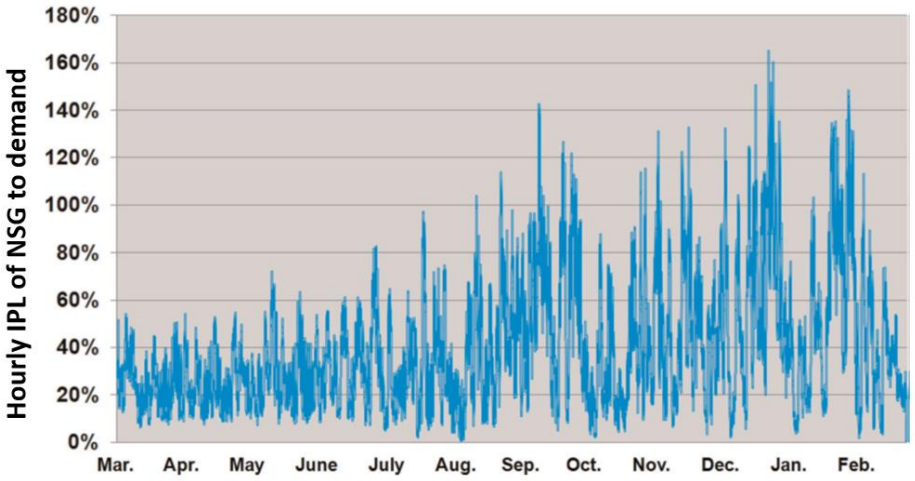

Figure 2-4. GB hourly instantaneous penetration level of NSG (%) to demand in 2030 under Two Degree scenario [11]

2.3 Operational challenges

With dramatically increasing penetration level of converters, operability challenges to the existing power systems have drawn great attention of the system operators. To achieve a secure and reliable system operation under high penetration of converters, it is important to overcome such issues and ensure a smooth and efficient transition of the current power networks. The main challenges on frequency stability and voltage stability are discussed in this section.

2.3.1 Frequency stability

Grid frequency is one of the most important indicators of the health of a power system. When generation and demand are balanced in a power network, frequency remains constant. As stated in [12, 13], the operational limits for contracted generators in the GB power system are ±0.2 Hz, i.e. 49.8 Hz to 50.2 Hz. As shown in Figure 2-5 within the ±0.2 Hz operational limits, the system will stay in continuous operation, and control system will regulate the system frequency to be as close as possible to its nominal value of 50 Hz.

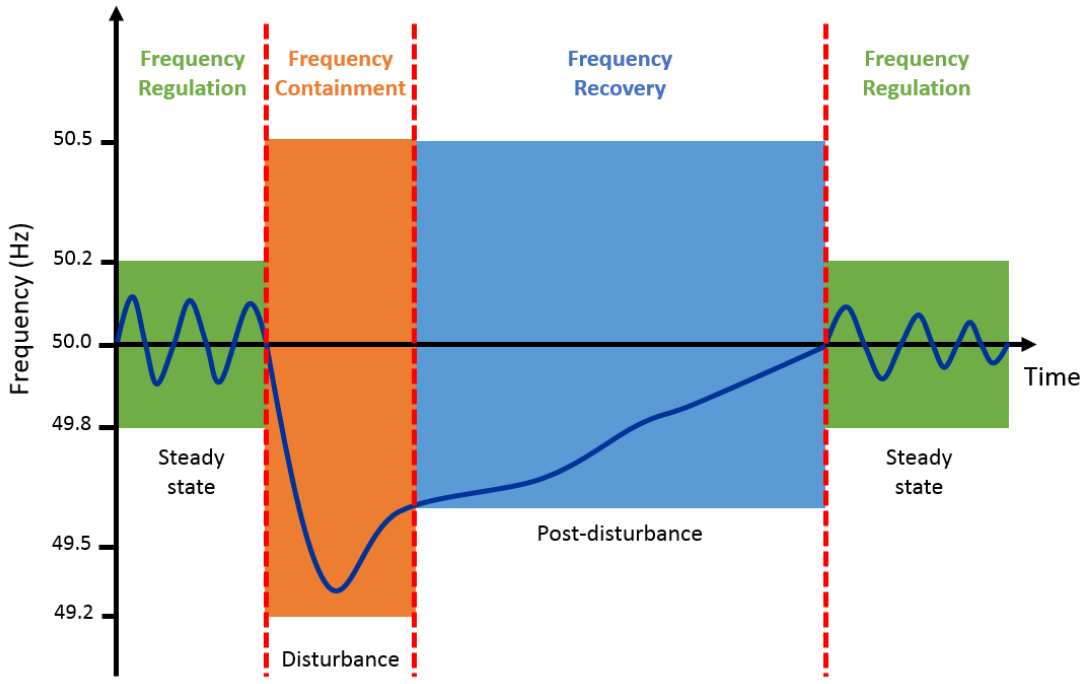

Figure 2-5. Illustrative frequency management requirement with respect to time [14]

When there is a power imbalance, for example due to loss of a generation, the electrical torque demand exceeds the mechanical torque being applied to the rotors of the generators connected to the power system. By Newton's second law applied to rotating bodies, this results in a natural deceleration of the rotors, as the power imbalance is compensated by the energy stored in the rotating masses of the machines. Given the intrinsic relationship between grid frequency and the rotor speed of directly connected synchronous machines, the grid frequency will drop in this scenario. On the other hand, e.g. following loss of a major load, system frequency will increase. Figure 2-5 shows the frequency response stages following a disturbance (generation and demand loss).

Figure 2-6. Generator with a synchronous coupling to the network (e.g. conventional SGs) [14] [3]

Figure 2-7. Generator without a synchronous coupling to the network (e.g. converter-interfaced generation) [14] [3]

System inertia is understood as the aggregated inertia of all the rotating machines in a power network (including generators and motors) that are directly coupled to the network. Such direct coupling allows power disturbances to be transferred to a change of mechanical torque that acts on the machine rotor, as shown in Figure 2-6, which can be visualised as a chain that connects a SG to the power system while a speed change can affect every component connected in the chain. Frequency in an infinitely strong system would never be shifted from nominal value, regardless of the magnitude of the transient event. Practically, the higher the system inertia, the slower the initial RoCoF in response to any transient, which results in less pronounced system dynamics following a

[3] This image has been removed by the author of the thesis for copyright reasons.

disturbance and contributes to a generally higher level of system stability. However, power electronic devices, i.e. non-synchronous devices, are decoupled from the AC system due to the static AC/DC converter interface, and therefore are not able to contribute to system inertia. It can be described as a roller which allows power transfer between the generator and the network while a change in the speed on one side will not affect the other, as shown in Figure 2-7.

In the GB power system, the system inertia level is already low during low demand periods and it is expected to decrease further between now and 2035. The system minimum inertia can even drop by over 60% between now and 2025/26 [15]. Even though the inertia level slowly increases after 2025/26 due to the construction of new synchronous generation, especially nuclear generation, it can still drop by more than 30%. The inadequate system inertia with increasing penetration of non-synchronous devices is already significantly affecting the operation of some synchronous areas.

Challenges have been raised by the decreasing system inertia levels worldwide, such as those discussed in [14] for GB and [16] for Ireland and Northern Ireland. First, the widespread high RoCoF value across the network following system disturbances, i.e. loss of a generation or demand, could easily trip the RoCoF relay and lead to cascading tripping of many affected generators. According to [15, 17], the RoCoF based Loss-of-Mains (LOM) protection setting which used to be 0.125 Hz/s, has been changed to 1 Hz/s for all distributed generators, with a delay of 500 ms (i.e. the RoCoF must be continually above the threshold for a period of 500 ms before tripping is permitted). This is to reflect the increasing penetration of converters and their impact on system dynamics. In Ireland, the RoCoF grid code standard has been updated to 1 Hz/s for Ireland and Northern Ireland calculated over 500 ms in 2014 and the suggested compliance of RoCoF for any studies up to 2 Hz/s [18]. Meanwhile the level of infrequent infeed loss in GB national electricity transmission system has been increased from 1320 MW to 1800 MW since April 1st 2014 [19].

With lowering inertia it is expected to become more difficult for the system to be maintained within the desired range, e.g. ±1% of 50 Hz in the GB transmission system, as stated in the Electricity Supply Regulations 1989 [20]. This is due to lack of natural/conventional frequency response provided by the converter.

2.3.2 Voltage stability

To facilitate economic, efficient and safe transfer of active power across the transmission and distribution networks, voltage levels must be controlled within acceptable operation margins. In the GB transmission system, normal operating voltage ranges are defined as ±5% at 400 kV and ±10% at lower transmission voltages, with reference to [12]. Similarly, the ranges for distribution networks can be found in [21].

Voltage depends primarily on the localised balance of reactive power supply and demand. When there is an excess of reactive power generation, the voltage at busbars nearby will rise; on the other hand, voltages will drop if there is more reactive power demand. When the power flows are high, electricity networks tend to absorb more reactive power (due to series reactance of the transmission lines and transformers), which requires additional source of reactive power to maintain voltages in the desired range.

After a disturbance, such as an short-circuit fault, voltage level at nearby busbars will drop rapidly due to increased current as well as increased reactive power consumption. It is therefore important to ensure a fast fault current injection to arrest the rapid drop of voltages during this period. Short-circuit level (or fault level) is an important factor as a measure of system strength. In the conventional power systems, synchronous machines can provide high fault currents, typically 6 times the value of the rated current [22], because such generators operate as voltage sources with low internal impedance. As the majority of non-synchronous devices are connected to the system via power electronic devices, their contribution to short circuit level is limited to a great extent by the maximum current allowed to flow to prevent over-heating of the converter hardware. Additionally, the characteristics of the three-phase current contribution from an inverter in response to balanced and unbalanced faults can be significantly different from that of a synchronous machine. Therefore, increasing penetration of converter-interfaced generation in the power networks will lead to a significant reduction in short circuit levels which will impact on various aspects of system operation such as voltage management.

Apart from the conventional regional voltage stability issues, another type of voltage stability issue related to the tracking performance of synchronous reference frame (SRF) PLL in the DQCI controller has also been discussed in the field specifically for weak networks, i.e. networks with high impedance, and/or high penetration of converters.

Traditional synchronous machines operate as balanced voltage sources connected to grid via a transient reactance [23]. However, conventional converters for non-synchronous devices typically use DQCI controller, where active and reactive power setpoints are translated into *dq*-axis rotating reference frame. This will be described in more detail in Chapter 2. Such method is used to control the switching bridges or multilevel modules to achieve actual injected currents closely marched to the reference values, resulting in a converter behaving as a balanced sinusoidal current source. This is required by the present GB and EU grid codes, such as [12, 24], even in the presence of voltage unbalance or harmonics. The DQCI converters also aim to have high equivalent impedance from the perspective of unbalance, harmonics and inter-harmonics. When there are harmonics or unbalance in the measured voltage waveforms, the feedback control signals could be affected in an undesirable way, leading to converter and system operation failures. Moreover, most of the existing analyses of the DQCI control scheme neglects the effects of the PLL. Given that the PLL has a low-bandwidth, it is more difficult for the PLL to track the phase of the grid at the point of common coupling, especially in a weak system where the voltage tends to be less stiff; hence, the performance of the PLL, and by extension the DQCI control scheme, deteriorates, which could affect the converter terminal voltage and lead to undesired cross-coupling in the *dq*-axis controller (as the measured voltage forms an input to the control loops). Such effects have been discussed widely such as by Lidong Zhang [25, 26], QingChang Zhong [27, 28], Ashabani Mahdi [29, 30], Dong Dong [31], as well as system operators, e.g. GB National Grid [32].

2.3.3 Sub-synchronous resonance

Resonant oscillatory modes at a range of frequencies can occur in all electrical and electromechanical power systems where most of them are harmless and short lived because of effective damping in the system, i.e. inertia stored in the various devices. However, there are cases where the oscillations can grow with significant magnitude for a sufficient period of time, which can cause damage to devices or system instability. This especially involves those with associated frequencies reflected at the terminals of the generators close to characteristic frequencies of the connected electrical power system, i.e. generally lies in the sub-synchronous frequency range below nominal system frequency, and cannot be damped sufficiently [33].

Conventionally, the sub-synchronous resonance (SSR) is mostly related to reinforcement such as series capacitor-formed compensation [23]. Recently and in the future power systems, the high speed active controls deployed in numbers of power system technologies, such as HVDC equipment and wind turbine controllers, tend to provide negative damping to the system and therefore exacerbate SSRs, or so-called sub-synchronous torsional interaction (SSTI) and sub-synchronous control interaction (SSCI) respectively [33], which could become increasingly relevant as regional levels of NSG increase [34]. Categories of SSR phenomenon are illustrated in Figure 2-8 [15]. In the GB national electricity transmission system, SSR has been a risk since the first HVDC interconnection between GB and neighbouring countries was established, which is generally related to current source converters operating in rectifier mode and it could become pragmatic when the negative electrical damping introduced by HVDC converter controller exceeds the positive mechanical damping from nearby synchronous generating units [35]. The GB Grid Code [12] requires the HVDC converter owner to hold the responsibility to mitigate any SSR risks that arise from the interactions between HVDC link and other plant by, for example, fitting the controller with an SSR damping loop.

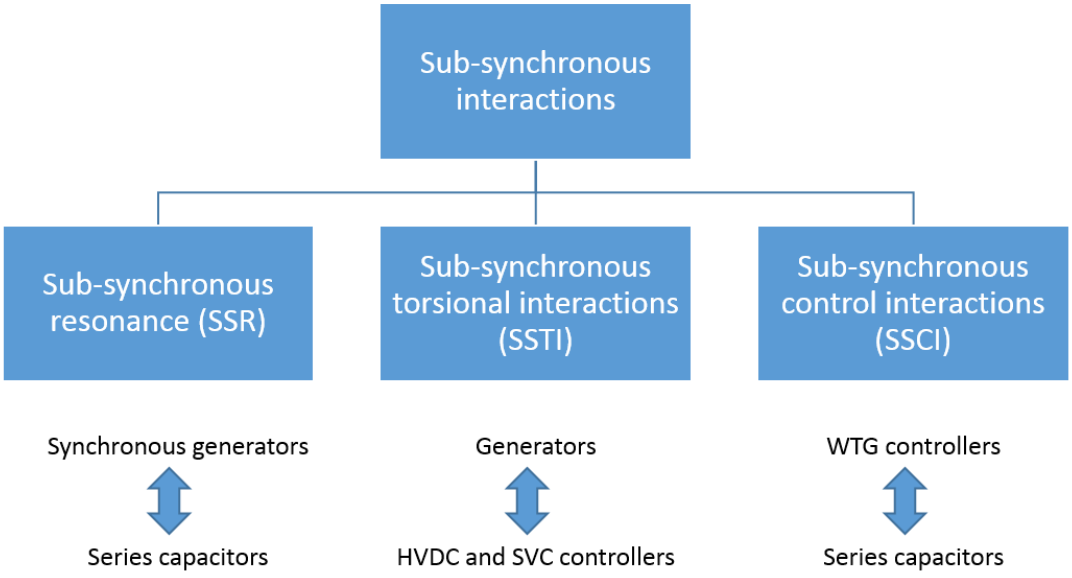

Figure 2-8. Classification of sub-synchronous interaction in power networks [15]

2.4 Grid code requirements for non-synchronous devices

2.4.1 Synthetic inertia

To overcome the problems of reduced system inertia, an idea of emulating the inertial response through control loops has been increasingly popular in recent years, which enables inverter power setpoint adjustment according to the measured value of RoCoF. Detailed examination of the synthetic inertia concept will be presented in Chapter 2 and Chapter 5.

Some guidance as well as regulation documents, including the grid codes, have considered the application of synthetic inertia in non-synchronous devices as one of the possible options to support system operation. For example, EU ENTSO-E requires that the non-synchronous devices 'shall be capable of providing synthetic inertia in response to frequency changes, activated in low and/or high frequency regimes by rapidly adjusting the active power injected to or withdrawn from the AC network in order to limit the RoCoF' [24, 36]. UK system operator National Grid discussed the need for synthetic inertia in [37].

2.4.2 Frequency and voltage control

Non-synchronous devices do not possess the inherent capability of frequency/active power support. With more and more non-synchronous devices to be installed in the power networks, the importance of providing frequency support from such devices has started to be realised. For example, in the GB Grid Code [12], it is required that the generating units, including the non-synchronous devices, be able to continuously adjust their output in relation to frequency across the normal operating range from 49.5 Hz to 50.5 Hz and maintain stable operation over the entire operating range from 47 Hz to 52Hz. It is also required that the non-synchronous devices are capable of performing a frequency droop between 3% and 5% and deliver a minimum frequency response of 10% of its capacity with no delay (or 2s delay maximum). Similarly, EU Network Codes [36] also have requirements regarding frequency droop response from non-synchronous devices for both under- and over-frequency situations.

Similarly, voltage regulation capability is required for non-synchronous devices by the grid codes [12, 24, 36] with reactive slope characteristic adjustable over a defined range, where reactive power control and power factor control modes could also be required.

Such requirements have also been introduced in USA [38, 39], China [40], and Ireland [41].

2.5 Synchronous generator

Synchronous generators have been the main source of the electromechanical power-conversion devices in power systems for more than a hundred years. They are so-called because the frequency of generated voltage is directly linked with the rotational speed of the generator. Synchronous generators can be found in coal, diesel, nuclear and hydro power plants. Machine ratings can be in excess of 1500 MW; however, most generators have ratings of a few hundred MVA.

2.5.1 Principles of operation

The two fundamental parts of a SG are the rotor (field) and the stator (armature). The rotor is equipped with a DC-excited winding. The combination of the excited rotor winding and the rotational motion of the rotor (driven by a prime mover) produces a rotating magnetic field in the air gap between the rotor and stator. As a result, alternating voltage will be induced in the stator windings. Note that a SG and a synchronous motor share the same configuration. The synchronous machines can be configured to operate in either mode by changing conversion direction between mechanical and electrical energy. An illustration of the operation of a SG is shown in Figure 2-9 (a) while the equivalent circuit is presented in Figure 2-9 (b), where E represents the induced voltage at the generator internal terminal, V represents voltage at the grid connection point, and X represents the equivalent reactance of the generator. Note that resistance in the stator winding is neglected in this equivalent circuit as it is typically much smaller than synchronous reactance.

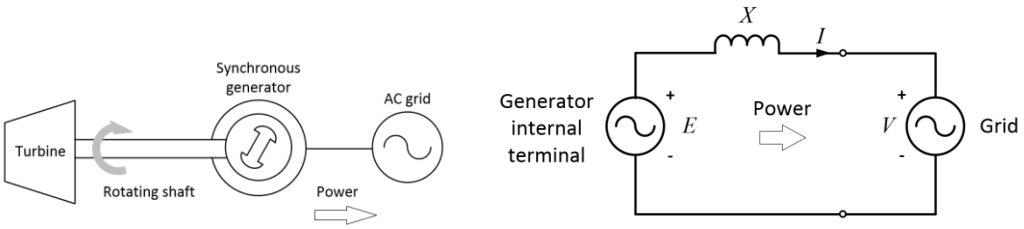

(a) (b)

Figure 2-9. (a) Illustration of operation in a single phase of a SG; and (b) its equivalent circuit when connected to a grid [42]

Active and reactive power transfer between the generator terminal and the grid connection point can be expressed in simplified forms by equation (2-1) and (2-2) respectively, where P is the active power, Q is the reactive power, and δ is the angular difference between the phasors E and V, i.e. the power angle.

$$P = \frac{|E||V|}{X}\sin\delta \tag{2-1}$$

$$Q = \frac{|V||E|\cos\delta - |V|^2}{X} \tag{2-2}$$

2.5.2 Motion mechanics

The rotor motion is determined by the Newton's second law, given by equation (2-3), where J is the total moment of inertia of the rotating masses in kg·m^2, α_m is the rotor angular acceleration in rad/s^2, T_a is the net accelerating torque in N·m, T_m is the mechanical torque in N·m and T_e is the electromagnetic torque in N·m. Additionally, the rotor acceleration is described by equations (2-4) to equation (2-6), where ω_m is the rotor angular velocity in rad/s, θ_m is the rotor angular position with respect to the stationary axis in rad/s, δ_m is the rotor angular position with respect to the synchronously rotating reference axis in rad and ω_{msyn} is the synchronous angular velocity of the rotor in rad/s.

$$T_a(t) = T_m(t) - T_e(t) = J\frac{d\omega_m(t)}{dt} \tag{2-3}$$

$$\alpha_m(t) = \frac{d\omega_m(t)}{dt} = \frac{d^2\theta_m(t)}{dt^2} \tag{2-4}$$

$$\omega_m(t) = \frac{d\theta_m(t)}{dt} \tag{2-5}$$

$$\theta_m(t) = \omega_{msyn}t + \delta_m(t) \tag{2-6}$$

When there is an imbalance between the electrical and mechanical torque, the net torque produces acceleration (or deceleration) which may be calculated using equation (2-3). In steady state, T_m and T_e and the rotor acceleration is zero, resulting in a constant rotor velocity. When the mechanical torque is larger than the electrical torque, the generator rotor will accelerate; conversely, it will decelerate if the electrical torque is larger.

By substituting equations (2-4) and (2-6) into equation (2-3),

$$J\frac{d^2\theta_m(t)}{dt^2} = T_m(t) - T_e(t) = T_a(t) \tag{2-7}$$

It is convenient to express equation (2-3) in terms of power rather than torque and also in p.u. rather than in physical units. In the per-unit form, the swing equation expressed in terms of power is given by equation (2-8). The power imbalance is calculated using equation (2-9). Here, $P_{m,pu}$ is the mechanical power in p.u. and $P_{e,pu}$ in p.u. is the electrical power output of the generator.

$$\frac{\omega_m(t)T_m(t) - \omega_e(t)T_e(t)}{S_{rated}} = \frac{P_m(t) - P_e(t)}{S_{rated}} = P_{m,pu}(t) - P_{e,pu}(t) \tag{2-8}$$

$$\frac{J\omega_m(t)}{S_{rated}}\frac{d^2\delta_m(t)}{dt^2} = P_{m,pu}(t) - P_{e,pu}(t) = P_{a,pu}(t) \tag{2-9}$$

The inertia constant H is defined by equation (2-10) with units in joules/VA, where the numerator part is the stored kinetic energy at the synchronous speed:

$$H = \frac{\frac{1}{2}J\omega_{msyn}^2}{S_{rated}} \tag{2-10}$$

With the p.u. rotor angular velocity ω_{pu} defined in equation (2-11) in rad/s, equation (2-9) can be rewritten as in (2-12), where ω_{sync} is the base angular frequency (set to be the 2π times the steady-state grid frequency), and δ is the power angle (rotor angle in electrical rad).

$$\omega_{pu}(t) = \frac{\omega_m(t)}{\omega_{msyn}} \tag{2-11}$$

$$\frac{2H}{\omega_{msyn}}\omega_{pu}(t)\frac{d^2\delta_m(t)}{dt^2} = \frac{2H}{\omega_{syn}}\omega_{pu}(t)\frac{d^2\delta(t)}{dt^2} = P_{m,pu}(t) - P_{e,pu}(t) = P_{a,pu}(t) \tag{2-12}$$

When taking into consideration the damping torque, whose value is proportional to the speed deviation, equation (2-12) can be expressed by (2-13), where $P_{d,pu}$ is the damping power introduced by the speed deviation in p.u. as expressed in equation (2-14) and D is the damping coefficient.

$$\frac{2H}{\omega_{syn}}\omega_{pu}(t)\frac{d^2\delta(t)}{dt^2} = P_{m,pu}(t) - P_{e,pu}(t) - P_{d,pu}(t) = P_{a,pu}(t) \tag{2-13}$$

$$P_{d,pu}(t) = \frac{D}{\omega_{syn}}\frac{d\delta(t)}{dt} \tag{2-14}$$

2.5.3 Controllers

To make sure the power quality indices are within standard limits, the system frequency and voltage have to be maintained close to their rated operational values. The frequency of a SG is exclusively given by the rotational speed of the generator shaft, which should be controlled within an acceptable operational range independent of torque fluctuations. Variations in the frequency are introduced by power imbalance in the network. Meanwhile, the excitation system must be able to automatically adjust the field current to maintain the required terminal voltage. An illustration of the main controllers of a SG is shown in Figure 2-10.

Kinetic energy stored in the rotational masses of a turbine-generator will be released naturally during a power-imbalance event, such as sudden an increase of load or a loss of generation. Rotor speed (or generator frequency) is a key indicator of network power balance (or imbalance). Hence, it may be used as a control signal for governing the mechanical output power of the turbine, as shown in Figure 2-10.

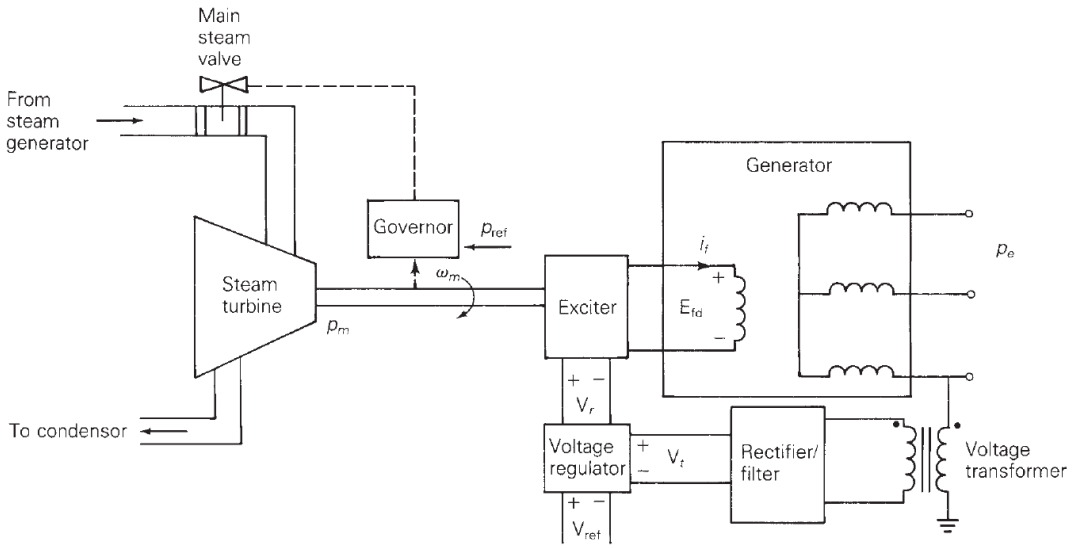

Figure 2-10. Main controllers of a SG including turbine-governor and voltage controller [43]

The main objective of the turbine-governor control is to ensure that the rotor speed is as close to its nominal value as possible. The frequency-active power relationship for turbine-governor control is shown in (2-15), where ΔP_m is the change in turbine mechanical power output, ΔP_{ref} is the change in the power reference value, D_f is the frequency droop slope and Δf is the change in frequency due to a system disturbance.

$$\Delta P_m = \Delta P_{ref} - \frac{1}{D_f}\Delta f \tag{2-15}$$

To maintain the generator terminal voltage V_t, an automatic voltage regulator (AVR) is required to adjust the output of the generator exciter. As seen in Figure 2-10, when the reference voltage V_{ref} decreases (or increases), the exciter voltage applied to the generator field winding is decreased (or increased) by the output voltage V_r, which then causes the V_t to decrease (or increase).

In addition to turbine-governor and AVR controllers, a power system stabiliser (PSS) is often implemented in the exciter of a SG. The role of the PSS is to damp the small magnitude and low frequency generator rotor angle oscillations introduced by the voltage regulator actions, which are in a broad range of frequencies in the power system rather than a single frequency, e.g. 0.1 to 2.5 Hz approximately, by controlling its excitation using auxiliary stabilising signal(s). This is to reduce any potential detrimental impact on the system steady-state stability and power transfer capability [44]. To provide damping, the

stabiliser must produce a component of electrical torque in phase with the rotor speed deviations, such as shown in Figure 2-11 [23].

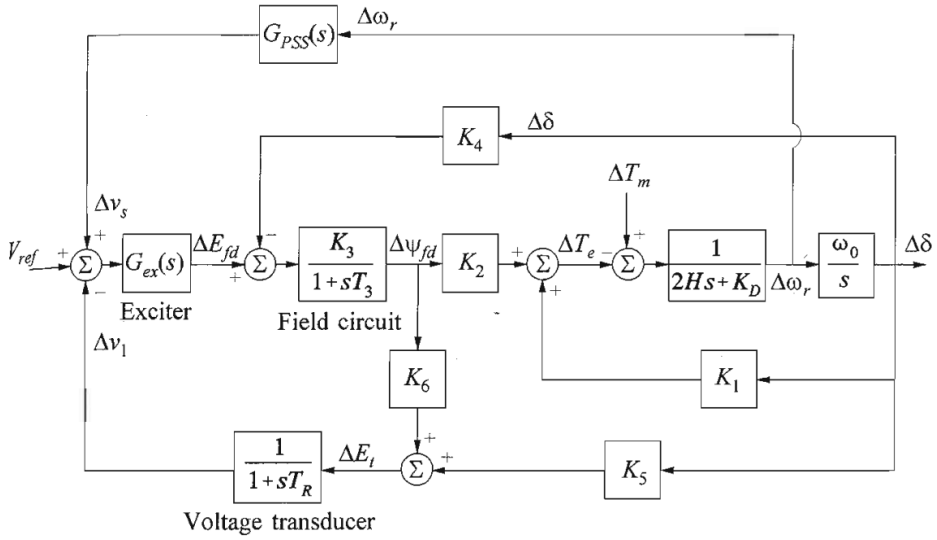

Figure 2-11. Example block diagram representation with AVR and PSS [23]

2.6 Power system stability

Power system stability has always been a major concern for secure system operation. As defined in [45], "*power system stability is the ability of an electric power system, for a given initial operating condition, to regain a state of operating equilibrium after being subjected to a physical disturbance, with most system variables bounded so that practically the entire system remains intact.*" Figure 2-12 gives an overall classification of the power system stability problems.

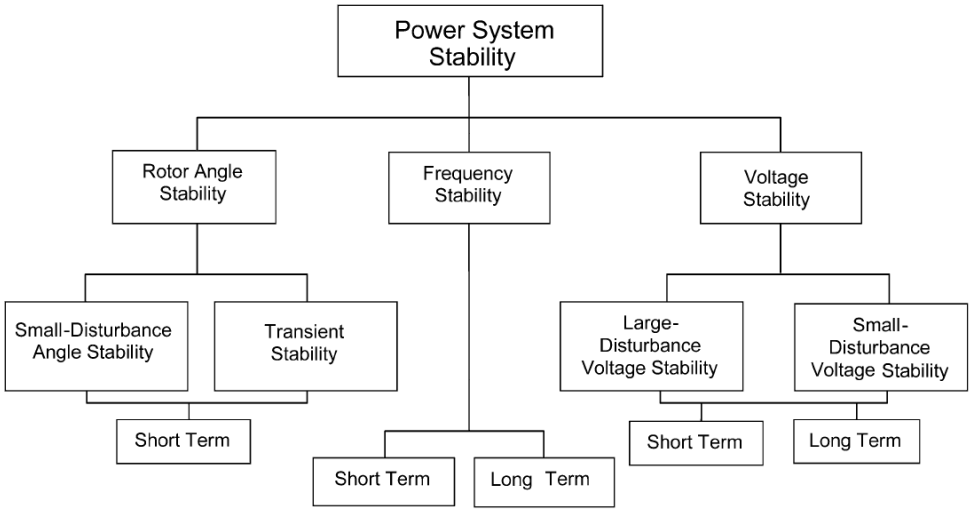

Figure 2-12. Classification of power system stability [45]

In conventional power networks dominated by synchronous machines, the main stability issue is to maintain synchronous operation after being subjected to a disturbance. Under steady-state conditions, there is an equilibrium between the mechanical torque and the electromagnetic torque of each generator, and their speed is kept constant. When the system is disturbed, the equilibrium will be disrupted and machine rotors will accelerate or decelerate accordingly based on the laws of motion. The resulting angle difference normally could be reduced by reducing the speed difference based on the power-angle relationship and the Equal Area Criterion, and hence, a new equilibrium will be achieved. However, when the angle separation is beyond a certain limit, there is insufficient restoring torque to react to the rotor speed differences, rotor angle instability will occur. When a synchronous machine losses synchronism with the rest of the system, large fluctuations will occur at the problematic machine(s) in the power output, current, and voltage, which will then cause protection system operate and trip the unstable machine. This stability issue is categorised as *rotor angle stability* which is defined as "*the ability of synchronous machines of an interconnected power system to remain in synchronism after being subjected to a disturbance*" [23].

Voltage stability refers to "*the ability of a power system to maintain steady voltages at all buses in the system after being subjected to a disturbance from a given initial operating condition*" where main factor causing the instability is the inability of the power system to meet the demand for reactive power [23]. "Voltage collapse" could occur following after a sequence of events accompanying voltage instability that leads to blackout or abnormally low voltages in a significant part of the power system [23, 46]. With increasing number of converters being introduced into the power systems, such as HVDC links and back-to-back applications [25, 47], they are usually associated with stability issues of the controller when connected to weak AC systems, as well as the unfavourable reactive power "load" characteristics [45].

For both rotor angle stability and voltage stability issues, there are subcategories based on the severity of the disturbance, i.e. small disturbance (or small signal) stability and large disturbance (transient) stability.

- Small disturbance/small signal stability is concerned with small disturbances in the system, such as continuous small variations in loads and generation, which are considered sufficiently small for linearisation of system equations to be

permissible for purposes of analysis. The time frame of interest is usually 10 to 20 seconds following the disturbance [45].

Analysis of small signal stability is usually established based on the linearised model (normally based on *dq* frame) of the network, including devices and its control systems, at a certain operating point and the stability is assessed based on eigenvalue analysis. The main challenge of the small signal stability analysis is to connect stability of a non-linear system to the properties of a linearised model at a certain operating point. For example, when analysing small signal stability of a network which contains a converter-interfaced generation/link connected with the grid via transformers and lines, efforts are required to connect the non-linear "converter frame" (shaped by the PLL) and "grid frame" to form the full stability analysis as they are based on different *dq* frames. This could become even more challenging due to difficulties on interpretation of its linearised model due to the non-linear blocks when ratings of the synchronous units is relatively low and/or system inertia is low.

- Large disturbance/transient stability is concerned with severe disturbances such as system faults, sudden loss of generation/load, etc. which is also relevant to the pre-disturbance operating state of the system. The time frame of interest in transient stability studies is usually 3-5 seconds following the disturbance which could be extended for very large disturbances.

Another type of the stability issues is the *frequency stability* which refers to "*the ability of a power system to maintain steady frequency following a severe system upset resulting in a significant imbalance between generation and load*" [45]. Frequency instability may result in sustained frequency swings which could then lead to cascaded tripping of generation units and/or loads.

In this thesis, time-domain stability analysis methods for systems that contains large amount of converters will be introduced and used to explore system stability thresholds, which could be beneficial to small signal stability analysis due to the difficulties to obtain the linearised weak AC system model with the existence of PLL. Both small signal stability and transient stability will be investigated.

2.7 Power converters

Power electronic converters have been used extensively in domestic, industrial and information technology applications. Figure 2-13 illustrates how the modern power networks work including electricity generation, transmission and distribution. With the exception of distributed generation, electricity is transferred over long distances through dedicated transmission lines, AC and/or DC, before being dispatched to users in the distributed network. To reduce transmission losses, the transmission lines operate at a high voltage. The distribution system will operate at a significantly lower voltage for safety and other practical reasons. To enable this mode of operation, power transformers are used to connect high voltage transmission lines to medium and low voltage distribution systems.

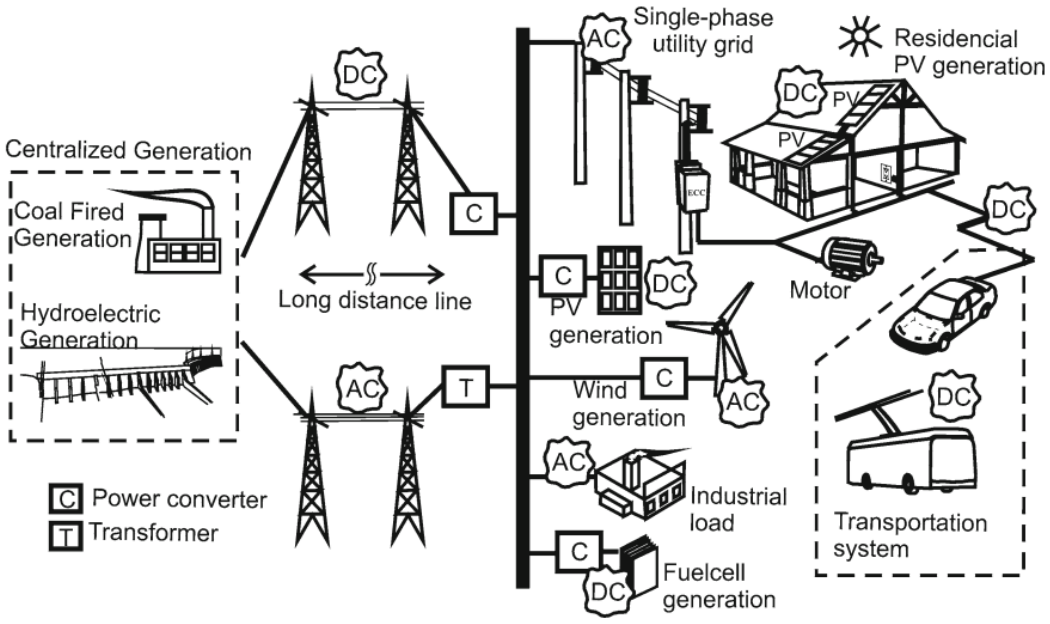

Figure 2-13. Illustrated structure of modern power networks and applications of power electronics [48]

Rapid development of power electronic converters has led to the steady increase of their usage in power systems over the past decades. The following examples are applications of converters:

- power filtering to enhance power quality [49],

- reactive power compensation to increase the power-transfer capability of the transmission lines,
- power conditioning to enable power exchange between two electrical networks in a controlled manner, such as back-to-back HVDC system which interfaces two AC subsystems at the same or different frequencies [50],
- AC/DC/AC conversion for wind generators to transfer power through a DC tie line between two electrically remote AC subsystems,
- DC/AC conversion (for PV solar array, a fuel cell, or a battery storage) to transfer power from a DC RES unit to the grid [51, 52],

The ability to connect two or more unsynchronised systems is a major benefit of using converters. This makes it possible for a wind turbine to operate at variable-speed, which is beneficial for both maximum energy capture and reduction of mechanical loading. Converters also make it possible to connect energy storage devices such as batteries.

Converters are referred to as either rectifiers, if the conversion is from AC to DC; or inverters if the conversion is from DC to AC. In this thesis, the main focus is on the stability of inverters under high penetration of converters in a power network.

2.7.1 HVDC transmission systems

Electric power transmission systems have been dominated by HVAC for more than a century. Debates on AC versus DC began in the 19th century, when the first DC power system was established by Thomas Edison and the first AC power system was founded by George Westinghouse and Nikola Tesla [43]. In recent years, HVDC transmission system has become increasingly more attractive to power system operators and companies compared to HVAC transmission for the following reasons [53-57]:

- Capability to transmit bulk power over long distances via overhead lines (or undersea cables) with significantly reduced power losses compared to AC.
- Capability to connect AC power networks with different operating frequencies, i.e. asynchronous connection between AC networks.
- Active power flow can be monitored and controlled accurately and quickly through VSC controllers.

- Capability to mitigate or prevent blackouts since correctly-controlled HVDC links cannot be overloaded and power flow can be fully controlled.
- Capability to segment different AC networks to prevent fault propagation from one system to another.
- Capability to provide "black-start" support to one AC system from another(s) (if the appropriate converter technology is employed).
- Capability to improve stability of interconnected systems as each system maintains its autonomy.
- Capability to reduce construction costs and complexity since HVDC system requires two conductors while HVAC system generally requires three conductors or more (although power transfer capability must also be taken into account).
- Capability, in some cases, to operate in a reduced power transfer mode following the loss of one conductor.

2.7.2 LCC-HVDC

Conventional HVDC systems are based on LCC (also known as current source converter) with thyristors as the main switching devices, an example of which is "HVDC Classic" by ABB [58]. The first commercial HVDC link in the world was constructed by ABB in 1954, which carried 20 MW of power at 100 kV level between the mainland of Sweden and the island of Gotland [59]. Presently, LCC-HVDC links can typically have rated power capacities as high as 1,000~5,000 MW [58]. LCC-HVDC transmission systems have been mainly used to transmit bulk power from large, concentrated but remote energy sources, e.g. large-scale hydropower plants [60], and over very large distances in countries such as Russia and China [61]. They are also used for short connections to interconnect independent AC systems, such as the connection between England and France [62].

The HVDC link is connected between the rectifier and the inverter stations to facilitate power transmission, normally in one pre-determined direction that is not easily changed. LCC-HVDC transmission systems utilise thyristor valves to enable the conversion between AC and DC. Based on the operating principles of thyristor, the thyristor valves can be switched to conduct current when the polarity of the voltages from AC system achieves the conditions required to trigger the thyristor. For LCC, the

thyristors are turned on by a gate signal, while they are turned off at the zero crossing of the AC current which is determined by the AC network voltage; this process is known as line commutation [63]. For normal operation of LCC-HVDC systems, the AC network has to be strong enough to facilitate completion of the commutation process and to avoid voltage instability. Strength of an AC network is measured by short-circuit ratio of the AC network to the rated power of the converter. The stronger the AC network, the higher the short-circuit ratio will be.

According to [63], HVDC converters need a certain minimum recovery time to allow the stored charge during forward conduction state of the thyristor devices be removed before re-establishing a forward voltage blocking capability at turn-off state. When there is no sufficient time for this recovery process, the converters may experience commutation failures. If the connected AC system is not strong enough and/or the AC network in the vicinity of the LCC-HVDC link is experiencing network transients (in particular, a short circuit fault which may cause an AC system voltage depression), commutation failures of the converters may occur.

Commutation failures can cause DC short circuits and a breakdown in the ability to transmit active power. This is the main drawback of LCC-HVDC transmission systems. Other disadvantages of LCC-HVDC transmission systems include: AC voltage stability issues when connected to relatively weak AC networks, requirement for large AC side filters, limited operating range due to maximum commutation delay, and inability to control the direction of power flow [54, 64, 65]. With the requirement to improve the performance and flexibility of HVDC transmission systems, VSC based HVDC technology has been developed. This is believed to be the main technology that will underpin the vast majority of HVDC systems in the future and will form the main focus of investigation in this thesis.

2.7.3 VSC-HVDC

VSC-HVDC systems are markedly different from conventional LCC-HVDC transmission systems: they are based on high-frequency pulse width modulation (PWM) techniques and the use of self-commutating insulated-gate bipolar transistors (IGBTs) (i.e. they can complete switching functions independently of the current flowing through them). An example of a VSC-HVDC system is the "HVDC Light ™" by ABB [66]. VSC-

HVDC systems are the preferred technology for connection of remote sources of generation, e.g. offshore wind farms, onshore wind farms, oil and gas offshore platforms, solar PV, etc., to AC grids. Furthermore, embedded VSC-HVDC links has been utilised to improve performance of existing HVAC grids [67].

Even though the VSC-HVDC technology is less mature compared to the LCC-HVDC systems, it is developing rapidly. The first VSC-HVDC project was commissioned in 1997 by ABB and was used to interface an HVDC connection between Hällsjön and Grängesberg in Sweden with a length of 10 km, rated at 3 MW, 10 kV [68]. According to [68], the highest capacity VSC-HVDC links that have been installed to date are the 1000 MW, including the two 320 kV links INELFE between France and Spain built by Siemens in 2015, a 320 kV link in Xiamen, Fujian in China built by C-EPRI in 2015, and a 350 kV link in Luxi, Yunnan in China built by China Southern Grid in 2016.

A more detailed description of the operating principles of VSC-HVDC and its control system will be presented in the next section.

2.7.4 Comparisons between LCC-HVDC and VSC- HVDC systems

Based on the findings of a literature review ([65, 69-75]) focused on the characteristics of both LCC-HVDC and VSC-HVDC transmission systems, a qualitative comparison outlining the key differences and merits of these technologies has been performed, as shown in Table 2-1.

For an LCC, the commutation process is controlled by the external circuit, i.e. the electrical AC system to which it is connected, where the turning-on and turning-off of the converter valves, is initiated by the reversal of the AC voltage polarity. Therefore, the LCC-HVDC will need additional equipment, such as synchronous compensators to provide AC commutation voltages for blackstart [74]. Conversely, the VSC is a self-commutated device whose commutation process is independent of the external AC voltage. That is, it creates its own AC voltages in case of blackstart. Furthermore, the LCC-HVDC can experience commutation failure as a result of a sudden drop in the amplitude or phase shift in the AC voltage, which results in temporary DC overcurrent. This does not occur in VSC-HVDC as it is immune to any voltage dips or transient AC disturbance due to the self-commutation [14, 55].

As the duration of the commutations in LCC depends on the voltage source level and the commutation reactance, i.e. mainly dominated by the converter transformer leakage reactance), even when the firing angle is 0º, LCC consumes reactive power, which can be as much as 50-60% of the active power of the converter [63, 74]. VSC is capable of generating voltage waveforms at any phase angle relative to the system that is being supplied, either leading or lagging, and therefore the real power and reactive power can be controlled independently. Therefore, reactive compensation is normally required for LCC-HVDC due to its inductive nature, while it is much less required for VSC-HVDC.

When the HVDC links are used as interconnectors between two subsystems or implemented in multi-terminal DC (MTDC) configuration, sometimes it is required to reverse the power flow direction on the link. This can easily be done on VSC-HVDC as the current direction can be changed which simultaneously changes the power flow direction and there is no need to invert DC voltage polarity. While for LCC-HVDC, the direction of power flow is determined by the polarity of DC voltage, i.e. the entire HVDC system must be taken offline for a short period of time to complete one-time power direction change of DC power flow [70]. Moreover, the amount of reactive power required in LCC varies with the active power conversion. This means that the converter filters and amount of reactive power compensation need to be continually adjusted when the load condition varies, while VSC can provide any amount of reactive power independently of the active power transfer [74].

Compared to transistors, thyristors have relatively slow switching processes. Consequently, the switching frequency of LCC-HVDC is normally less than 1 kHz, whereas VSC-HVDC systems can have switching frequencies as high as 20 kHz. This way VSC-HVDC systems can produce cleaner waveforms. However, higher switching frequencies are also associated with higher losses. Hence, a trade-off must be made between waveform quality and losses when designing an HVDC system.

An additional consideration to be taken into account when designing an HVDC system is the transformer linking the HVDC system to the AC grid. For LCC-HVDC, special converter transformers are required to be designed to withstand a harsher electrical operating environment, such as exposure to high levels of harmonics contained in the generated voltage waveforms [70, 71]. As the VSC-HVDC systems produce cleaned voltage waveforms they can connect to the grid via a conventional transformer.

Table 2-1. Comparisons between LCC-HVDC and VSC-HVDC technologies [65, 69-75]

Attributes	LCC-HVDC	VSC-HVDC
Maturity of technology	Mature	Developing
Adopted valve	Thyristor	Transistor (IGBT)
Operation	Line-commutated	Self-commutated
Commutation failure	Can occur	Does not occur
Requirements on AC system for satisfying performance	Strong AC grid	No
Power control	Active power control	Active power and reactive power independently
Reactive power exchange with AC system	~50% of active power transferred	No
Reactive compensation	Required	Much less required
Power flow reversal	Not achievable	Achievable
Black start capability	Require additional equipment	Yes
Harmonic filter	Large AC and DC filter devices required for removal of distortion and harmonics	Small or no filters required due to insignificant level of harmonics
Output voltage	Contains significant lower-order harmonics (if no filters applied)	Near-perfect sinusoidal voltage waveforms
Switching frequency	≤ 1kHz	Few kHz to 20 kHz
Converter loss	0.7% to 0.8% of transmitted power	1% of transmitted power (as a result of the PWM which is switched on and off many times in a cycles)
Converter transformers	Special design required	Conventional transformers can be used
Multiterminal configuration	Complex, limited to 3 terminals	Simple, no limitations
Mostly used for	Transmitting bulk power for a long distance	Transmitting power from remote area with renewable energy
Converter station footprint (relative size)	Large due to volume of harmonic filters, 200m x 120m x 22m (100%)	More compact, 120m x 60m x 22m (~40%)

As the process of changing direction of current is not dependent on the direction of DC voltage, it is relatively more viable to build VSC-HVDC with more than a few terminals, i.e. VSC-MTDC system. They could be either radial, meshed, or a combination of both [54]. For LCC-HVDC it is much more challenging to form multi-terminal direct current (MTDC) network due to its operation principles and it is practically limited to a maximum of three terminals [69].

Bearing in mind the aforementioned points, the footprint of the LCC converter station is normally larger than that of VSC converter station [71].

Besides the high switching losses disadvantage of VSC-HVDC, its switching devices can be fatally damaged under overcurrent situations such as DC fault. As the continuous conduction in the diode will cause a rapid increase in DC fault current (even when the IGBTs are blocked) the fault can only be cleared by the dedicated DC breakers at both ends of the link which significantly increases the delay in restoring normal system operation [69]. LCC-HVDC outperforms VSC-HVDC under these circumstances due to the combination of smoothing reactors (that are used to limit the current peak) and fast converter control which drives the DC current to zero. The process of restarting the LCC can be achieved within 100 to 300 ms [74].

In summary, as VSC-HVDC overcomes most of the drawbacks of LCC-HVDC technology, it is almost certain that it will be developed further and utilised in a wider range of power applications. Therefore, the VSC-HVDC technology is also the main focus for detailed modelling and analysis presented later in Chapters 3 and Chapter 4 of this thesis.

2.8 Operation principles of VSC-HVDC and its control system

2.8.1 Models of VSC

Generally, the most common VSC models are the detailed switching model and the average-value model. The detailed representation of VSC includes the modelling of IGBT valves which allows accurate replication of the switching procedure. This approach is suitable for electromagnetic studies where the converter switching process is of great importance. A detailed operation principles of VSC will be introduced in Appendix C.

However, it requires small sampling time step to ensure an accurate representation of the fast switching actions; naturally this introduces a large computational burden, which would be considered unacceptable for carrying out studies of large power networks. The attenuation of high frequency content by the phase reactor (and possibly a capacitor bank) means that any high frequency content generated specifically by the switching process can be ignored [76]. Therefore, for the studies in this thesis, the average-value model is used which represents the average response of the switching devices, controls and converters by applying controllable voltage and current sources and switching functions, while neglecting the effects of high order harmonics introduced by the switching process, as shown in Figure 2-14.

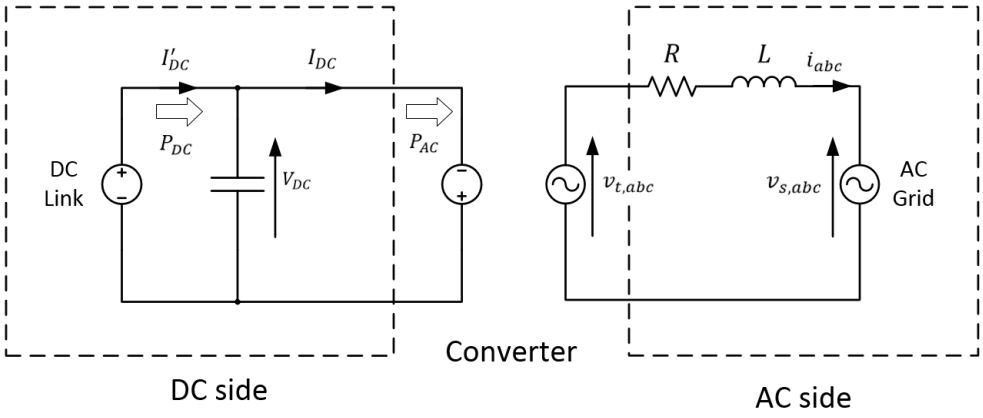

Figure 2-14. Average-value model (AVM) of VSC in single line diagram

Note that as the power flow direction of VSC-HVDC transmission system is bi-directional, each converter can be controlled as either rectifier or inverter. The rectifier and inverter VSC operation modes are quite similar except that their power reference values have the opposite polarities due to different power flow direction. In this section, operation of VSC in the inverter mode, when it is interfaced with an AC grid, is illustrated.

Control of the DC voltage of the VSC is derived from the power conservation principle, i.e. power flowing on the DC side should be equal to power flowing on the AC side plus the converter losses. Considering ideal conversion, the formula (2-16) links powers on AC and DC side, where $v_{t,abc}$ is the voltage generated at the converter terminal, $i_{t,abc}$ the current flowing at the AC side of the converter (into the AC grid), V_{DC} is the DC voltage across the capacitor on the DC-side of the converter, I_{DC} is the DC current flowing from the DC side to AC side of the converter.

$$v_{t,a}i_a + v_{t,b}i_b + v_{t,c}i_c = V_{DC}I_{DC} \tag{2-16}$$

The relationship between the ac-side voltages and DC link voltage is shown in equation (2-17), where m_{abc} is the modulation index of the PWM which is the amplitude of the modulating signal divided by the amplitude of the carrier signal.

$$v_{t,abc} = \frac{V_{DC}}{2} m_{abc} \tag{2-17}$$

2.8.2 Configuration of a VSC-HVDC

Figure 2-15. Historically, the preferred control algorithm has been based on vector current control, denoted by DQCI in this thesis. The topology of said control system is illustrated in Figure 2-16. Note that power flow of the VSC-HVDC link can be controlled to be in either direction between the two AC systems.

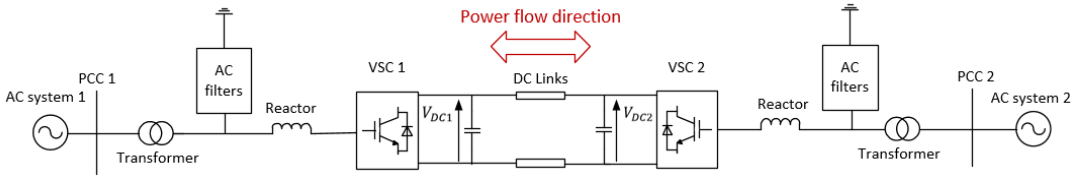

Figure 2-15. Generic configuration of a symmetrical mono-polar VSC-HVDC link

A generic configuration of a two-level VSC-HVDC transmission system is shown in

Typically, there are transformers, phase reactors and AC filters connected between the converter and the AC grid to provide satisfactory performance and to meet the transmission specifications.

- Phase reactors are applied to enable the control of both active and reactive power by regulating the current flowing through them. In addition, since the phase reactor is an inductive element, it also acts as a filter to reduce high-frequency harmonic components introduced by the switching process of the converter.
- Normally, transformers are required to ensure that the voltages of the VSC output and the AC system have the correct magnitudes. The transformer, being an inductive element also, acts as a filter similar to the phase reactor.

- For two-level HVDC systems, the harmonic content is significant even with the filtering capabilities of the phase reactor and transformer. Consequently, a shunt AC filter (featuring a capacitor) is often implemented.

Capacitors on the DC bus provide a means of energy storage since there is never a perfect instantaneous balance between the energy being extracted from the DC bus and that being injected into it. The DC capacitor also provides a low inductive path for the turned-off current, i.e. current flowing in the switch valves that have been turned off. Furthermore, the capacitor also reduces the voltage ripple on the DC side of the HVDC link.

2.8.3 DQCI control

As an established control algorithm, vector current control is well-documented [54, 72, 76]. In this thesis it is termed as DQCI control. Referring to Figure 2-16, it can be noted that the vector current control utilises a *dq* frame. The *dq* frame typically employs a Park and Clarke transform which will be introduced in Appendix B.

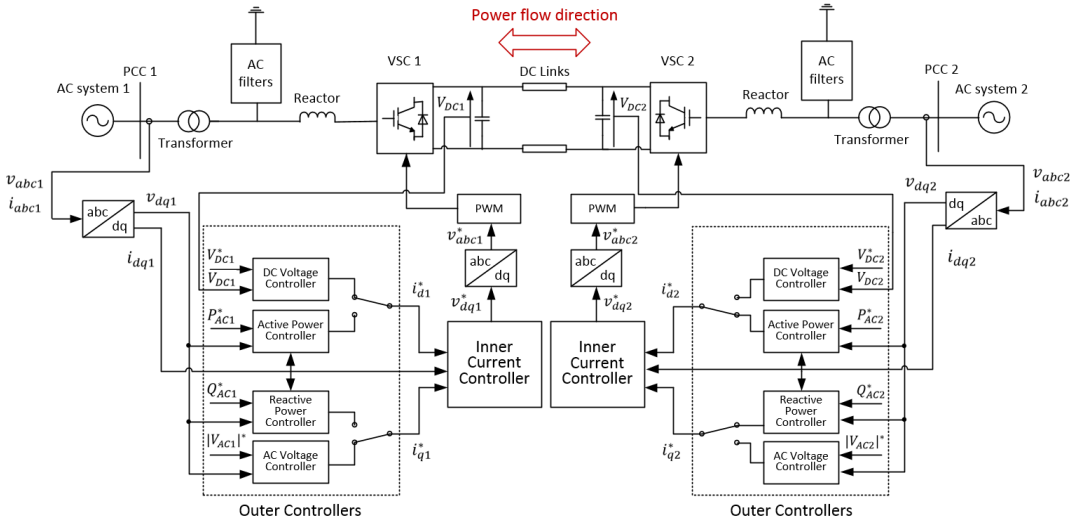

Figure 2-16. VSC-HVDC configuration with its vector current control system, i.e. DQCI control (* represents reference value)

The active power *P*, and reactive power *Q*, flowing through a point of interest as expressed in a *dq*-frame are given by equations (2-18) and (2-19), where v_d and v_q are the *dq* components of voltage measured at the point of interest and i_d and i_q are the associated currents in *dq* reference frame.

$$P = \frac{3}{2}(v_d i_d + v_q i_q) \tag{2-18}$$

$$Q = \frac{3}{2}(-v_d i_q + v_q i_d) \tag{2-19}$$

Active and reactive power through the effective impedance between the converter and the grid can be fully controlled by modulating the converter terminal voltage, as shown in equations (2-20) and (2-21).

$$P = \frac{v_t v_s \sin\delta}{\omega L} \tag{2-20}$$

$$Q = \frac{v_s(v_s - v_t)\cos\delta}{\omega L} \tag{2-21}$$

2.8.3.1 Phase-locked loop (PLL)

Essentially, the PLL acts as a closed control loop, i.e. the synchronisation loop, which drives the *q* part (v_q) of the measured PCC voltage in the converter *dq* frame to zero, and the phase signal it measures is also used to control the power flow from the converters. The basic topology of a SRF-PLL is shown in Figure 2-17 [77, 78].

Normally, a proportional and integral (PI) control is required to act as the loop filter and estimate the phase to be used in the Park transform, such that the *dq* components are controlled to become constant in steady state. The three-phase voltage v_{abc} measured at the converter PCC is transformed to *dq* variables v_{dq}. The *q*-axis component v_q is sent to the PI controller as the phase error signal and then is added on the grid nominal frequency ω_0 to form the measured PLL frequency ω_{PLL}. The output phase angle measured by the PLL θ_{PLL} is finally calculated by integration of PLL frequency. Therefore, the voltage controlled oscillator (VCO) generates a sinusoidal signal whose phase angle is proportional to the integral of the measured ω_{PLL}.

Conventionally, the objective of the SRF-PLL is to achieve a *dq* frame in which the voltage at the PCC is aligned with the *d*-axis in order to synchronise the VSC to the AC grid. Consequently, in ideal conditions, the *q* component of the voltage v_q the PCC as expressed in the PLL *dq*-frame is zero. Hence, if the PLL performs satisfactorily, it follows

that the DQCI control should make it possible to control active power and reactive power independently as v_q is zero in equations (2-18) and (2-19). This is one of the main advantages of the DQCI control.

However, conventional DQCI control based on PLL to synchronise with the AC grid operates under the assumption that the grid is stiff, i.e. has a relatively low impedance, and the v_q is controlled to zero. However, when the converters are connected to a weak AC grid, the voltage waveform measured at the converter PCC could be more variable when disturbed, which introduces a weakened phase reference generated by the PLL, i.e. worsened tracking of the transmission network, and could lead to instability of the converter. This issue has been widely discussed such as in [25, 31]. In [32], it shows that the capability of PLL based converters to remain stable operation and fault-ride-through is compromised with reduced system short circuit levels. This is potentially the major barrier to achieving very high penetration of converters in power networks and has drawn a lot of attention from researchers and manufacturers in this field.

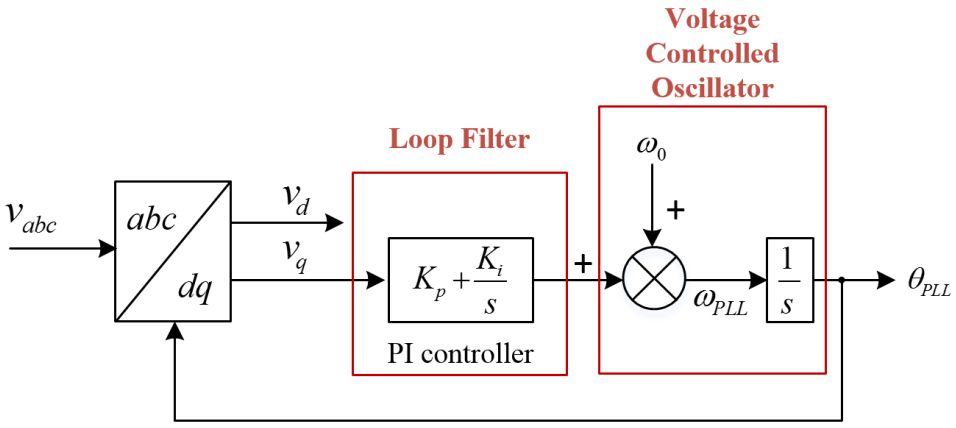

Figure 2-17. Schematic of a SRF PLL

2.8.3.2 Inner current control

The objective of the inner current control loop is to track the current reference vectors with a feed-forward control scheme and then provide updated voltage reference vectors to be used by the PWM to generate proper output voltage waveforms, where a fast independent control of the currents under system disturbances can be achieved, through voltage orientation from *abc* reference frame to *dq* reference frame.

The voltage at the converter terminal may be related to the current flowing through the converter and the voltage at the point of common coupling by the following expression:

$$v_{s,abc} = Ri_{abc} + L\frac{d}{dt}i_{abc} + v_{t,abc} \tag{2-22}$$

By applying the Clark and Park transformations, the three-phase variables can be transformed into the rotational *dq*-frame, where ω refers to the angular speed of frequency in the AC grid,

$$v_{t,d} = v_{s,d} + Ri_d + L\frac{di_d}{dt} - j\omega i_q \tag{2-23}$$

$$v_{t,q} = v_{s,q} + Ri_q + L\frac{di_q}{dt} + j\omega i_d \tag{2-24}$$

It can be seen that both expressions contain a mixture of *d* and *q* current terms. This is an artefact of operating in the *dq* frame (derivative terms expressed in the *dq* frame produce cross-coupling). For this reason, the feed-forward terms previously mentioned are introduced. These compensate for the cross coupling terms. Under the assumption of well-established *dq*-frame (with v_q aligned to zero), the active power and reactive power outputs can be controlled independently by varying the reference current values i_{dqref} by employing outer controllers as will be introduced in the next section.

To represent procedure of the inner current control loop, equations (2-23) and (2-24) can be rewritten as follows:

$$v_d^* = v_{s,d} - \omega L i_q + k_p(i_d^* - i_d) + \frac{k_i}{s}(i_d^* - i_d) \tag{2-25}$$

$$v_q^* = v_{s,q} + \omega L i_d + k_p(i_q^* - i_q) + \frac{k_i}{s}(i_q^* - i_q) \tag{2-26}$$

Accordingly, the structure of the inner current controller is shown in Figure 2-18. The proportional and integral gains for the inner current controller need to be selected based on specific converter and system parameters, such as the converter switching frequency, DC and AC voltage levels, phase reactor impedance, AC filter design, etc.

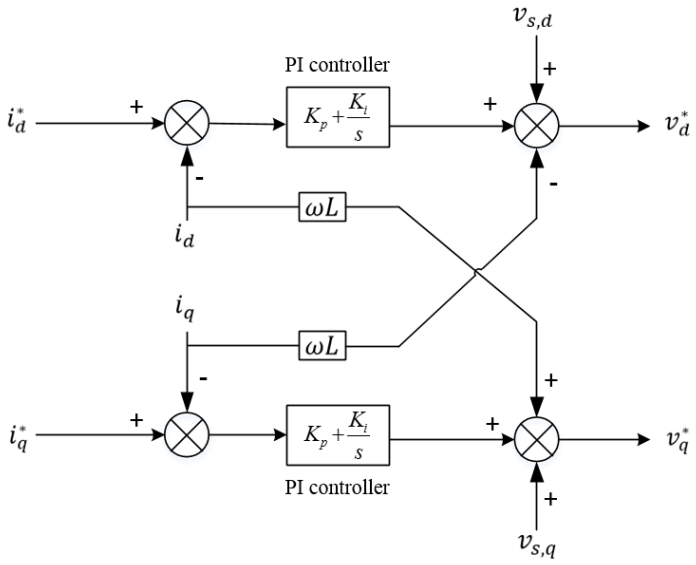

Figure 2-18. Illustration of the inner current controller in the DQCI control algorithm

2.8.3.3 Outer controllers

The outer controllers for VSC-HVDC system generate reference current values for the inner controllers. i_{dref} is set by either an active power controller or a DC bus voltage controller; i_{qref} is set by either a reactive power controller or an AC voltage controller. The modes can be selected according to specific system operation requirements. For a HVDC system, one of the converters must employ a DC voltage controller to make sure the active power flow in the system is balanced. The control laws of the aforementioned controllers are given in Table 2-2.

Table 2-2. Equations for the outer controller modes

Reference variable	Type of controller	Equation based on the circuit	Equation with PI controller
i_d^*	Active power	$i_d^* = \frac{2P^*}{3v_d}$	$i_d^* = \frac{2P^*}{3v_d} + (Kp + \frac{K_I}{s})(P^* - P)$
	DC voltage	$i_d^* = \frac{2V_{DC}^*}{3v_d}(C\frac{dV_{DC}}{dt} + I_{DC}^{'})$	$i_d^* = (Kp + \frac{K_I}{s})(V_{DC}^* - V_{DC})$
i_q^*	Reactive power	$i_q^* = \frac{2Q^*}{3v_d}$	$i_q^* = \frac{2Q^*}{3v_d} + (Kp + \frac{K_I}{s})(Q^* - Q)$
	AC voltage	$i_d^* = \frac{2v_{abc}^*}{3v_d}(C\frac{dv_{abc}}{dt} + I_{DC}^{'})$	$i_q^* = (Kp + \frac{K_I}{s})(\lvert V_{AC}^* \rvert - \lvert v_{AC} \rvert)$

2.8.4 Active and reactive power capability

While active power and reactive power in a VSC-HVDC transmission system can be controlled independently, there are few factors that will affect its power transfer capability, such as discussed in [79, 80].

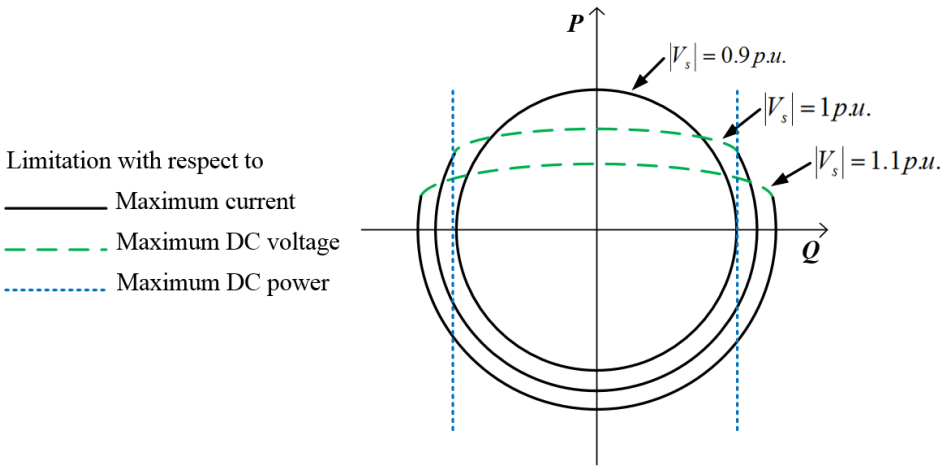

Figure 2-19. Active and reactive power capability for VSC-HVDC transmission system

IGBTs have a limitation on the maximum current flowing through the transistor in case of damage to the device. This establishes the maximum MVA circle in the PQ plane, as shown in Figure 2-19, which is the result of multiplying the maximum allowed current through the device by the measured voltage at the AC-side PCC of the link. Due to this limitation, the MVA capability will be reduced proportionally when the AC grid voltage drops, as seen in the dashed lines in Figure 2-19.

The second limitation is the maximum DC voltage level. As explained in section 2.7.2, the maximum voltage the VSCs can generate at the AC side is dependent on the voltage at the DC side, and the amplitude difference between the converter terminal voltage and grid voltage will then decide the reactive power flow along the system, referring to equation (2-21). Therefore, when the AC grid voltage is higher, the voltage magnitude difference will be higher, which enables increased reactive power capability; and vice versa.

The third limitation is the maximum DC current/power flowing through the transmission link which will affect the active power transfer capability directly.

As explained before, the VSCs can alter their operating points almost instantaneously within the power capability range, such as rapid active power flow direction reversal by changing the DC current direction without changing the DC voltage polarity.

2.9 Alternative converter control techniques to assist system stability under high penetration of converters

In this section, converter control techniques that have the potential of resolving system stability issues under high penetration of converters will be reviewed and discussed. In section 2.8, the principles of operation of the DQCI controller are based on the assumption of a perfect PLL; that is, one which perfectly tracks the grid voltage at the point of common coupling. The departure from perfect phase tracking, as would occur with any real PLL (particularly in weak systems) leads to a cross-coupling phenomenon in the inner current control loop which could lead to converter and system instability issues. Therefore in this chapter, the various control techniques are categorised based on whether DQCI control and PLL are used or not. VSM concepts, also termed as grid-forming converters, which have been the most popular topic in this field, mimic the behaviour and characteristics of a real synchronous machine based on the converter interface. Two representative models of VSM are covered in detail in this thesis: VSM0H and VSM-type converter. Both are considered helpful for system stability studies and promising to assist the high penetration of converters.

2.9.1 Stability enhancing solutions based on DQCI control

This section discusses the control strategies which may supplement the baseline DQCI controller (defined as the combination of an SRF-PLL, inner current controllers and the power/reactive power controllers). These solutions are grouped according to their objective(s): the emulation of inertia, the provision of frequency droop, the provision of voltage droop, and/or enhancement of PLL.

2.9.1.1 Inertia emulation

It is known that the displacement of conventional generators in favour of renewables will result in a lower overall system inertia with the effect being a higher sensitivity of the grid frequency to power imbalances. Most power systems impose strict limits on grid frequency. Furthermore, the rate of change of frequency, which is inverse proportional to the inertia of the system, is a critical parameter. This is because distributed generators use measured frequency to detect islanding. When a distributed generator observes the RoCoF to be above a certain threshold, its protection system assumes that it has become disconnected from the main power system. Subsequently, to protect itself and de-energise what the protection system perceives to be a small power island, the generator trips. Because of this arrangement, events on the main power system may produce unwanted tripping when the inertia is low leading to a cascade-style instability.

To compensate for the lower system inertia, synthetic inertia can be adopted. In the simplest case, the power setpoint is adjusted as shown in Figure 2-20. In this thesis, such a concept is quoted as the swing equation based inertial response (SEBIR) control, with the fundamental principle expressed by equation (2-27) which is derived from the commonly known swing equation [23]. Similar to the response of a synchronous machine, when there is a power imbalance in the system, e.g. a loss of infeed, the system frequency drops and the RoCoF becomes negative; as a result, the NSGs equipped with SEBIR control contribute active power (proportional to the measured RoCoF and inertia constant H) which has an effect of counteracting the impact of the original ΔP and thus supports the system recovery.

$$\Delta P = -2H\frac{df}{dt} \tag{2-27}$$

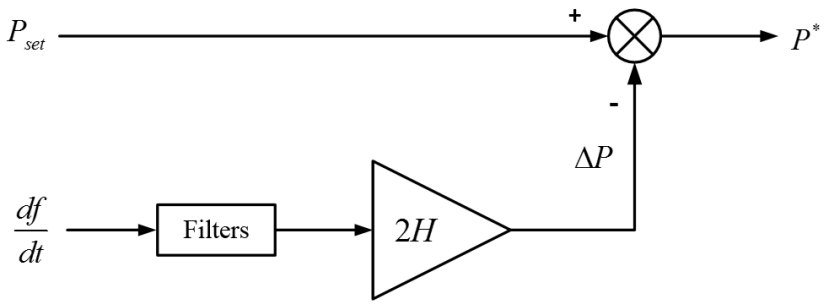

Figure 2-20. Configuration of SEBIR control applied as additional loop to DQCI control

SEBIR-type control algorithms have been widely discussed for practical devices, ranging from battery storage to wind turbines. Also, a number of technical publication discussed implementations of SEBIR-like control in various applications:

- [81-87] discussed control algorithms that make it possible to extract natural kinetic energy stored in the rotating elements of wind turbines and/or virtual inertial response from the temporary power surge of the wind farm.
- [88-91] presented control techniques to support system frequency by manipulating energy stored in the DC capacitors based on power balance between the DC and AC side.
- [92-95] proposed virtual inertia support method via SEBIR control and a virtual prime mover on energy storage system which can help with frequency restoration and active support after a power imbalance event.
- [96, 97] discussed about enhancing frequency control via small scale distributed energy resources such as EVs.
- It is also considered by system operators, such as EU ENTSO-E [24], GB National Grid [12, 37] and Ireland [41], and manufacturers such as US GE [98], SIEMENS [94, 99] and ABB [100] with its product EssPro Energy Storage Power Conversion System [101].

Accurate RoCoF estimation and fast response are crucial to achieve the desired effect. Normally, frequency is measured by differentiating the measured phase angle. For RoCoF measurement, there is another stage of differentiation. Differentiation term naturally involves an amplification of signal noise, and therefore the two stages of differentiation to assess RoCoF make it even harder to obtain clean and useable signal for the control processes. To overcome this, carefully designed filters are required with sufficiently long measuring windows to ensure accurate and noise-free measurement of RoCoF. Unfortunately, this comes at the expense of additional signal delays [102, 103]. Therefore, there is a trade-off between RoCoF measurement accuracy and control response time which should be considered carefully in the design process. Due to such reasons, in [14, 104], SEBIR-type inertia emulation technique is termed as fast frequency response or fast

active power injection, which is distinct from the inherent inertial response of a synchronous machine.

A PLL can be used to determine the grid frequency. However, it was shown in [105] that PLL Alternative algorithms include, but are not limited to the second-order generalised integrator (SOGI) and the Phasor Measurement Units (PMUs). In [106-109], it was shown that PMUs provide frequency (and RoCoF) measurements with an acceptable accuracy, speed and robustness against faults, which has been used for many monitoring, control and protection applications. For that reason, the frequency measurement methods that will be investigated in this thesis are those used in P and M class PMU. A high level overview of such methods can be found in [103].

Unlike traditional synchronous machines, the inertia constant in such inertia emulation strategies can be set in theory to any value as it is a control parameter. However, there are limitations introduced by the converter capacity and frequency measurement accuracy [110]. The amount of power requested is bound by the amount of energy available on the DC bus (conservation of energy). In addition, a constraint is also imposed on the current (to avoid damage being done to the switching devices). Finally, as illustrated by Figure 2-20, the inertia constant acts as a proportional gain in the control sense. It, therefore, has the ability to amplify noise if set too high but also lead to negative gain and/or phase margins, resulting in instability.

2.9.1.2 Frequency and voltage droop controllers

Provision of frequency and voltage response is crucial to ensure the network frequency and voltage are controlled within the required operational limits, and to avoid damage to connected devices, such as rotating machines, transmission lines, and other components. This service is normally provided by conventional synchronous machines, In recent years with increasing penetration of converters, researchers and system operators (such as grid code documents [12, 111]) have been focusing on implementing such capabilities on converters.

Associated expressions for active power-frequency droop control and reactive power-voltage droop control are shown in equations (2-28) and (2-29), with corresponding characteristics shown in Figure 2-21 (a) and (b) respectively, which are effectively straight lines with negative slopes. For example, in frequency droop control, when the measured

frequency drops from f_1 to f_2, the active power output from this unit will be increased from P_1 to P_2 (according to the characteristic with a frequency droop slope of D_f) to facilitate the restoration of power balance in the system. The reactive power-voltage droop control react similarly with a voltage droop slope of D_v.

$$f_1 - f_2 = -D_f(P_1 - P_2) \tag{2-28}$$

$$V_1 - V_2 = -D_V(Q_1 - Q_2) \tag{2-29}$$

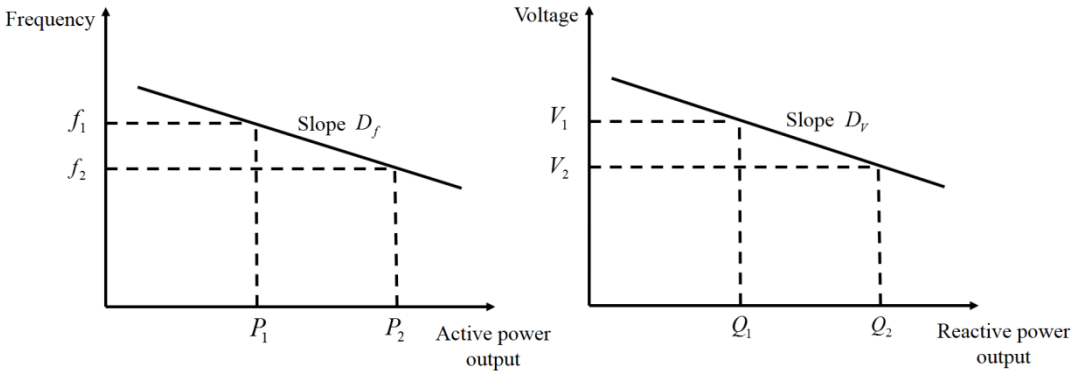

(a) (b)

Figure 2-21. Droop characteristics for (a) active power-frequency and (b) reactive power-voltage

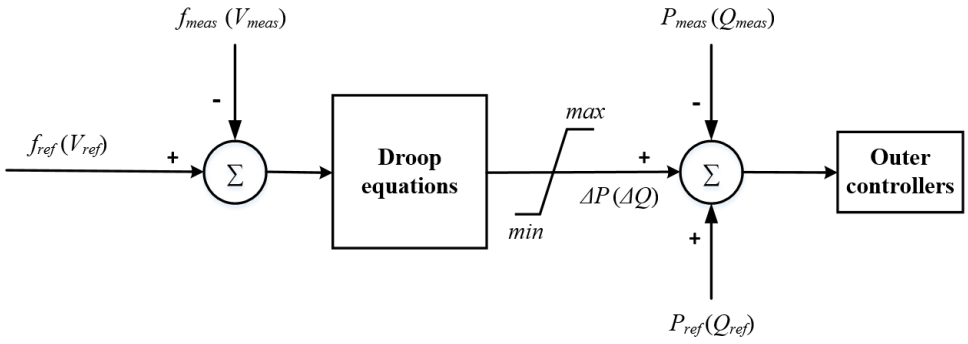

Figure 2-22. Implementation of active power-frequency and reactive power-voltage droop controllers as additional control loop on outer controllers of DQCI converter control

Droop controllers are implemented to provide an additional power reference to the outer controllers of DQCI converter control system, where the power reference value P_{ref} (Q_{ref}) sent to the active power controller and reactive power controller will be adjusted

when the measured value, i.e. frequency f (or voltage V) at the converter PCC differs from the reference frequency f_{ref} (or voltage V_{ref}) based on the droop equation, as shown in Figure 2-22.

Droop controllers have been used widely in the microgrids, which are regarded as effective control methods for active power and reactive power sharing when there are several paralleled converters. This is discussed in [112-114] (frequency droop control) and in [115, 116] (voltage droop control). Paper [117] used frequency droop control from both wind turbines and VSC-HVDC system where parameters for such controller should be selected carefully, otherwise will deteriorate the frequency response instead of improving it. Both active power-frequency droop and reactive power-voltage droop characteristics are required by [12, 24, 41] on the converter interfaces, such as HVDC links and DG converters.

2.9.1.3 Enhanced PLL algorithms

Stability issues with the PLL in DQCI control are related to the influence of the converter operation on the voltage measurement used for grid synchronisation, especially when system impedance is high. Corresponding effects on the converter dynamics could partially be mitigated by reducing the PLL bandwidth, which will however result in a slower dynamic response of the converter, as discussed in [118]. In [119], rather than synchronising with the weak PCC, a voltage sensor-less approach is proposed for synchronising to a remote and stronger point in a weak grid by a virtual flux based estimation. Paper [120] proposed an impedance based compensation term which was introduced in the traditional SRF-PLL which could ensure quasi-stationary synchronisation to a virtual remote point and an extension of stability range in a weak grid. The principles of improving performance of the PLL phase tracking and DQCI control is to synchronise converter control with a stiff source in the network, such as a slack bus. However, the existence of slack bus in real power networks is not guaranteed. Especially under significant penetration of converters, future power networks are expected to be much weaker and therefore, it is even more difficult to find a reliable point for the PLL to synchronise with. Moreover, although method discussed in [120] established a virtual remote point to facilitate PLL synchronisation by compensating for an estimated equivalent grid impedance, it is impractical to obtain the precise value which

in practice is likely to vary due to the constantly changing generation and demand, especially in the future power networks where intermittent generation such as wind and PV could be dominant. Therefore, stability issues of DQCI converter could still remain unsolved in the long-term, even with such enhanced PLL algorithms, such as discussed in [25, 121].

2.9.2 Stability improvement solutions without DQCI control

Taking into account the control stability issues with the DQCI control and unsatisfying grid synchronisation using a SRF-PLL in a weak grid, converter control algorithms have been proposed and widely discussed to replace the conventional DQCI controller. Considering the benefits for existing system operation, stability enhancement and infrastructure, including protection and system control units, it is of great advantage to mimic operation principle of a traditional synchronous machine on a converter interface. Moreover, traditional synchronous machines with speed governor control and excitation control provide favourable features to support system operation in either transmission or distribution networks, including the provision of natural inertia and damping of disturbances and system oscillations, frequency regulation through governor droop control, control of voltage and reactive power flow, islanding operation, and high level of fault current infeed (as a synchronous machine operates as a voltage source rather than current source). Therefore, a VSM concept which enables the converters to operate (to a certain degree) in a fashion similar to SGs, or often quoted as the grid forming converter in grid code documents such as [122], has been one of the most popular topics in the studies of converter control algorithms to assist system stability under high penetration of converters.

The current state of art of the VSM concept has been reviewed in [110, 123, 124]. In this section, VSM techniques for converters without DQCI control (or a PLL) will mainly be discussed. System inertia is considered necessary to damp system frequency and voltage oscillations; therefore, implementation of virtual inertia based on the Swing Equation, i.e. the second order model which describes only the rotor dynamics, has been discussed in [125, 126]. Higher order models of VSM have been proposed too, such as the first VSM concept [127], 'VISMA' concept [128, 129], 'synchronverter' concept [27, 28, 130-132],

and 'inducverter' concept [29, 30, 133]. [127] proposed the first VSM algorithm, which allows a grid compatible integration of predominantly RES even in weak grids, with properties such as interaction between grid and generator as in a remote power dispatch, reaction to transients, full electrical effects of a rotating mass, and primary frequency response. The 'VISMA' concept [128, 129] controls the inverter current to follow the current reference generated from its control system which emulate a traditional synchronous machine. [27, 28, 130-132] proposed the 'synchronverter' concept where the inverter is controlled to generate an output voltage via embedding most of the major properties of a synchronous machine and act as voltage source to the grid similar as the traditional synchronous machine. Authors in [30, 133] presented a high order VSM model which provide virtual inertia and synchronising and damping power components and later proposed a 'inducverter' concept in [29] which controls the converters to act as an induction machine with the ability to self-synchronise with the grid without need of grid information and provision of virtual inertia and damping.

Rather than implementing key features of synchronous machines, control algorithms have also been proposed aiming to solve the issues with conventional DQCI control and PLL performance, such as the power synchronisation control introduced in [25, 26, 134], where the VSC synchronises with the AC system through an active power control loop, similar to the operation of a synchronous machine, and a strong voltage support can be provided from such VSC terminal to the weak AC grid.

VSM concepts provide the possibility for converters to act in a similar way to the traditional synchronous machines and assist with system stability and operation under high penetration of converters. Meanwhile, it also provides a high flexibility of the converter configuration, as its parameters are not constrained by the physical design, cost or mechanical/practical considerations that are present in a traditional synchronous machine. Therefore, it is possible to control and achieve desired behaviour which can be advantageous for both operational and economic considerations, such as desired inertia constant (could be limited by controller performance), high efficiency as rotor friction no longer exists, and critically damped oscillations.

However, as the majority of VSM techniques drive the converter as a voltage source, in a similar way as the traditional synchronous machines, it is important to implement current limitation (even short-term current overloads) in the control system to avoid

damage to converter hardware, especially when there are faults presented. For most of the VSM techniques discussed above, insufficient consideration to current limitation have been given, or otherwise it is common for them to switch back to conventional DQCI control when there are faults detected, such as discussed in [26, 135]. [136] proposed a voltage drive mode of the VSC in a similar way to the power synchronisation concept with a fast-acting current limitation block which is capable of providing balanced or unbalanced fault current, which is believed to be a simple and effective way of current limitation and provision of balanced or unbalanced fault currents.

In this thesis, for dynamic studies of system stability and tipping points, two representative VSM techniques have been used, i.e. the VSM0H algorithm based on [136, 137] and a VSM-type architecture which emulates virtual inertia and damping power. Both algorithms are equipped with the current limitation blocks discussed in [136].

2.9.2.1 VSM0H control

The VSM0H method of controlling a converter represents a VSM, but with zero inertia constant H. Figure 2-23 shows a block diagram of the control philosophy, and how it relates to the 3-phase switching bridge and line filter. The main control strategy is notable in that the only measurements needed are the currents flowing from the switching bridge, I_{abc}. Additional measurements of voltages and currents at the grid-side of the filter inductor can be used for fault current limiting and to optimise active and reactive power setpoints. There are a number of important points to note in relation to the VSM0H controller.

Firstly, there is no PLL to be used for grid synchronisation. The phase angle of the voltage synthesised at the switching bridge is derived purely from an integrator which advances at a rate determined from a conventional droop slope of frequency versus measured active power output. This will effectively eliminate the effects of PLL performance and make the converter controller more reliable in a weak AC grid.

Secondly, there is no inner current loop which attempts to produce sinusoidal balanced currents. Instead, the measurements of active and reactive power, averaged over 1 cycle using adaptive boxcar filters tuned to the fundamental, are used to determine target frequency f and voltages $|E|$ using the conventional droop equations. The resulting

frequency and voltages are used directly to derive the angle and magnitude of the drive voltage. Filtering the measurements of active power P and reactive power Q over 1 cycle is extremely useful, because when unbalance or harmonic voltages or current occur on the network, P and Q tend to ripple at twice fundamental (for unbalance) or higher frequencies for unbalanced or negative-sequence harmonics. The filtering removes these components entirely and leads to a steady values of f and $|E|$ during scenarios of unbalance and harmonics.

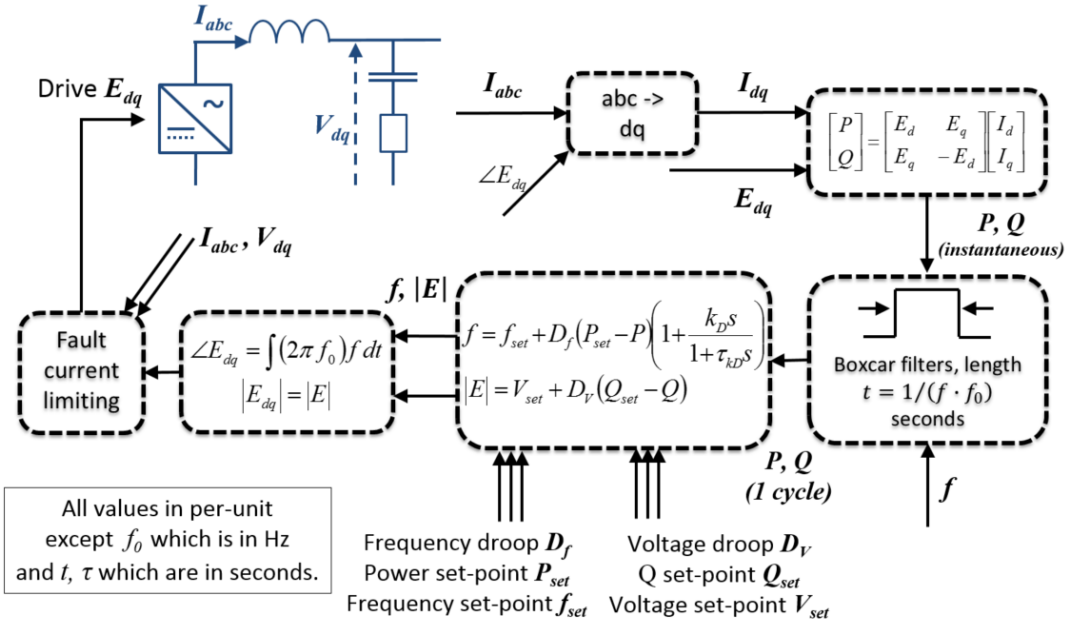

Figure 2-23. VSM0H converter control algorithm and single-line diagram of switching bridge and line filter

Thirdly, there is nothing in the VSM0H control strategy which attempts to introduce any synthetic inertia. In fact, if a VSM0H converter (alone) is feeding a power island and an active power load-step occurs, then the frequency would experience a rapid ramp from the initial frequency to the new frequency, as determined by the droop slope settings, over one fundamental cycle. The ramp occurs over 1 cycle due to the boxcar filtering. If the filtering was removed then the frequency ramp could in theory occur "instantly", although in practical terms this could never be measured. Although there is no inertia, the response rapidly tracks the droop slope, with only a small time lag. As a result this control strategy does not directly mitigate against RoCoF immediately following after an event. However the frequency nadir can be well managed by the VSM0H strategy. This is true under the

assumption that sufficient energy and power are available at the DC bus to provide the required response, which may be significant and is dependent on the change in the balance in load and generation.

In this way, the converter behaves as a stable voltage source, connected to the grid via its filter impedance. The result is a converter which mitigates power quality in a very similar manner to a SG which behaves as "a voltage source behind a transient reactance" [138]. This is in contrast to the DQCI-controlled converter which has the objective of behaving as a balanced sinusoidal current source (with PLL and controller-related imperfections). This voltage-source behaviour is important, and as a consequence, the VSM0H mitigates power quality and high-frequency oscillations in the voltage waveforms at its connection point.

The controller design of VSM0H is not dissimilar compared to the concept of power synchronisation control proposed in [139]. However, the implementation used in VSM0H also includes single-cycle boxcar filtering which introduces a damped resonance into the closed-loop response (typically at ~20 Hz), while being extremely beneficial for power quality, as well as an effective current limitation block with fault current provision to both balanced and unbalanced faults.

2.9.2.2 VSM-type control

Among various VSM techniques discussed in the industry which provide different characteristics of a synchronous machine, a simple VSM-type model (instead of the complex full order models) which emulates the basic characteristics of a SG is built and used for the comparison studies. The VSM-type algorithm has a similar output stage with that of the VSM0H algorithm, where waveform sent to VSC is derived from a model of a rotor with associated mass and damping, as shown in Figure 2-24.

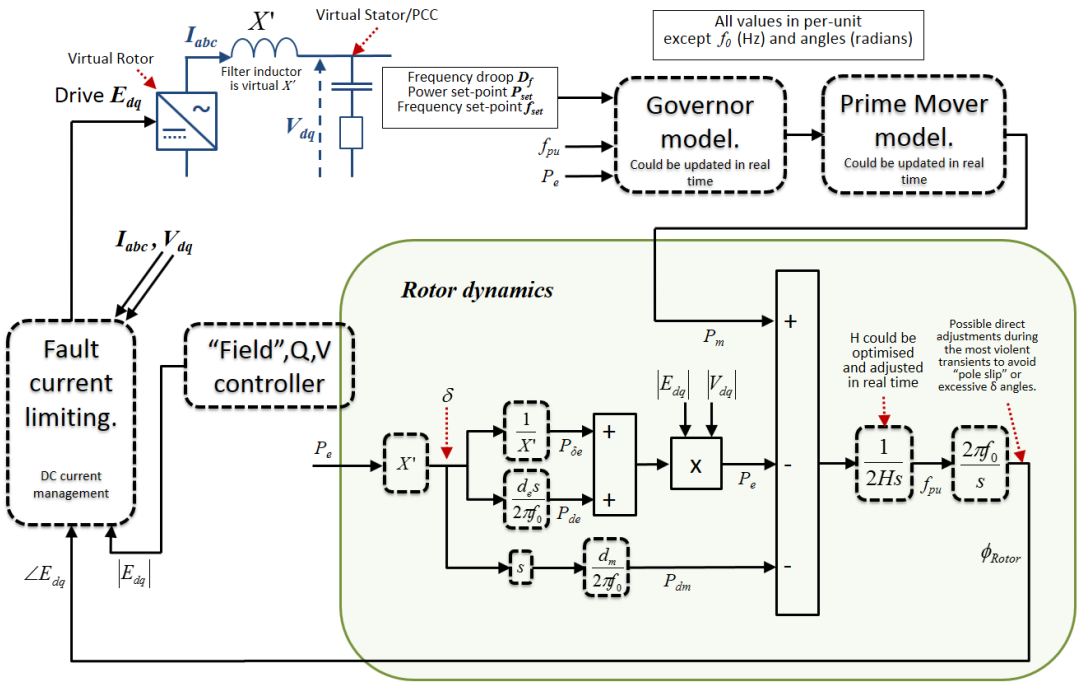

Figure 2-24. High-level control diagram for a 'true' VSM converter controller with virtual rotor angle measured from active power output at the converter PCC

Referring to the power angle equation shown in equation (2-1), the electrical angle across the filter impedance X (p.u.) can be written as δ and considered to be equivalent to a rotor angle. Using this analogy, the VSM-type response contains only "spring" (power output is proportional to δ) and "damper" (power output is proportional to $d\delta/dt$) terms. The VSM-type response adds an extra "mass" term - via a finite value of inertia constant H. This term adds a response proportional to $d^2\delta/dt^2$. This changes the response of the device from a purely damped response, to one with a 2nd-order transfer function with an associated natural resonant frequency determined by,

$$f_n = \frac{1}{2\pi}\sqrt{\frac{2\pi f_0}{2HX}} \qquad (2\text{-}30)$$

Resonance in the VSM rotor is exact analogy of rotor oscillation in a real synchronous machine, and is generally in the 2-5 Hz region for normal values of H (2-10 s) and X (≈0.1 p.u.). In some literatures, damping is considered to be a mechanical or droop-related effect, such as in [27, 131], but in reality any real synchronous machine with significant mechanical damping, i.e. friction or viscous windage, would be rejected on efficiency grounds. By far, the dominant damping effect in a real synchronous machine is the

electrical damping, whose amount is limited by physical constraints on the damper windings and also on electrical losses associated with them. These operate as an induction machine to provide a torque proportional to slip (power proportional to $d\delta/dt$), with the associated inefficiency and reactive power losses inherent in an induced-rotor-current machine. Real SGs have damping ratios ζ of the order of 0.2 and hence the decaying post-transient rotor oscillations observed after system events and changes in operating point.

Therefore, in a VSM, electrical damping should be dominant as a function of the rotor slip angle derived from either the measured active power (as shown in Figure 2-24). Meanwhile, there are no efficiency or mechanical design constraints on the damping ratio ζ and the resulting damping term magnitude. Essentially, ζ is a freely variable parameter, settable in software. It is therefore possible to choose ζ=1 which will lead to critical damping of the rotor, and this would be a highly desirable network stabilisation tool and potentially omits the need for complex PSS (Power System Stabilisers) as found on SG. However, damping the rotor resonance right down too much might detract from some of the beneficial inertial response.

As a result, the VSM-type converter has a control bandwidth much lower than 50 Hz, configurable droop settings via a virtual governor, and a damped rotor resonance which provides virtual inertia. The fact that the control bandwidth is which smaller than 50 Hz (compared to the conventional DQCI controller) with a 2^{nd}-order transfer function response and virtual rotor inertia means that the voltage source induced by the virtual rotor filters is capable of generating unbalance and harmonics which appear at higher frequencies, while most of the conventional DQCI converters do not react to them unless special control blocks are designed. Similar to the VSM0H, the VSM-type converter behaves as a robust balanced three-phase voltage set which mitigates voltage power quality problems in a manner proportionate to its rating and filter reactance X.

During close-in faults, action needs to be taken to avoid convertor destruction, as it is operated as a voltage source. This intervention is described in [136] and has the advantage that it can service unbalanced, resistive and non-linear fault currents, rather than the "balanced reactive current" prescribed by existing grid codes. For the VSM-type algorithm in this thesis, a dynamic braking is introduced, which involves setting the virtual inertia constant H to an extremely high value (such as 1000 s) when there is a fault event

detected, i.e. when the converter terminal voltages are less than 0.85 p.u. chosen as the GB Grid Code [12], to prevent the integrator changing the frequency of the converter and advancing the operating angle under such circumstances. Such implementation reduces the post fault power oscillations and minimises rating requirements for converters, and therefore could potentially increase system stability. Related studies will be introduced in Chapter 5. It is rather convenient to implement such algorithm in VSM-type control as it is simply based on software, while for traditional synchronous machines, it requires additional expensive plant such as resistor banks.

2.10 Summary

In this chapter, the reasons for the presence of non-synchronous devices have been reviewed against the background of anticipated increasing energy demand and CO_2 emission limitation efforts around the world. With the ambition to achieve 100% renewable energy resources, renewable energy targets have also been set by the majority of countries in the world. Great efforts have been made worldwide towards achieving those targets. The current status and future energy scenarios for non-synchronous devices have also been summarised. With increasing penetration of converters, the existing power networks are expected to face various types of operational challenges, such as frequency and voltage management, system stability and power quality issues which result from the control mode of the conventional DQCI converters. Grid code requirements for non-synchronous devices to deal with those issues have been briefly outlined.

The operation principles and motion mechanics of a SG have been introduced. Common controllers for a SG have been discussed, including turbine-governor control, voltage regulator control and PSS, which ensure a reliable, stable and securable operation of the generator itself and also the power network it is connected to. Most of the renewable power generation are connected to the AC grid via power electronic converters. The two most common types, LCC and VSC based HVDC transmission systems have been described and compared. LCC-HVDC has been the main HVDC technology for decades and the drawbacks of this technology, such as commutation failure and lack of flexibility to change the power flow direction, have been recognised. Those limitations

can be overcome by the VSC-HVDC technique. Configuration of VSC-HVDC and its conventional control system have been discussed.

Conventional DQCI control for VSC, i.e. vector current control with PLL to synchronise with the AC grid, has been introduced. It has also been discussed that satisfactory performance of the PLL and DQCI control is based on the assumption that the converter is connected to a stiff grid. This is no longer be true under high penetration of converters in the future power networks and could lead to serious stability issues. Converter control algorithms need to be designed and validated to improve converter performance as well as make it possible to achieve high penetration. Additionally, converter control techniques that have the potential of assisting system stability under high penetration of converters have been reviewed and discussed. To deal with the inadequate performance of the conventional DQCI control scheme in a weak AC grid, additional controllers have been proposed based on the conventional DQCI control, such as inertia emulation, frequency and voltage droop control and enhanced PLL techniques, which have been reviewed. While removing the DQCI control and PLL, the most popular choice for converter control are the VSM concepts, which have been widely discussed in the field. A brief review of the current state-of-art of VSM algorithms have been provided. Among the various techniques of VSM, two representative models, i.e. VSM0H and VSM-type controller, have been selected to be systematically investigated in this thesis according to their outstanding advantages.

References

[1] U.S. Energy Information Administration, "International Energy Outlook 2016," 2016. Available: http://www.eia.gov/forecasts/ieo/, accessed in 2017/6/1.

[2] P. R. China Government, "13th Five-Year Plan for the National Economic and Social Development," 2016. Available: http://www.gov.cn/xinwen/2016-03/17/content_5054992.htm, accessed in 2017/2/3.

[3] U.S. Deparment of Energy, "Renewable Energy Data Book," 2015. Available: http://www.nrel.gov/docs/fy17osti/66591.pdf, accessed in 2017/5/25.

[4] European Commission, "Climate Action: Climate strategies and targets," 2009. Available: http://ec.europa.eu/clima/policies/strategies/index_en.htm, accessed in 2017/2/7.

[5] European Commission, "Renewable Energy Progress Report," 2015. Available: http://ec.europa.eu/energy/node/70, accessed in 2017/5/24.

[6] ENTSO-E, "Scenario Outlook & Adequacy Forecast," 2015. Available: https://www.entsoe.eu/Documents/SDC%20documents/SOAF/150630_SOAF_2015_publication_wcover.pdf, accessed 2017/5/24.

[7] National Grid (GB), "Future Energy Scenario," 2017. Available: http://fes.nationalgrid.com/, accessed in 2018/2/12.

[8] UK Government, "Climate Change Act," 2008. Available: http://www.legislation.gov.uk/ukpga/2008/27/contents, accessed in 2017/2/7.

[9] UK Department of Energy & Climate Change, "Third Progree Report on the Promotion and Use of Energy from Renewable Sources for the United Kingdom," 2016. Available: https://www.gov.uk/government/publications/third-progress-report-on-the-promotion-and-use-of-energy-from-renewable-sources-for-the-united-kingdom, accessed in 2017/6/5.

[10] Ofgem, "Electricity interconnectors," 2017. Available: https://www.ofgem.gov.uk/electricity/transmission-networks/electricity-interconnectors, accessed in 2017/6/1.

[11] H. Urdal, "Future system challenges ahead with high penetration of PEIPS," Public Workshop on Frequency Stability Parameters for CNC Implementation, 2017. Available: https://www.entsoe.eu/Documents/Events/2017/170309_%20ENTSO-E%20workshop%20on%20%20CNC_frequency%20paramentes%20_all%20presentations.zip, accessed in 2017/11/15.

[12] National Grid (GB), "The Grid Code," 2016. Available: http://www2.nationalgrid.com/UK/Industry-information/Electricity-codes/Grid-Code/, accessed in 2017/5/25.

[13] National Grid (GB), "Report of the investigation into the automatic demand disconnection following multiple generation losses and demand control response that occured on the 27th May 2008," 2009. Available: http://www.nationalgrid.com/NR/rdonlyres/D680C70A-F73D-4484-BA54-95656534B52D/26917/PublicReportIssue1.pdf, accessed in 2017/5/12.

[14] National Grid (GB), "System Operability Framework," 2016. Available: http://www2.nationalgrid.com/UK/Industry-information/Future-of-Energy/System-Operability-Framework/, accessed in 2017/2/10.

[15] National Grid (GB), "System Operability Framework," 2015. Available: http://www2.nationalgrid.com/UK/Industry-information/Future-of-Energy/System-Operability-Framework/, accessed in 2017/2/10.
[16] EirGrid and SONI, "Delivering a Secure, Sustainable Electricity System (DS3 Programme)," 2015. Available: http://www.eirgridgroup.com/site-files/library/EirGrid/DS3-Programme-Overview-2015.pdf, accessed in 2017/5/26.
[17] Ofgem, "Distribution Code G59," 2015. Available: https://www.ofgem.gov.uk/licences-codes-and-standards/codes/electricity-codes/distribution-code, accessed in 2017/2/13.
[18] Northern Ireland Utility Regulator, "Rate of Change of Frequency Modification to the Northern Ireland Grid Code," 2014. Available: https://www.uregni.gov.uk/sites/uregni.gov.uk/files/media-files/Decision_Paper_on_the_Rate_of_Change_of_Frequency_Grid_Code_Modification.pdf, accessed in 2018/2/12.
[19] National Grid (GB), "National Electricity Transmission System Security and Quality of Supply Standard (NETS SQSS)," 2017. Available: http://www2.nationalgrid.com/uk/industry-information/electricity-codes/sqss/the-sqss/, accessed in 2017/2/17.
[20] UK Government, "Electricity Act 1989," 1989. Available: http://www.legislation.gov.uk/ukpga/1989/29/contents, accessed in 2017/1/27.
[21] Energy Networks Association (ENA), "The Distribution Code of Licensed Distribution Network Operators of Great Britain," 2016. Available: http://www.dcode.org.uk/the-distribution-code, accessed in 2017/2/17.
[22] J. Keller and B. Kroposki, "Understanding Fault Characteristics of Inverter-Based Distributed Energy Resources," National Renewable Energy Laboratory (NREL), NREL/TP-550-46698, 2010.
[23] P. Kundur, N. J. Balu, and M. G. Lauby, *Power system stability and control* vol. 7: McGraw-hill New York, 1994.
[24] ENTSO-E, "Network Code on High Voltage Direct Current Connections and DC-connected Power Park Modules," 2016. Available: https://www.entsoe.eu/major-projects/network-code-development/high-voltage-direct-current/Pages/default.aspx, accessed in 2017/2/16.
[25] L. Zhang, "Modeling and Control of VSC-HVDC Links Connected to Weak AC Systems," School of Electrical Engineering (EES), Electrical Machines and Power Electronics, KTH, Stockholm, 2010, Available: http://www.diva-portal.org/smash/record.jsf?pid=diva2%3A322475&dswid=1654, accessed in 2017/5/24.
[26] L. Zhang, H. Lennart, and H. P. Nee, "Interconnection of Two Very Weak AC Systems by VSC-HVDC Links Using Power-Synchronization Control," *Power Systems, IEEE Transactions on,* vol. 26, pp. 344-355, 2011.
[27] Q. C. Zhong and G. Weiss, "Synchronverters: Inverters That Mimic Synchronous Generators," *IEEE Transactions on Industrial Electronics,* vol. 58, pp. 1259-1267, Apr 2011.
[28] Q. C. Zhong, P. L. Nguyen, Z. Ma, and W. Sheng, "Self-Synchronized Synchronverters: Inverters Without a Dedicated Synchronization Unit," *IEEE Transactions on Power Electronics,* vol. 29, pp. 617-630, 2014.

[29] M. Ashabani, F. D. Freijedo, S. Golestan, and J. M. Guerrero, "Inducverters: PLL-Less Converters With Auto-Synchronization and Emulated Inertia Capability," *IEEE Transactions on Smart Grid,* vol. 7, pp. 1660-1674, 2016.

[30] M. Ashabani and Y. A. R. I. Mohamed, "Novel Comprehensive Control Framework for Incorporating VSCs to Smart Power Grids Using Bidirectional Synchronous-VSC," *IEEE Transactions on Power Systems,* vol. 29, pp. 943-957, 2014.

[31] D. Dong, B. Wen, D. Boroyevich, P. Mattavelli, and Y. Xue, "Analysis of Phase-Locked Loop Low-Frequency Stability in Three-Phase Grid-Connected Power Converters Considering Impedance Interactions," *IEEE Transactions on Industrial Electronics,* vol. 62, pp. 310-321, 2015.

[32] National Grid (GB), "Performance of Phase-Locked Loop Based Converters," Sep 2017. Available: https://www.nationalgrid.com/sites/default/files/documents/Phase%20locked%20loop%20FINAL.pdf, accessed in 2018/1/8.

[33] National Grid (GB), "Information Required to Evaluate Subsynchrononous Resonance on the Transmission System," July 2011. Available: https://www.nationalgrid.com/sites/default/files/documents/15783-Information%20Required%20to%20Evaluate%20Subsynchrononous%20Resonance%20on%20the%20Transmission%20System.pdf, accessed in 2018/6/1.

[34] L. Livermore, C. E. U. Loo, Q. Mu, J. Liang, J. B. Ekanayake, and N. Jenkins, "Damping of subsynchronous resonance using a voltage source converter-based high-voltage direct-current link in a series-compensated Great Britain transmission network," *IET Generation, Transmission & Distribution,* vol. 8, pp. 542-551, 2014.

[35] National Grid (GB), "GSR018/GC0077: Sub-Synchronous Oscillations (SSO)," Jan 2017. Available: https://www.nationalgrid.com/sites/default/files/documents/8589938896-GSR018-GC0077%20SSO%20Report%20to%20the%20Authority%20Resubmission.pdf, accessed in 2018/6/1.

[36] ENSTO-E, "Network Code for Requirements for Grid Connection Applicable to all Generators," 2016. Available: https://www.entsoe.eu/major-projects/network-code-development/requirements-for-generators/Pages/default.aspx, accessed in 2017/5/25.

[37] A. Johnson and S. Whyte, "System Inertia and Development," Grid Code Frequency Response Working Group, National Grid (GB), 2012.

[38] US Federal Energy Regulatory Commission (FERC), "661A Interconnection for Wind Energy," 2005. Available: https://www.ferc.gov/EventCalendar/Files/20051212171744-RM05-4-001.pdf, accessed in 2017/5/24.

[39] International Organization for Standardization (ISO), "ISO 50001 Energy Management," 2011. Available: https://www.iso.org/obp/ui/#iso:std:iso:50001:ed-1:v1:en, accessed in 2017/5/25.

[40] P.R.China National Electricity Regulatory Standardization Technical Committee, "GB/T 19963-2011 Technical rule for connecting wind farm to power system," 2011. Available:

http://www.chinesestandard.net/default.aspx?PDF-English-ID=GB/T%2019963-2011, accessed in 2017/5/25.
[41] EirGrid, "The Grid Code," 2015. Available: http://www.eirgridgroup.com/site-files/library/EirGrid/GridCodeVersion6.pdf, accessed in 2017/5/26.
[42] P. Schavemaker and L. V. D. Sluis, *Electrical Power System Essentials*: Wiley, Apr 2008.
[43] J. D. Glover, M. S. Sarma, and T. J. Overbye, *Power System Analysis and Design (Fifth Edition)*. USA: Cengage Learning, 2012.
[44] E. V. Larsen and D. A. Swann, "Applying Power System Stabilizers Part I: General Concepts," *IEEE Transactions on Power Apparatus and Systems,* vol. PAS-100, pp. 3017-3024, 1981.
[45] P. Kundur, J. Paserba, V. Ajjarapu, G. Andersson, A. Bose, C. Canizares, N. Hatziargyriou, D. Hill, A. Stankovic, C. Taylor, T. V. Cutsem, and V. Vittal, "Definition and classification of power system stability IEEE/CIGRE joint task force on stability terms and definitions," *IEEE Transactions on Power Systems,* vol. 19, pp. 1387-1401, 2004.
[46] C. W. Taylor, *Power system voltage stability*: New York, NY: McGraw-Hill, 1994.
[47] "IEEE Guide for Planning DC Links Terminating at AC Locations Having Low Short-Circuit Capacities," *IEEE Std 1204-1997,* pp. 1-216, 1997.
[48] E. R. C. D. Silva and M. E. Elbuluk, "Chapter 2 Fundamentals of Power Electronics," in *Power Electronics for Renewable and Distributed Energy Systems*, ISBN 978-1-4471-5103-6, M. G. S. Sudipta Chakraborty, William E. Kramer, Ed. London: Springer-Verlag, 2013, pp. 7-59.
[49] H. Akagi, E. H. Watanabe, and M. Aredes, *Instantaneous Power Theory and Applications to Power Conditioning*: Wiley-IEEE Press, 2007.
[50] T. Larsson, A. Petersson, A. Edris, D. Kidd, and F. Aboytes, "Eagle Pass back-to-back tie: a dual purpose application of voltage source converter technology," in *2001 Power Engineering Society Summer Meeting. Conference Proceedings (Cat. No.01CH37262)*, 2001, pp. 1686-1691 vol.3.
[51] O. Wasynczuk and N. A. Anwah, "Modeling and dynamic performance of a self-commutated photovoltaic inverter system," *IEEE Transactions on Energy Conversion,* vol. 4, pp. 322-328, 1989.
[52] M. N. Marwali and A. Keyhani, "Control of distributed generation systems-Part I: Voltages and currents control," *IEEE Transactions on Power Electronics,* vol. 19, pp. 1541-1550, 2004.
[53] A. Kalair, N. Abas, and N. Khan, "Comparative study of HVAC and HVDC transmission systems," *Renewable and Sustainable Energy Reviews,* vol. 59, pp. 1653-1675, 6// 2016.
[54] D. Jovcic and K. Ahmed, *High Voltage Direct Current Transmission: Converters, Systems and DC Grids*, 2015.
[55] D. V. Hertem, O. G. Bellmunt, and J. Liang, *HVDC Grids: For Offshore and Supergrid of the Future*: Wiley-IEEE Press, 2016.
[56] ABB, "Why HVDC?," Available: http://new.abb.com/systems/hvdc/why-hvdc, accessed in 2017/5/19.
[57] D. V. Hertem, O. G. Bellmunt, and J. Liang, "Comparison of HVAC and HVDC technologies," in *HVDC Grids:For Offshore and Supergrid of the Future*. 4: Wiley-IEEE Press, 2016, pp. 79-96in 2017/5/18.

[58] ABB, "HVDC Classic (LCC)," Available: http://new.abb.com/systems/hvdc/hvdc-classic, accessed in 2017/5/19.
[59] ABB, "The Gotland HVDC link," Available: http://new.abb.com/systems/hvdc/references/the-gotland-hvdc-link, accessed in 2017/5/19.
[60] O. Heyman, L. Weimers, and M. L. Bohl, "HVDC-A key solution in future transmission systems," *ABB,* 2010.
[61] H. Ding, M. X. Han, Q. Chen, W. Y. Yin, and B. H. Liu, "Detailed modeling of China-Russia Heihe back-to-back HVDC project using PSCAD/EMTDC," in *2008 Third International Conference on Electric Utility Deregulation and Restructuring and Power Technologies*, 2008, pp. 1916-1921.
[62] UK Department of Energy & Climate Change, "More interconnection: improving energy security and lowering bills," 2013. Available: https://www.gov.uk/government/publications/more-interconnection-improving-energy-security-and-lowering-bills, accessed in 2017/5/22.
[63] P. F. d. Toledo, "Modeling and control of a line-commutated HVDC transmission system interacting with a VSC STATCOM ", Department of Electrical Engineering, KTH, Stockholm, 2007, Available: http://www.diva-portal.org/smash/get/diva2:12532/FULLTEXT01.pdf, accessed in 2017/5/15.
[64] B. T. Ooi, "Feasibilty, Stability, and Voltage Collapse in Weak Back-to-Back HVDC Links," *IEEE Transactions on Power Delivery,* vol. 1, pp. 211-217, 1986.
[65] ENTSO-E, "Offshore Transmission Technology," 2011. Available: https://www.entsoe.eu/fileadmin/user_upload/_library/publications/entsoe/SDC/European_offshore_grid_-_Offshore_Technology_-_FINALversion.pdf, accessed in 2017/5/22.
[66] ABB, "HVDC Light (VSC)," Available: http://new.abb.com/systems/hvdc/hvdc-light, accessed in 2017/5/19.
[67] J. Danielsson, S. Patel, J. PAN, and R. Nuqui, "Transmission Grid Reinforcement with Embedded VSC-HVDC " in *2015 Grid of the Future Symposium* Paris, 2015.
[68] "HVDC VSC Projects to Date," *VSC-HVDC Newsletter,* vol. 5, p. 8, December, 2017.
[69] J. Pan, R. Nuqui, K. Srivastava, T. Jonsson, P. Holmberg, and Y. J. Hafner, "AC Grid with Embedded VSC-HVDC for Secure and Efficient Power Delivery," in *2008 IEEE Energy 2030 Conference*, 2008, pp. 1-6.
[70] O. E. Oni, I. E. Davidson, and K. N. I. Mbangula, "A review of LCC-HVDC and VSC-HVDC technologies and applications," in *2016 IEEE 16th International Conference on Environment and Electrical Engineering (EEEIC)*, 2016, pp. 1-7.
[71] National Grid (UK), "High Voltage Direct Current Electricity - Technical Information," 2013. Available: http://www2.nationalgrid.com/WorkArea/DownloadAsset.aspx?id=13784, accessed in 2017/5/22.
[72] N. Mohan, T. M. Undeland, and W. P. Robbins, *Power Electronics: Converters, Applications, and Design (Third Edition)*: Wiley, 2003.
[73] N. Ray Chaudhuri, B. Chaudhuri, R. Majumder, and A. Yazdani, "The Voltage-Sourced Converter (VSC)," in *Multi-Terminal Direct-Current Grids*, ISBN

9781118960486: John Wiley & Sons, Inc, 2014, pp. 23-75. Available: http://dx.doi.org/10.1002/9781118960486.ch2, accessed in 2017/5/19.

[74] J. Arrillaga, Y. H. Liu, and N. R. Watson, *Flexible Power Transmission: The HVDC Options*: John Wiley & Sons Ltd, 2007.

[75] D. V. Hertem, O. G. Bellmunt, and J. Liang, "HVDC technology overview," in *HVDC Grids:For Offshore and Supergrid of the Future*. 3: Wiley-IEEE Press, 2016, pp. 45-78.

[76] A. Yazdani and R. Iravani, *Voltage-Sourced Converters in Power Systems : Modeling, Control, and Applications*: Wiley-IEEE Press, 2010.

[77] L. Harnefors, M. Bongiorno, and S. Lundberg, "Input-Admittance Calculation and Shaping for Controlled Voltage-Source Converters," *IEEE Transactions on Industrial Electronics,* vol. 54, pp. 3323-3334, 2007.

[78] K. G. Masoud, "PLL Basics and Standard Structure," in *Enhanced Phase-Locked Loop Structures for Power and Energy Applications*, ISBN 9781118795187: Wiley-IEEE Press, 2014, p. 232. Available: http://ieeexplore.ieee.org/xpl/articleDetails.jsp?arnumber=6798225, accessed 2017/5/19.

[79] G. A. Stefan G Johnasson, Erik Jansson, Roberto Rudervall (ABB), "Power system stability benefits with VSC DC-transmission systems," in *Cigre*, Paris, France, 2004.

[80] L. Zhang, L. Harnefors, and P. Rey, "Power system reliability and transfer capability improvement by VSC-HVDC (HVDC light)," in *Cigre Regional Meeting on Security and Reliability of Electric Power Systems*, Tallinn, Estonia, 2007.

[81] F. Gonzalez-Longatt, E. Chikuni, W. Stemmet, and K. Folly, "Effects of the synthetic inertia from wind power on the total system inertia after a frequency disturbance," in *Power Engineering Society Conference and Exposition in Africa (PowerAfrica), 2012 IEEE*, 2012, pp. 1-7.

[82] A. S. Overjordet, "Synthetic inertia from wind farms - Impacts on rotor angle stability in existing synchronous generators," Department of Electric Power Engineering, Norwegian University of Science and Technology, June, 2014, Available: http://www.diva-portal.org/smash/get/diva2:751075/FULLTEXT01.pdf, accessed in 2017/5/26.

[83] M. Seyedi and M. Bollen, "The utilization of synthetic inertia from wind farms and its impact on existing speed governors and system performance," Report of Vindforsk Project V-369, January 2013. Available: http://goo.gl/Okhizx, accessed in 2017/5/26.

[84] J. Licari, J. Ekanayake, and I. Moore, "Inertia response from full-power converter-based permanent magnet wind generators," *Journal of Modern Power Systems and Clean Energy,* vol. 1, pp. 26-33, 2013.

[85] B. Silva, C. L. Moreira, L. Seca, Y. Phulpin, and J. A. P. Lopes, "Provision of Inertial and Primary Frequency Control Services Using Offshore Multiterminal HVDC Networks," *IEEE Transactions on Sustainable Energy,* vol. 3, pp. 800-808, 2012.

[86] E. Lidström and D. Wall, "Frequency support by synthetic inertia from variable speed wind turbines," in *CIRED Workshop 2016*, 2016, pp. 1-4.

[87] W. He, X. Yuan, and J. Hu, "Inertia Provision and Estimation of PLL-Based DFIG Wind Turbines," *IEEE Transactions on Power Systems,* vol. 32, pp. 510-521, 2017.

[88] J. Zhu, J. M. Guerrero, W. Hung, C. D. Booth, and G. P. Adam, "Generic inertia emulation controller for multi-terminal voltage-source-converter high voltage direct current systems," *IET Renewable Power Generation,* vol. 8, pp. 740-748, 2014.

[89] J. Zhu, C. D. Booth, A. P. Grain, A. J. Roscoe, and C. G. Bright, "Inertia Emulation Control Strategy for VSC-HVDC Transmission Systems," *IEEE Transactions on Power Systems,* vol. 28, pp. 1277-1287, 2013.

[90] J. Zhu, J. Hu, W. Hung, C. Wang, X. Zhang, S. Bu, Q. Li, H. Urdal, and C. D. Booth, "Synthetic Inertia Control Strategy for Doubly Fed Induction Generator Wind Turbine Generators Using Lithium-Ion Supercapacitors," *IEEE Transactions on Energy Conversion,* vol. 33, pp. 773-783, 2018.

[91] L. Orellana, V. Matilla, S. Wang, O. D. Adeuyi, and C. E. U. Loo, "Fast frequency support control in the GB power system using VSC-HVDC technology," in *2017 IEEE PES Innovative Smart Grid Technologies Conference Europe (ISGT-Europe)*, 2017, pp. 1-6.

[92] M. Torres and L. A. C. Lopes, "Frequency control improvement in an autonomous power system: An application of virtual synchronous machines," in *8th International Conference on Power Electronics - ECCE Asia*, 2011, pp. 2188-2195.

[93] M. P. N. v. Wesenbeeck, S. W. H. d. Haan, P. Varela, and K. Visscher, "Grid tied converter with virtual kinetic storage," in *PowerTech, 2009 IEEE Bucharest*, 2009, pp. 1-7.

[94] "Synthetic inertia issue in future grids and frequency stabiliser as a solution," Available: http://resourcecenter.ieee-pes.org/product/-/download/partnumber/PESSLI1315, accessed in 2017/5/26.

[95] E. Spahic, C. P. S. S. Reddy, M. Pieschel, and R. Alvarez, "Multilevel STATCOM with power intensive energy storage for dynamic grid stability - frequency and voltage support," in *2015 IEEE Electrical Power and Energy Conference (EPEC)*, 2015, pp. 73-80.

[96] M. Rezkalla, A. Zecchino, S. Martinenas, A. M. Prostejovsky, and M. Marinelli, "Comparison between synthetic inertia and fast frequency containment control based on single phase EVs in a microgrid," *Applied Energy,* vol. 210, pp. 764-775, 2018/01/15/ 2018.

[97] M. Rezkalla, S. Martinenas, A. Zecchino, M. Marinelli, and E. Rikos, "Implementation and validation of synthetic inertia support employing series produced electric vehicles," *CIRED - Open Access Proceedings Journal,* vol. 2017, pp. 1197-1201, 2017.

[98] GE Energy, "Impact of frequency responsive wind plant controls on grid performance," 2010 Available: http://web.mit.edu/windenergy/windweek/Presentations/GE%20Impact%20of%20Frequency%20Responsive%20Wind%20Plant%20Controls%20Pres%20and%20Paper.pdf, accessed in 2017/5/26.

[99] E. SPAHIC, M. PIESCHEL, R. ALVAREZ, G. KUHN, V. HILD, G. BECK, and N. PLATT, "Power Intensive Energy Storage and Multilevel STATCOM for frequency and voltage grid support," in *CIGRE 2016*, Paris, France, 2016.

[100] S. Seman and R. Sakki, "Inertial response - generators and the power electronics," in *Active Power Control from Wind Power Workshop*, At Boulder, Colorado, 2011.
[101] "EssPro Energy Storage Power Conversion System (PCS)," Available: http://www.abb.com/product/seitp322/a51aa1b820acf3164825770c001a4e30.aspx?productLanguage=us&country=GB, accessed in 2017/5/27.
[102] A. J. Roscoe, I. F. Abdulhadi, and G. M. Burt, "P-Class Phasor Measurement Unit algorithms using adaptive filtering to enhance accuracy at off-nominal frequencies," in *2011 IEEE International Conference on Smart Measurements of Future Grids (SMFG) Proceedings*, 2011, pp. 51-58.
[103] A. J. Roscoe, I. F. Abdulhadi, and G. M. Burt, "P and M Class Phasor Measurement Unit Algorithms Using Adaptive Cascaded Filters," *IEEE Transactions on Power Delivery,* vol. 28, pp. 1447-1459, 2013.
[104] R. Eriksson, N. Modig, and K. Elkington, "Synthetic inertia versus fast frequency response: a definition," *IET Renewable Power Generation,* vol. 12, pp. 507-514, 2018.
[105] P. Rodriguez, A. Luna, M. Ciobotaru, R. Teodorescu, and F. Blaabjerg, "Advanced Grid Synchronization System for Power Converters under Unbalanced and Distorted Operating Conditions," in *IECON 2006 - 32nd Annual Conference on IEEE Industrial Electronics*, 2006, pp. 5173-5178.
[106] F. Ding, C. D. Booth, and A. J. Roscoe, "Peak-Ratio Analysis Method for Enhancement of LOM Protection Using M-Class PMUs," *IEEE Transactions on Smart Grid,* vol. 7, pp. 291-299, 2016.
[107] A. J. Roscoe, G. M. Burt, and G. Rietveld, "Improving frequency and ROCOF accuracy during faults, for P class Phasor Measurement Units," in *2013 IEEE International Workshop on Applied Measurements for Power Systems (AMPS)*, 2013, pp. 97-102.
[108] V. Terzija, G. Valverde, D. Cai, P. Regulski, V. Madani, J. Fitch, S. Skok, M. M. Begovic, and A. Phadke, "Wide-Area Monitoring, Protection, and Control of Future Electric Power Networks," *Proceedings of the IEEE,* vol. 99, pp. 80-93, 2011.
[109] A. G. Phadke and J. S. Thorp, *Synchronized Phasor Measurements and Their Applications*: Springer US, 2008.
[110] H. Bevrani, T. Ise, and Y. Miura, "Virtual synchronous generators: A survey and new perspectives," *International Journal of Electrical Power & Energy Systems,* vol. 54, pp. 244-254, 2014.
[111] ENTSO-E, "Network Code for Requirements for Grid Connection Applicable to all Generators," 2015.
[112] E. Rokrok and M. E. H. Golshan, "Adaptive voltage droop scheme for voltage source converters in an islanded multibus microgrid," *IET Generation, Transmission & Distribution,* vol. 4, pp. 562-578, 2010.
[113] W. Zhang, D. Remon, and P. Rodriguez, "Frequency support characteristics of grid-interactive power converters based on the synchronous power controller," *IET Renewable Power Generation,* vol. 11, pp. 470-479, 2016.
[114] J. E. S. de Haan, C. Escudero Concha, M. Gibescu, J. van Putten, G. L. Doorman, and W. L. Kling, "Stabilising system frequency using HVDC between the Continental European, Nordic, and Great Britain systems," *Sustainable Energy, Grids and Networks,* vol. 5, pp. 125-134, 2016.

[115] P. Piagi and R. H. Lasseter, "Autonomous control of microgrids," in *2006 IEEE Power Engineering Society General Meeting*, 2006, p. 8 pp.
[116] L. Y. Lu and C. C. Chu, "Consensus-Based Secondary Frequency and Voltage Droop Control of Virtual Synchronous Generators for Isolated AC Micro-Grids," *IEEE Journal on Emerging and Selected Topics in Circuits and Systems,* vol. 5, pp. 443-455, 2015.
[117] J. V. d. Vyver, J. D. M. D. Kooning, B. Meersman, L. Vandevelde, and T. L. Vandoorn, "Droop Control as an Alternative Inertial Response Strategy for the Synthetic Inertia on Wind Turbines," *IEEE Transactions on Power Systems,* vol. 31, pp. 1129-1138, 2016.
[118] Z. J. Z, "Impact of short circuit ratio and phase locked loop parameters on the small-signal behaviour of a VSC-HVdc converter," in *2016 IEEE Power and Energy Society General Meeting (PESGM)*, 2016.
[119] J. A. Suul, M. Molinas, and P. Rodríguez, "Exploring the range of impedance conditioning by virtual inductance for grid connected voltage source converters," in *2012 3rd IEEE PES Innovative Smart Grid Technologies Europe (ISGT Europe)*, 2012, pp. 1-9.
[120] J. A. Suul, S. D. Arco, P. Rodríguez, and M. Molinas, "Impedance-compensated grid synchronisation for extending the stability range of weak grids with voltage source converters," *IET Generation, Transmission & Distribution,* vol. 10, pp. 1315-1326, 2016.
[121] A. D. Giles, A. J. Roscoe, and L. Recalde-Camacho, "Assessment of HVDC control algorithms for weak and strong AC systems," *IEEE Transactions on Power Systems,* vol. 14, 2018 (under review).
[122] "Implementation Guidance Document (IGD) on High Penetration of Power Electronic Interfaced Power Sources (HPoPEIPS)," 2017 Available: https://www.entsoe.eu/Documents/Network%20codes%20documents/Implementation/CNC/170322_IGD25_HPoPEIPS.pdf, accessed in 2017/8/15.
[123] S. D'Arco and J. A. Suul, "Virtual synchronous machines - Classification of implementations and analysis of equivalence to droop controllers for microgrids," in *2013 IEEE PowerTech (POWERTECH)* Grenoble, France, 2013, pp. 1-7.
[124] H. A. Alsiraji and R. El-Shatshat, "Comprehensive assessment of virtual synchronous machine based voltage source converter controllers," *IET Generation, Transmission & Distribution,* vol. 11, pp. 1762-1769, 2017.
[125] S. D'Arco and J. A. Suul, "Equivalence of Virtual Synchronous Machines and Frequency-Droops for Converter-Based MicroGrids," *Smart Grid, IEEE Transactions on,* vol. 5, pp. 394-395, 2014.
[126] Y. Chen, R. Hesse, D. Turschner, and H. P. Beck, "Investigation of the Virtual Synchronous Machine in the island mode," in *2012 3rd IEEE PES Innovative Smart Grid Technologies Europe (ISGT Europe)*, 2012, pp. 1-6.
[127] H. P. Beck and R. Hesse, "Virtual synchronous machine," in *9th International Conference on Electrical Power Quality and Utilisation*, 2007, pp. 1-6.
[128] Y. Chen, R. Hesse, D. Turschner, and H.-P. Beck, "Improving the grid power quality using virtual synchronous machines," in *Power Engineering, Energy and Electrical Drives (POWERENG), 2011 International Conference on*, 2011, pp. 1-6.

[129] Y. Chen, R. Hesse, D. Turschner, and H.-P. Beck, "Comparison of methods for implementing virtual synchronous machine on inverters " in *International Conference on Renewable Energies and Power Quality (ICREPQ'12)*, Santiago de Compostela, Spain, 2012.
[130] Q. C. Zhong, G. C. Konstantopoulos, B. Ren, and M. Krstic, "Improved Synchronverters with Bounded Frequency and Voltage for Smart Grid Integration," *IEEE Transactions on Smart Grid,* 2016.
[131] R. Aouini, B. Marinescu, K. B. Kilani, and M. Elleuch, "Synchronverter-Based Emulation and Control of HVDC Transmission," *IEEE Transactions on Power Systems,* vol. 31, pp. 278-286, 2016.
[132] Q. C. Zhong, "Virtual Synchronous Machines: A unified interface for grid integration," *IEEE Power Electronics Magazine,* vol. 3, pp. 18-27, 2016.
[133] M. Ashabani and Y. A. R. I. Mohamed, "Integrating VSCs to Weak Grids by Nonlinear Power Damping Controller With Self-Synchronization Capability," *IEEE Transactions on Power Systems,* vol. 29, pp. 805-814, 2014.
[134] P. Mitra and L. Zhang, "Real-time simulation of a wind connected HVDC grid," in *10th IET International Conference on AC and DC Power Transmission (ACDC 2012)*, 2012, pp. 1-6.
[135] R. Rogersten, L. Zhang, and P. Mitra, "Applying power-synchronization control in a multi-terminal DC system," in *2014 IEEE PES General Meeting | Conference & Exposition*, 2014, pp. 1-5.
[136] A. J. Roscoe, G. Jackson, I. M. Elders, J. McCarthy, and G. M. Burt, "Demonstration of sustained and useful converter responses during balanced and unbalanced faults in microgrids," in *Electrical Systems for Aircraft, Railway and Ship Propulsion (ESARS), 2012*, 2012, pp. 1-6.
[137] L. Zhang, H. Lennart, and N. H. P., "Power-Synchronization Control of Grid-Connected Voltage-Source Converters," *IEEE Transactions on Power Systems,* vol. 25, pp. 809-820, 2010.
[138] P. C. Krause, O. Wasynczuk, S. D. Sudhoff, and S. Pekarek, "Analysis of Electric Machinery and Drive Systems (Second Edition)." Chapter 5 New York: IEEE Press, 2002, pp. 229-232.
[139] L. Zhang, L. Harnefors, and H. P. Nee, "Power-Synchronization Control of Grid-Connected Voltage-Source Converters," *Power Systems, IEEE Transactions on,* vol. 25, pp. 809-820, 2010.

Chapter 3

Methodology, Models and Analytical Tools

3.1 Introduction

In this chapter, simulation models used in the studies of system stability and tipping point will be introduced, including a RGBT model based on RMS-simulation in DIgSILENT PowerFactory, and a higher-fidelity APS model based on EMT-simulation in MATLAB SimPowerSystems. A dedicated method termed in this thesis as TPS will be introduced along with a set of detection criteria to determine whether the system is viable or unviable. The method is utilised to establish the tipping points under a variety of system conditions and inverter control regimes. Moreover, a frequency response analysis tool, termed as NFP method, will also be presented. All associated definitions and terms used in further simulation studies are also explained and discussed.

3.2 Tipping point search method

In order to evaluate stability issues under high penetration of conventional converters, a TPS method along with a set of realistic criteria from the network operator perspective is defined in this thesis. The TPS method can be used to assess the tipping points using time-domain dynamic power system models. System stability indicators including frequency, RoCoF, voltage magnitude, voltage THD, locking signal from PLL in the DQCI controller, and voltage flicker perception level have been considered to determine whether the system is unstable (either unstable or have unacceptable performance, termed here as unviable). In this thesis, when any of the following statements become true, the system is recognised as unstable:

- System frequency is outwith the operating range 47 Hz to 52 Hz for a period longer than 500 ms, with reference to [1, 2];
- Magnitude of RoCoF exceeds 1 Hz/s;
- Magnitude of the terminal voltage out of the range of ±30% of the nominal voltage level, with reference to [2, 3] but with additional headroom for capturing the instability phenomenon;
- Voltage THD level is higher than 8% for a period longer than 1 s, with reference to [2, 3];

- The PLL locking signal in converter DQCI control is unlocked for a period longer than 1 s;
- Flicker perception level of voltage exceeds 1.96% [4] for duration of 1 s.

Frequency, RoCoF and terminal voltages are usually monitored in traditional power networks. Given the ongoing transformation of power networks occurring through the introduction of converter-interfaced generation, monitoring both the state of the PLL and voltage flicker perception level should also be monitored. In the case of the PLL state, if the PLL cannot synchronise with the power network, the DQCI controller will perform in an undesirable manner; specifically, modifications to the active power setpoint could influence AC voltage or reactive power output more than active power output, while modifications to the reactive power setpoint of the converter could influence active power output more than reactive power output, as has been suggested by [5].Voltage flicker perception level is selected as well to detect the oscillatory modes appeared in the system at certain marginal unviable case, as when increasing the instantaneous penetration level of converters, oscillations will firstly be seen before the system collapses. Such marginal unviable cases will be introduced in detail in Chapter 4. Note that indicators mentioned above will be measured for both SG and DQCI converter.

For different types of test events, the instability detection mechanism will be activated with certain time delay following the event, so that the actual instability can be detected rather than the system dynamic response during the recovery time period. In this work, the TPS searching is activated 1.5 s after the load step event, and 5 s after the fault event.

There have been several types of instantaneous penetration level definitions discussed in literature such as [6-8], where either a specific equation has been developed for instantaneous penetration level, or a set of capacity values for implemented non-synchronous devices are stated. Examples for instantaneous penetration level equation are shown in formulas (3-1)~(3-3), where P_{NSG} and S_{NSG} are the combined active power output and apparent power rating of all of the NSG, P_{SG} and S_{SG} are the combined active power output and apparent power rating of all the SGs, P_{Demand} is the total system demand, P_{HVDC_import} is the imported active power into the network via HVDC links (as part of the total NSG output power in the system), and P_{HVDC_export} is the exported active power from the power network via HVDC links (as an element of total system demand).

$$\frac{P_{NSG}}{P_{Demand}} \times 100\% \tag{3-1}$$

$$\frac{S_{NSG}}{S_{SG} + S_{NSG}} \times 100\% \tag{3-2}$$

$$\frac{P_{NSG} + P_{HVDC\_import}}{P_{Demand} + P_{HVDC\_export}} \times 100\% \tag{3-3}$$

Generally, when exploring the effects of various factors/converter controllers on the tipping points, the trends of penetration level should be similar regardless of which definition is used. However, in order to achieve a meaningful TPS result based on a certain definition, it is important to consider how the operating conditions of a power system are defined. For example, using definition (3-1), it would be preferable to fix the value of demand in order to have a common denominator in all calculations but it is not a realistic assumption as demand in a power network fluctuates significantly during the day. Therefore, in this thesis, definition (3-2) is used for the APS model in Matlab, which is defined as the ratio of VA ratings of the NSG to the total generation ratings (those of the NSG and SG) in a power network. In such way, while conducting the TPS studies, system rating is defined and fixed, which is closer to the reality as the total capability of installed generation should be a known value and generally does not change continuously unless one is commissioned or decommissioned. And the definition (3-3) is used for the RGBT model in PowerFactory which includes the import and export power through the international HVDC links.

3.3 Simulation models

For studies of tipping points for converters, appropriate APS model is necessary which should fulfil following requirements:

- It should contain detailed representative models of different generation types with their corresponding controllers, and basic infrastructure such as loads and transmission lines. The focus of this thesis is the converter interaction with the AC grid it is connected to, and effects of penetration of converters on system

stability at transmission level. Therefore, it is assumed that DC side of the converters are well controlled, i.e. DC link voltage stays at constant.

- Ratings and/or power output of the generators should be adjustable to achieve various penetration levels of converters and capable of conducting TPS studies. Moreover, for the APS models, parameters such as transmission line impedance can be configured either to be a fixed or a variable one, where the variable impedance reflects the realistic network condition changes when penetration of converters varies in a real network. In this work, line impedance following after a certain type of generation is set as per-unit values where higher penetration of this generation will lead to lower line impedance.
- Parameters in the network, including system impedance, generation/load settings, controller settings, and any other parameter of interest should be easily adjustable to make sure the effects of various factors on system tipping points can be investigated.
- As much as possible the simulation model should be computationally efficient as the search engine performs a great number of repeated simulations to identify the tipping points which should be completed within a reasonable timescale.

In this thesis, two power system models have been used; a RGBT model in DIgSILENT PowerFactory (provided by GB National Grid) and an APS model built in MATLAB SimPowerSystems. The RMS-simulation based RGBT model is an equivalent network model representing the GB National Electricity Transmission System built and used by GB National Grid for system analysis and research purposes. It has mainly been used in this thesis for quantifying system issues under high penetration of converters. In order to conduct system dynamic studies based on EMT-simulation and improve simulation efficiency, the APS model is built not only for studies of system stability issues, but also the studies of TPS and exploring of effects of various types of converter controllers on the tipping points.

3.3.1 RGBT model in PowerFactory

A 37-bus equivalent network representing the National Electricity Transmission System of GB (based on dynamic phasor-type RMS simulation) has been made available for the purposes of this research. The network was modelled in DIgSILENT

PowerFactory by GB National Grid and it is presented schematically on the transmission map in Figure 3-1. Each node in the model represents a part of the system and is composed of relevant generation (represented as a mix of different energy sources), demand and HVDC interconnectors. As shown in Figure 3-2, generators within each zone were catagorised by fuel type, including coal, gas, nuclear, oil, hydro, pump storage, marine, biomass, wind, interconnectors, and synchronous compensation or embedded SG if this option is selected (shown as 'others'), all of which are represented by SGs or static generators, including corresponding dynamic controllers as well as Static Var Compensators (SVCs)/static synchronous compensators (STATCOMs) to reflect system reinforcements under high NSG scenarios.

The estimated active and reactive power demand (including contribution from embedded generation) is modelled in each zone. Transmission lines are modelled where the overall impedance is derived based on the line topology in each zone. All conventional generation is fitted with a basic governor which provides a degree of frequency control. Appropriate excitation systems and AVR are selected for each fuel type.

As a number of assumptions are made in the creation of the reduced model, there will inevitably be limitations in terms of the accuracy of the obtained results. As a central substation is selected to represent the connection point of all generators contained in a specific zone, the electrical distance between individual generators is not captured, which could have an impact on the ability to capture local oscillatory modes. This RGBT model has been validated using the full GB model held by National Grid by conducting a series of tests including load flow and dynamic response. Thus, this reduced model is considered sufficient for the TPS studies in this thesis.

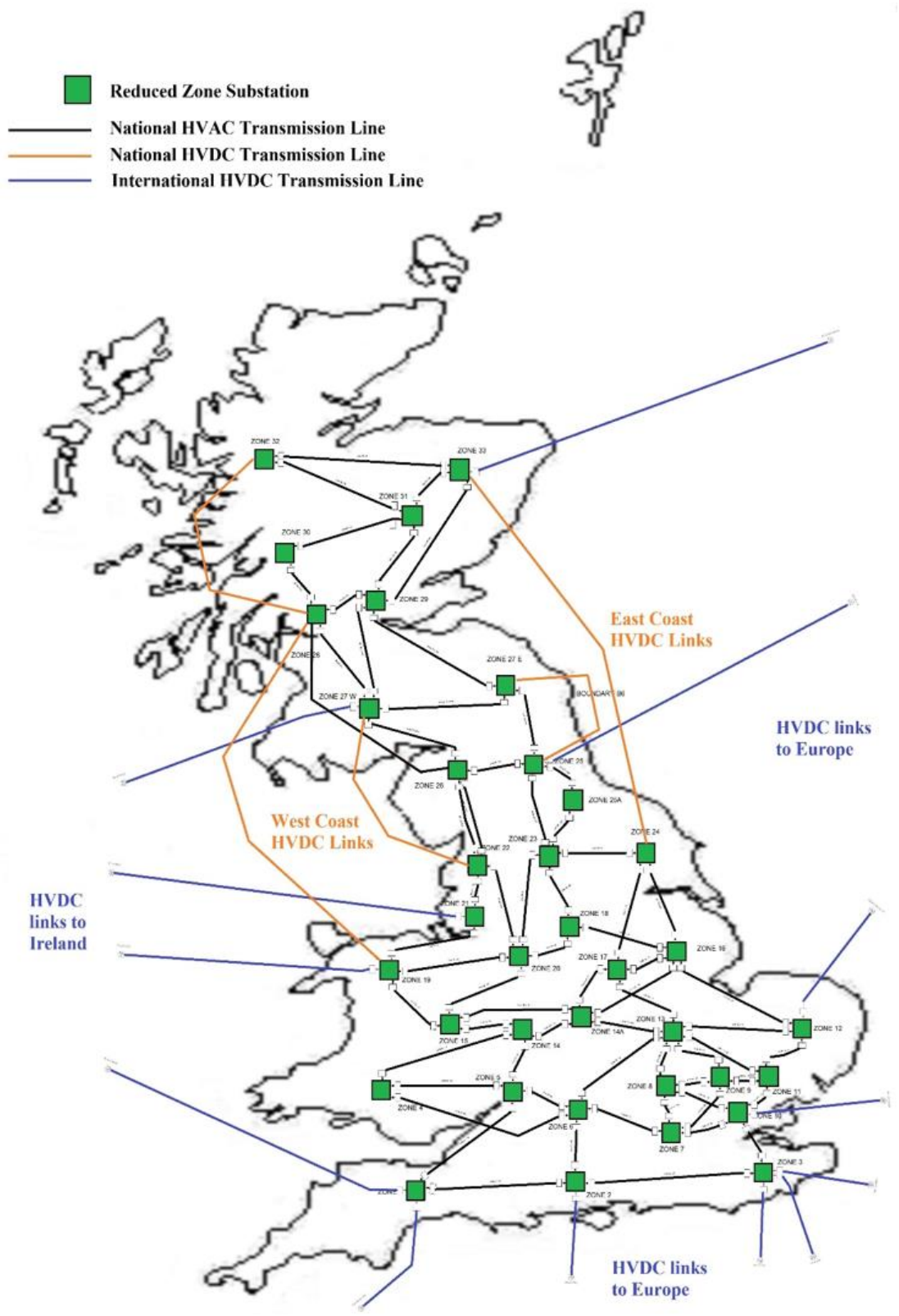

Figure 3-1. Reduced GB 36-bus/substation transmission model under 2030 Two Degrees Scenario in DIgSILENT Power Factory with UK map outline from [9]

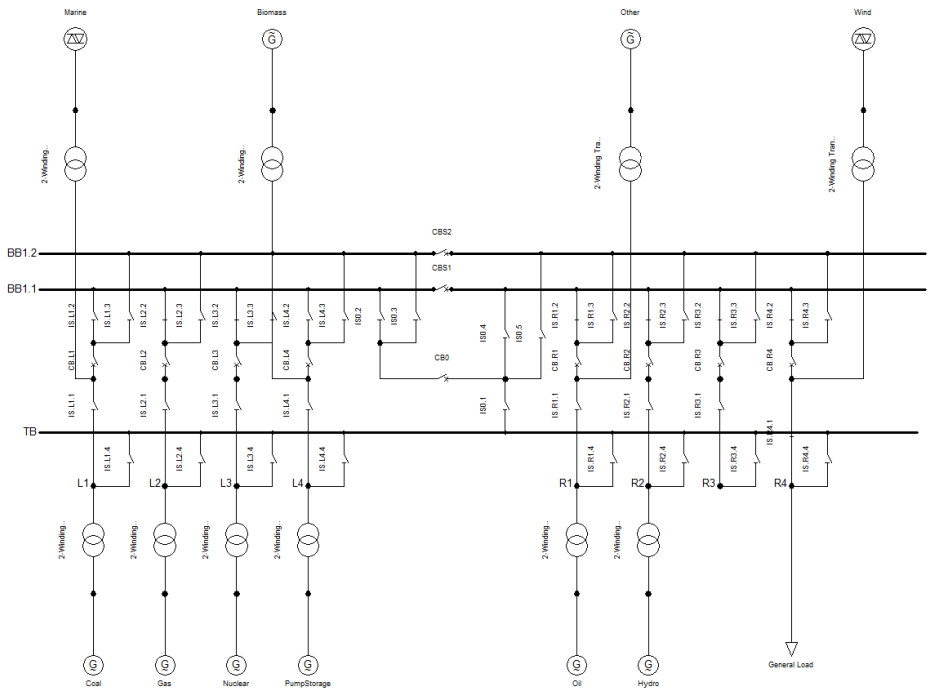

Figure 3-2. General layout of each substation in the RGBT model (HVDC interconnectors and static compensators are not shown)

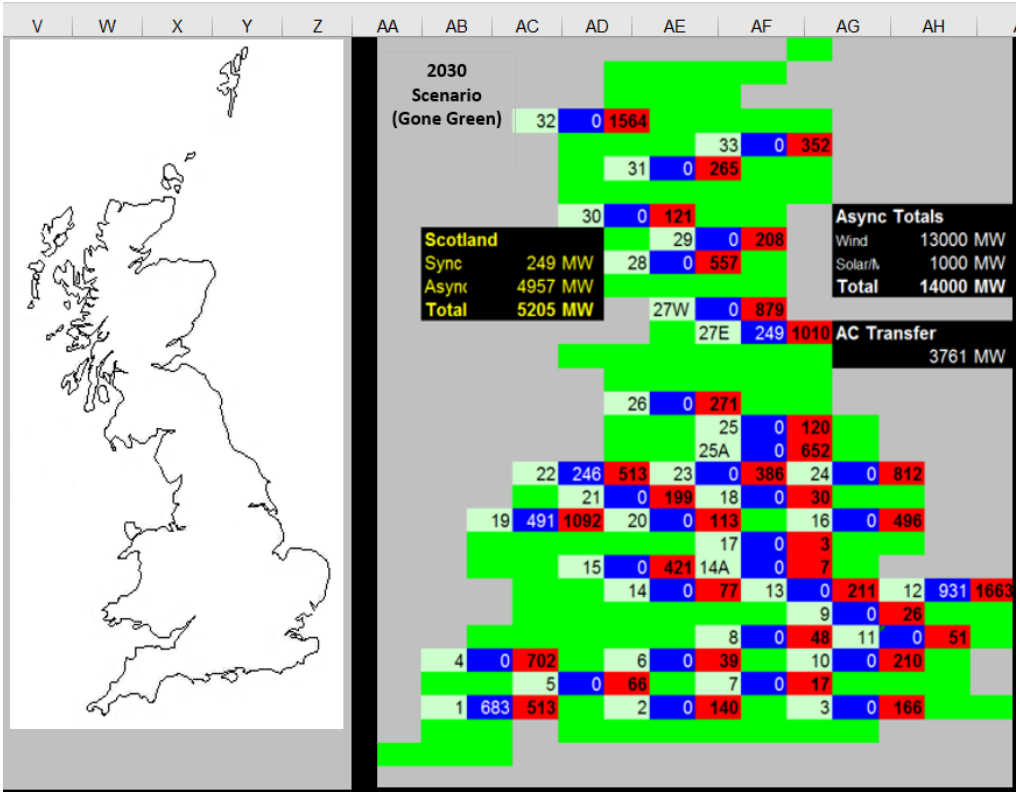

Figure 3-3. Example section of the spreadsheet for dispatching the generation in the RGBT model to achieve various instantaneous penetration levels

For the case studies in this thesis, the reduced GB model has been dispatched according to the GB 2030 Two Degrees scenario [10]. An Excel spreadsheet has been used to vary the proportion of power provided from SG and NSG to achieve different instantaneous penetration levels of NSG in the system, with an example snapshot shown in Figure 3-3. Generation are dispatched zone by zone, prioritizing by fuel type and scaling the MVA rating of each machine and step up transformer accordingly. Loads connected at each substation can be scaled similarly.

Studies in [6] have shown that the maximum penetration level of NSG is in the region of 65% of dispatched generation (MW), or 75% in terms of connected generation capacity (MVA) for the GB power system. These limits were established using the same RGBT model in DIgSILENT PowerFactory as used in this thesis.

3.3.2 APS model in MATLAB

In order to carry out dynamic studies over a wider range of frequencies, it is more suitable to utilise higher fidelity models with a smaller amount of generators, so that it is more focused on each of the types of the generators, rather than allowing simulations to become complicated and to have to incorporate an excessive amount of factors in the investigations and scenarios. Accordingly, an aggregated power network model based on EMT-simulation has been built in MATLAB SimPowerSystems, as shown in Figure 3-4. The model includes a single/aggregated SG, converter models with different types of controllers, transmission lines and loads.

A conventional synchronous machine model has been used in this model with standard IEEEG1 steam turbine and governor model [11] and AC1A excitation system applied on the control for the SG, operating at minimum loading of 60%. In this thesis, the main purpose is to study the interaction of converters with the AC grid and its maximum instantaneous penetration level into an AC network without leading to unstable situation. Therefore, it is of importance to be able to investigate the dynamics of the inverters and their impact on the AC grid. The model of a VSC-HVDC link is chosen (as it is the most common converter technology) to represent the non-synchronous devices in the network, i.e. the DQCI converter. As it is assumed that the DC link voltage is constant and well-controlled, a fixed DC voltage source is used to represent the rectifier

side of the link, as shown in Figure 3-5. Loading of the DQCI converter is set to 60% referred to [12, 13]. Conventional active and reactive power controllers are chosen as the outer controllers to achieve desired power flow in the system. To test the steady-state stability, a small load step of 1% with respect to the main load, is chosen. For transient stability testing a balanced three-phase solid fault is applied at the SG PCC with a fault clearance time set to 100 ms which is a typical expected clearance time at the transmission level in the GB network [2].

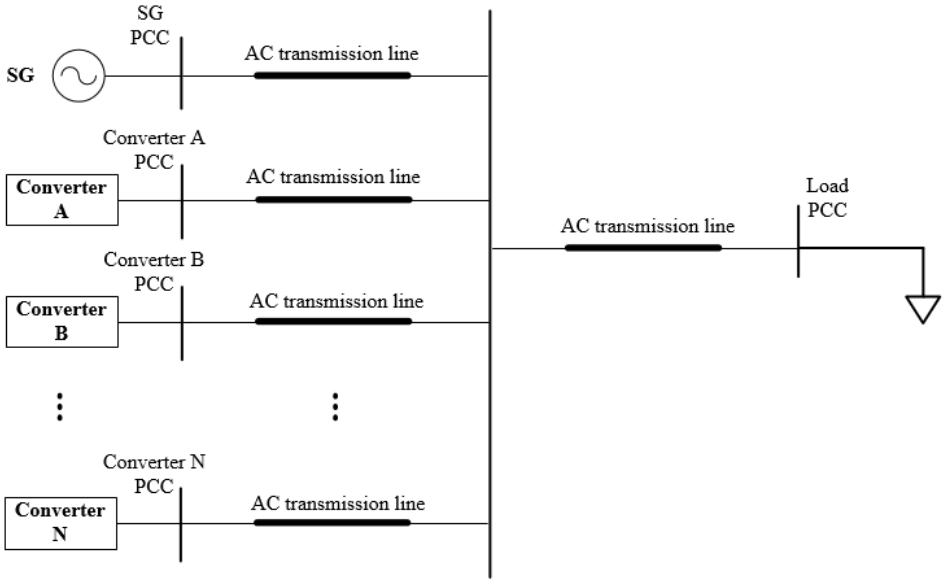

Figure 3-4. Configuration of the APS model in MATLAB SimPowerSystems

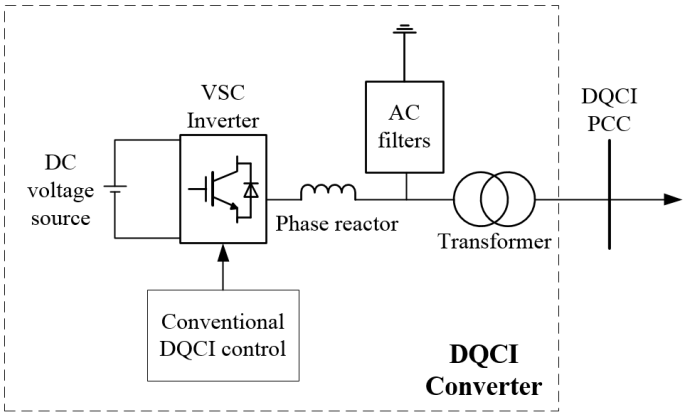

Figure 3-5. Model of DQCI converter in the APS model in MATLAB SimPowerSystems

One difficult aspect of simulating high penetration of converter-connected generation is that of initialising the simulation components, i.e. machines, governors, AVRs, and all converter components including PLLs and *dq*-axis control loops. The simulation of interest must not contain an infinite bus since frequency, voltage and power quality deviations from nominal are crucial part of the simulation. In this scenario, standard initialisation techniques based on load-flow solution are not sufficient. The approach taken in this thesis is to start the simulation with the base load, SG and an infinite bus initially connected together. Subsequently, the converter-based devices can be connected to the simulation, after their PLLs have synchronised with the voltage at the PCC. These devices are best added in the order of most-stable first, and least-stable last. The appropriate active and reactive power setpoints for each device can be estimated before the simulation, based upon the scenario load, the desired power split, and the droop slopes. However, the simulation model contains power losses, voltage drops, and line/transformer reactive power demands, which can be hard to estimate exactly until all the devices are connected and stabilised. Therefore, after all devices have been connected, small adjustments are made to the setpoints (termed as "power balancing control"), so that the active and reactive power exchange with the infinite bus reduces to almost zero, i.e. 0.002 p.u. based on the total system rating. Once this is achieved, the infinite bus can be disconnected from the simulation, and removing it should not introduce a significant disturbance to the system. The simulation after that point represents the behaviour of the network in the absence of any infinite bus, which may, or may not, be stable.

In the APS model, the instantaneous penetration level of converters is varied based on the VA ratings of the generations as shown in (3-2), with a fixed total system VA rating (including both SG and converters) of 60 GVA with reference to the GB system rating in 2016/17 [14]. The active power consumption of the main load is set as the sum of total active power from all generation, and the reactive power consumption is defined using the assumed power factor of 0.95 lagging. Therefore, when the instantaneous penetration level defined for converters in the APS model is increased, the VA rating as well as the actual power output from the DQCI converter are increased. Transmission lines are connected between each type of generation and the main load which are defined in per-unit (p.u.) with base power the same as the VA rating of the generation they are connected to.

3.4 NFP method

In a meshed AC electrical network with many generators and loads, fundamental frequency changes continuously and it is therefore important to gain understanding of how individual devices contribute to frequency stability and active power balance. This can be achieved by examining how a device responds to a change in network frequency. The novel NFP method described in this section facilitates a useful visualisation of the response of a device to variations in network frequency over a range of dynamic frequencies. A clear distinction can be observed between devices that provide frequency support through droop-slope type response and inertial-type response. Even though the method is not a classical stability assessment technique, the graphical representation is similar to the commonly used Bode type plots, and therefore, gives a useful and easily understood insight into the device's dynamic behaviour, and can offer indication of potential instability due to interaction of various types of devices at specific frequencies.

The NFP method places the device within a hypothetical or "test" power system in which frequency is forced and modulated in a sinusoidal fashion at frequency f_{NFPmod}, with a small amplitude Δf (1% is assumed in this thesis) about the nominal frequency f_0, which can be expressed as shown in equation (3-4).

$$f = f_0 + \Delta f \cos(2\pi f_{NFP\,\mathrm{mod}}) \tag{3-4}$$

The value of f_{NFPmod} changes from 10^{-3} Hz to 20 Hz. The device responds to this changing frequency with a modulated active power output, as shown in equation (3-5). Figure 3-6 gives a schematic illustration of the model setup used in NFP method.

$$P_{out} = P_{set} + \Delta P \cos(2\pi f_{NFP\,\mathrm{mod}} + \phi_{\Delta P}) \tag{3-5}$$

The amplitude of the frequency modulation Δf is kept small so that no unnatural saturation of device control loops occur. The active power amplitude modulation ΔP (in p.u.) and phase modulation $\Phi_{\Delta P}$ together form a response *R*, as defined in equation (3-6), when normalised to Δf.

$$R = \frac{\Delta P \angle \varphi_{\Delta P}}{\left(\frac{\Delta f}{f_0}\right)} \tag{3-6}$$

Due to the potential complexity of the systems being analysed, it may not be a trivial exercise to derive transfer functions representing the system dynamics, particularly in low inertia systems where PLL control systems are present in [15], with which Bode plots can be generated. Consequently, the combination of the time domain simulation, in which a frequency perturbation is applied (see Figure 3-6), with Fourier analysis will, in some situations, be easier to realise. In both cases, the amplitude of the voltage is assumed to remain constant at 1 p.u., so that the analysis is purely an examination of the interaction between active power and frequency. The NFP charts for amplitude and phase are plotted by setting on the x axis, and plotting the amplitude and phase of *R*.

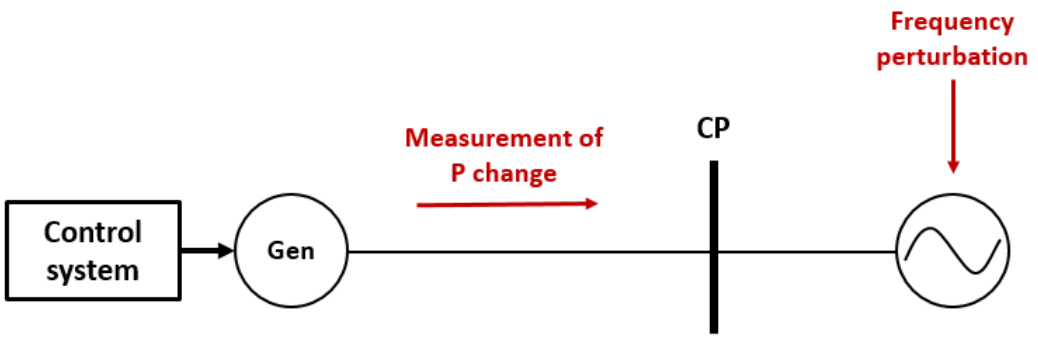

Figure 3-6. Illustrative schematic of NFP method where network frequency is perturbed and amplitude and phase of the active power change is measured

3.4.1 Linearised model of a SG

The analytical model of SG used for the NFP analysis is introduced in this section. In this thesis, the SG is modelled with the IEEEG1 steam turbine and governor model [11] as shown in Figure 3-7. For the purpose of the NFP analysis, the linearised model of SG, which is essentially the relationship between measured frequency f_{pu} and active power output P_e is derived based on the schematic shown in Figure 3-8. Six main transfer functions representing various functions of the SG are denoted in Figure 3-8.

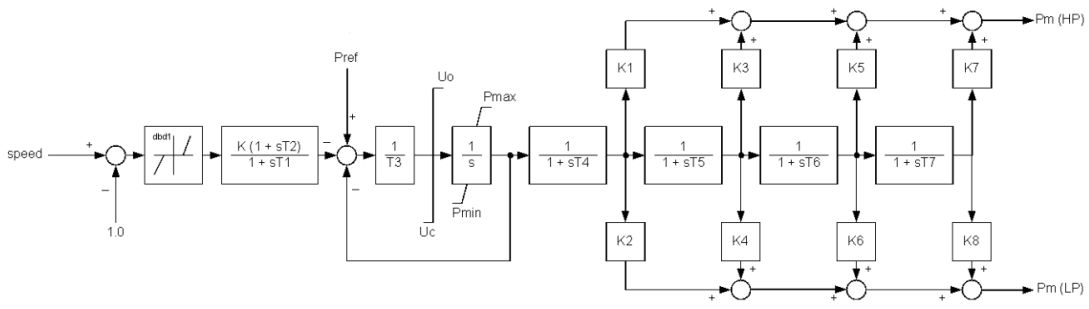

Figure 3-7. Diagram of the IEEEG1 steam turbine and governor model [11]

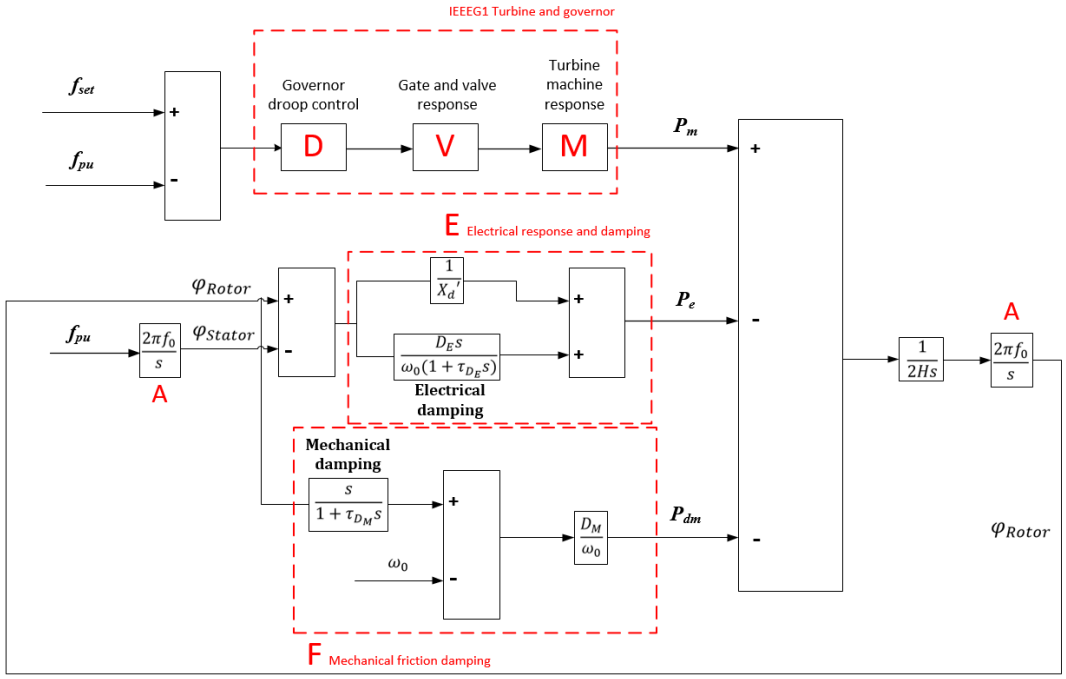

Figure 3-8. Schematic of the SG model in this thesis

Transfer function *A(s)* represents the derivation of angle (rad/s) from measured frequency (pu) with transfer function written as in (3-7), where f_0 is the nominal frequency in Hz. The stator angle φ_S is derived from the measured frequency (pu) based on *A(s)* and rotor angle φ_R is taken from the output of the SG.

$$A(s) = \frac{2\pi f_0}{s} \tag{3-7}$$

The operating principles of the electrical part in the SG as well as the electrical damping are represented by *E(s)* as shown in (3-8). The first part of *E(s)* is the

representative of the power-angle relationship discussed in (2-1) assuming sinδ≈δ and both generator terminal voltage and voltage at the connection point of the SG to the network are 1 pu. X'_d is the transient reactance of the SG in pu. The second part of *E(s)* represents the electrical damping of the machine whose amount is limited by physical constraints on the damper windings and also on electrical losses associated with them. D_E is the electrical damping factor, τ_{DE} is the time delay simulated for the electrical damping, and ω_0 is the nominal frequency in rad/s. Similarly, the mechanical damping is represented in (3-9) while the mechanical damping factor D_M is fairly low as for any real synchronous machine with significant mechanical damping, i.e. friction or viscous windage, would be rejected on efficiency grounds.

$$E(s) = \frac{1}{X'_d} + \frac{D_E s}{\omega_0 (1 + \tau_{D_E} s)} \tag{3-8}$$

$$F(s) = \frac{D_M s}{\omega_0 (1 + \tau_{D_M} s)} \tag{3-9}$$

Based on the diagram of IEEEG1 turbine and governor shown in Figure 3-7, it can be divided into three sub-parts to represent the functions of governor droop control *D(s)*, fate and valve response *V(s)*, and turbine machine response *M(s)*, whose transfer functions are shown below in (3-10), (3-11) and (3-12) with standard time constants *T* and gains *K* set with reference to [11], and D_f is the frequency droop gain in percentage (pu/pu) set as 4% as default.

$$D(s) = \frac{1 + sT_2}{(1 + sT_1) D_f} \tag{3-10}$$

$$V(s) = \frac{1 + sT_4}{1 + sT_3} \tag{3-11}$$

$$M(s) = K_1 + \frac{K_3}{1 + sT_5} + \frac{K_5}{1 + sT_6} + \frac{K_7}{1 + sT_7} \tag{3-12}$$

The relationship between rotor angle φ_R and active power output is shown in (3-13), with representations of mechanical power output from the turbine and governor model

P_m, electrical power output P_e and mechanical damping power P_{dm} expressed in (3-14), (3-15) and (3-16) respectively.

$$\varphi_R = \frac{A}{2Hs}(P_m - P_e - P_{dm}) \tag{3-13}$$

$$P_m = MVD(f_{set} - f_{pu}) \tag{3-14}$$

$$P_e = E(\varphi_R - \varphi_S) \tag{3-15}$$

$$P_{dm} = F\varphi_R \tag{3-16}$$

The relationship between rotor angle φ_R and stator angle φ_S can then be derived as shown in (3-17).

$$\frac{\varphi_R}{\varphi_S} = \frac{AE}{2Hs + MVD + A(E+F)} \tag{3-17}$$

Considering (3-7), (3-15) and (3-17), the relationship between electrical power output Pe and measured frequency fpu can be expressed as below shown in (3-18).

$$\frac{P_e}{f_{pu}} = AE(\frac{\varphi_R}{\varphi_S} - 1) = -AE\left[\frac{2Hs + MVD + AF}{2Hs + MVD + A(E+F)}\right] \tag{3-18}$$

Therefore, the NFP responses in both magnitude and phase can be analysed when the network frequency is perturbed.

3.4.2 Key trendlines

On the NFP plots, the x axis is the dynamic frequency of a network perturbation that is applied to the device, and the y axis shows the ΔP magnitude and phase respectively, which the device responds with. On the chart there are three key features, plus a number of more subtle details which can be interpreted to give further understanding of the device response, as shown in Figure 3-9 (a) and (b), for amplitude and phase respectively, which are explained in detail in this section. Note that asymptotes R_{Droop}, R_H and R_{HD} shown in Figure 3-9 are obtained from classical linear analysis.

Firstly, if the generator is configured with a governor and frequency droop, this creates an asymptote where $R \rightarrow 1/D_f$ as $f_{NFP\ mod} \rightarrow 0$ where D_f is the frequency droop slope. If the governor and droop slope are operating correctly, the device response must approach this asymptote, as the frequency of the perturbation tends to zero, which is illustrated as response R_{Droop}. The amplitude of R_{Droop} is expected to stay at 25% of ΔP. This is due to 1% network frequency change with the assumed 4% frequency droop slope. At the same time the phase tends to 180° due to the inverse relationship between active power and frequency in the drooped control arrangement.

At lower frequencies on the x axis, the plots reveal the combined effect of droop control, together with governor and prime-mover response (in the frequency range 0~0.2 Hz on the x axis, i.e. response time longer than 5 s).

The effects in the frequency range of 0.2~2 Hz, i.e. time response between 0.5 s and 5 s, represent rotor dynamics and everything that would be encompassed in any device

$$R_H = -j2H\left(\frac{f_{NFP\,\mathrm{mod}}}{f_0}\right) \tag{3-19}$$

claiming to provide true inertia. This creates a second key asymptote R_H as depicted in Figure 3-9 (drawn for the idealistic synchronous machine without damping), and is expressed by equation (3-19). The response must intercept this asymptote (in both amplitude and the 90 phase advance relative to the droop asymptote R_{Droop}).

One key point about the true inertia is that by definition, rotor angle has a 2nd-order transfer function relationship with active power (refer to the swing equations introduced in section 2.5.2), i.e. perform as resonance due to the finite value of inertia constant H. Such resonance is unavoidable in any device which provides true inertia and must be damped to avoid sustained oscillations, as in a real synchronous machine.

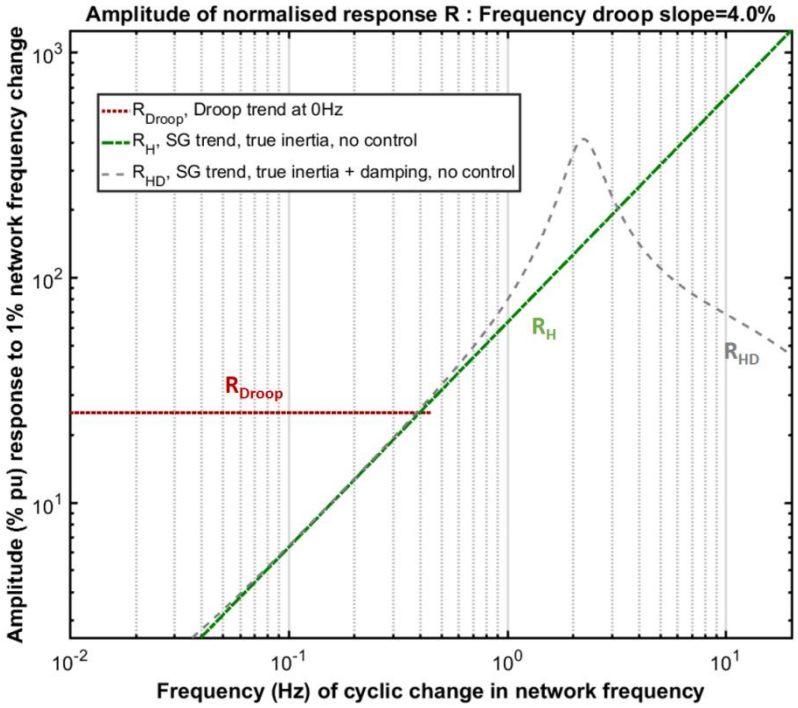

(a) Amplitude chart

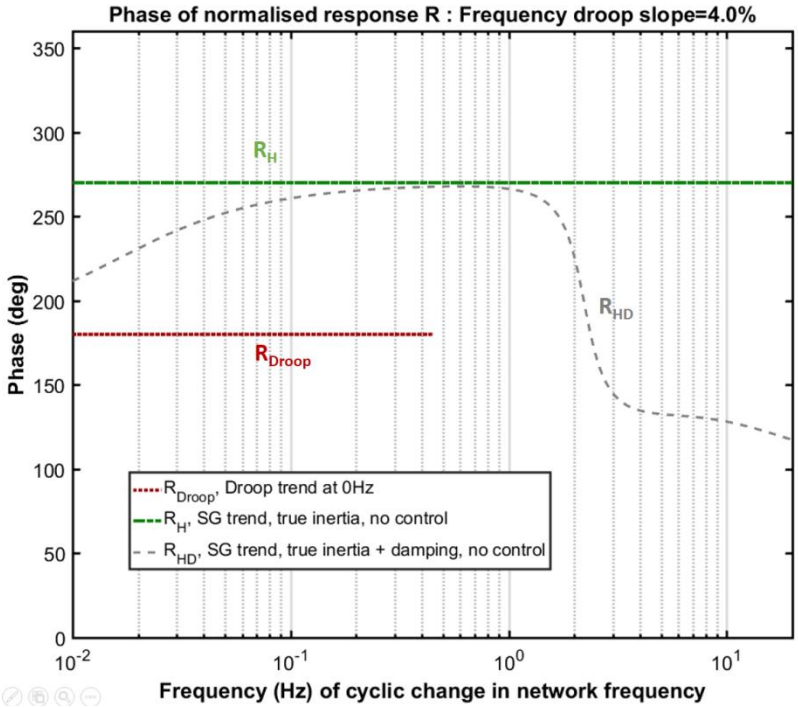

(b) Phase chart

Figure 3-9. Illustration of the key featured responses *R* introduced by the NFP method based on linear analysis method

The third key feature is that for any device which intercepts the inertia asymptote R_H, there must be a resonant peak that occurs, typically in the region of 1-3 Hz. The resonant frequency is dependent on inertia (real or synthetic), impedance X_d' and damping (real or synthetic), and is shown as response R_{HD}. Both responses R_H and R_{HD} are presented with the assumption that there is no governor controller attached to the generator (i.e. the machine operates like a synchronous compensator or a flywheel). NFP response plots of SG and DQCI converter with all associated controllers will be introduced and analysed in Chapter 4.

One important bi-product of the 2-nd order transfer function relationship in a real synchronous machine is that there is an upper bandwidth (in terms of modulations of network frequency) at which the swing equation is applicable. This upper bandwidth is bounded by the rotor resonant frequency, generally in the 2~5 Hz region for normal values of H (2~10 s) and X_d' (~0.1 p.u.). Meanwhile, for low modulation frequencies of the network, i.e. < 0.1~0.2 Hz, the inertial contribution drops towards zero and instead the effect of droop settings and governor response become dominant.

3.5 Summary

In this chapter, two types of power system models used in this thesis have been introduced and discussed. The RMS-simulation based RGBT model in DIgSILENT PowerFactory will be used for studies of system stability under high penetration of converters, and further studies considering the effects of various types of converter controllers will be carried out in the EMT-simulation based on APS model in MATLAB SimPowerSystems.

The TPS method applied for investigations of tipping point has also been described with a set of detection criteria on system indicators including frequency, voltage, voltage THD, locking signal in the DQCI converter control and voltage flicker perception level designed specifically to capture the instability introduced by high penetration of converters.

A frequency-domain analysis tool, NFP method, has been presented which can be used to compare response of converters with different types of control with that of a SG, with three key featured responses such as droop, inertia and damping.

References

[1] Ofgem, "Distribution Code G59," 2015. Available: https://www.ofgem.gov.uk/licences-codes-and-standards/codes/electricity-codes/distribution-code, accessed in 2017/2/1.

[2] National Grid (GB), "The Grid Code," 2016. Available: http://www2.nationalgrid.com/UK/Industry-information/Electricity-codes/Grid-Code/, accessed in 2017/5/25.

[3] ENSTO-E, "Network Code for Requirements for Grid Connection Applicable to all Generators," 2016. Available: https://www.entsoe.eu/major-projects/network-code-development/requirements-for-generators/Pages/default.aspx, accessed in 2017/5/25.

[4] BSI, "BS EN 61000-4-15:2011 Electromagnetic compatibility (EMC)," July 2011.

[5] L. Zhang, "Modeling and Control of VSC-HVDC Links Connected to Weak AC Systems," School of Electrical Engineering (EES), Electrical Machines and Power Electronics, KTH, Stockholm, 2010, Available: http://www.diva-portal.org/smash/record.jsf?pid=diva2%3A322475&dswid=1654, accessed in 2017/5/24.

[6] H. Urdal, R. Ierna, Z. Jiebei, C. Ivanov, A. Dahresobh, and D. Rostom, "System strength considerations in a converter dominated power system," *IET Journal on Renewable Power Generation,* vol. 9, pp. 10-17, 2015.

[7] M. Yu, A. J. Roscoe, C. D. Booth, A. Dysko, R. Ierna, J. Zhu, and H. Urdal, "Use of an Inertia-less Virtual Synchronous Machine to Stabilise Networks with High Penetrations of Converters," in *Power Systems Computation Conference (PSCC)*, Genoa, Italy, 2016.

[8] J. O'Sullivan, A. Rogers, D. Flynn, P. Smith, A. Mullane, and M. O'Malley, "Studying the Maximum Instantaneous Non-Synchronous Generation in an Island System: Frequency Stability Challenges in Ireland," *IEEE Transactions on Power Systems,* vol. 29, pp. 2943-2951, 2014.

[9] UK Electrical Network Strategy Group, "Our Electricity Transmission Network: a Vision for 2020," February 2012. Available: https://www.gov.uk/government/uploads/system/uploads/attachment_data/file/48274/4263-ensgFull.pdf, accessed in 2017/12/1.

[10] National Grid (GB), "Future Energy Scenario," 2015. Available: http://fes.nationalgrid.com/, accessed in 2017/3/1.

[11] IEEE Power & Energy Society (PES), "Dynamic Models for Turbine-Governors in Power System Studies," 2013. Available: http://sites.ieee.org/fw-pes/files/2013/01/PES_TR1.pdf, accessed in 2017/4/3.

[12] EirGrid, "All-Island Generation Capacity Statement 2016-2025," 2016. Available: http://www.eirgridgroup.com/site-files/library/EirGrid/Generation_Capacity_Statement_20162025_FINAL.pdf, accessed in 2017/4/3.

[13] UK House of Parliament, "Postnote 464: Intermittent Electricity Generation," 2014. Available: http://researchbriefings.parliament.uk/ResearchBriefing/Summary/POST-PN-464, accessed in 2017/4/5.

[14] National Grid (GB), "Electricity Ten Year Statement," 2015. Available: http://www2.nationalgrid.com/UK/Industry-information/Future-of-Energy/Electricity-Ten-Year-Statement/, accessed in 2017/3/1.
[15] A. D. Giles, A. J. Roscoe, and L. Recalde-Camacho, "Assessment of HVDC control algorithms for weak and strong AC systems," *IEEE Transactions on Power Systems,* vol. 14, 2018 (under review).

Chapter 4

Instability and Tipping Points with DQCI Converters

4.1 Introduction

In this chapter, system instability introduced by high penetration converters will be investigated in both the RMS-simulation based RGBT model in DIgSILENT PowerFactory and the EMT-simulation based APS model in MATLAB SimPowerSystems, along with the system tipping points in terms of transient stability and small signal stability. A sensitivity analysis investigating the effects of various selected factors including system inertia, system impedance, DQCI converter capacity factor and non-linear rectifier load on the tipping points is presented. Most of the sensitivity is analysis is conducted using the APS model due to the lower computational cost and preferable modelling flexibility.

4.2 Instability introduced by converters

Traditionally, power system stability analysis has been based on the physics of electrical machines. This is because power systems have, historically, been mostly powered by synchronous machines. However, as power systems transition from the classical (SG dominated) power system to a converter dominated system, the validity of the traditional analysis is called into question; accordingly, a revised approach to stability analysis is required which accounts for the converters and their control systems, i.e. the TPS method introduced in this thesis. In this section, system instabilities introduced by high penetration of converters will be demonstrated.

4.2.1 RGBT model in DIgSILENT PowerFactory

The RMS-simulation based RGBT model in DIgSILENT PowerFactory reflects the generation capacity under 2030 Two Degrees scenario; the simulation has a sampling time of 0.5 ms. A three-phase solid fault is applied on two of the four HVAC England-Scotland interconnectors (lines between Zone 26 and Zone 27 W shown in Figure 3-1) to test the system stability, i.e. the N-2 criterion (one of the common test cases chosen by GB National Grid as stated in [1]). This fault is applied at different instantaneous penetration levels, where the instantaneous penetration level is defined by equation (3-3) which involves import/export power from HVDC transmission systems.

In the RGBT model, a variety of case studies are considered including all combinations of the following influencing factors: varied NSG, varied demand level, and varied import and export from international HVDC links as shown below and also in Table 4-1.

- High (37 GW), Medium (30 GW) and Low (24 GW) RES production from 73 GW of installed capacity;
- 30 GW, 35 GW and 40 GW demand compared with present variation from 18 GW to 60 GW;
- 0 GW HVDC import/export, 3 GW HVDC import and 10GW export, and 10 GW HVDC export only.

The fault event is applied at 1 s with a duration of 140 ms [2] and total simulation time is 5 s. When the instantaneous penetration level of the DQCI converters is low, the system is able to return to normal operation shortly after the fault clearance as shown in Figure 4-1. However, as the instantaneous penetration level increases, transient instability and even small signal instability occur as can be observed in Figure 4-2 and Figure 4-3 respectively. For the transient instability case shown in Figure 4-2, the system is able to maintain normal operation before the fault is applied; however, the system becomes unstable after the fault, indicating a loss of synchronism within the network. When the instantaneous penetration level is increased further, the system becomes unstable even before the fault event as can be observed in Figure 4-3. In this scenario, steady state stability cannot be maintained. It is noticeable that the waveforms, immediately after the loss of stability, contain high frequency components which are different from typical transient instability cases with conventional SGs. This highly nonlinear unstable response can sometimes lead to numerical converge issues at a later stage of the simulation which is sometimes unable to complete, such as that shown in Figure 4-2.

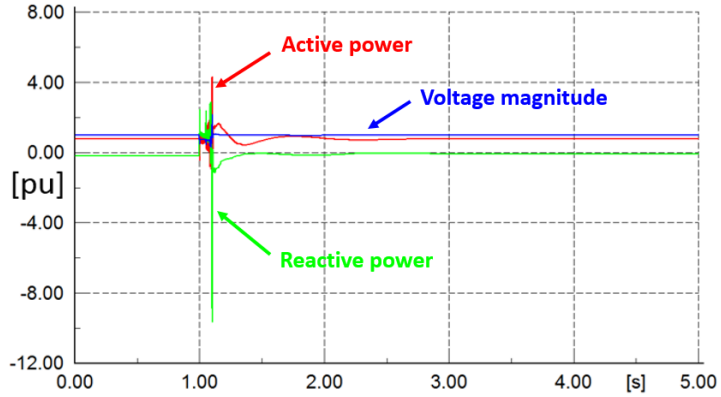

Figure 4-1. Active power, reactive power and terminal voltage for a Scottish SG in the RGBT model under a stable case with converter penetration level slightly below tipping point

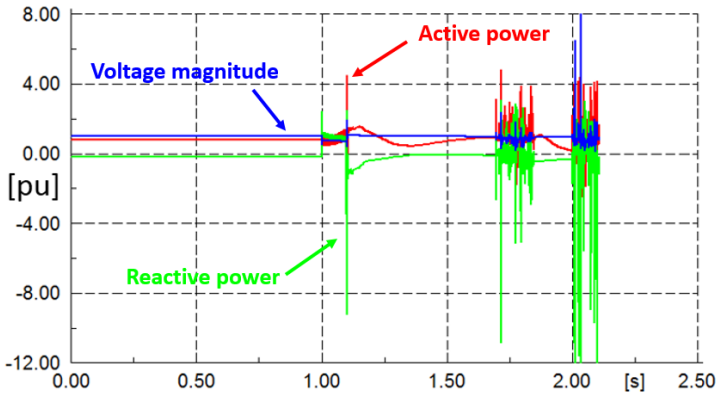

Figure 4-2. Active power, reactive power and terminal voltage for a Scottish SG in the RGBT model under an unstable case with converter penetration level slightly above tipping point

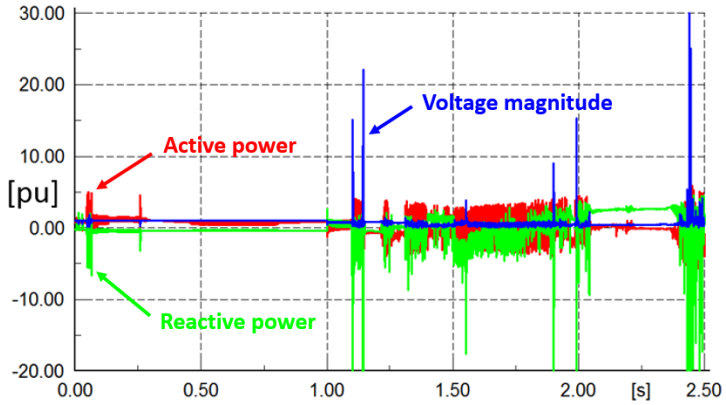

Figure 4-3. Active power, reactive power and terminal voltage for a Scottish SG in the RGBT model under an unstable case with converter penetration level significantly above tipping point

Table 4-1. Operating range in relation to NSG%, demand, and HVDC import and export in the RGBT model in DIgSILENT PowerFactory (✓ stands for the presence of stability and ✕ stands for the absence of stability)

Instantaneous penetration level of NSG	**No HVDC Import/Export**			**3GW HVDC Import 10GW HVDC Export**			**No HVDC Import 10GW HVDC Export**		
	Load (GW)			Load (GW)			Load (GW)		
	40	35	30	40	35	30	40	35	30
Low (24 GW)	✓	✕	✕	✓	✓	✕	✓	✓	✓
Medium (30 GW)	✕	✕	✕	✓	✕	✕	✓	✓	✕
High (37 GW)	✕	✕	✕	✕	✕	✕	✕	✕	✕

Table 4-1 shows the system stability thresholds in terms of instantaneous penetration level of NSG for varied system demand level and HVDC import/export in GB power system. It can be seen clearly that the instantaneous penetration level of NSG could have a significant impact on system stability; indeed, all cases with a "High" instantaneous penetration level of DQCI converters appear to be unstable. Using the definition of instantaneous penetration level adopted in this thesis, when the demand level in the network decreases, the instantaneous penetration level of NSG increases; thus, it is no surprise that the system tends to become more unstable.

Owing to seasonal variations in wind, solar radiation, weather and human activities (energy consumption wise), the daily demand profile varies from season to season. As a result, the instantaneous penetration level of NSG also changes continually and the network could potentially reach a tipping point. Meanwhile, power flows via HVDC links in and out of the GB power system could also have an impact on the system stability; this is particularly true when the HVDC is exporting power since it leads to lower instantaneous penetration level of NSG and therefore higher system tipping points.

Tipping points found in the RGBT model with the base settings are approximately 70% for transient stability and 85% for small signal stability in terms of dispatched MW based on equation (3-3).

4.2.2 APS model in MATLAB SimPowerSystems

The system instability has been found in the higher-fidelity EMT-simulation based APS model in MATLAB. Similarly, a small load step (1% with respect to rating of the main load) is used to test the system small signal stability, and a 140 ms three-phase solid fault is applied in the middle of the system to test the transient stability.

As introduced in 3.3.2, an infinite bus is connected at the beginning of the simulation to assist model initialisation, which will be disconnected when power (both active and reactive) contributed from the infinite bus is shared by the generation, i.e. smaller than 0.01 p.u. based on the system MVA rating for 1 s. Total simulation time is 30 s and the test events are applied at 20 s where the system is expected to be stable following the initialisation process. Note that the APS model is configured according to the base case (with setups summarised in Appendix A).

Infinite bus control is activated 2 s after the DQCI converter is switched on, which will distribute the active and reactive power output from the infinite bus to each type of generation (SG and DQCI converter in this case). This way, when the infinite bus is disconnected, there will not be a significant disturbance to the network which itself could lead to instability. As seen in Figure 4-4, both the SG and converter operate satisfactorily during the initialisation process where frequency and voltage is controlled within the desired operational range. Note that the voltages measured at both the SG and converter terminals are 1 p.u. before the power balance control is activated, after which the voltage set points of both the generator and converter have been adjusted to fulfil the requirements of reactive power flow including losses on the transmission lines and transformers. No significant disturbance is introduced by the process of removing the infinite bus from the system (which occurs at ~7.4s).

In terms of small signal stability (with load step test), at relatively low penetration levels, the system operates satisfactorily as shown in Figure 4-4. When the load step event is applied at 20 s, both SG and DQCI react to the event due to their control systems (governor and AVR control for the SG, and frequency and voltage droop control for the DQCI-controlled converter) and get back to a small signal quickly after the event. The PLL is able to maintain satisfactory synchronization during the entire simulation, which indicates a stable operation of the converter control system.

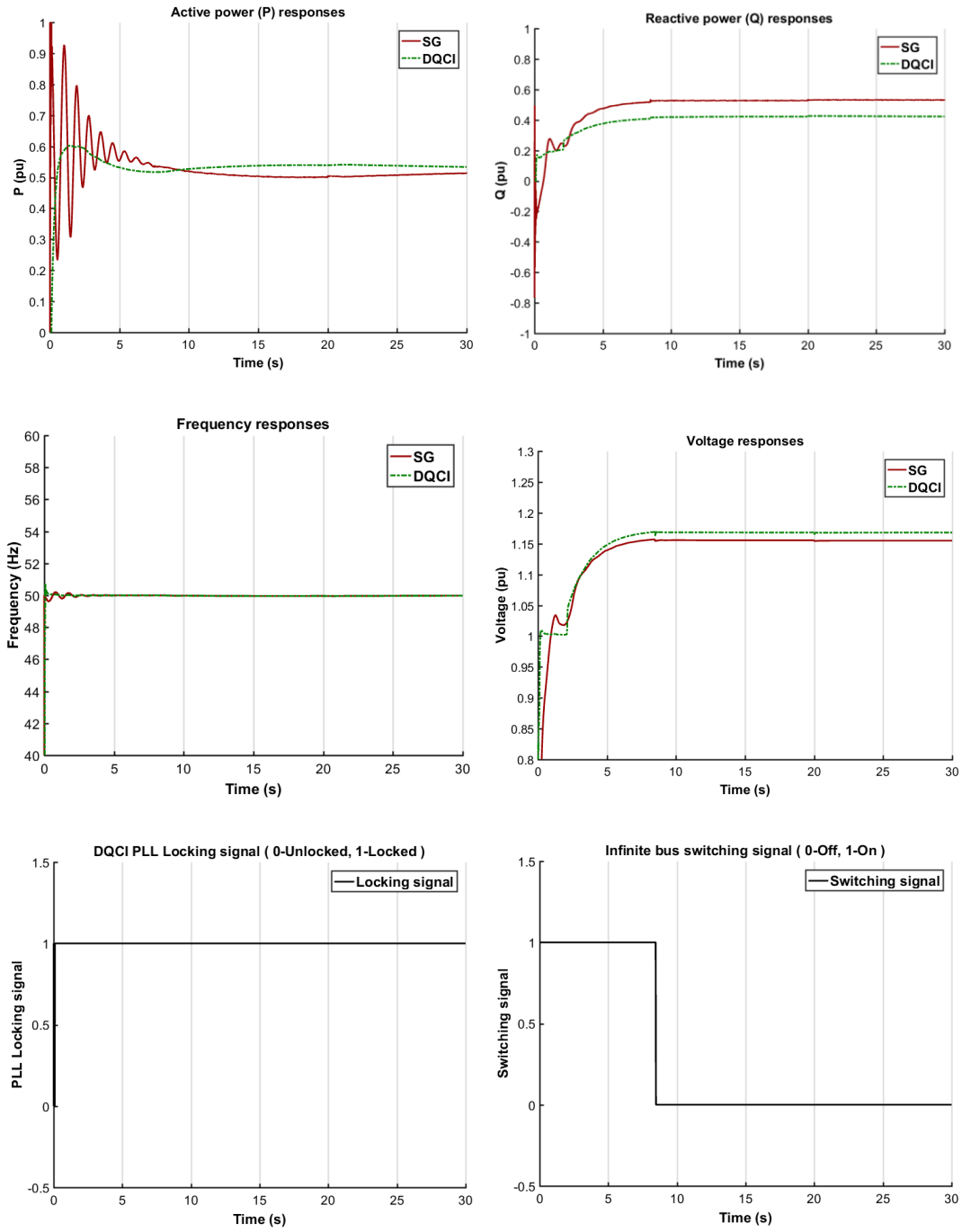

Figure 4-4. System performance for an example under a stable case with converter penetration level below tipping point for small signal stability (60% instantaneous penetration level based on generation VA ratings)

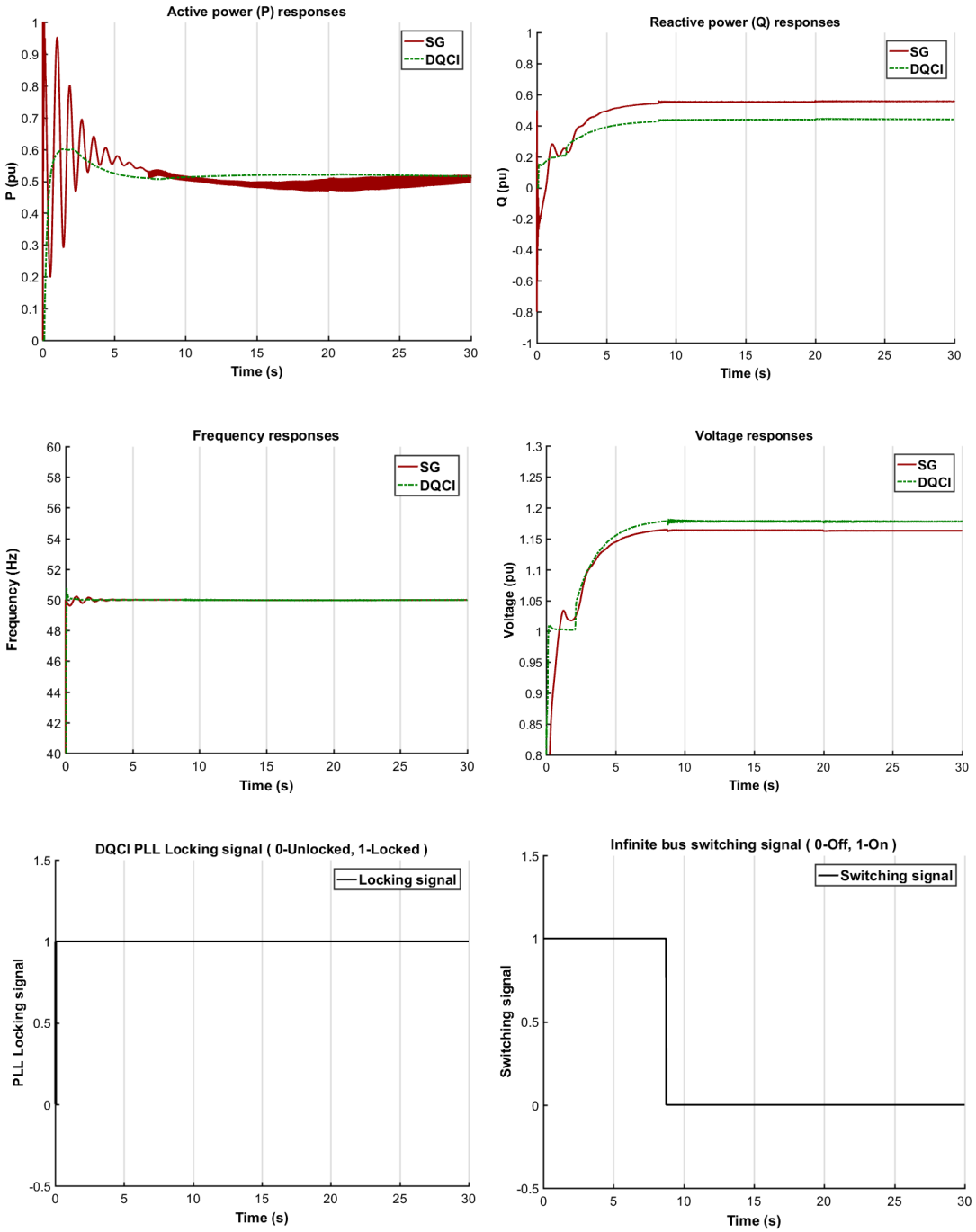

Figure 4-5. System performance for an example under a stable case with converter penetration level slightly below tipping point for small signal stability (71% instantaneous penetration level based on generation VA ratings)

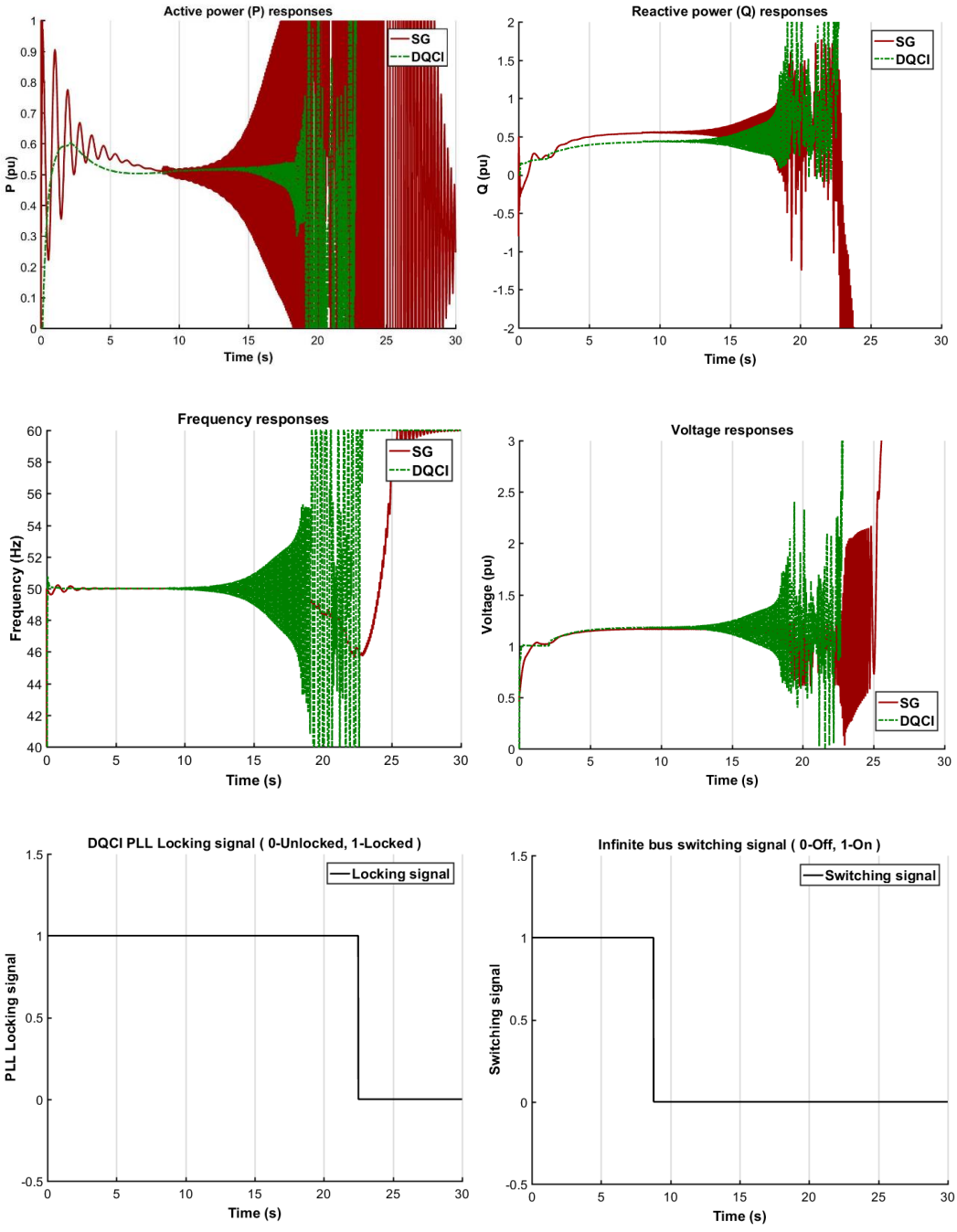

Figure 4-6. System performance for an example under an unstable case with converter penetration level slightly above tipping point for small signal stability (72% instantaneous penetration level based on generation VA ratings)

As the instantaneous penetration level increases, increasing oscillations following after the infinite bus disconnection and load step events can be seen in the power outputs and terminal voltages. Figure 4-5 demonstrates a marginally stable scenario in which large, but decaying, oscillations can be seen following islanding of the network.

However, as the instantaneous penetration level increases further, significant oscillations whose amplitudes grow with time (as opposed to decay in the previous scenario) are found in the system frequency, voltage and power outputs from the generation after the initialisation stage as shown in Figure 4-6. The fact that the system cannot even survive the disconnection of the infinite bus, which in this setup is equivalent to a very small load step, definitively demonstrates that small signal stability is compromised in weak systems. It should be noted that under these conditions, the frequency of DQCI converter ramps between 40 Hz and 60 Hz which is a result of the frequency limitations applied to the PLL. In this case, this is where a tipping point is reached. It is obvious that almost all the stability indicators introduced in the TPS method are expected to be tripped in this unstable case, such as frequency, RoCoF, voltage, flicker perception level, and converter PLL locking signal. Voltage THD levels do not exceed the operation limitation as there is no harmonic content existed.

A similar phenomenon has been found with the transient stability (with the fault test) as shown in Figure 4-7~Figure 4-9, where system performance under stable, marginally stable, and marginally unstable cases are displayed respectively. With a relatively low penetration level of the converters, it can be seen that both the SG and DQCI converter behave satisfactorily without the infinite bus connected to the network; furthermore, the generator and converter are both able to survive the 140ms three-phase fault, returning to steady state operating conditions quickly after the disturbance. In marginally stable cases, the system can still continue normal operation before the fault event; the generator and converter are able to return to steady state after the disturbance as well; however, significant oscillations can be seen in the generation power outputs, terminal voltages and frequencies. As the instantaneous penetration level increases, the instability started to present and the oscillations grow with time. Tipping points found in the APS model based on the base model are 71.5% for small signal stability and 65.8% for transient stability.

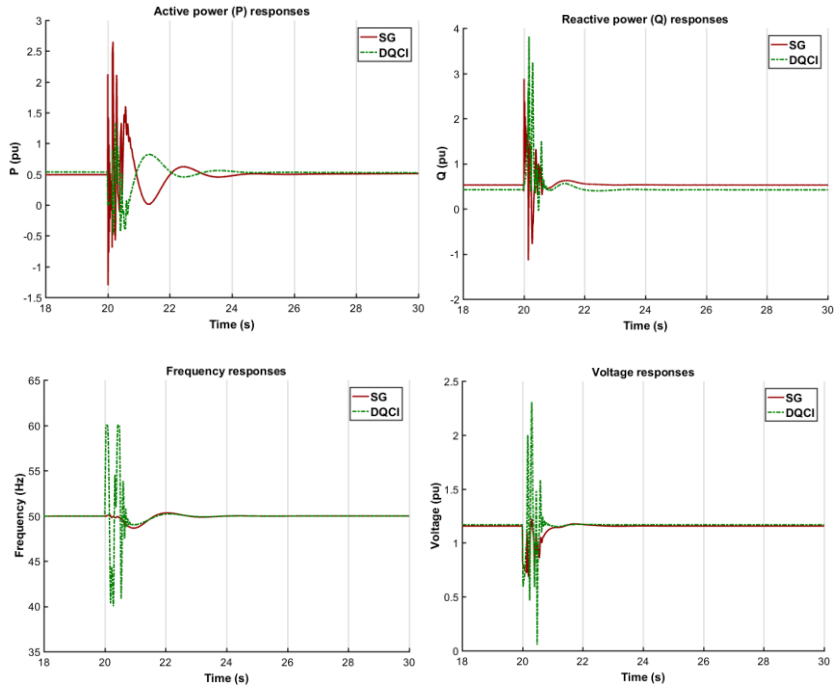

Figure 4-7. System performance for an example under a stable case with converter penetration level below tipping point for transient stability (60% instantaneous penetration level based on generation VA ratings)

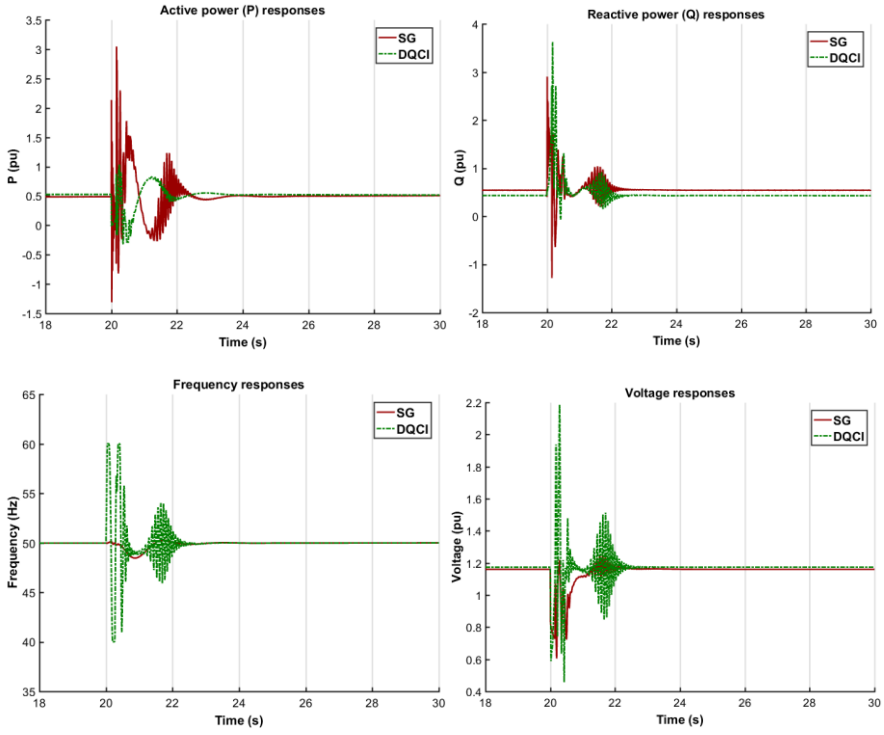

Figure 4-8. System performance for an example under a stable case with converter penetration level slightly below tipping point for transient stability (65% instantaneous penetration level based on generation VA ratings)

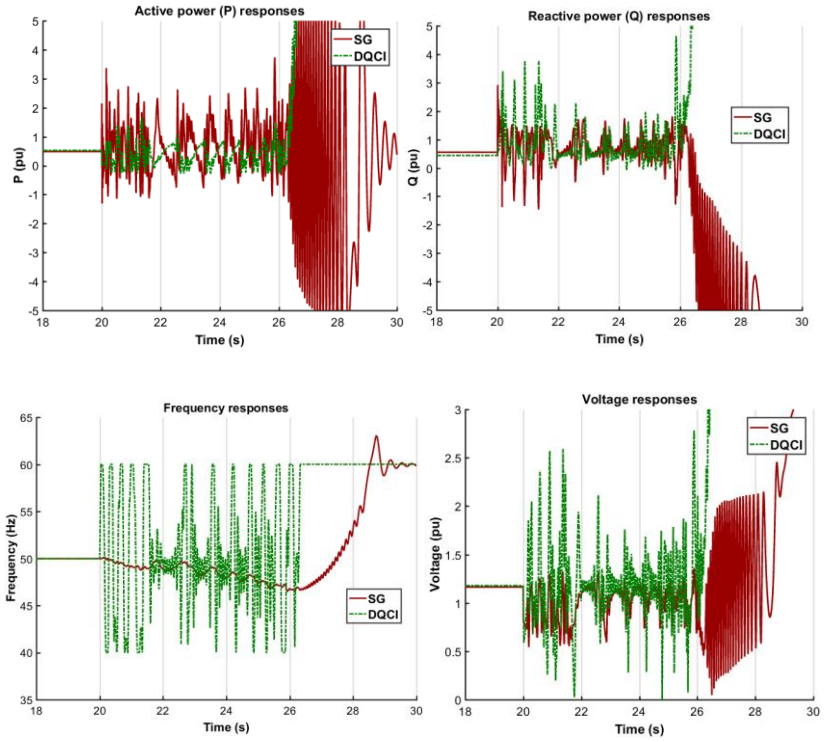

Figure 4-9. System performance for an example under an unstable case with converter penetration level slightly above tipping point for transient stability (66% instantaneous penetration level based on generation VA ratings)

Note that, in general, tipping points found in different simulation models could vary because system configuration and settings are significantly distinguished from one simulation to another. However, the existence of the tipping points is important to be revealed.

Figure 4-10 and Figure 4-11 show the *dq*-axis currents in the DQCI converter control under a stable case and an unstable case for transient stability and small signal stability respectively. It can be seen that, for the stable cases, both i_d and i_q are well controlled with reference i_{dref} and i_{qref}, where the magnitude of i_{dq} is constrained to around 2 p.u. (in RMS value) by its corresponding PI controllers in recognition of the semiconductors' limitation on overcurrent capability. A small disturbance can be seen at 20 s where the load step event occurs as shown in Figure 4-10(a), and significant spikes present in both i_d and i_q due to the fault occurrence but they can return to original small signal levels after the fault is cleared as shown in Figure 4-11(a).

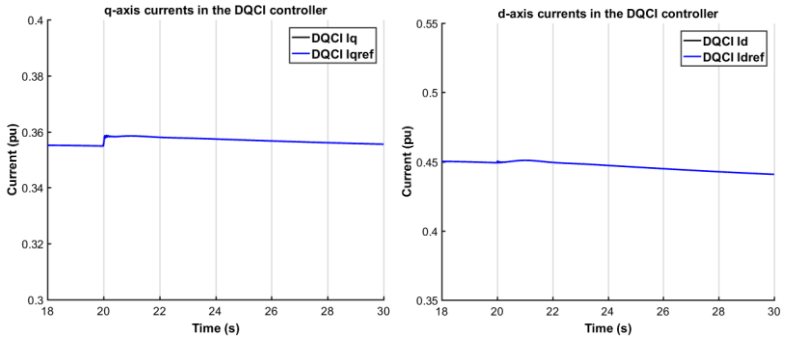

(a) 71% instantaneous penetration level based on generation VA ratings (a stable case)

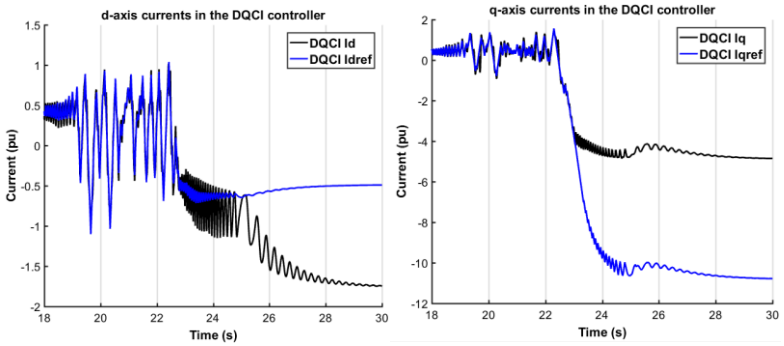

(b) 72% instantaneous penetration level based on generation VA ratings (an unstable case)

Figure 4-10. Responses of *dq*-axis currents for small signal stability

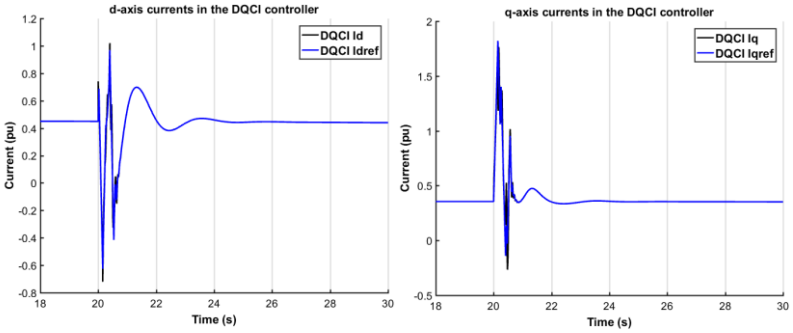

(a) 65% instantaneous penetration level based on generation VA ratings (a stable case)

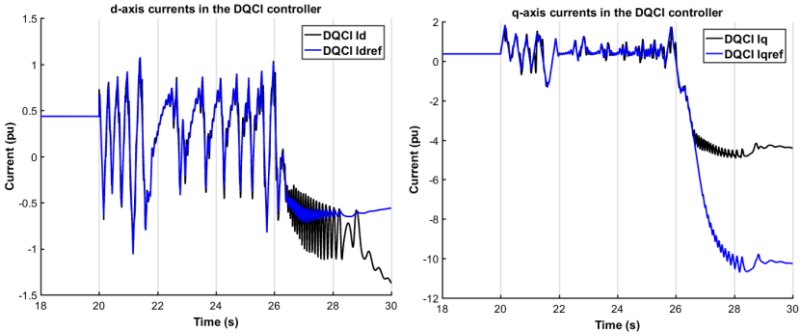

(b) 66% instantaneous penetration level based on generation VA ratings (an unstable case)

Figure 4-11. Responses of *dq*-axis currents for transient stability

However, for the unstable cases, it can be seen that oscillations are introduced in i_{dq} and i_{dqref}, due to the poor track of PLL when the system becomes weaker. Also as voltages measured at the DQCI converter connection point will be used in the PLL and inner current control loop in the DQCI converter control system, the increasing oscillations in the voltage waveforms will cause further deterioration of the network stability.

In [3], it is discussed and proven based on state-space linear analysis that small-signal stability of the DQCI control is directly related to the phase angle output of the PLL relative to the system reference angle. The system reference angle is ideally that of a stiff point in the network, such as a strong grid connection point. In this thesis, as there is no infinite bus connected in the APS model, the stiffest point is considered to be the connection point of the SG. Intuitively and based on analysis in [3], the higher the angle difference between DQCI converter measurement point and the SG connection point, the system is expected to be more unstable; this is because of phase tracking errors which lead to undesirable cross-coupling in the inner current control loop. In this thesis, such angle difference is quoted as steady-state angle difference (SSAD).

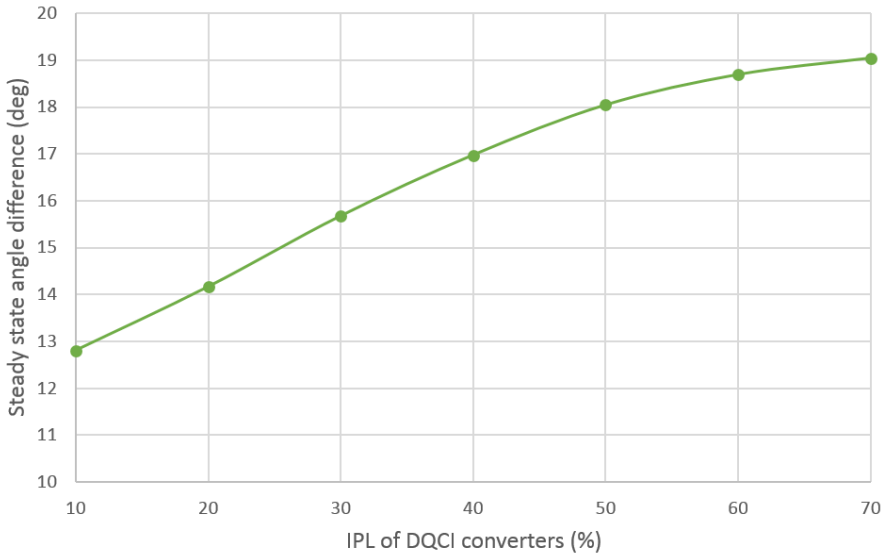

Figure 4-12. Effects of penetration level of converters on the SSAD in APS model

Figure 4-12 shows the SSAD in the APS model with instantaneous penetration level of converters increases from 10% to 70% (as tipping point of small signal stability for the base model is 71.5%). It can be seen that the angle difference increases while penetration level increases, from 12.8° to 19.0° which is aligned with discussion above. Such angle

disturbances directly affect the operation of the inner current controllers in the DQCI converter by introducing unexpected cross-coupling in the *dq*-axis currents i_{dq}. Note that for later case studies, the SSADs in the APS value are all measured with a fixed instantaneous penetration level of 50% and based on the base model except for the factors to be investigated which will be varied.

4.2.3 NPF analysis

As introduced in 3.4, response, *R*, of a specific type of generation and its controllers can be analysed using the NFP method, either using classical analysis of the device transfer function (if known), or by time-domain simulation (and Fourier analysis). To carry out analysis based on transfer functions, main function blocks of the generation controllers have to be linear, such as that of a SG. In this section, the NFP charts describing responses of the SG and a DQCI converter will be demonstrated based on the time-domain simulation analysis method, while the simulation model for NFP analysis is validated by comparing the response of a SG obtained by both linear analysis and time-domain simulation analysis. As shown in Figure 4-13, the two approaches are generally consistent both in terms of the amplitude and phase. Note that the models for SG and DQCI with their controllers are the same as in the APS model in aspects of both configuration and settings, and both are set with a 4% frequency droop slope.

NFP charts of SG and DQCI converters are shown in Figure 4-14, marked as R_{SG} and R_{DQCI} along with the three key features R_{Droop}, R_H and R_D discussed in 3.4. The results indicate that the modulation frequency f_{NFPmod} requires actions which are faster than the prime mover and governor are physically capable of, but that the modulation frequency is too slow to initiate a large inertial contribution. For a real SG attached to a prime mover, there is usually a band of modulation frequencies between these two initial regions, i.e. 0.001 to 0.2 Hz which represents dynamics of 5s or longer, for which the amplitude of R_{SG} both diminishes in value and approaches the droop asymptote. The convergence with droop asymptote is due to the dominance of the turbine governor. For a modulation frequency range of approximately 0.2 to 2 Hz, i.e. 0.5 to 5 s dynamics, R_{SG} follows the inertia asymptote R_H (and R_{HD}) for both amplitude and phase, until it reaches a rotor oscillation mode at around 2 Hz. For modulation frequencies higher than 2 Hz, i.e.

dynamics faster than 0.5s, R_H (and R_{HD}) is dominated by the machine damping effect, where amplitude response decreases and phase lags with increasing frequency. The response R_{SG} follows R_H and R_{HD} in their corresponding modulation frequency regions as expected.

In comparison, the response R_{DQCI} is quite different. In the region 10^{-3} to 10^{-1} Hz, R_{DQCI} follows the droop asymptote; this is due to the 4% frequency droop slope applied in the DQCI converter. It starts to drop off in amplitude for modulation frequencies higher than 0.2 Hz, which does not follow the inertia asymptote. This is to be expected since there is no inertia contribution from the DQCI converter. Similarly, the phase of R_{DQCI} begins to drop from around 0.02 Hz and experiences an even deeper slope after 4 Hz. Note that the 'spike' seen in the phase chart of R_{DQCI} is the wrapped phase which is displayed in the range of 0º to 360º. This reduction in phase response of the DQCI converter can become nearly anti-phase with the SG rotor oscillation. A significant phase difference up to 130º between R_{SG} and R_{DQCI} can be introduced when the SG is following the inertia asymptote at around 0.3 to 0.5 Hz. Even larger differences can be found at high modulation frequency regions beyond 4 Hz, which can be easily affected by any settings in the DQCI control system and would be difficult to predict in any actual power system. In addition, oscillations found in APS model when approaching marginally unstable cases have frequencies in the range of 4 to 8 Hz, which is consistent with the NFP charts where large phase differences are evident. Therefore, the steep phase slopes shown in the NFP charts could indicate a tendency for instability at high penetrations.

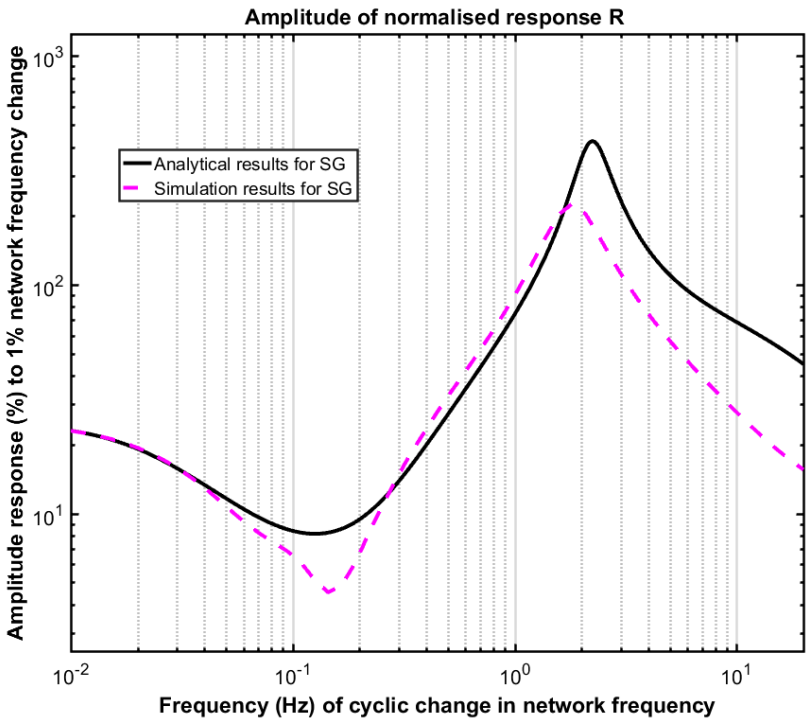

(a) Amplitude chart

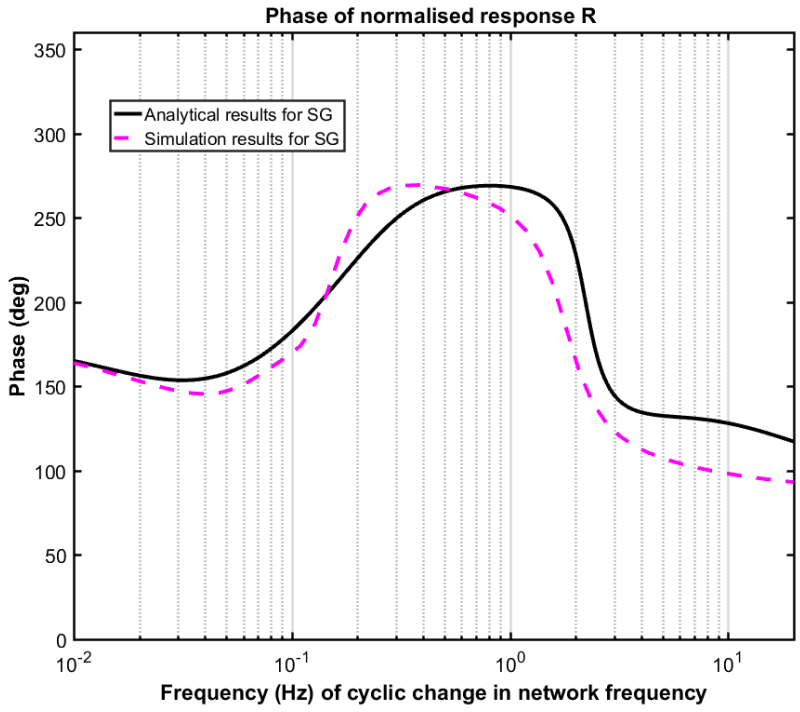

(b) Phase chart

Figure 4-13. Comparisons of NFP responses for SG obtained based on classical linear analysis and numerical simulation

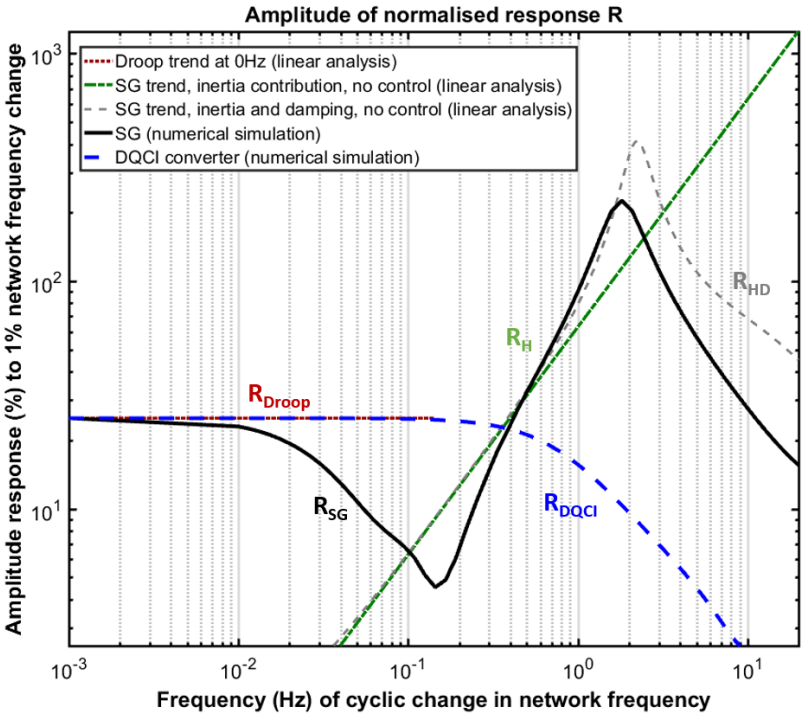

(a) Amplitude chart

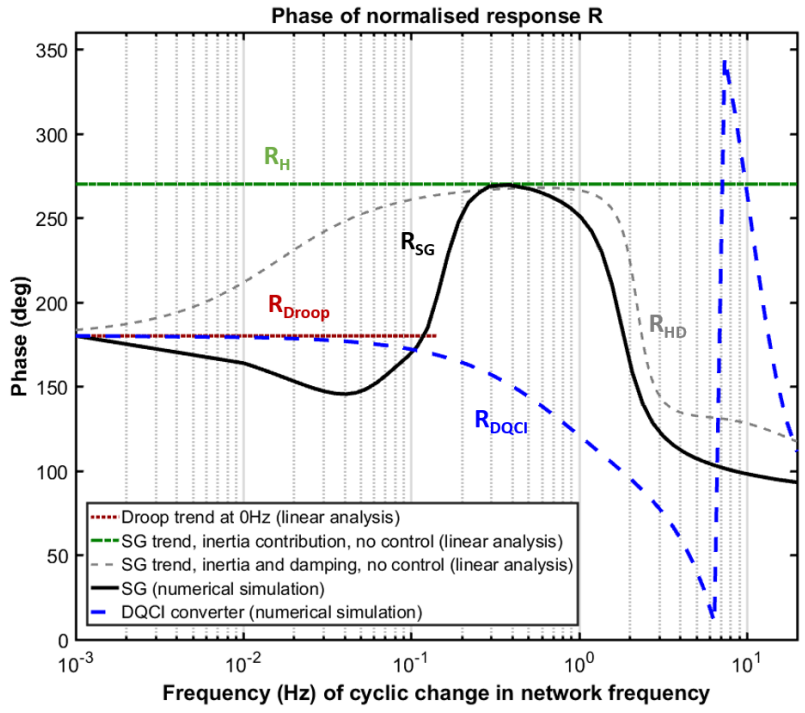

(b) Phase chart

Figure 4-14. NFP charts for SG (R_{SG}) and DQCI converter (R_{DQCI}) obtained by time-domain simulation along with the three key trend-lines R_{Droop}, R_H, R_{HD} predicated by classical linear analysis

4.3 Investigation of possible reasons for instability

Among the significant number of factors in a power system that can have an effect on the system stability and tipping points, factors of interest, such as system inertia, system impedance and load types, will be explored as the most influential in this section. Note that the APS model in MATLAB is used in this section to limit the complexity and required simulation time for conducting numerous tipping point studies which could be excessive in the DIgSILENT PowerFactory RGBT model due to large number of generators.

4.3.1 System inertia

In a power network, the overall system inertia is typically defined by (4-1), where N is the total number of generators, H_i is the inertia constant of generator (measured in seconds), S_i is the VA rating of generator , S_{system} is the total system VA rating, and H_{system} is the aggregated system inertia constant (measured in seconds). When the combined ratings of converters increases, generation that contributes to system inertia decreases and therefore, overall system inertia will decrease as well. In the TPS studies for the effects of inertia, besides of the "natural" changing of system inertia with different penetration levels, the inertia constant in the SGs, H_{SG}, is varied. Normally, H_{SG} for a single turbine generator is in the range of 2~10 s depending on the turbine type and number of poles of the rotor [4].

$$H_{system} = \frac{\sum_{i=1}^{N} S_i H_i}{S_{system}} \tag{4-1}$$

In the MATLAB APS model, the inertia constant of the SG, H_{SG}, is varied between 1 s and 10 s, and two extreme test cases are also included where H_{SG} is 50 s and 100 s. This is to explore the effect of high inertia constant in the simulation model, even though the values are unrealistic in the real world. As seen in Figure 4-15, system inertia does not affect the tipping points in terms of small signal stability significantly, with tipping point only varying less than 0.6% while H_{SG} increases, even with the extreme cases (not shown on the graph). Additionally, the SSAD measured at steady state with varying inertia is shown in Figure 4-16. With H_{SG} increases, the SSAD only changes less than 0.4°, which

is in agreement with the tipping point results. The relationships between tipping points and SSAD cannot be visualised clearly in this case study as the effect of system inertia is fairly less significant. Note that when measuring the SSAD in this section, system settings are the same with that in the base model whilst the factor to be investigated (such as system inertia) is varied to explore its effects.

In terms of transient stability, inertia has a positive effect on the tipping point as shown in Figure 4-15. It appears that system inertia affects more significantly in the range of 1~3s of H_{SG} by increasing the tipping points from 59.3% to 67.8% (was 67.8% for base model where H_{SG}=5 s). This is understandable as inertia only play an effect during a short time period after disturbances and is expected to influence more on the transient stability, rather than long-term small signal stability.

It leaves no doubt that system inertia is important to maintain normal system operation, such as discussed in system operator documents [5, 6] and research papers [7, 8]. However, based on the studies above, the system inertia turns out to be a non-significant factor for tipping points as well as the system stability defined in this thesis.

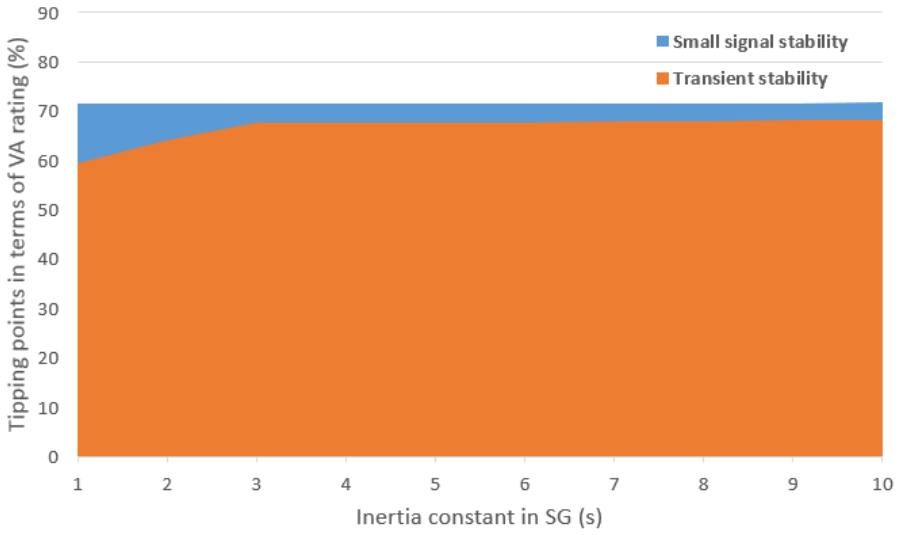

Figure 4-15. Effects of system inertia on tipping points in terms of small signal stability and transient stability based on the APS model in MATLAB

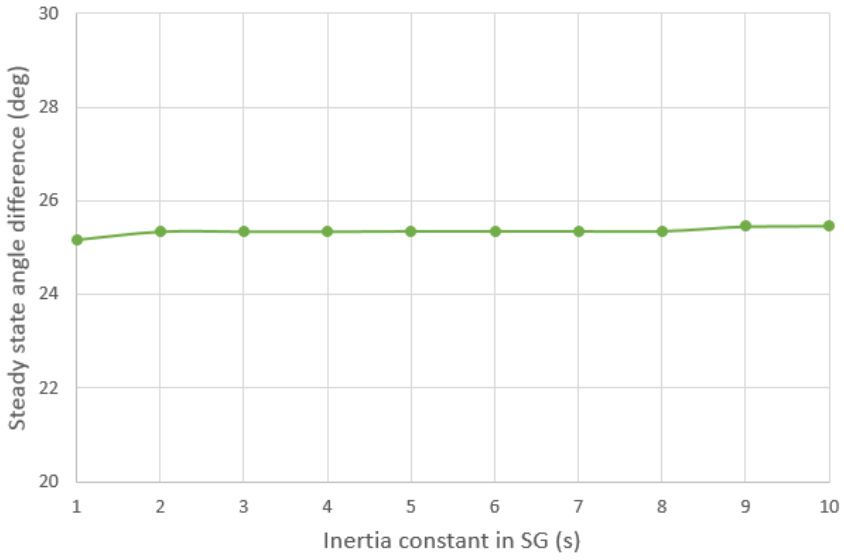

Figure 4-16. Effect of system inertia on SSAD in the APS model

4.3.2 System impedance

In a power network, system impedance could change constantly/continuously with varying system configurations, for example, removing/adding of transmission lines, varying loads and generation, etc. With increasing penetration of RES and HVDC links, system impedance is expected to increase, which makes the power networks weaker. In order to investigate on the effects of system impedance in a more intuitive way, in the APS model, the impedance (both resistance and reactance) of the transmission line connected after the DQCI converter is varied, i.e. increased from 4 km to 36 km (20km in the base model).

The tipping point results are shown in Figure 4-17 in terms of both small signal stability and transient stability. With the converter transmission line longer, i.e. system impedance higher, it can be seen that the system is liable to become unstable in terms of both small signal stability and transient stability, with tipping points dropped to approximately 51.6% and 53.1% respectively in the investigated range. This is in corresponding with the expectations as the higher the system impedance, the larger voltage deviation is introduced at the converter connection point due to increasing disturbances shown in the PLL and inner current controller in the DQCI control, and

therefore affect the network stability as a whole. It also shows that the increased system impedance has slightly higher impact on the tipping points in terms of transient stability.

Figure 4-18 shows the SSAD measured in the APS model when varying the converter transmission line length. As the line length increases, i.e. system impedance increases, increasing SSAD has been introduced to the system which is as expected. Across the investigation range, the SSAD varied for about 37.4º. It can be noticed that the trend of SSAD shown in Figure 4-18 aligns with that of the tipping points for small signal stability shown in Figure 4-17. By showing the results of the SSAD with relationship to tipping points, as shown Figure 4-19, it confirms the theoretical analysis that the system could become more unstable with higher angle difference between the converter PCC and grid reference point.

Figure 4-18 shows the SSAD measured in the APS model when varying the converter transmission line length. As the line length increases, i.e. system impedance increases, increasing SSAD has been introduced to the system which is as expected. Across the investigation range, the SSAD varied for about 37.4º. It can be noticed that the trend of SSAD shown in Figure 4-18 aligns with that of the tipping points for small signal stability shown in Figure 4-17. By showing the results of the SSAD with relationship to tipping points, as shown Figure 4-19, it confirms the theoretical analysis that the system could become more unstable with higher angle difference between the converter PCC and grid reference point.

The studies show a clear effect of the system impedance on system stability, which also implies the negative effect of converters when they are connected with the grid due to the high impedance between the converter terminal and grid connection point. Also it is preferable to keep the system impedance lower the possible within an acceptable range related to the system ratings to maintain stability and enhance system strength. However, this value is difficult to estimate for a real power system due to the complex system architecture and configuration, including constantly varying generation and load.

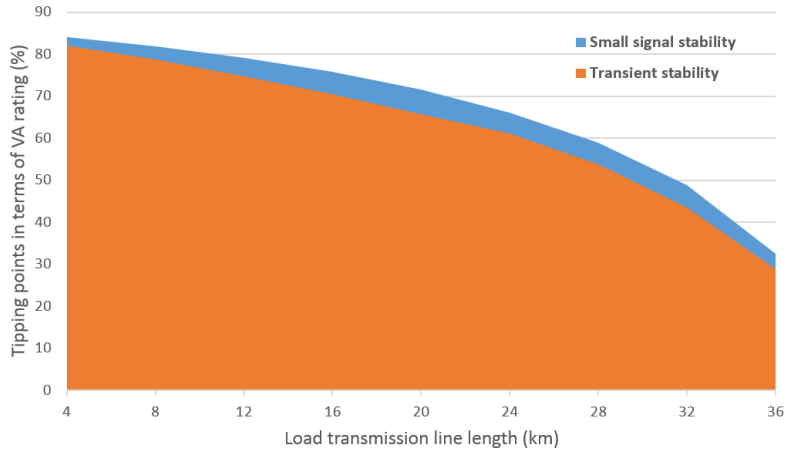

Figure 4-17. Effects of system impedance on tipping points in terms of small signal stability and transient stability based on the APS model in MATLAB

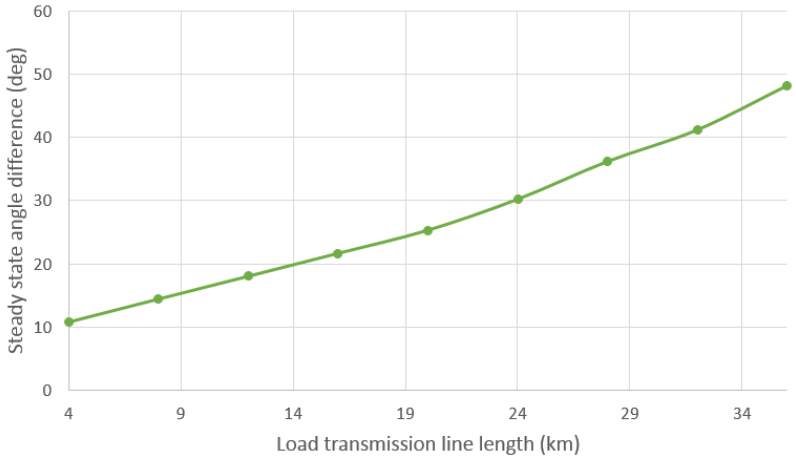

Figure 4-18. Effects of system impedance on SSAD in the APS model

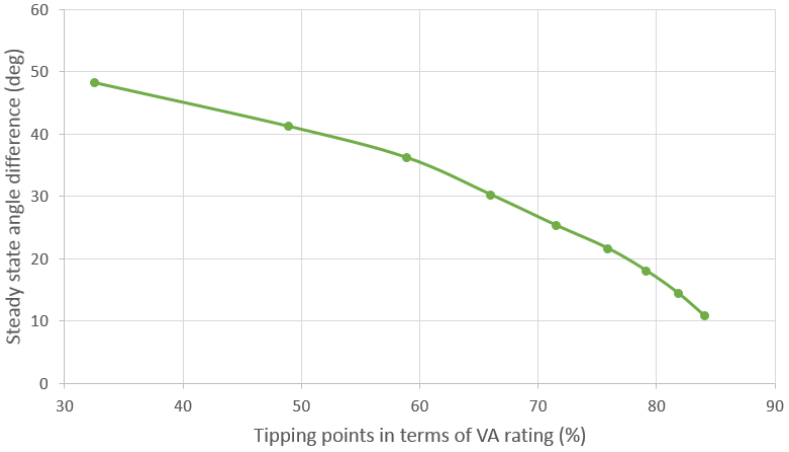

Figure 4-19. Relationship between tipping points in terms of small signal stability and SSAD with effects of system impedance

4.3.3 Converter capacity factor

The actual average electrical energy output from various types of generation over a certain time period divided by their maximum rated electrical energy output in the same period of time is quoted as the generation's capacity factor [9]. Normally, capacity factor of a specific generation can vary depending on various factors such as their capability and reliability of electricity production, electricity demand, as well as constraints from regulations and market forces. For conventional generation such as coal fired power plants and nuclear power plants, the capacity factors are at an average of 60% to 90% mainly due to their operation efficiency and running costs [10]. However, for RESs, capacity factors could be much lower, at an average around 10% to 40% [10]. One of the key reasons for such low capacity factors in renewable devices (besides of that have been mentioned above) is the nature of the RESs, which come from natural sources and local weather conditions could become an important impact factor, such as wind, solar and hydro. Ongoing technology improvements on RES are making them more reliable and competitive electricity sources with increasing capacity factors. According to [11], the capacity factors for onshore wind, offshore wind and solar PV averaged across the world are 33%, 31% and 26% respectively. Examples of estimated capacity factors for different types of utility-scale renewable energy generation in 2017 in the U.S. are shown in Figure 4-20.

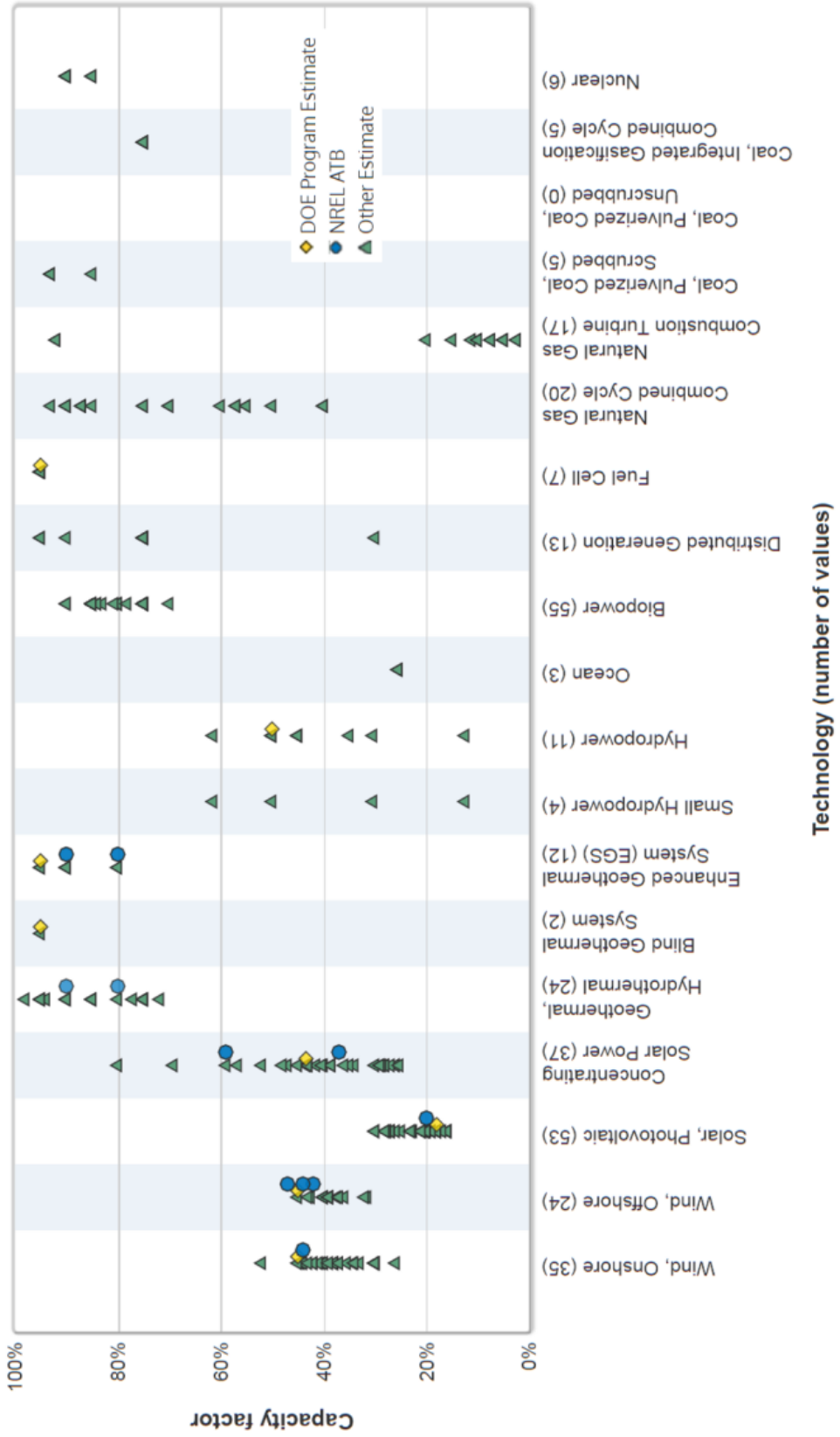

Figure 4-20. Range of recent capacity factor estimates in 2017 for utility-scale renewable energy technologies in the U.S. [12]

For the case studies in this thesis, capacity factor is defined as the actual power output from the generation and its rated power. The range of capacity factor to be explored on the DQCI converter is selected as 10% to 100% taking account of the current status and expected future scenarios.

Effects of capacity factor in the DQCI converters on the tipping points for both small signal stability and transient stability are shown in Figure 4-21, while generally the tipping point increases slightly for capacity factor lower than 40~50% but drops rapidly (for about 17.7%) beyond that. The highest tipping points that occur in the APS model are 72.3% for small signal stability (with DQCI capacity factor of 50%) and 68.6% for transient stability (with DQCI capacity factor of 40%).

It can be observed that the tipping point is relatively insensitive to capacity factor when the capacity factor is between 0 and 50%; conversely, the tipping points exhibit strong sensitivity to capacity factor once the capacity factor is increased beyond 50%. This is reasonable as the power angle between the DQCI converter PCC and the stiffest point in the network, i.e. the SG PCC, could be larger due to increased power outputs from the converters based on their ratings, based on power angle equation in (3-1). In Figure 4-22, it can be seen that the SSAD decreases slightly within 5º but increases greatly by about 23.1º with capacity factor increased from 50% to 100%. The relationship between tipping points in terms of small signal stability and SSAD, again, confirms the theory where higher SSAD could leads to lower tipping points, as seen in Figure 4-23.

Therefore, despite the obvious economic advantages of operating at a higher capacity in the DQCI converters, there could potentially be a danger of system becoming unstable when DQCI converters are at high capacity factors, which should be considered by system operators and manufacturers. It is assumed that all the DQCI converters operate under the same capacity factor in this section; however, in reality, a set of converters at any instant can have a set of values of capacity factor (potentially one unique value for each converter), which could produce different results. However, it is believed that it is of more importance to show that there could potentially be an impact from the capacity factor in DQCI converters but rather than the exact values of tipping points.

Compared with the system impedance case studies discussed in section 4.3.2, where tipping point in terms of small signal stability changes for 51.6% with SSAD changes for

37.4°, the DQCI capacity factor case studies have a change in tipping point of 17.7% in terms of small signal stability with SSAD changes for 23.7°. The trends confirm the theory that a power system is expected to be more unstable with higher SSAD between the converter terminals and the stiffest point in the network.

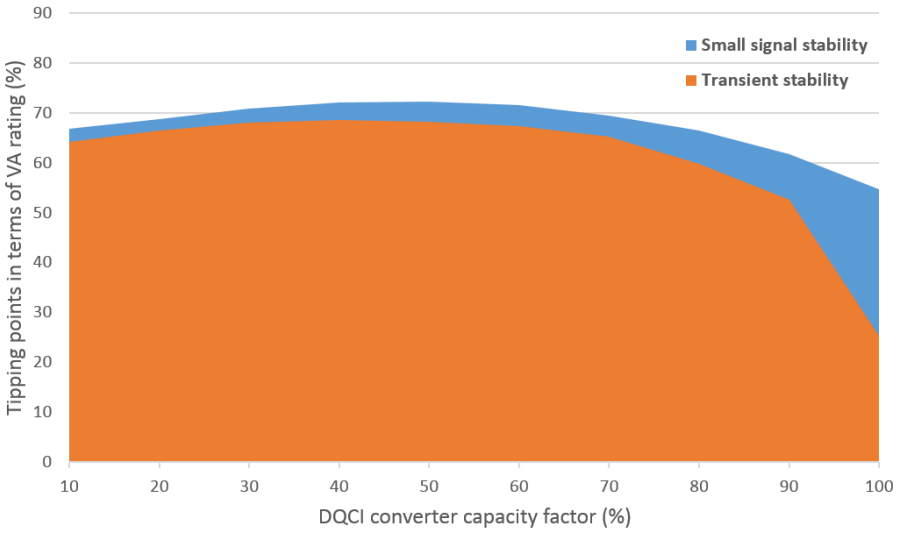

Figure 4-21. Effects of DQCI converter capacity factor on tipping points in terms of small signal stability and transient stability based on the APS model in MATLAB

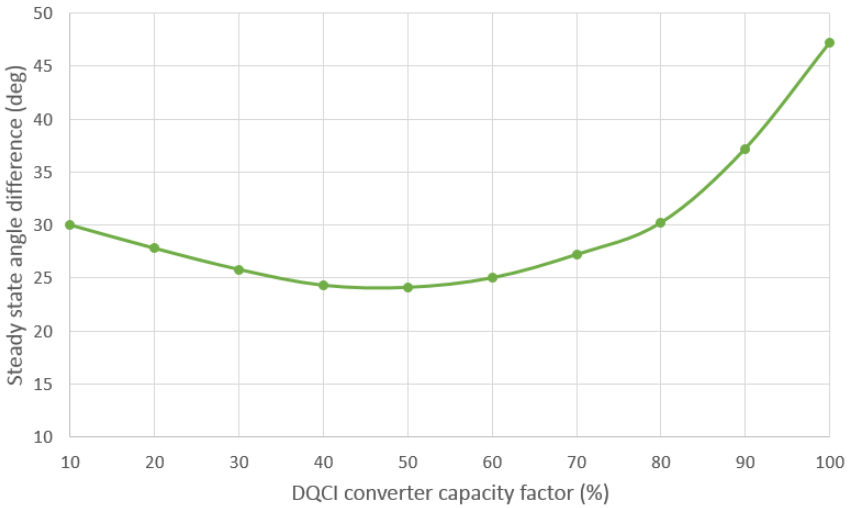

Figure 4-22. Effects of DQCI converter capacity factor on SSAD in the APS model

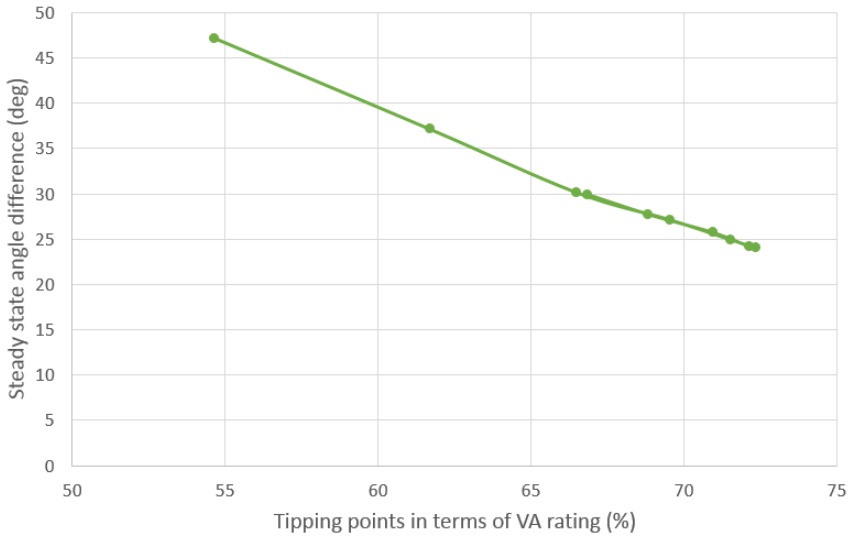

Figure 4-23. Relationship between tipping points in terms of small signal stability and SSAD with effects of DQCI converter capacity factor

Table 4-2. Comparisons of changes in tipping point (in terms of small signal stability) and SSAD for system impedance and DQCI CF case studies

Case studies	Tipping point change	SSAD change
System impedance	51.6%	37.4°
DQCI capacity factor	17.7%	23.7°

4.3.4 NLL

Power systems are designed to operate at frequencies of 50 or 60 Hz; however, certain types of devices could produce currents and voltages with frequencies that are integer multiples of the nominal fundamental frequency, which are known as power system harmonics. As a form of electrical pollution, the presence of harmonics in the power networks leads to voltage and current distortion. Conventionally, harmonics problems could mainly be caused by saturated devices, e.g. the third harmonic currents caused by saturated iron in transformers and machines has been encountered by using delta connection of the transformer to block the third harmonic currents [13]. Recently, these

power quality issues have become more complicated due to the increasing use of power electronic devices in the power networks.

Normally, in a stiff power system with a relatively low impedance and high short-circuit level, the power quality problems are not significant as the voltage/current distortion in such networks is usually small. However, when the system is weak with high impedance and low short-circuit level, problems caused by the harmonics cannot be ignored anymore. Unlike some of the transient events, such as lightening which only lasts a few milliseconds, harmonics will produce continuous distortion of voltage and current waveforms which is a small signal periodic phenomena, and so does the side effects it could produce, such as device overheating, impact on measurement accuracy, and nuisance tripping.

Note that the THD is used as the measure of the harmonic distortion in this thesis, as introduced in Chapter 3.

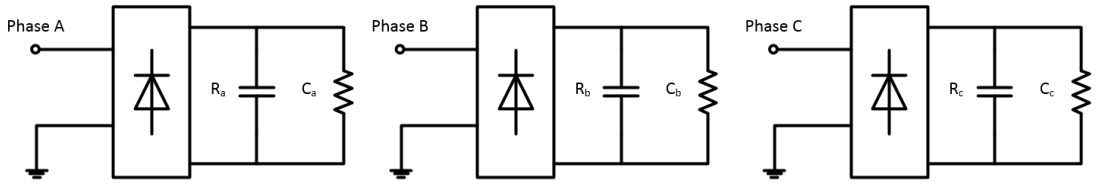

Figure 4-24. Configuration of three parallel single-phase rectifier (with resistor and capacitor connected in parallel at the DC side) forming as the NLL

In this section, three single-phase bridge rectifiers are connected in parallel to form the three-phase NLL, as shown in Figure 4-24, which normally produce voltage distortion with odd number harmonics. A resistor load is connected at the DC side of the rectifier along with a capacitive filter in parallel, while their values (for single phase) are calculated based on (4-2) and (4-3). V_{dc} is the voltage level at the DC side of the single-phase rectifier, P_{NLL} is the total power consumption at the NLL (whose a third is the power consumption at each rectifier), f_0 is the nominal frequency in Hz, and k_{ripple} is the percentage of voltage ripple which is normally set to 5%. A test model in MATLAB is built to test the non-linear rectifier load as shown in Figure 4-25, which consists of a three-phase source block to represent the network (with X/R ratio of 10 and short-circuit level of 10 GVA), a delta-wye 275kV/11kV transformer, a total load of 100MW where a resistive load and a non-

linear rectifier load share equally. The delta-wye transformer is used to eliminate the triple harmonics at the load side.

$$R_{NLL} = \frac{V_{dc}^2}{P_{NLL}/3} \tag{4-2}$$

$$C_{NLL} = \frac{P_{NLL}/3}{2\pi f_0 V_{dc}^2 k_{ripple}} \tag{4-3}$$

To visualise the harmonic distortion, the Fourier Analysis Tool in MATLAB Powergui is used where 10 cycles are selected for the measurement based on the IEC 61000-4-7 standard and phase A of selected voltages/currents is analysed as example. When there is no non-linear rectifier load connected, i.e. the resistive load consumes 100MW, no harmonic contents are seen in both voltages and currents in the system, with an example of Fourier Analysis on the network voltages as shown in Figure 4-26, and also the magnitudes of the voltages and currents stay at 1 p.u.

However, when the rectifier NLL is connected (consuming 50 MW of the total load), both voltage and current waveforms are distorted with significant harmonic contents. As shown in Figure 4-27 and Figure 4-28, significant odd order harmonics are seen in both the voltage and current waveforms at the load PCC, which are the unique characteristics of the single phase NLL. It can also be seen that both of the waveforms are distorted from the normal sinusoidal ones, with significantly increased magnitude of the current at the load PCC; however, the magnitudes of voltages and currents at the fundamental frequency are lower (0.9879 p.u. and 0.9322 p.u. respectively) as a fact due to the effects of increased harmonics. THD levels are increased significantly as well, i.e. 7.61% and 43.09% shown in the load voltage and current waveforms respectively.

Since the delta-wye transformer connected in between of the load PCC and network PCC, it is clearly that the 3n harmonics, i.e. 3rd, 6th, 9th, etc. generated from the NLL are greatly suppressed, as seen in Figure 4-29 and Figure 4-30 of the Fourier analysis of the voltage and current at the network PCC. Increased THD levels have been witnessed in the analysed waveforms at the network PCC but which are less than that are measured at the load PCC due to effects of the transformer.

In the APS model, the rectifier NLL (three single phase rectifier loads connected in parallel) is connected in parallel with the system main load. A delta-wye isolation transformer (with nominal system voltage level of 275 kV set to both primary and secondary side of the transformer) is connected right after the NLL to assist system performance under the presence of harmonic contents.

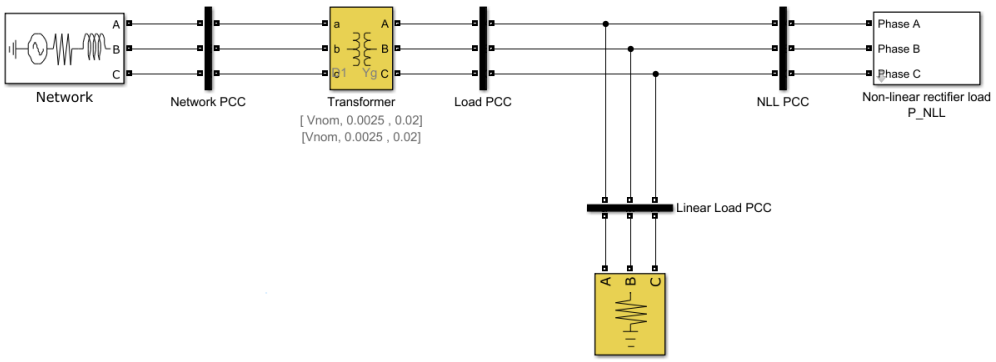

Figure 4-25. Model configuration for testing the single-phase rectifier NLL

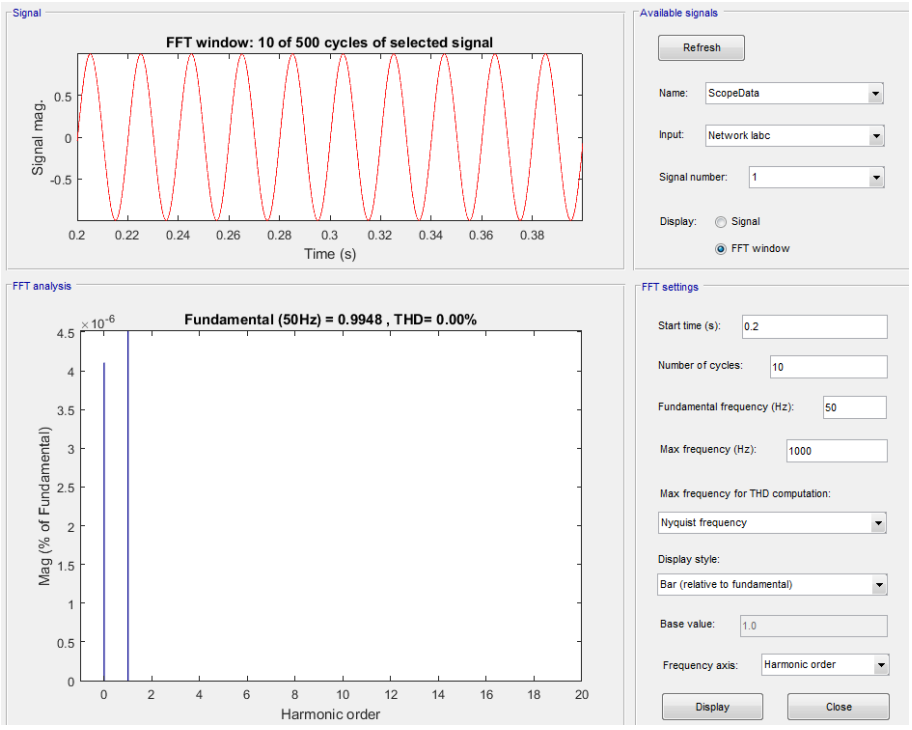

Figure 4-26. Fourier analysis of harmonic distortion of phase A of the network PCC currents when NLL is not connected

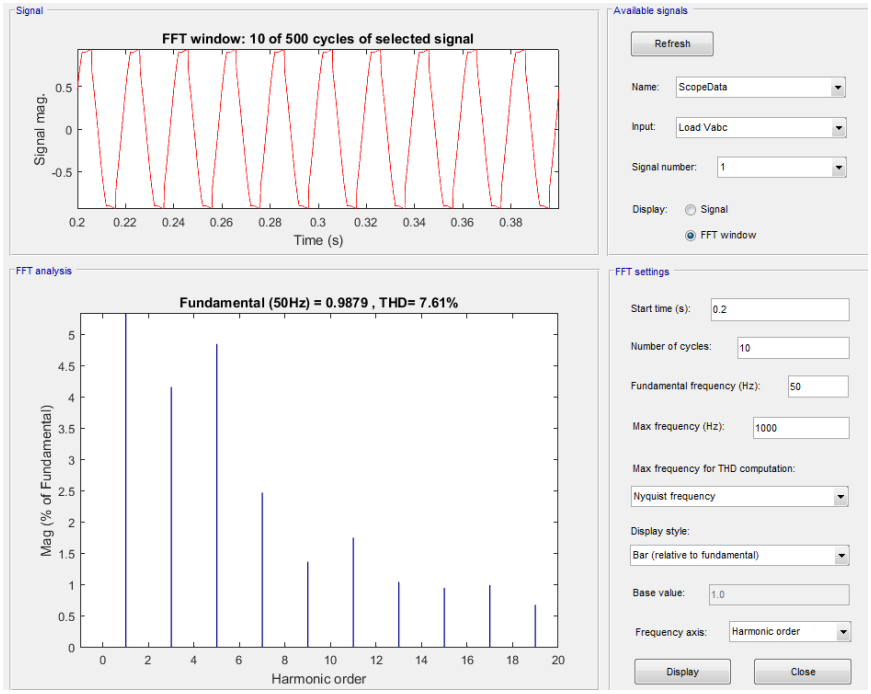

Figure 4-27. Fourier analysis of harmonic distortion of phase A of the load PCC voltages when NLL is connected

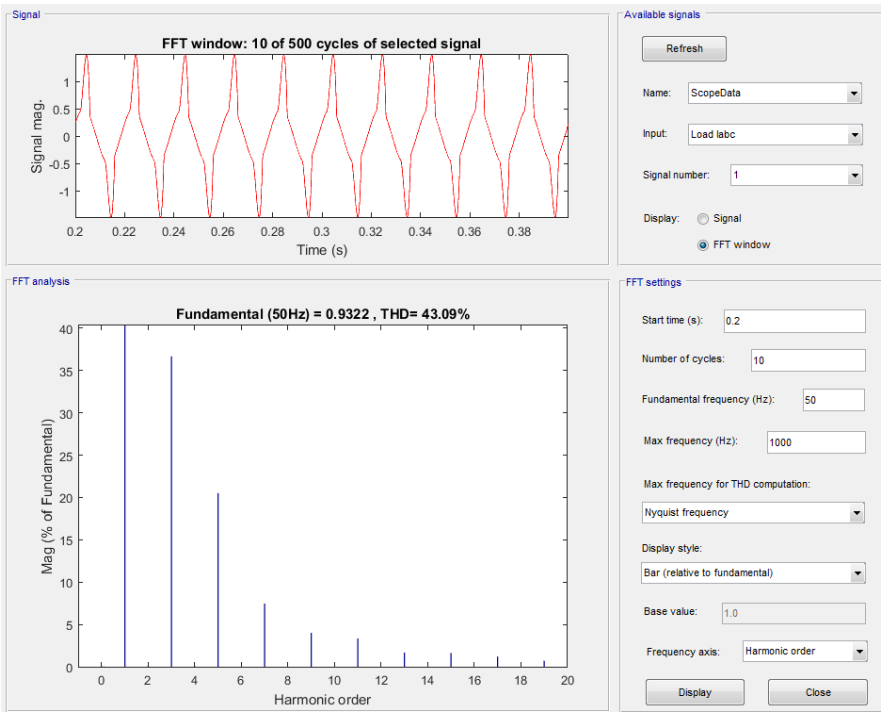

Figure 4-28. Fourier analysis of harmonic distortion of phase A of the load PCC currents when NLL is connected

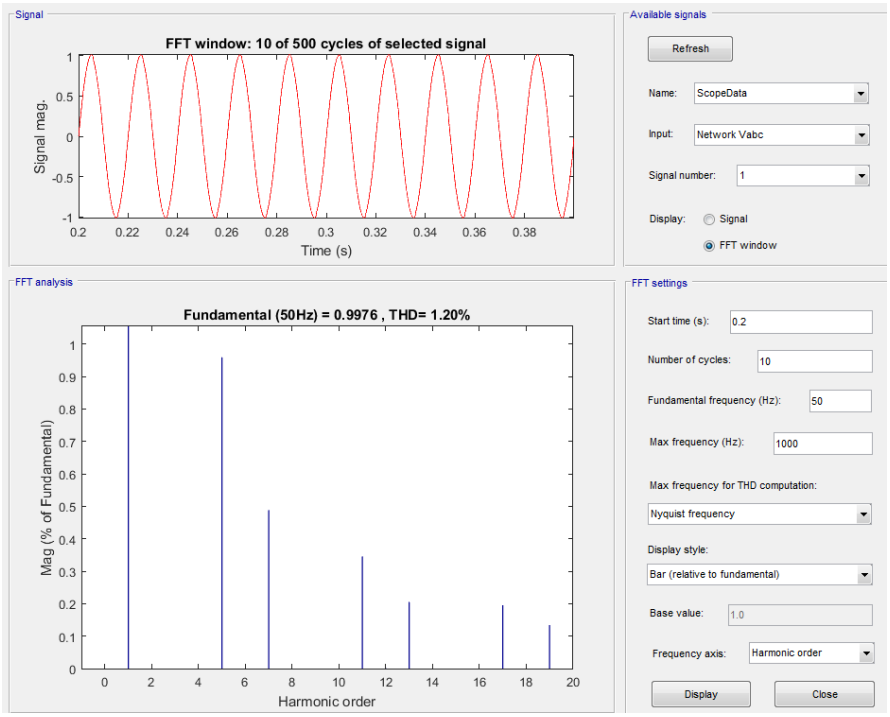

Figure 4-29. Fourier analysis of harmonic distortion of phase A of the network PCC voltages when NLL is connected

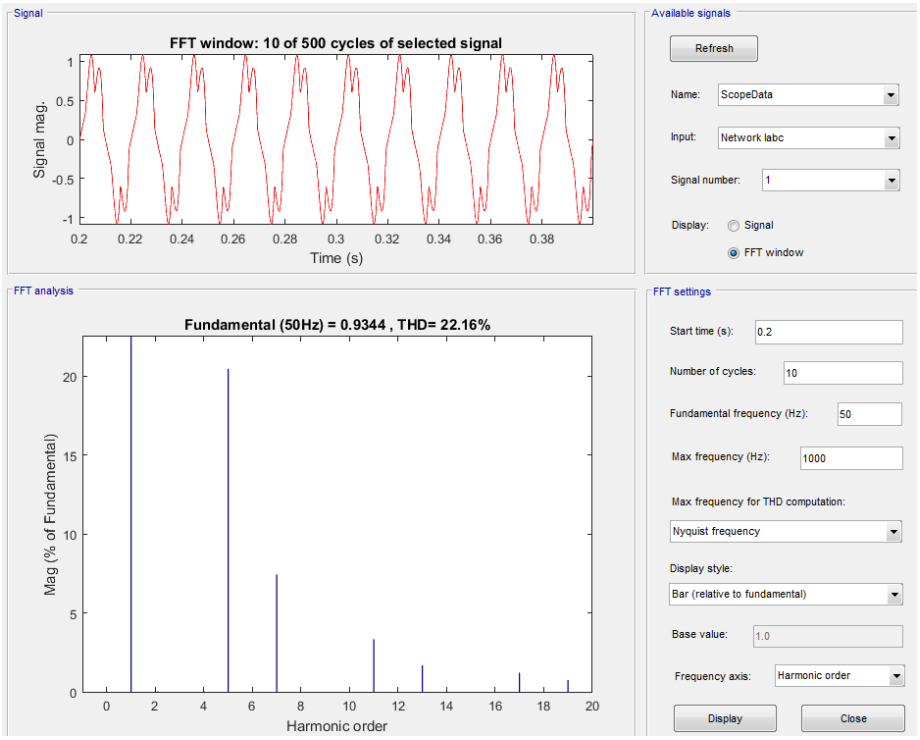

Figure 4-30. Fourier analysis of harmonic distortion of phase A of the network PCC currents when NLL is connected

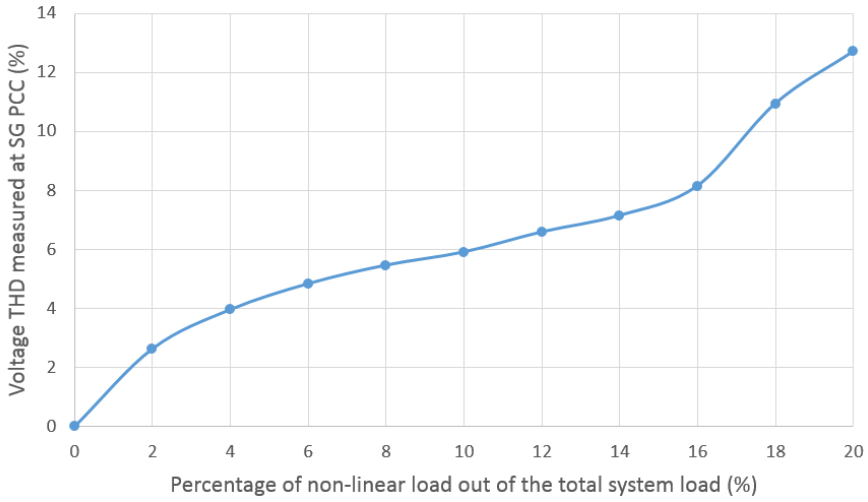

Figure 4-31. Voltage THD measured at the SG PCC with various percentages of NLL in the APS model

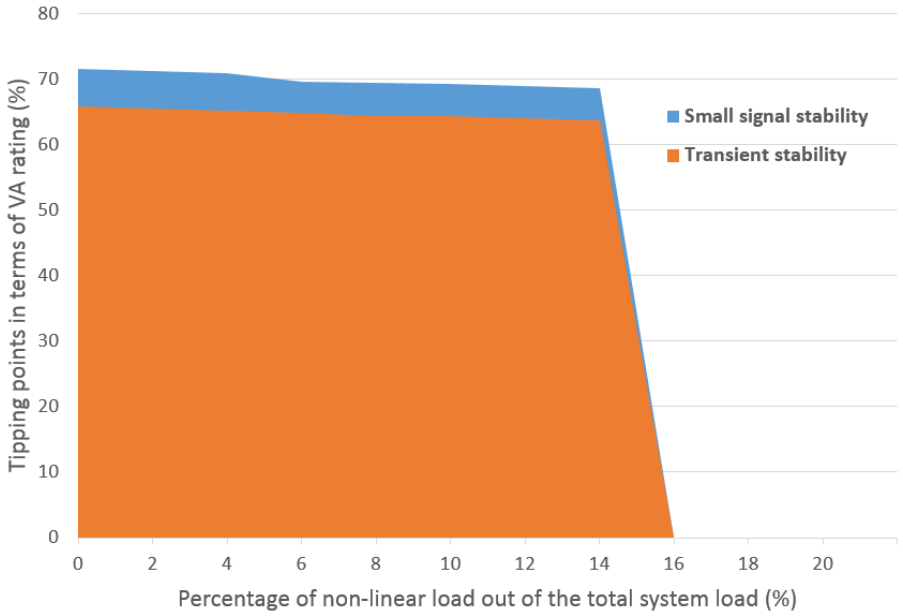

Figure 4-32. Effects of various percentages of NLL out of total system load on tipping points in terms of small signal stability and transient stability based on the APS model in MATLAB

As seen in Figure 4-31, with increasing penetration of NLL in the network model, the voltage THD level experiences a dramatic change, increasing from 0% to 12.7%. In the TPS method, limitation on voltage THD level selected for instability detection is 8%. Therefore, with it is expected that when the non-linear rectifier load increases to above about 16% out of the total system load in this APS model, the system could be classified as unstable, which is aligned with the tipping point results shown in Figure 4-32. It can

be seen that tipping points in terms of both small signal stability and transient stability drops slightly due to the increased percentage of NLL which could slightly bring "forward" the instability phenomenon, but the system will be unstable with more than 16% of NLL where the power quality could be problematic.

4.4 Summary

In this chapter, the system instability introduced by high penetration of converters, as well as the stability thresholds, i.e. the tipping points, in terms of transient stability and small signal stability have been investigated in both power system models in DIgSILENT PowerFactory (RMS-based simulation) and MATLAB SimPowerSystems (EMT-based simulation).

Effects of system parameters, including system inertia, system impedance, converter capacity factor and NLL, on system tipping points have been investigated using the TPS method in the APS model. It has been found that there is a direct relationship between the voltage SSAD between the converter terminal(s) and the stiffest point in a network with the system stability as well as tipping points, where higher SSAD could lead to lower tipping points, i.e. negative effect on system stability.

The ranges and trends of tipping points are useful to system operators and manufacturers. However, learning in details of the combined effects of all the various factors in a power network (which could be more than a hundred) could end up in a complicated multi-dimensional studies which does not sits in the aims of this thesis. Note that the tipping points could vary in a different model with various configuration and setups. Meanwhile, poor power quality contents in real power networks, such as converter switching noises, could potentially decrease the tipping points and destabilise the system significantly.

References

[1] National Grid (GB), "GB SQSS Fundamental Review," 2008. Available: www2.nationalgrid.com/WorkArea/DownloadAsset.aspx?id=12734, accessed in 2017/10/24.

[2] National Grid (GB), "The Grid Code," 2016. Available: http://www2.nationalgrid.com/UK/Industry-information/Electricity-codes/Grid-Code/, accessed in 2017/5/25.

[3] L. Zhang, "Modeling and Control of VSC-HVDC Links Connected to Weak AC Systems," School of Electrical Engineering (EES), Electrical Machines and Power Electronics, KTH, Stockholm, 2010, Available: http://www.diva-portal.org/smash/record.jsf?pid=diva2%3A322475&dswid=1654, accessed in 2017/5/24.

[4] P. Kundur, N. J. Balu, and M. G. Lauby, *Power system stability and control* vol. 7: McGraw-hill New York, 1994.

[5] National Grid (GB), "System Operability Framework," 2016. Available: http://www2.nationalgrid.com/UK/Industry-information/Future-of-Energy/System-Operability-Framework/, accessed in 2017/2/10.

[6] National Grid (GB), "System Operability Framework," 2015. Available: http://www2.nationalgrid.com/UK/Industry-information/Future-of-Energy/System-Operability-Framework/, accessed in 2017/2/10.

[7] P. Tielens and D. Van Hertem, "The relevance of inertia in power systems," *Renewable and Sustainable Energy Reviews,* vol. 55, pp. 999-1009, 2016.

[8] "Future GB Power System Stability Challenges and Modelling Requirements," 2015 Available: http://www.theiet.org/sectors/energy/resources/modelling-reports/papers.cfm, accessed in 2017/7/27.

[9] U.S. Nuclear Regulatory Commission (NRC), "Capacity factor (net)," Available: https://www.nrc.gov/reading-rm/basic-ref/glossary/capacity-factor-net.html, accessed in 2018/07/13.

[10] "Electric Power Annual," 2016. Available: https://www.eia.gov/electricity/annual/, accessed in 2018/7/13.

[11] "Renewables 2016 Global Status Report," Renewable Energy Policy Network for the 21st Century (REN21), Paris, France, 2016. Available: http://www.ren21.net/wp-content/uploads/2016/10/REN21_GSR2016_FullReport_en_11.pdf, accessed in 2017/10/25.

[12] "U.S. Generation Capacity Factor Database," Available: http://en.openei.org/apps/TCDB/index.php?pMin=2009&pMax=2015&dMin=2009&dMax=2014&gf=h&ggt=c&pub=&t=capacityFactor&ct=s, accessed in 2017/7/27.

[13] W. M. Grady and S. Santoso, "Understanding Power System Hannonics," *IEEE Power Engineering Review,* vol. 21, pp. 8-11, 2001.

Chapter 5

Effectiveness of Alternative Converter Control Methods in Enhancing System Tipping Points

5.1 Introduction

In this chapter, the effectiveness of the converter control techniques reviewed and discussed in Section 2.9 will be investigated in the APS model based in MATLAB Simulink. The NFP analysis tool is used to compare the performance of the aforementioned control algorithms against that of a synchronous generator. Distinct from the DQCI converter, which causes the converter to behave as a current source, the VSM algorithm makes the converter operate as a voltage source. The latter is regarded as preferable from a system stability perspective as it compensates for the loss of critical services that synchronous generators naturally provide. Case studies including load step and balanced/unbalanced fault events have been carried out on the VSM0H converter and VSM-type converter to provide insights of their dynamic responses.

5.2 Frequency and voltage droop controllers on DQCI converter

In the APS model, frequency and voltage droop controllers are implemented as an augmentation of the DQCI converter control; more specifically, the active power and reactive power setpoints are based on frequency and voltage variations respectively. First-order low-pass filters (LPFs) are applied to both droop controller outputs. Principles and implementation of the droop controllers are shown and discussed in section 2.9.1.2.

In this section, the effects of frequency and voltage droop controllers on system stability and tipping points are investigated. The droop slopes (D_f and D_v) and time constants in the LPFs ($\tau_{\_Df}$ and τ_{L_Dv}) of both the frequency and voltage droop controllers are included in the analysis. Based on [1-3], the droop slope gain to be investigated ranges from 4%, representing an aggressive droop response, to infinity, representing no frequency/voltage droop response with actual setting in the model to be $1e^9$. Based on [4] the maximum admissible value for the time constants that enable full initialisation of the simulation (i.e. settling into a steady state) in 30 s is 0.5 s. Therefore, in this section, time constant to be investigated for both controllers varies between 0.01 s to 0.5 s.

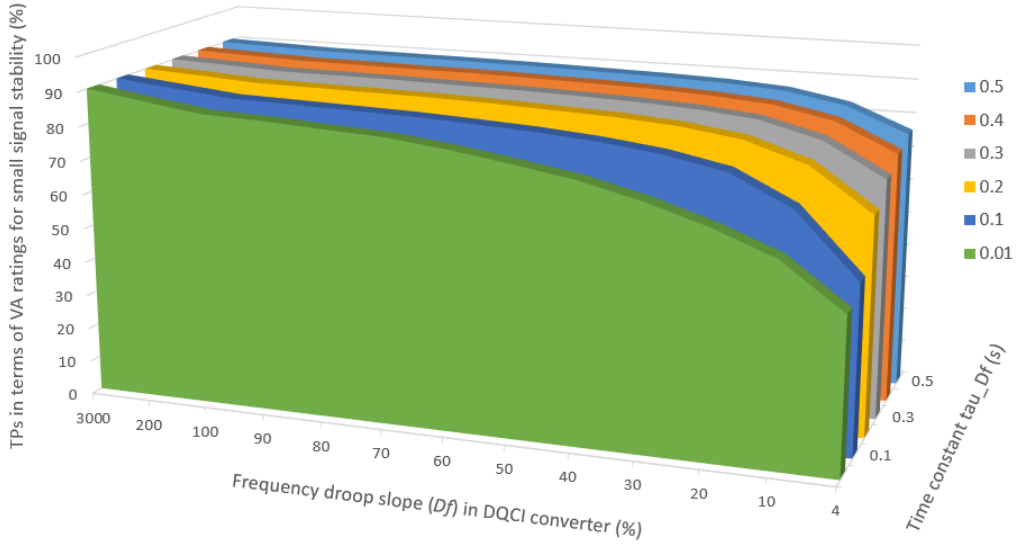

Figure 5-1. Effects of frequency droop slope D_f in DQCI converter and its LPF time constant $\tau_{\_Df}$ on system tipping points for small signal stability

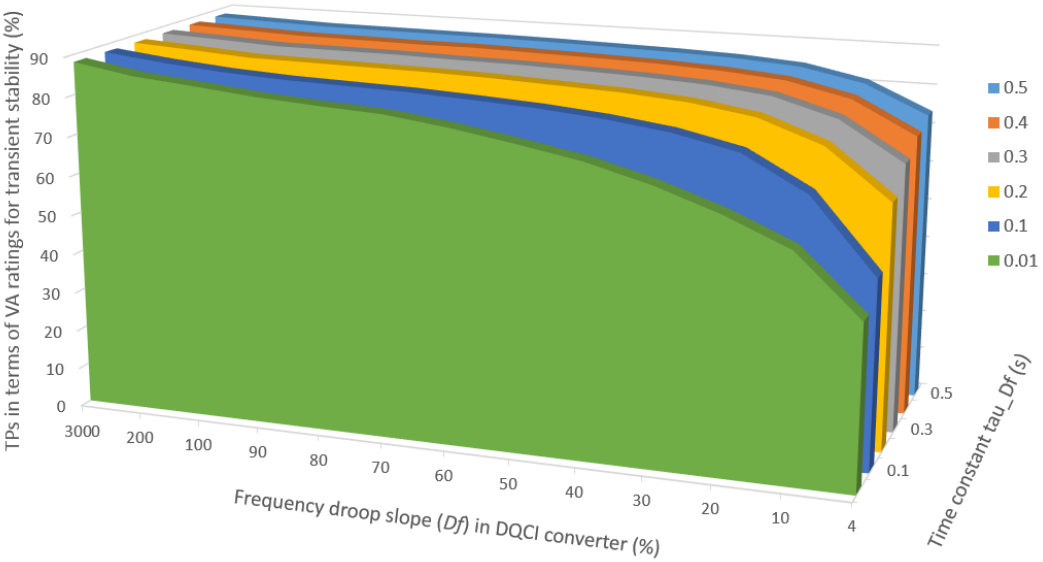

Figure 5-2. Effects of frequency droop slope D_f in DQCI converter and its LPF time constant $\tau_{\_Df}$ on system tipping points for transient stability

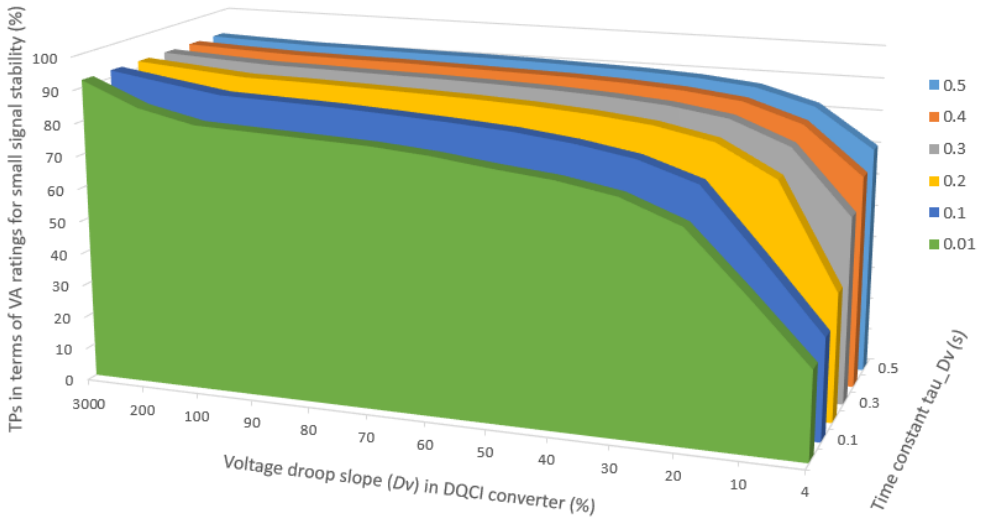

Figure 5-3. Effects of voltage droop slope D_v in DQCI converter and its LPF time constant τ_{L_Dv} on system tipping points for small signal stability

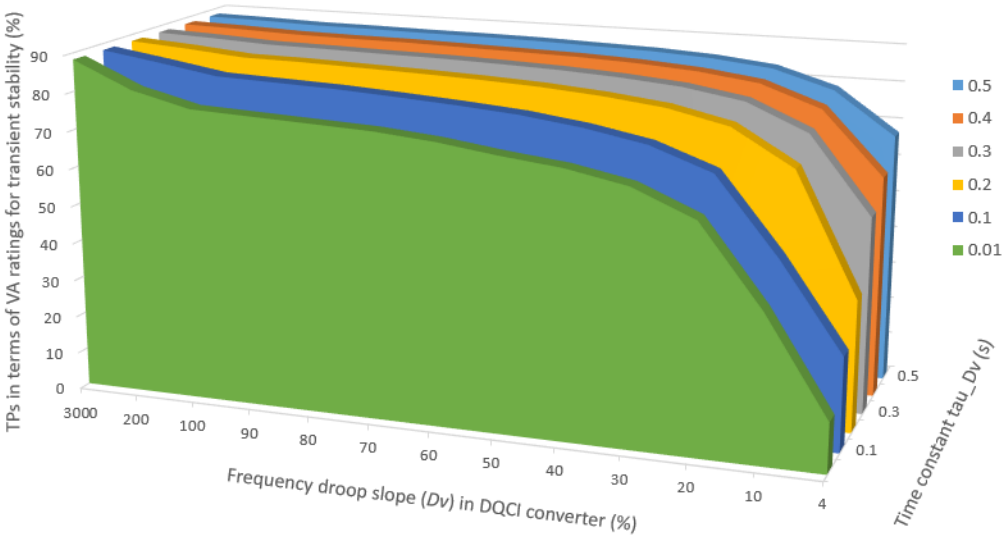

Figure 5-4. Effects of voltage droop slope D_v in DQCI converter and its LPF time constant τ_{L_Dv} on system tipping points for transient stability

Effects of frequency and voltage droop slopes in the DQCI converter and time constant in their corresponding LPFs on the system tipping points in terms of both small signal stability and transient stability are shown in Figures 5-1~Figure 5-4. The figures demonstrate that the tipping points can be affected significantly when changing the selected settings in both controllers. However, with high droop slopes, i.e. 100% and beyond, the time constants in the LPFs have very little impact on the tipping points.

It can be also seen that the droop controllers can have a negative effect on system stability; system stability is further compromised when the drooped signal is poorly filtered. These results are reasonable as the introduction of droop controllers increases the interactions in the inner current control loop in the DQCI converter. Meanwhile, less filtering means there could be more noise produced by the measurement process.

When comparing the results from both droop controllers, it can be seen that the voltage droop controller has a greater influence on the tipping points than does the frequency droop controller. This also reveals the main cause of instability, i.e. the disturbed drive voltages at the converter terminal when the network is weak that are then fed back to the DQCI control system could definitely worsen the control performance.

5.3 SEBIR control in DQCI converter

SEBIR control is considered to have the potential to improve system stability during loss of generation. Effectively, the converters with SEBIR control attempt to measure frequency and provide a power adjustment proportional to RoCoF and a particular chosen value of emulated inertia constant H_{SEBIR} as explained in Section 2.9.1.1. The control principle for the SEBIR controller is as given in (5-1), where *M(s)* represents a measurement window/filter for RoCoF, *F(s)* represents post-filtering applied to the measurement of RoCoF, and *R(s)* represents the response of the actual power control in the converter. Note that df/dt is the measured RoCoF in Hz/s and system nominal frequency is f_0 in Hz.

$$\Delta P_{pu} = -R(s)F(s)M(s)\frac{2H_{SEBIR}}{f_0}\frac{df}{dt} \tag{5-1}$$

It is important to note that particular measurement methods used to measure frequency and RoCoF are of great importance to the performance of SEBIR control. For example, the PLL found in the conventional control topology could be used to measure frequency, from which RoCoF is estimated. However, it has been shown (e.g. in [5]) that using a PLL to measure frequency is not always accurate or effective. Therefore, frequency measurement methods to be investigated in this section for SEBIR control include both P class Phasor Measurement Unit (PMU) and M class PMU. A high level review of the PMUs can be found in [6].

The P class PMU uses a symmetrical filter with a length of 3 cycles, and so the measured value is vulnerable to disturbances and noise from transients, inter-harmonics, flicker and instrumentation noise. Using a P class PMU to measure either frequency or RoCoF is generally not recommended for these reasons. Nevertheless, it is selected to highlight the sensitivity of SEBIR control to RoCoF measurement quality.

The M class uses a filter with a substantially longer measuring window of 11 cycles; consequently, the measured value contains significantly reduced noise and ripple levels in comparison to the P class measurement. A low-pass filter is added to the power setpoint adjustment signal ΔP_{SEBIR}, separately from the low-pass filter applied for the frequency droop signal ΔP_{Df}, as shown in Figure 5-5.

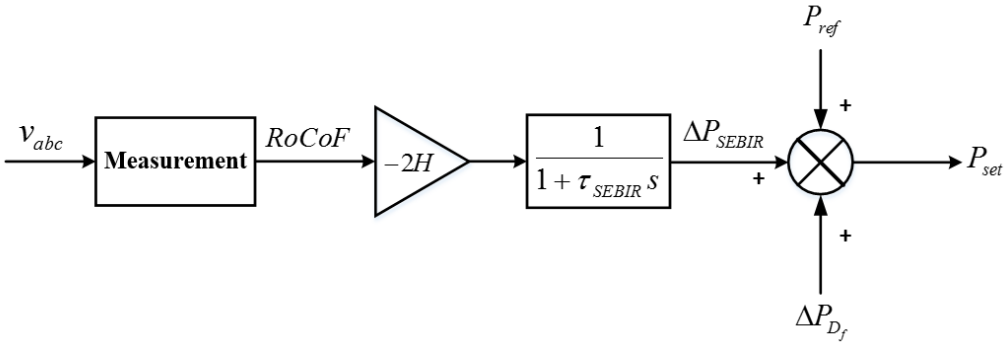

Figure 5-5. Implementation of SEBIR control in addition to the active power controller for DQCI converter in the APS model

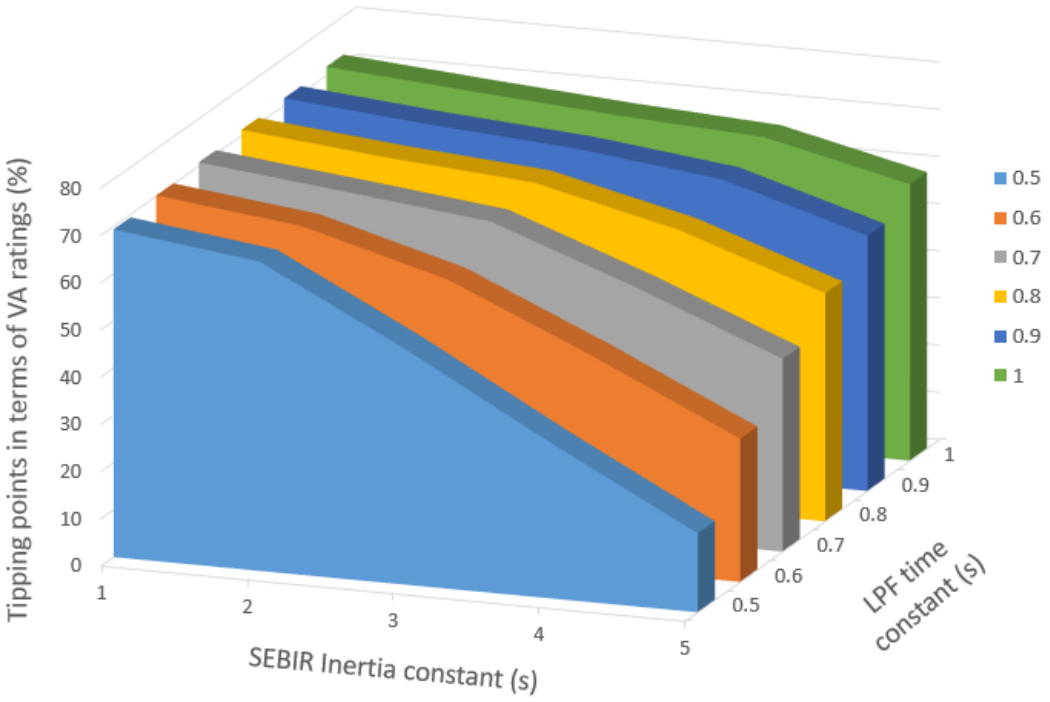

Figure 5-6. Tipping points in terms of steady state stability in APS model with SEBIR control implemented on DQCI converter using M class PMU to measure the RoCoF

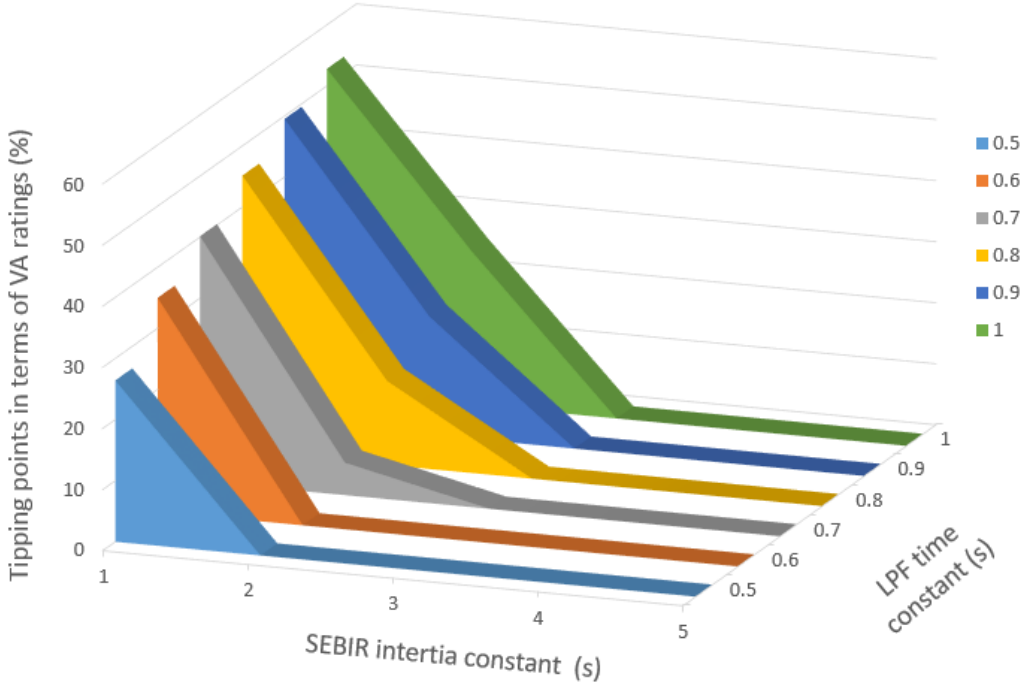

Figure 5-7. Tipping points in terms of steady state stability in APS model with SEBIR control implemented on DQCI converter using P class PMU to measure the RoCoF

It has been found that significant filtering is required for the SEBIR signal ΔP_{SEBIR} in the APS model due to noise generated from the measurement process, even when using PMU measurement. Otherwise, system stability limits could easily be reached even with a small amount of converters. For this reason, the time constant in the SEBIR low-pass filter to be investigated is chosen to be from 0.5 s to 1 s.

Intuitively, with increasing inertia constant in the SEBIR control, i.e. increasing effect of SEBIR control in the system, the system should become more stable, with higher tipping points. However, Figure 5-6 and Figure 5-7 show that the introduction of SEBIR control is counter-productive; that is, stability margins are diminished, rather than enhanced. This phenomenon is independent of choice of PMU (P or M class), and also independent of the noise levels in the signals. It is also noticed that using M class PMU to measure the RoCoF produces much better results (with respect to tipping points) than using the P class PMU.

In this "inadequate" provision of "synthetic inertia", a total time lag of more than approximately 1 cycle produces a response markedly different from that of a synchronous generator. The time/phase lags mean that although the power response may be "useful" in terms of dealing with frequency nadir, the phase of the response can be quite different to the 90º phase advance that the true inertia possesses. If the delays are too long, the SEBIR control will provide no mitigation of the initial RoCoF during an event. Furthermore, if the delay happens to cause a phase lag that is 180º different from the equivalent true inertial response, the output power adjustments provided by the SEBIR control could operate in anti-phase to the rotor swings of a real synchronous machine, magnifying classical rotor oscillations, and thereby, degrading network stability.

One of the key problems in abetting short-term changes in grid frequency through SEBIR controllers is determining RoCoF. RoCoF measurements are notoriously susceptible to large errors and ripples in the presence of noise, potentially due to various power quality imperfections. DQCI converter designers would typically expect smooth power targets to their inner current control loops. To achieve this, long measurement windows and long filtering time constants are applied, such as the P class and M class PMUs. If the total measurement window and response lag become too great, it poses a serious doubt on whether the SEBIR control could be helpful at all in mitigating system

RoCoF. Publications [7, 8] discussed similar effects of SEBIR control which was better termed as "Fast Frequency Response".

To visualise the impact of measurement and control delays, the SEBIR control has been applied on the NSG in the RGBT model with manually-adjustable control delay, as the frequency/RoCoF measurement appears to be "instantaneous" in PowerFactory. Analysis of the impact of measurement delay in the SEBIR control on the converter response is shown in Figure 5-8. It can be seen that even a short time delay of two cycles (40ms) causes instability in the network.

A deeper understanding of the critical difference between a true inertial response from a synchronous machine and the SEBIR response from a DQCI converter can be gained by studying the NFP charts shown in Figure 5-9. Clearly, the SEBIR response is different to that of the real synchronous machine, particularly with respect to phase of the response. It appears that the SEBIR-equipped DQCI converters, either with P or M class PMUs, can act in antiphase to SG rotor oscillations, at particularly "unfortunate" combinations of RoCoF measurement window and/or filter lags. The response is good in terms of the low-frequency dynamics, but is quite different to a real synchronous machine in terms of modulation frequencies above 0.2 Hz. The results might look quite different if different RoCoF measurement windows or filter windows were applied. Nevertheless, it is interesting to note that implementing SEBIR control on conventional DQCI converters may not assist system stability as has previously been suggested.

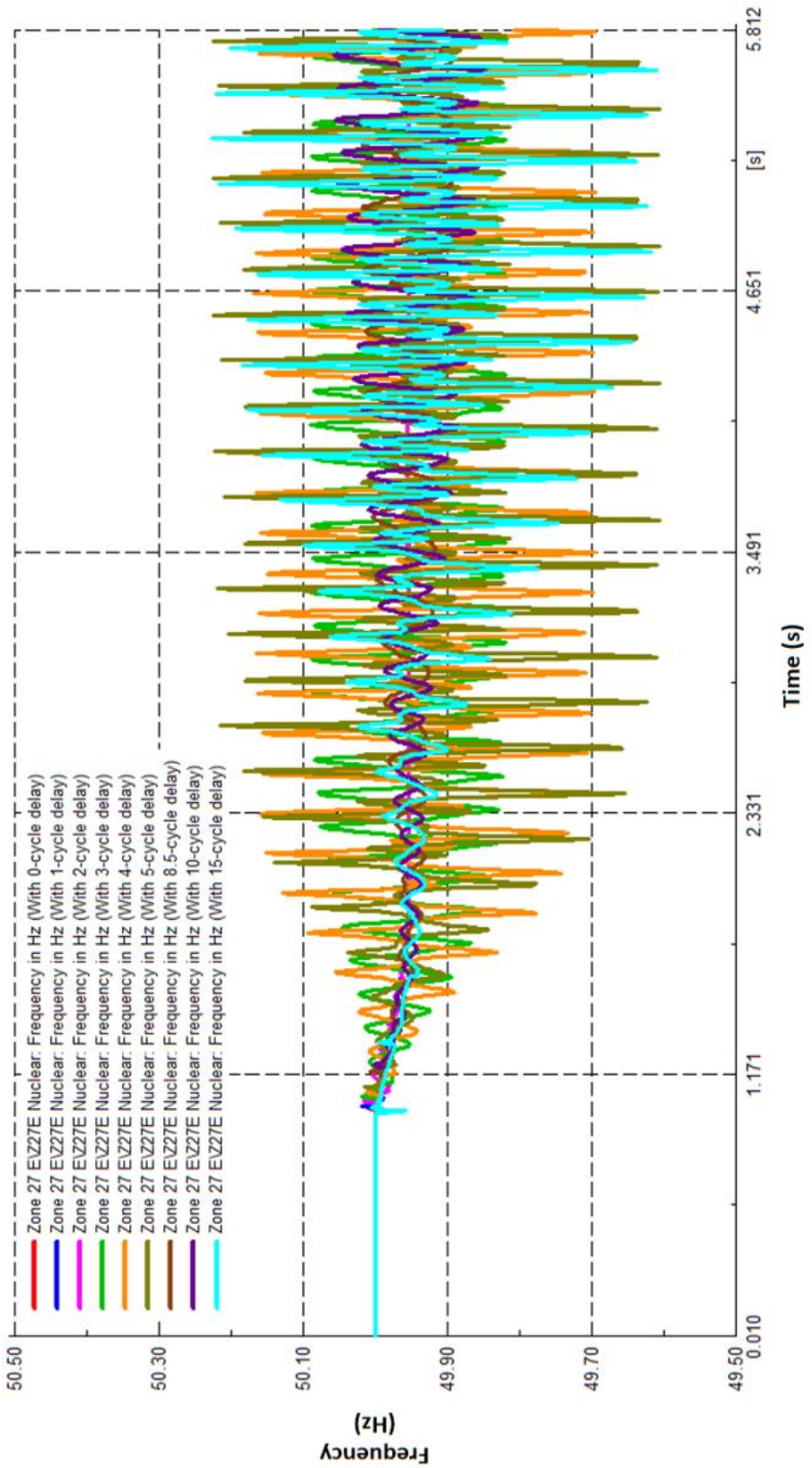

Figure 5-8. Effects of SEBIR control with various delay in the control loop in the RGBT model shown from frequency measured at a Scottish nuclear station in GB network

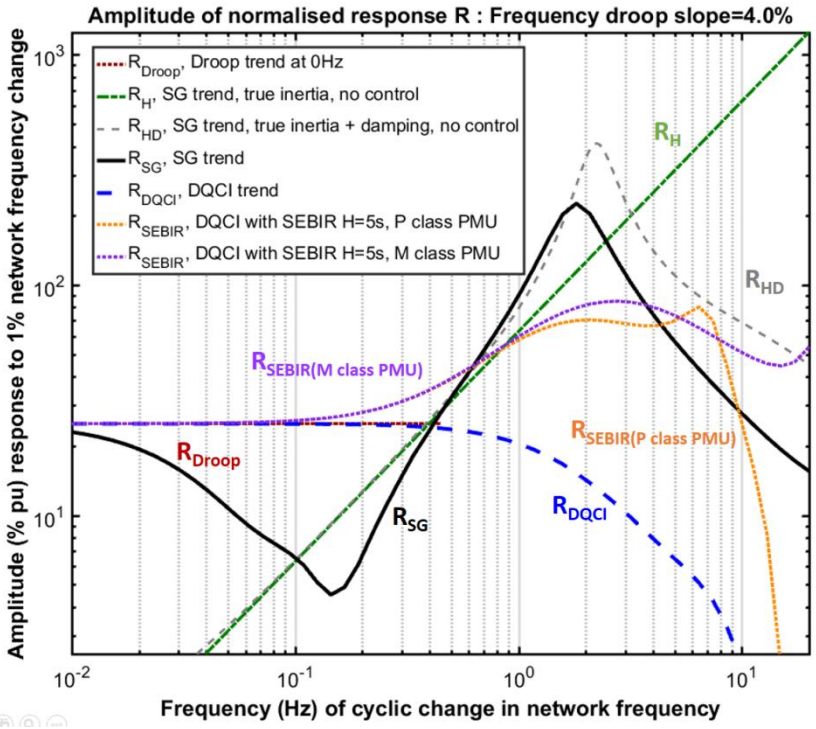

(a) Amplitude chart

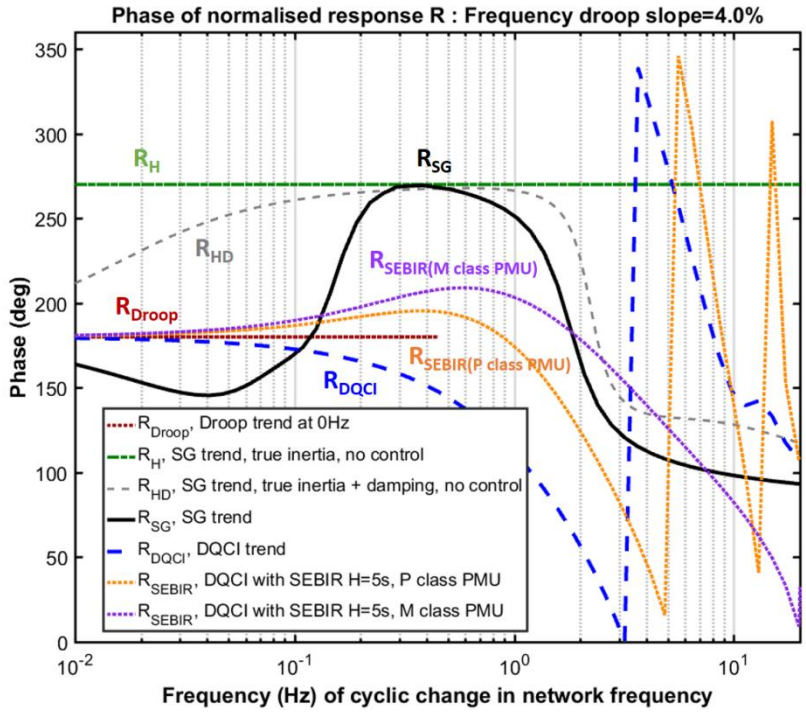

(b) Phase chart

Figure 5-9. NFP charts for SG, DQCI and SEBIR-equipped DQCI obtained by time-domain simulation along with the key trend-lines R_{Droop} and R_H predicated by classical linear analysis

5.4 VSM0H converter control

As introduced in 2.9.2.1, VSM0H control algorithm makes converter behave like a voltage source. Such a converter control technique is expected to be less insensitive to power quality issues and high frequency oscillations in the voltage waveforms at the point of common coupling (PCC). Accordingly, the VSM0H algorithm is beneficial to system stability under high penetration of converters.

In this section, responses of VSM0H converter to system disturbances such as load steps and faults are simulated. The results of NFP analysis are also studied and compared with the synchronous generator. Subsequent to this, an APS model is developed comprising a VSM0H converter connected in parallel with SG and DQCI converter. This model is then used to evaluate the tipping points in terms of small signal stability and transient stability.

5.4.1 VSM0H dynamic response

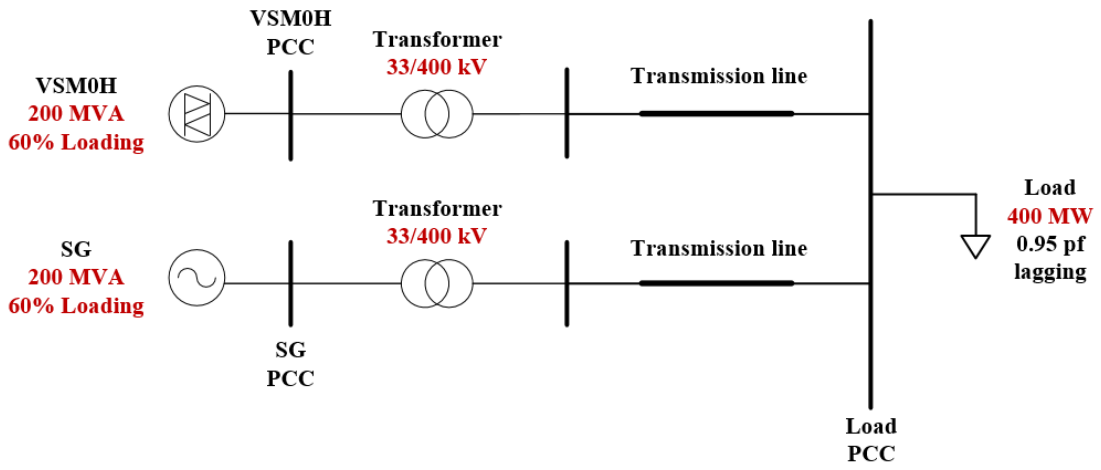

Figure 5-10. Network model for comparison studies of SG and VSM0H-type converter

Figure 5-10 shows a schematic diagram of the electrical network modelled in MATLAB Simulink which is used in the comparative studies of a SG and a VSM0H-type converter under various system disturbances including a 5% load step, a balanced three-phase fault, and an unbalanced phase-to-phase fault. The two types of generation are connected in parallel and share the 400 MW load (with a lagging power factor of 0.95), equally. The transformers, rated at 200 MVA with 0.15 p.u. reactance and 0.005 p.u. resistance, step up the voltage from 33 kV (distribution level) to 400 kV (transmission level). Both lines have a reactance of 0.04 p.u. and resistance of 0.005 p.u. (X/R ratio of

8) on 200 MVA base. The two types of generation are configured so that their responses are comparable. The test events are applied at 30 s and the total simulation time is 40 s.

5.4.1.1 Load step with VSM0H converter

A 5% load step relative to the system main load with a lagging power factor of 0.95 is applied in this case to test responses of the generation to a power imbalance event.

Responses of both SG and VSM0H are shown in Figure 5-11. It can be seen that both generators respond to the additional load step and a new system equilibrium is achieved. As soon as the frequency starts to deviate from its nominal value, the active power output of both generators ramp up. In the SG, inertia and governor controller contribute to frequency response and help to regain power balance in the network. The peak value of the first pulse in SG active power response is determined by the machine inertia and is proportional to RoCoF. On longer time scales, the increased power output is achieved through governor control.

With the VSM0H being a static voltage source, its current output instantly increases, causing the active and reactive power to evolve accordingly. As the input to the core control loop, the drive voltage magnitude and angle are changed correspondingly based on the droop equations. Such responses take place over a cycle due to the one-cycle boxcar filter applied to the measured active and reactive power. After the initial cycle, its power outputs (P & Q) gradually increase to support the additional load. Values of active and reactive power of both generators settle at the same levels due to the same frequency and voltage droop slopes applied.

It can be noticed that voltage measured at the SG PCC dropped more than that measured at the VSM0H PCC. This is due to the slower response of the voltage regulator than the droop response and reactive power support from VSM0H. It is also worth mentioning that under an event featuring power imbalance, the frequency experiences a rapid ramp from the initial frequency to the new frequency over one fundamental cycle. This could be beneficial to frequency nadir after the disturbance (under the assumption that sufficient energy is available at the DC bus); however, it could also introduce a high initial value for RoCoF, which needs careful consideration to avoid the unnecessary tripping of RoCoF-sensitive protection devices.

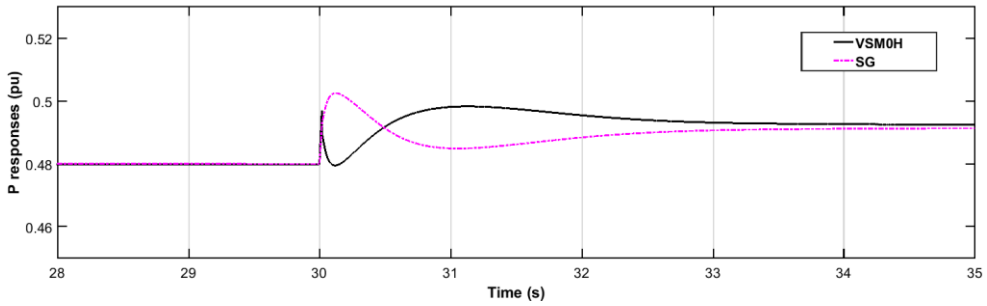

(a) Active power output

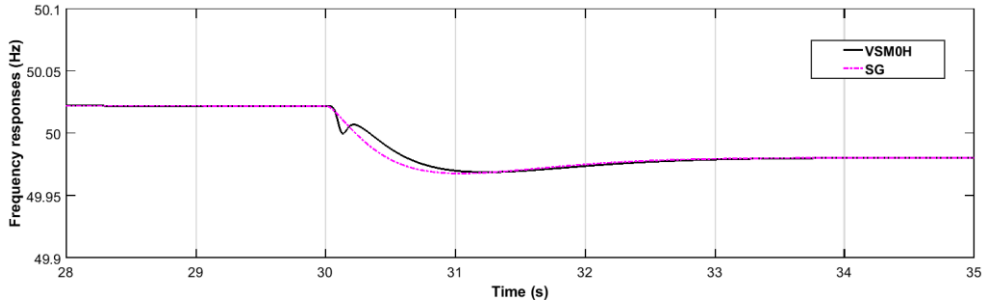

(b) Frequency

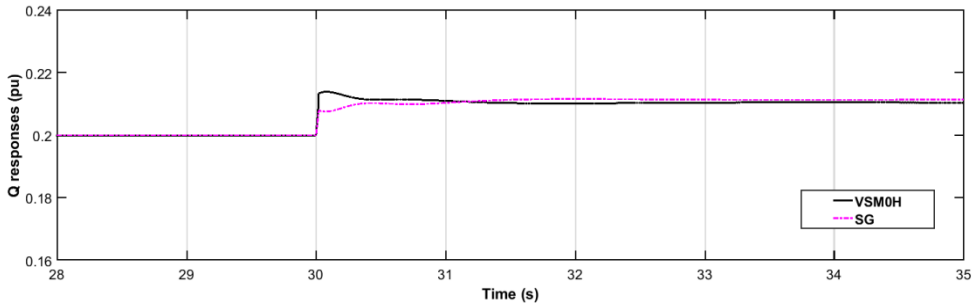

(c) Reactive power output

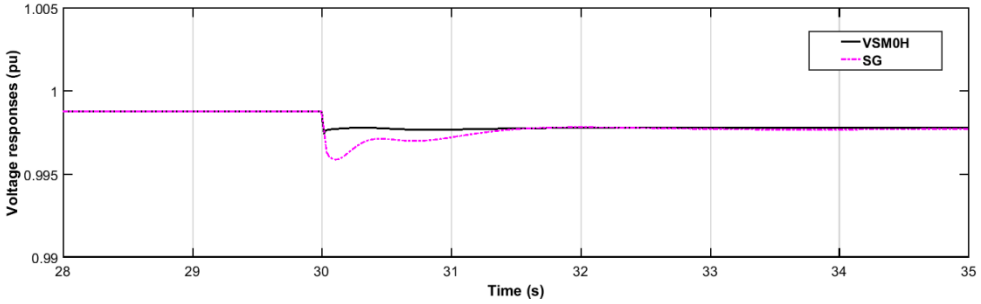

(d) Voltage

Figure 5-11. Responses of SG and VSM0H converter under the event of a load step

5.4.1.2 Balanced three-phase fault

In this case study, a balanced three-phase fault is applied in at the load PCC at 30 s with a duration of 140 ms. Current limitation of the VSM0H converter is set to ± 2 p.u. Response waveforms including voltages, currents, frequency, active power, voltage and reactive power of SG and VSM0H converter are shown in Figures 7-12~Figure 5-14.

Both generators perform satisfactorily, producing balanced currents during the fault; both recover after the fault is removed. It can be seen that, similar to the SG, VSM0H starts to provide current injection to the fault location immediately after the fault is applied. Contributing to fault current is required and desired in power systems so that the fault event can be detected by protection devices and cleared effectively before causing more serious problems. However, due to the hardware limitation on the converter itself, converter currents are normally limited to 1.5~2 p.u. as seen in Figure 5-13(b) compared to 4~10 p.u. as seen in Figure 5-12(b) (instantaneous current contribution from synchronous sets). Therefore, with high penetration of converters (regardless of the type of control technique) in the future power networks, it is important to bear in mind that the fault current contribution will be significantly reduced such as discussed in [7].

The voltages of both generators experience a significant drop due to the vicinity of the fault. The voltage magnitudes are determined by the electrical proximity (impedance) of the relevant generator to the fault location, which are the same for SG and VSM0H converter in this model. Similarly, active power outputs from the generators dropped significantly during the fault due to the reduced voltage levels.

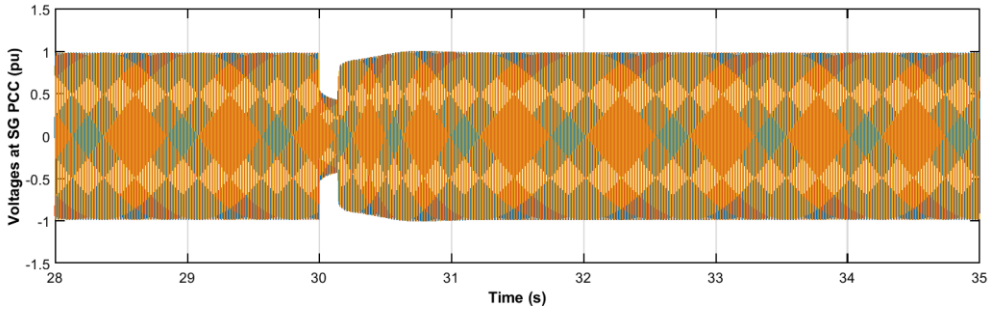

(a) SG terminal voltages

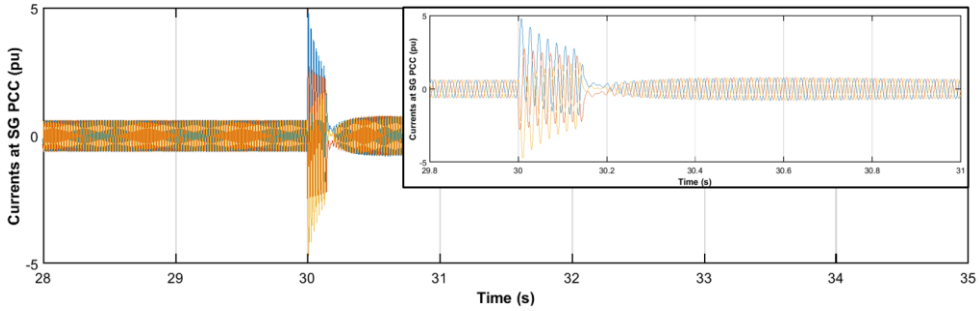

(b) SG currents

Figure 5-12. Responses of SG under a balanced three-phase fault

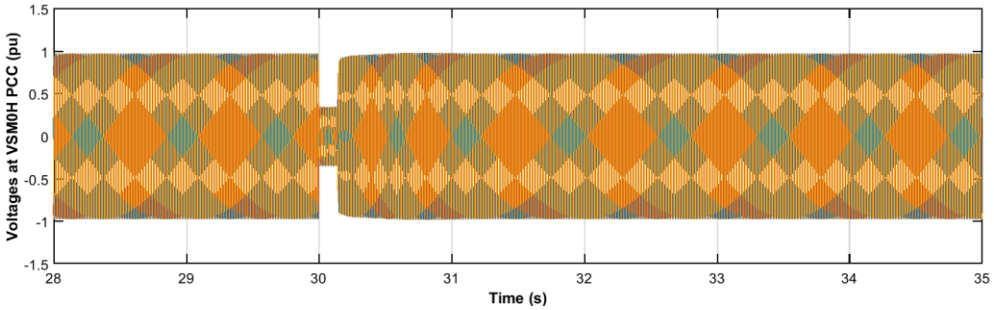

(a) VSM0H terminal voltages

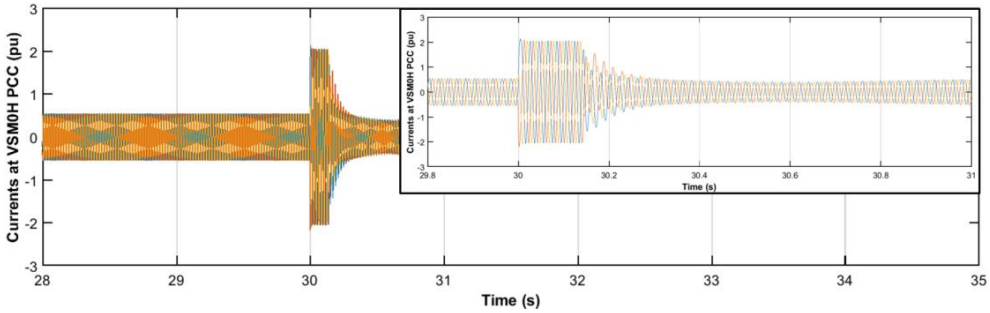

(b) VSM0H currents

Figure 5-13. Responses of VSM0H converter under a balanced three-phase fault

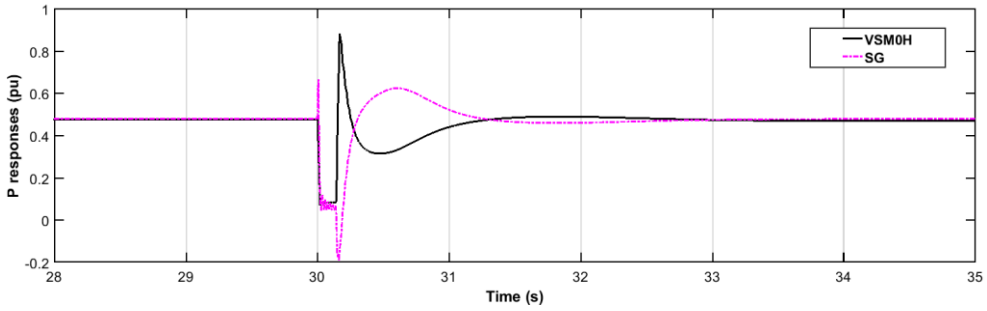

(a) Active power output

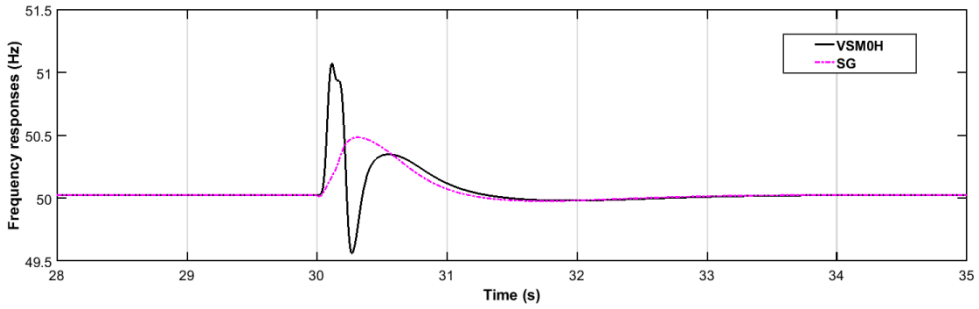

(b) Frequency

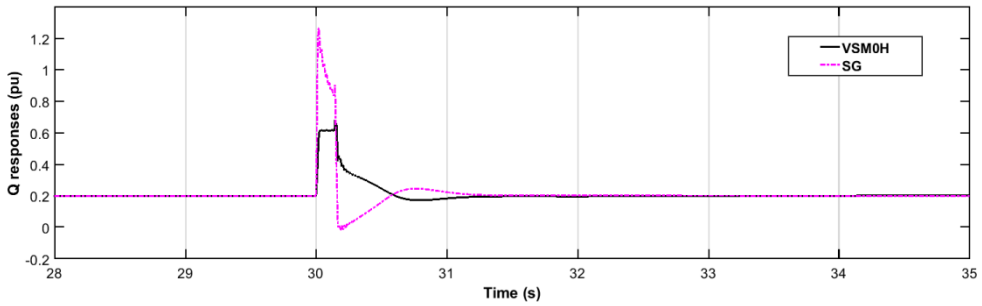

(c) Reactive power output

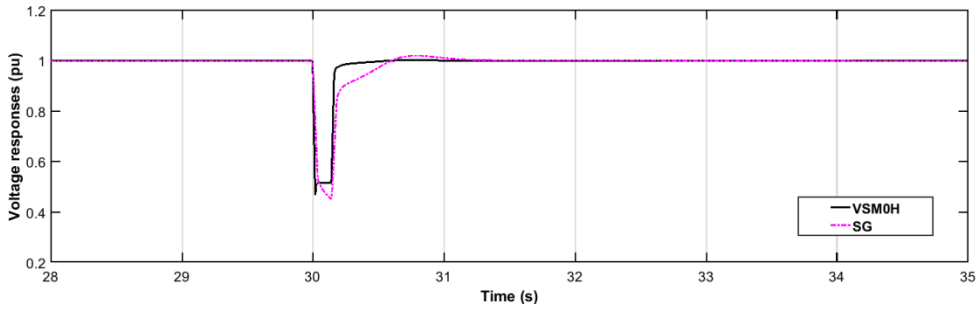

(d) Voltage

Figure 5-14. Responses of SG and VSM0H converter under the event of a balanced three-phase fault

5.4.1.3 Unbalanced phase-to-phase fault with VSM0H converter

Under unbalanced phase-to-phase fault, similar to the case with balanced three-phase fault, the VSM0H converter responds quickly in a similar way as the SG. It is worth mentioning that during the phase A to phase B fault VSM0H (as a voltage source) produces corresponding unbalanced currents naturally, in the way similar to SG. On the other hand, a DQCI-controlled converter typically has the objective of behaving as a balanced sinusoidal current source and a modified control algorithm is required to provide the capability of generating unbalanced currents, e.g. to meet the requirements stated in grid code documents such as [4]. The voltage-source behaviour of the VSM0H is therefore critical. It mitigates power quality and high-frequency oscillations in the voltage waveforms at the connection point. On the other hand, behaving in a similar way to the SG makes it possible to inherit fundamental ways of operation and control of the traditional power systems, such as the conventional protection schemes, and therefore, reduces various barriers and challenges during the transition to networks with significant penetration of converters.

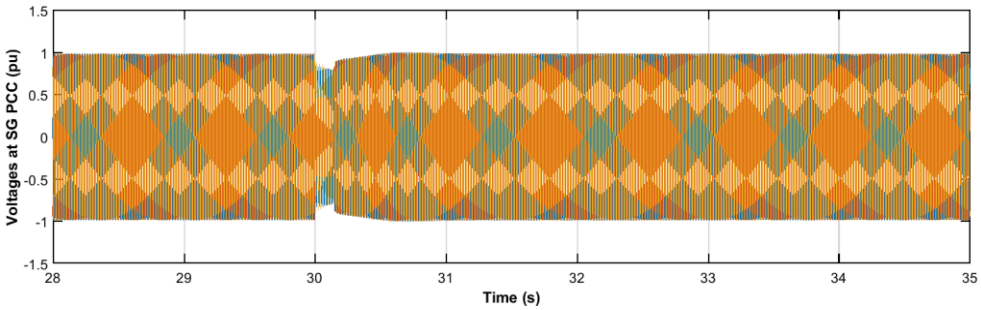

(a) SG terminal voltages

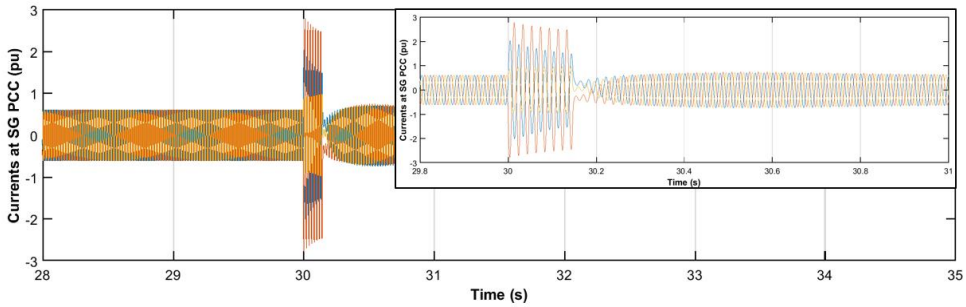

(b) SG terminal currents

Figure 5-15. Responses of SG under the event of an unbalanced phase A to phase B fault

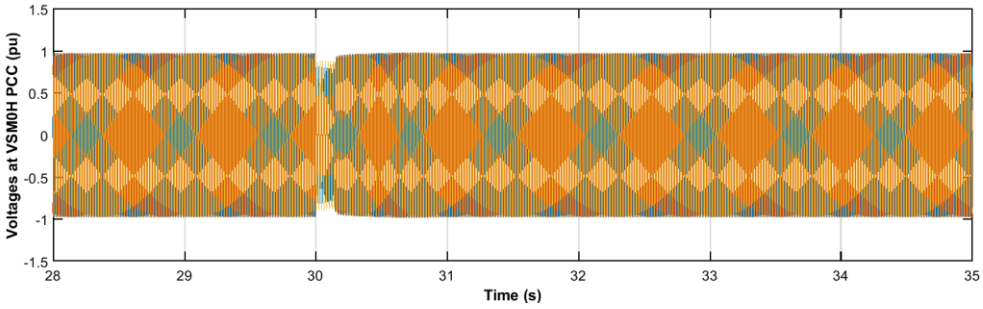

(a) VSM0H terminal voltages

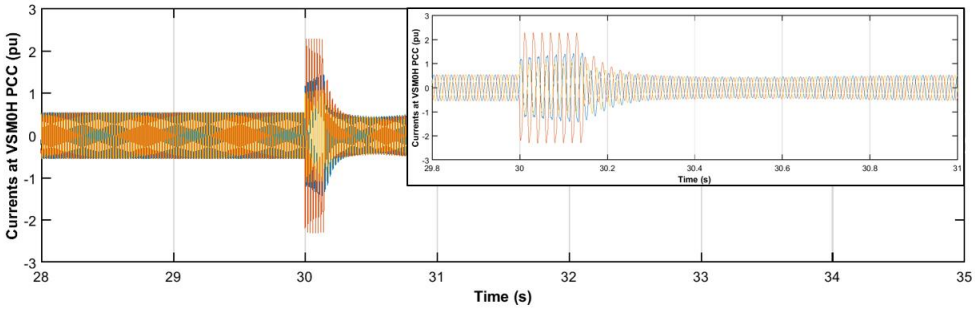

(b) VSM0H terminal currents

Figure 5-16. Responses of VSM0H converter under the event of an unbalanced phase A to phase B fault

5.4.2 Tipping point studies

For this study the VSM0H converter was implemented in the APS model in MATLAB Simulink. The VSM0H model is connected in parallel with the SG and DQCI converter to explore the system tipping points with various penetration levels of VSM0H-type converter, as shown in Figure 5-17. As introduced in section 3.3.2, impedance (resistance and reactance) of the transmission lines is the same in p.u. while its value in Ohms is scaled according to the VA rating of the generation connected behind of the line. In this model, the penetration level of VSM0H represents its percentage VA rating relative to the total converter VA ratings, i.e. DQCI converter and VSM0H converter combined rating. For example, with 60 GVA system rating, 50% of converter penetration and 5% of VSM0H represent SG rating of 30 GVA, DQCI converter rating of 28.5 GVA, and VSM0H converter rating of 1.5 GVA.

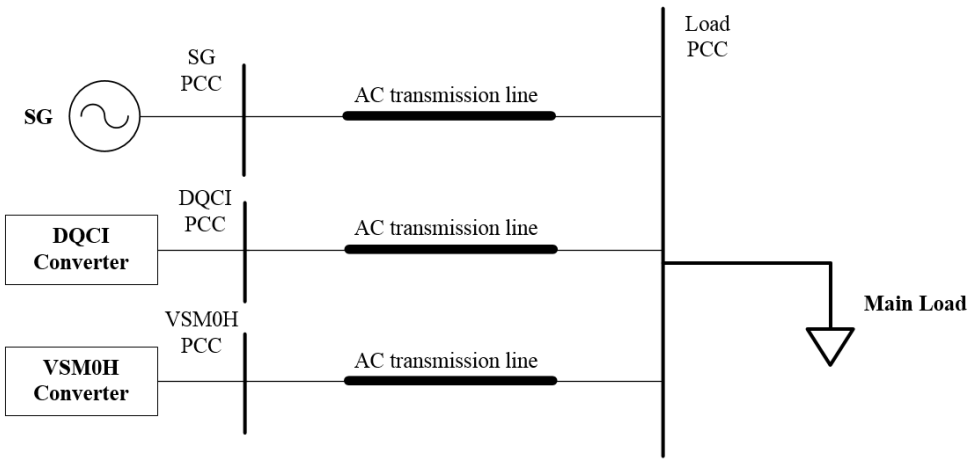

Figure 5-17. APS model in MATLAB Simulink with implementation of VSM0H converter in parallel with SG and DQCI converter for tipping point studies

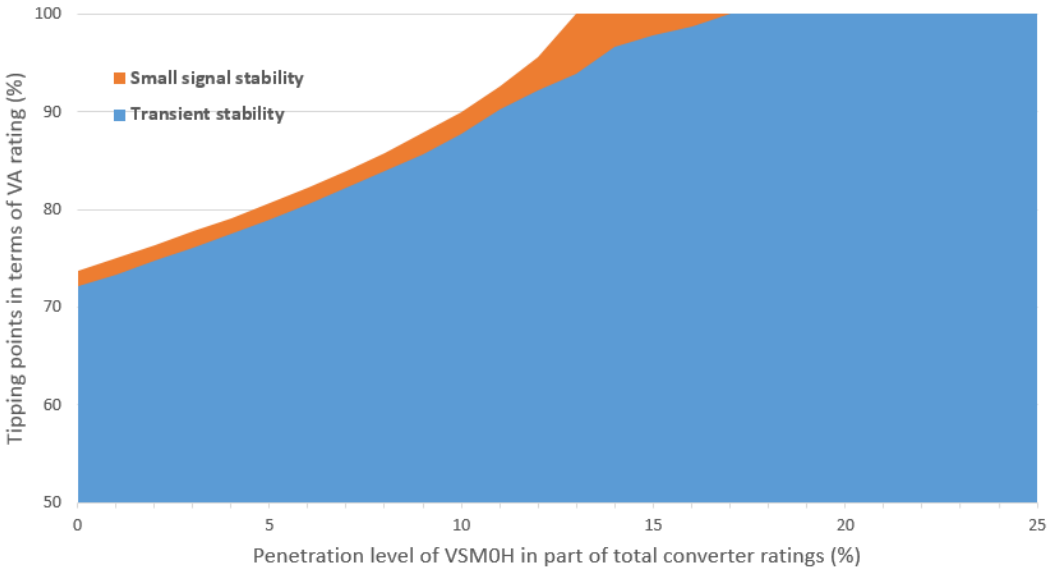

Figure 5-18. Tipping points in terms of steady state stability and transient stability in APS model with VSM0H converter implemented

The tipping point results in terms of both small signal stability and transient stability, found using the APS MATLAB model with implementation of VSM0H converter, are shown in Figure 5-18. It can be seen that utilisation of VSM0H converter in a power network with high penetration of converters could have a positive effect on the system tipping points and overall system stability both in terms of small signal and transient stability. For small signal stability, with VSM0H converter contributing to 13% of the total converter connected generation capacity, the tipping point can be pushed up to 100%

from around 72% where no VSM0H converter is used. To achieve system transient stability with 100% penetration of converters approximately 17% of VSM0H is needed only, based on this specific model configuration. Although the results found in a different simulation model or in the real power networks could vary, studies in this thesis clearly show the potential of the VSM0H control algorithm to increase penetration levels of converter connected generation in the future and the feasibility of achieving 100% converter penetration by utilising such control algorithm.

Work in [9] has employed the VSM0H control in converters based on the duplicated real site network model (with parameters defined as in the real devices such as lines and transformers) in MATLAB Simulink where multiple DQCI converters and VSM0H converters are connected at various locations in the network. It has been demonstrated that algorithms similar to VSM0H permit system configurations where all power is provided by converters. Furthermore, it has been demonstrated that the VSM0H converter has certain advantages during balanced/unbalanced fault, and in mitigating power quality issues.

5.4.3 NFP analysis

The NFP charts of VSM0H converter are compared against that of the SG and the three key characteristics as shown in Figure 5-19. VSM0H responses obtained from both linear analysis and numerical simulation are shown with acceptable differences. Unlike the SG responses and the three key characteristics, VSM0H performs steadily across the various modulation frequency ranges in both magnitude and phase. Furthermore, they mostly follow the droop asymptotes due to the droop equations applied in the VSM0H converter, except for the slight differences which occur at around 10~20 Hz; this could be due to the use of boxcar filter in the VSM0H converter. These results are consistent with the tipping point results which revealed the positive effect of VSM0H converter on system stability.

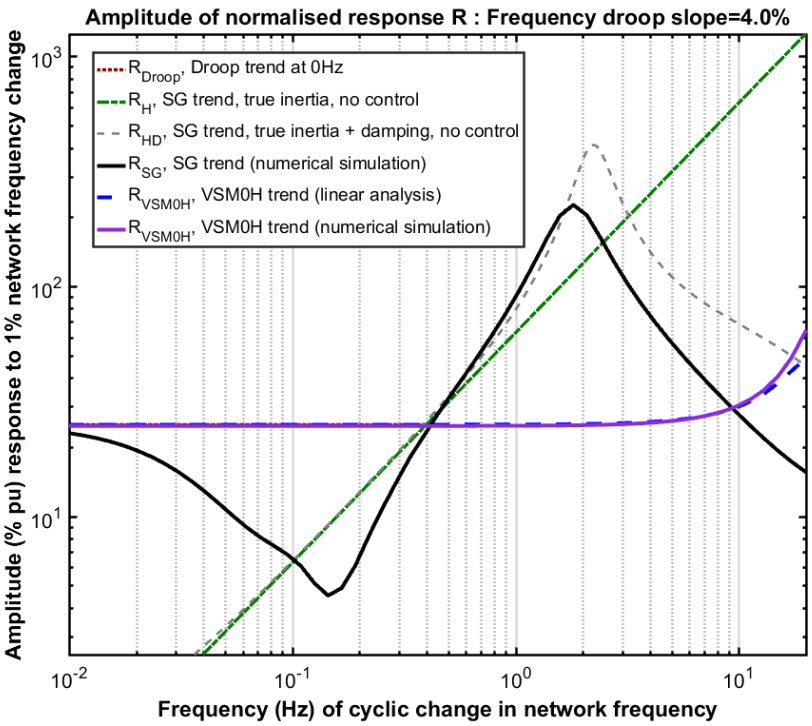

(a) Amplitude chart

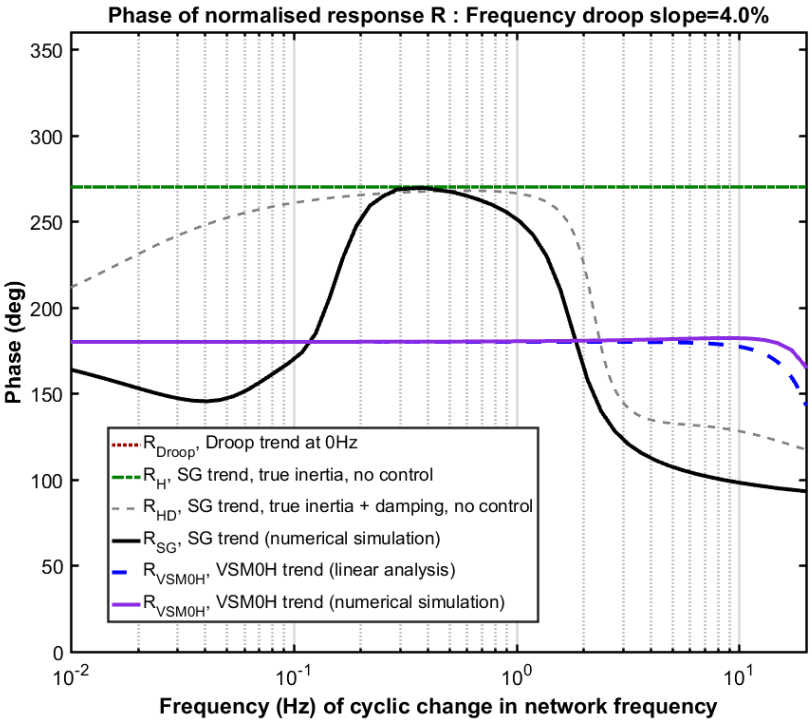

(b) Phase chart

Figure 5-19. NFP charts for SG and VSM0H converter obtained by time-domain simulation along with VSM0H trend and the key trend-lines R_{Droop}, R_H and R_{HD} predicated by classical linear analysis

5.5 VSM-type control

The VSM-type control technique is expected to provide many of the benefits of the VSM0H algorithm, but with the added ability of providing "true" inertial support. Both techniques drive the converter as a voltage source, similar to synchronous machine. Among various VSM techniques discussed in technical literature which can provide different features of a synchronous machine, a relatively simple VSM-type model which emulates the basic SG functionality was built and is utilised in this section for the purposes of comparative analysis.

The VSM-type converter responses to system disturbances (load step change and faults) as well as the NFP analysis are investigated and compared with the responses from SG. Tipping points obtained from the APS model with implementation of VSM converter are also explored.

5.5.1 VSM-type converter dynamic response

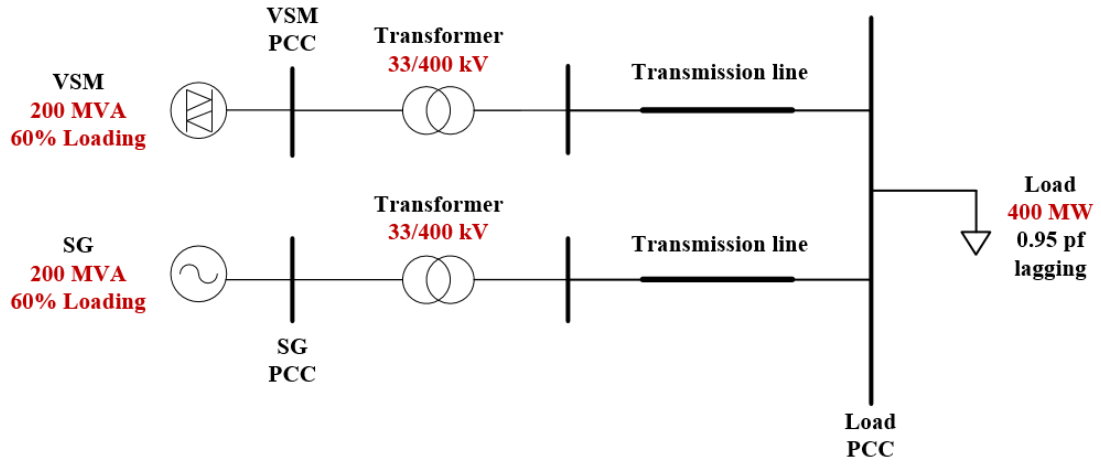

Figure 5-20. Network model for comparison studies of SG and VSM-type converter

Similar to the case study model used in the previous section with VSM0H converter, VSM-type converter is connected in parallel with a SG supporting the system main load as shown in Figure 5-20. Similar system configuration is adopted so that the results can be compared directly. Disturbances including load step, balanced and unbalanced faults are applied. The test events are applied at 30 s and the total simulation time is 40 s. For the VSM-type converter, its virtual inertia constant is set to 5 s which is the same as that of the SG. Damping factor of the VSM-type converter is set to 0.5 in the base case. Note

that theoretically the VSM damping factor could be set to 1, i.e. providing critically damped generator, as there is no physical limitations on the VSM compared to a real SG.

5.5.1.1 Load step with VSM-type converter

Responses of SG and VSM-type converter to 5% load step are shown in Figure 5-21. With the same IEEEG1 Governor applied, both generators are able to respond to the load step in a stable way and a new steady state condition is reached. It can be seen that both generators react quickly and in a similar manner due to the same governor control and similar operation mechanism. When there is more load connected to the network, both generators accelerate and generate more power to support the additional load based on the droop settings in the governor and voltage regulator. As both generators have either real or virtual inertia, oscillations introduced by the interactions between the two generators can be witnessed from their power outputs, and it takes longer for the frequencies to settle to a new level after the event.

In the case studies carried out in this section the damping factor, ζ (Zeta), in the VSM-type control algorithm is set to 0.5. Unlike conventional SG where many of the parameters are determined by the physical design of the machine, in VSM-type converters, all parameters are defined in software and could be changed in real time with no additional hardware cost (subject to converter physical limitations). Therefore, the damping factor ζ can be increased significantly without incurring extra cost or real energy loss. Effects of the damping factor ζ in VSM-type converter on its active power response following after the same load step event is shown in Figure 5-22. It can be seen that the post-event oscillations observed in the active power output of VSM-type converter decay with increasing damping factor ζ. This would be highly desirable in aspect of system operation for network stabilisation, although damping the rotor resonance too much might detract from some of the beneficial inertial response which will be investigated using the NFP method.

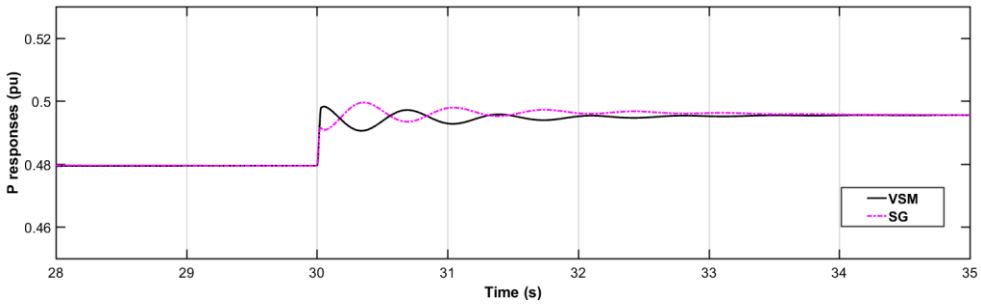

(a) Active power

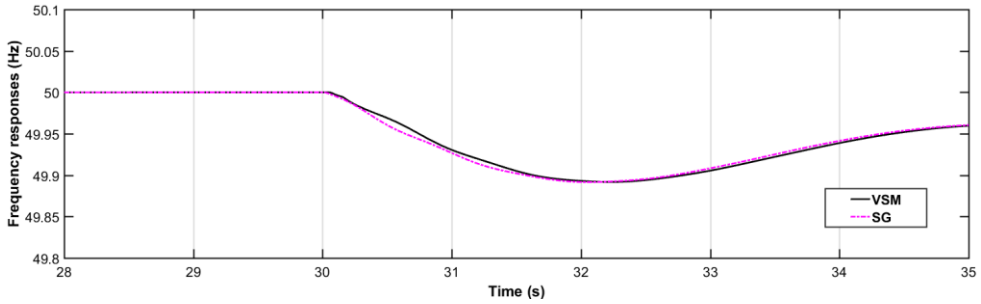

(b) Frequency

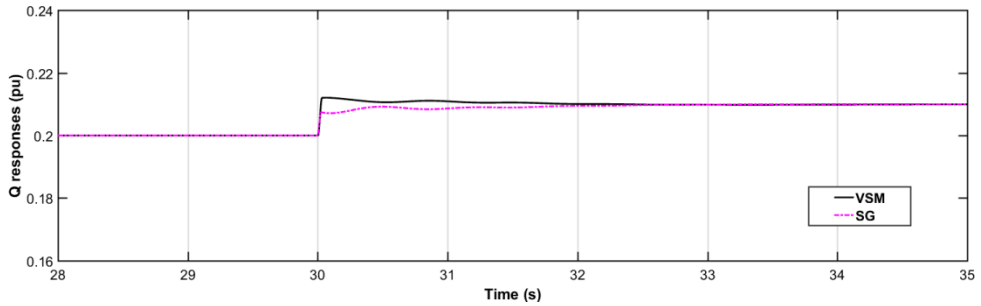

(c) Reactive power

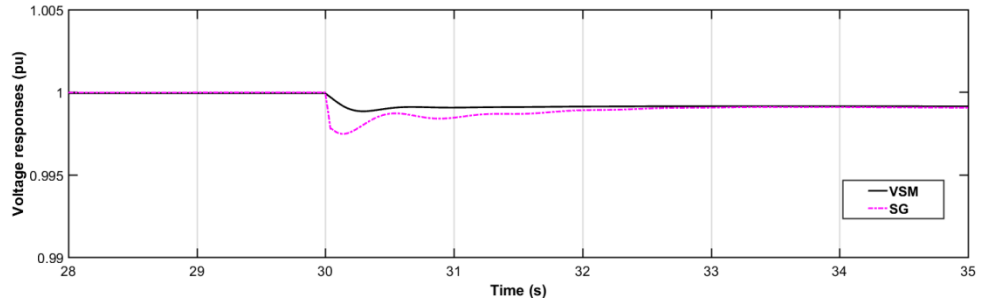

(d) Voltage

Figure 5-21. Responses of SG and VSM-type converter under the event of a load step

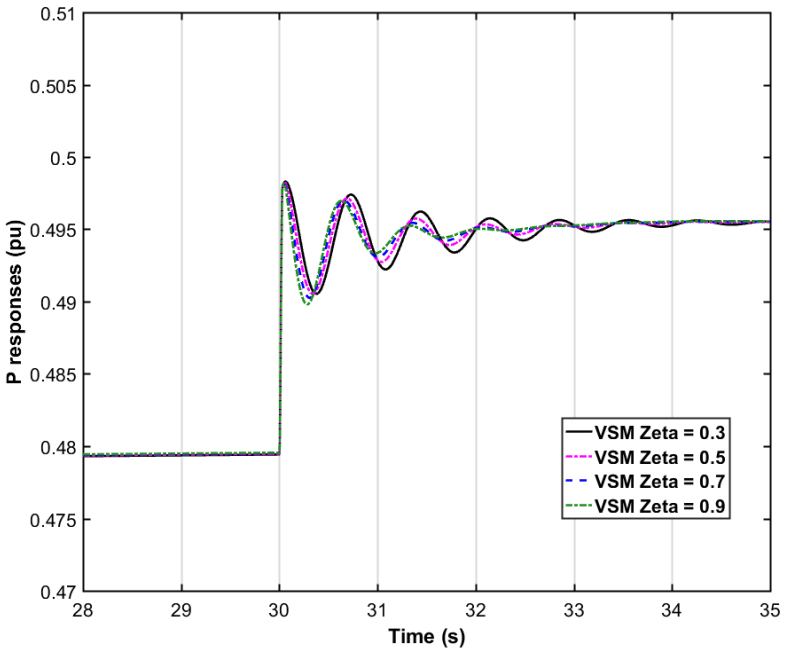

Figure 5-22. Effects of various damping factor zeta in VSM-type converter on its active power output measured at the PCC

5.5.1.2 Balanced three-phase fault with VSM-type converter

For the case of the 140 ms balanced three-phase fault in the middle of the network, i.e. at right side of the load PCC, resulting voltages and currents measured at the PCCs of SG and VSM-type converter are shown in Figure 5-23 and Figure 5-24. Similar to the VSM0H converter, the VSM-type converter starts to output fault currents instantaneously after the fault is applied as it is a voltage source like the SG, while the injected fault currents are limited to 2 p.u. compared to the 5 p.u. contribution from SG.

Waveforms of active power, frequency, reactive power and voltage amplitude of SG and VSM-type converter are shown in Figure 5-25. It can be seen that both generators perform satisfactorily and can recover from the fault after the fault is cleared. During the fault event, active power outputs of the two generators drop significantly while reactive power outputs boost to support the fault currents. With the dynamic breaking applied in the VSM controller, the virtual inertia constant is significantly increased when fault events are detected, i.e. when voltage drops to below 0.85 p.u.

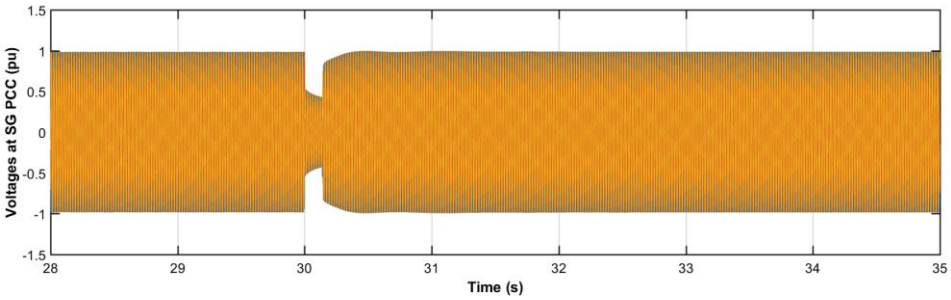

(a) SG terminal voltages

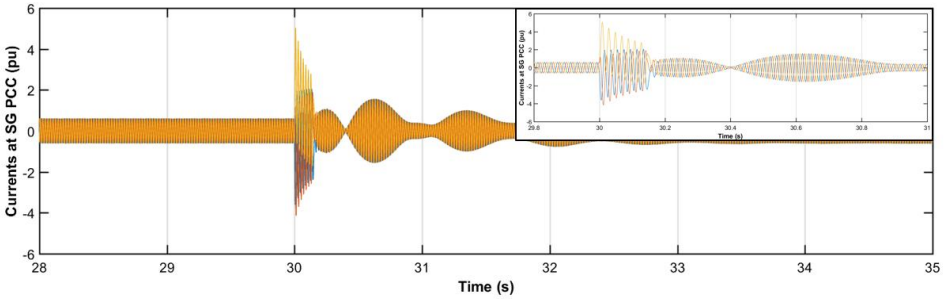

(b) SG terminal currents

Figure 5-23. Responses of SG under the event of a balanced three-phase fault

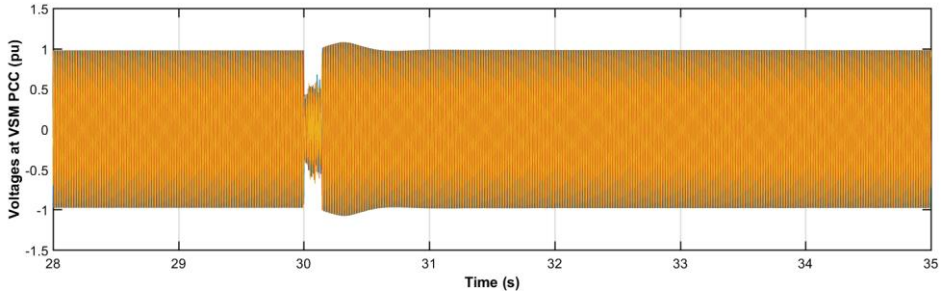

(a) VSM-type converter terminal voltages

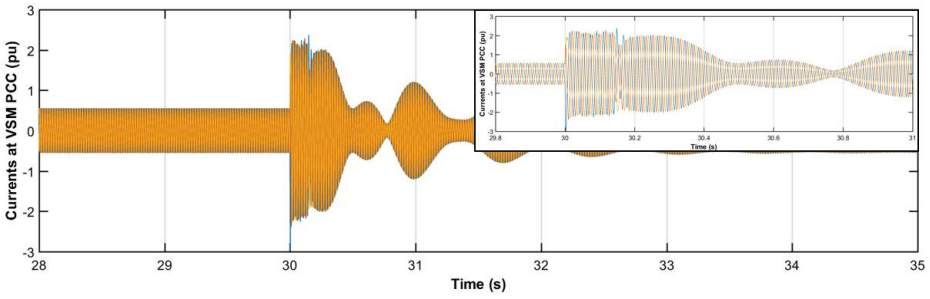

(b) VSM-type converter terminal currents

Figure 5-24. Responses of VSM-type converter under the event of a balanced three-phase fault

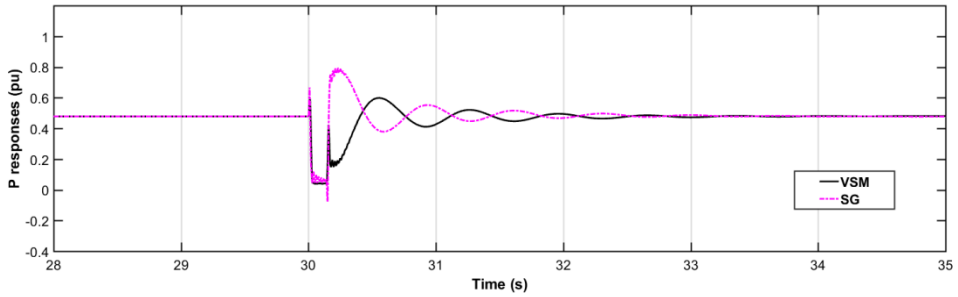

(a) Active power output

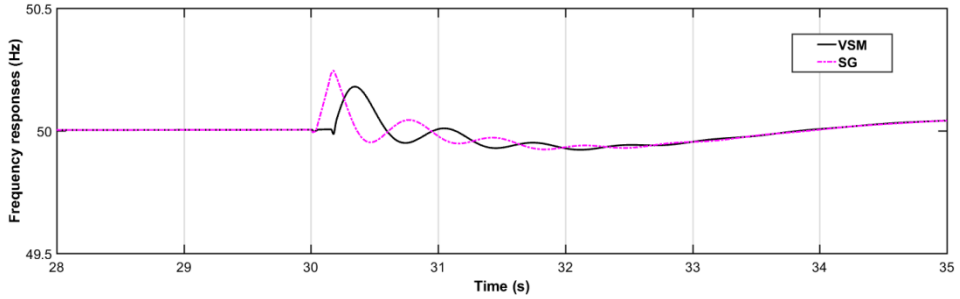

(b) Frequency

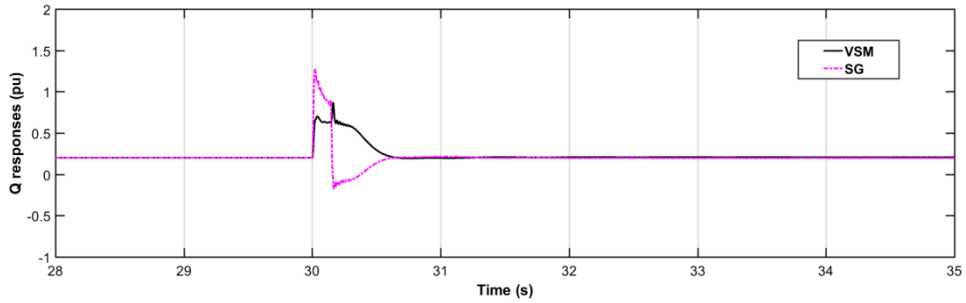

(c) Reactive power output

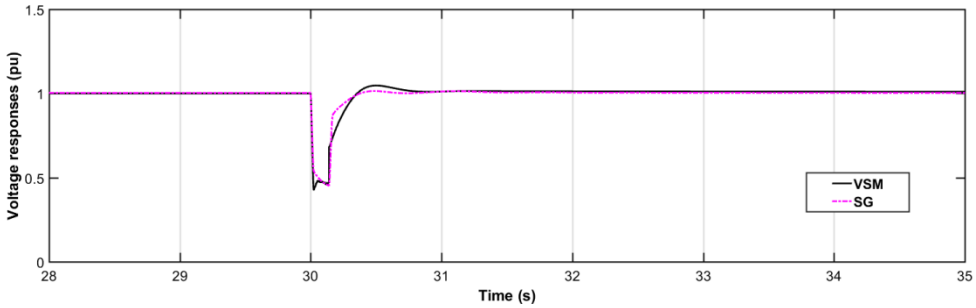

(d) Voltage

Figure 5-25. Responses of SG and VSM-type converter under the event of a balanced three-phase fault

As a result, the frequency deviation of VSM-type converter is arrested with its pre-fault operating frequency maintained while SG accelerates with an increasing frequency. However, once the fault clearance is detected, virtual inertia constant is changed back to its original value (5 s in this case) and both generators will continue to work resynchronised and settle down to reach the steady state. As the current of VSM-type converter during fault is limited by the converter hardware, the reactive power output is lower than that from the SG. However, with reactive power naturally reduced on fault clearance, the risk of post-fault over-voltages is lower.

5.5.1.3 Unbalanced phase-to-phase fault with VSM-type converter

In this case, the unbalanced phase A to phase B fault is applied at the same fault location, i.e. next to the load PCC, at 30 s with a duration of 140 ms. Responses of SG and VSM-type converter to this unbalanced fault are shown in Figure 5-26 and Figure 5-27. As a voltage source, VSM-type converter naturally produces unbalanced currents according to the type of the fault in a similar way as the VSM0H converter and SG.

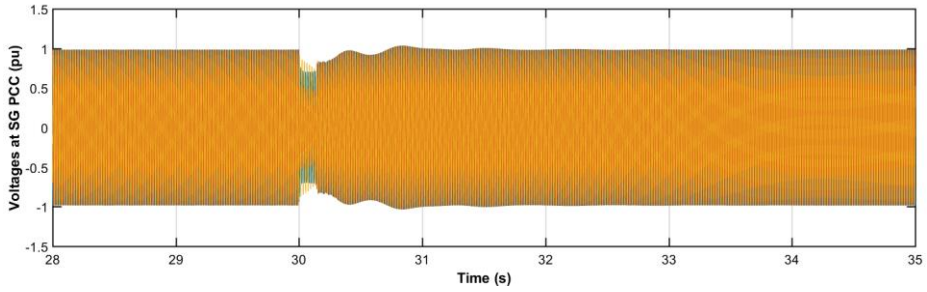

(a) SG terminal voltages

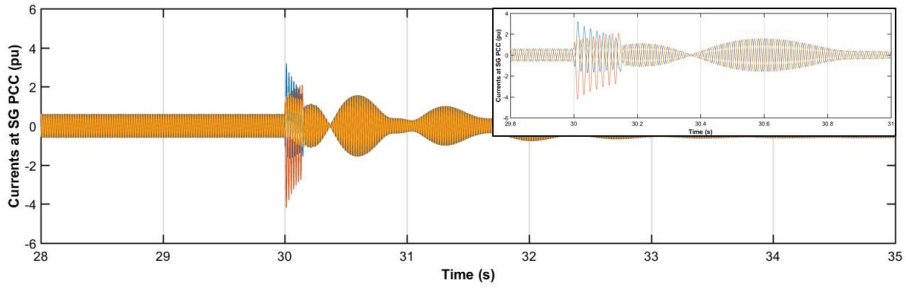

(b) SG terminal currents

Figure 5-26. Responses of SG under the event of an unbalanced phase A to phase B fault

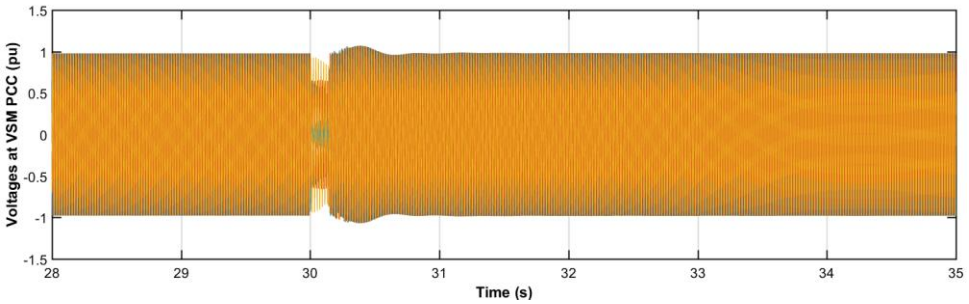

(a) VSM-type converter terminal voltages

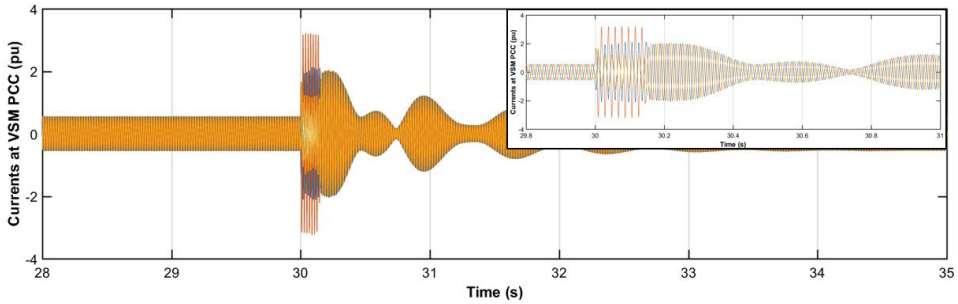

(b) VSM-type converter terminal voltages

Figure 5-27. Responses of VSM-type under the event of an unbalanced phase A to phase B fault

5.5.2 Tipping point studies

The VSM-type converter model is implemented in the APS model and connected in parallel with the SG and DQCI converter to explore the system tipping points with existence of VSM-type converter, in a similar way as described in section 5.4.2 with the VSM0H tipping point studies. Settings of the VSM-type converter are the same as those used for the comparison case studies as well. Tipping point results in terms of both small signal stability and transient stability are shown in Figure 5-28. It can be seen that with introduction of VSM-type converter, system stability can be significantly improved. Under 100% converter penetration the system can achieve stable operation in terms of small signal stability with only 14% of VSM converter VA rating contribution. However, to ensure system transient stability under 100% converter penetration, 18% of VSM-type converter contribution is required.

Both the VSM0H and VSM algorithms can provide a significant benefit to system stability. The results demonstrate that 100% converter penetration can be achieved. With moderate contribution from those converters both transient and small signal stability can be satisfied.

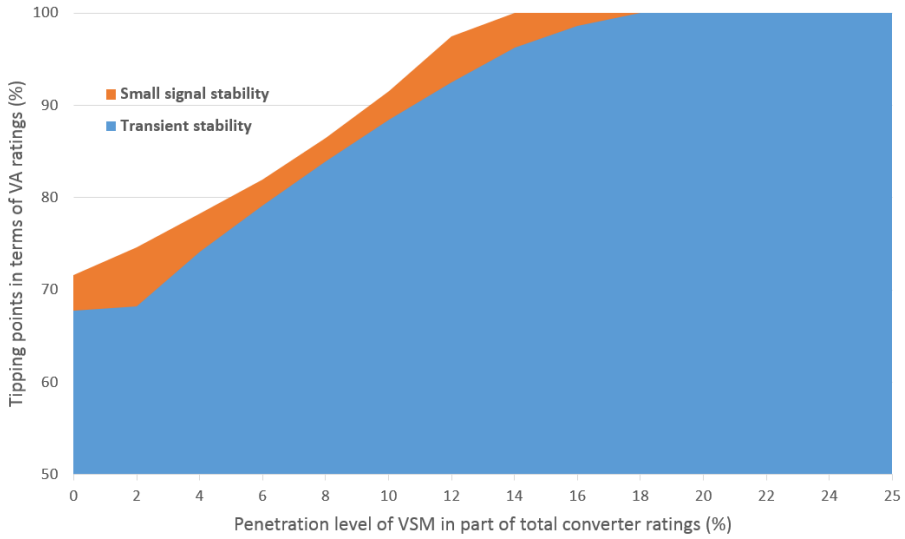

Figure 5-28. Tipping points in terms of steady state stability and transient stability in APS model with VSM-type converter implemented

5.5.3 NFP analysis

Responses of VSM-type converters to network frequency perturbation are investigated using the NFP analysis method and compared against that of the SG and the three key characteristics as shown in Figure 5-29. Results of VSM-type converter from both linear analysis and numerical simulation are shown. It can be seen that the responses of VSM-type converter are similar to that of the SG as they employ the same governor controller. Within the modulation frequency range, the response R_{VSM} firstly follows the droop asymptote, diminishes in value due to the dominant effect of the governor controller with modulation frequency slower than 0.2 Hz, then rises up following the inertia trendline and finally decreases after it reaches a rotor oscillatory mode and the damping effect starts to dominate. Compared with the NFP charts of VSM0H converter in section 5.4.3, which does not resemble the SG characteristic, the VSM-type converter behaves rather similarly to the SG including the inertia contribution and rotor dynamics.

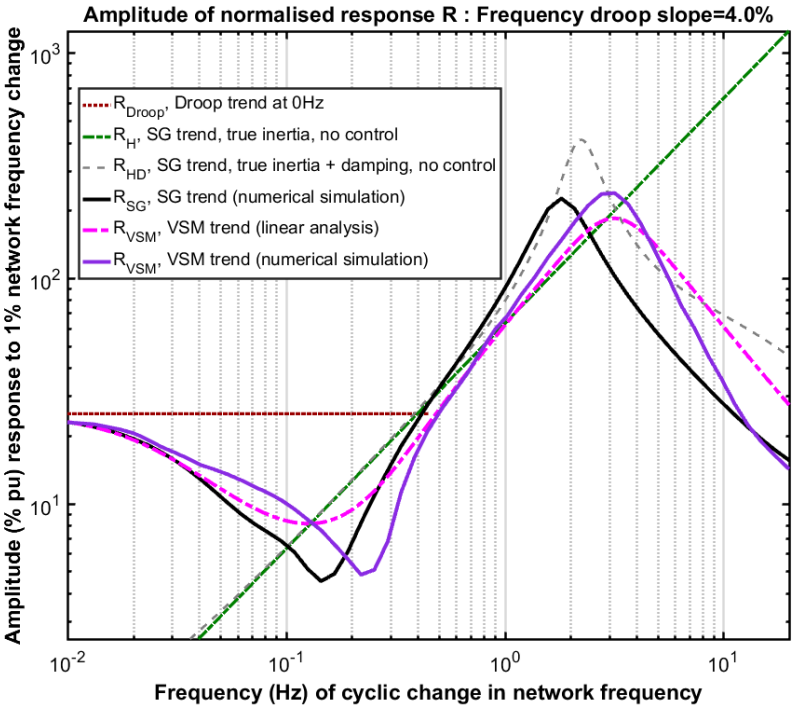

(a) Amplitude chart

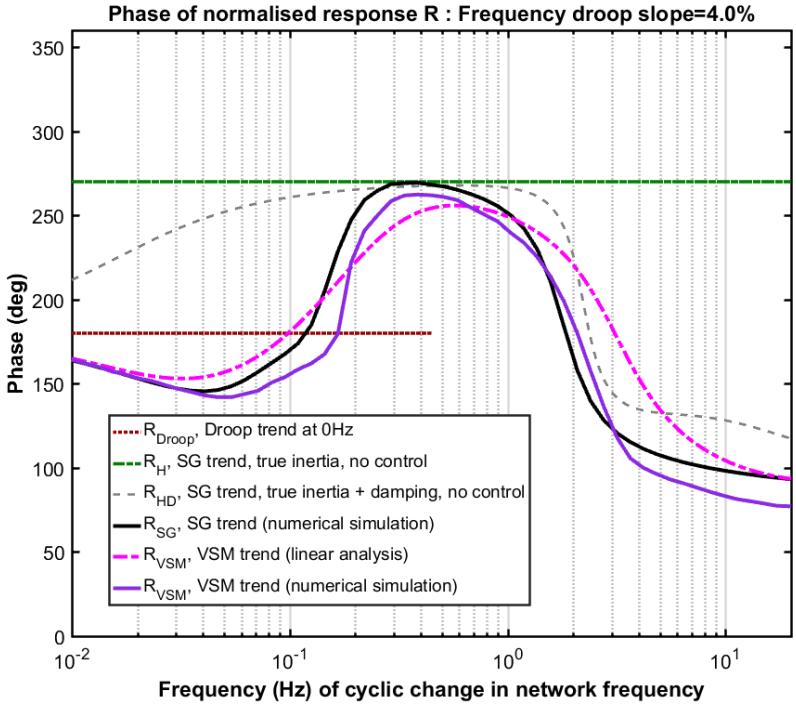

(b) Phase chart

Figure 5-29. NFP charts for SG and VSM-type converter obtained by time-domain simulation along with VSM trend and the key trend-lines R_{Droop}, R_H and R_{HD} predicated by classical linear analysis

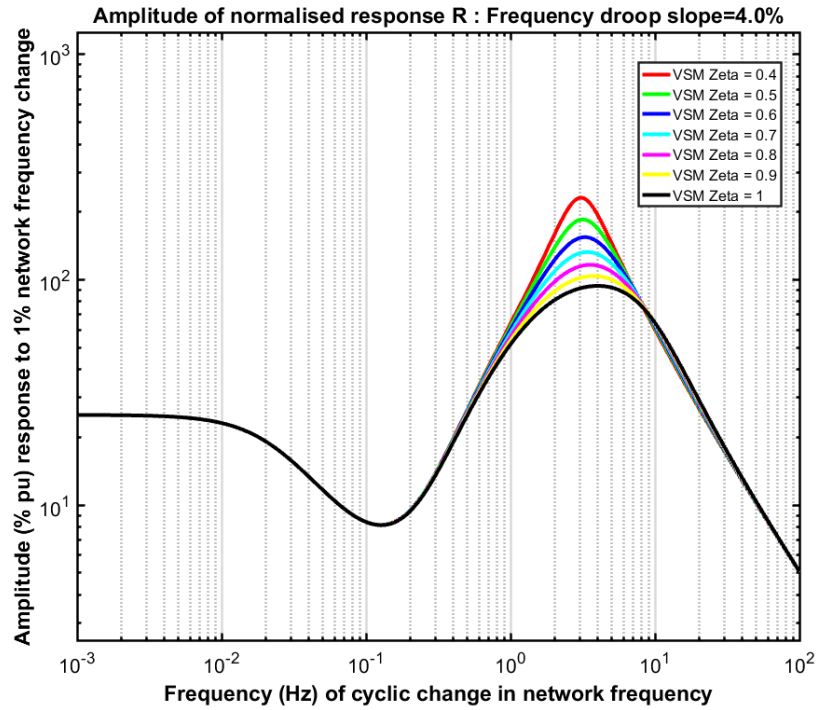

(a) Amplitude chart

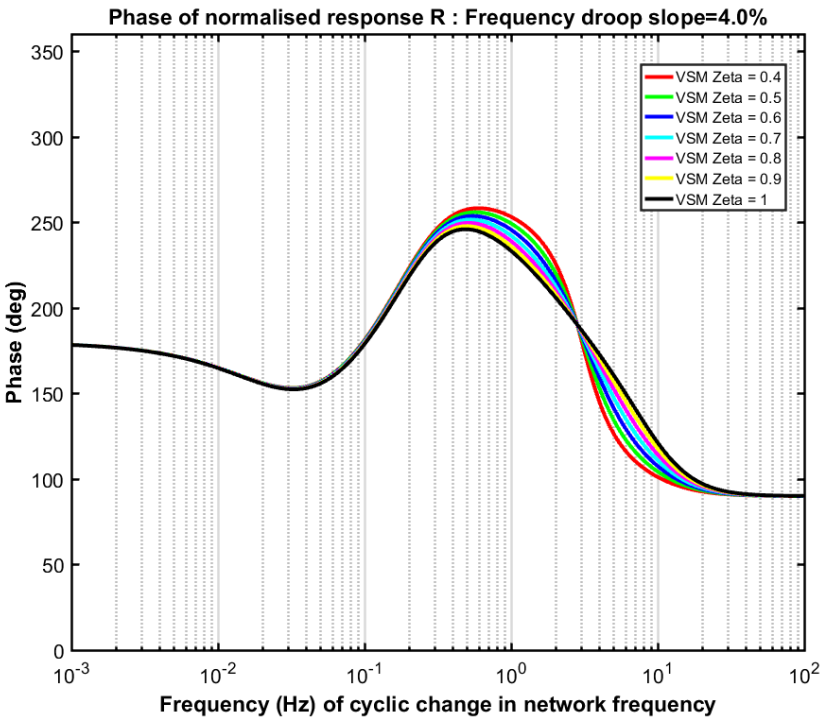

(b) Phase chart

Figure 5-30. Effects of damping factor Zeta in the VSM-type control on the NFP charts (obtained by time-domain simulation)

Additionally, the effect of electrical damping in the VSM-type converter is investigated in the NFP charts and is shown in Figure 5-30. It can be seen that with higher damping factor ζ, the rotor oscillation at around 2 Hz can be reduced, which means decreased settling time for the converter to settle down after events. However, it could also be noticed that both NFP magnitude and phase of VSM-type converter could be tilted away from the inertia trendline; therefore, a trade-off between inertia contribution and damping should be taken into consideration while configuring ζ.

5.5.4 Test of VSM-type control algorithm in PowerFactory

The VSM-type technique has been implemented in the RGBT model in DIgSILENT PowerFactory and tested by National Grid (UK) with details published in [10]. In the RGBT model, the generation termed as "Marine" (which represents the marine and solar) is equipped with VSM-type technique while the "Wind" model is controlled based on the conventional DQCI control algorithm. Three studies have been carried out including (a) the investigation of the required proportion of VSM-type converter to rectify instability problem associated with conventional DQCI converters, (b) trip of a 1600 MW generation, and (c) system split between Scotland and the rest of GB. Findings from those studies are briefly discussed below. Note that the penetration level of either NSG or VSM is defined according to (3-2) stated in section 3.2.

(a) With a double circuit fault applied on two of the four HVAC interconnectors connected between Scotland and England and trip on the Scottish border, the proportion of VSM-type converter required to rectify the instability problem associated with conventional DQCI converters has been studied. It has been found that maximum of VSM-type converter needed to achieve stable operation of the network is around 25% (~35% maximum of VSM-type converter is required for a low noise result) which showed a realistic possibility of achieving 100% converter penetration.

(b) A severe case was simulated where a 1600 MW SG is tripped under 97% penetration level of NSG with 75% of the NSG modelled as VSM-type converter (the remaining 25% were DQCI converters). It was found the system can survive and all generators operate satisfactorily sharing the power, with power limiting

algorithm installed on the VSM-type converters so that the close-up VSM units would not operate beyond their ratings.

(c) With the same double circuit trip applied on all four HVAC interconnectors crossing the England/Scotland border and after which the GB network is split, i.e. equivalent to England and Wales experiencing a loss of 4.6 GW generation, it has been found that the system can survive such severe event with VSM-type converter contributing 25% of the total capacity of NSG under 93% penetration level of NSG. It has also been found that with higher penetration level of VSM-type converter in the network, this capability required to get through such event could be reduced.

5.6 Benefits of grid forming converters

Studies in this chapter demonstrated the potential of grid forming converters (with VSM0H and VSM-type control algorithms explored as representatives) to allow 100% penetration of NSG. The grid forming converters have been considered as promising solutions to the future power networks with high penetration of converters by system operators such as in [11] by National Grid (GB) and [8] by ENTSO-E (Europe). Such converters behave as a balanced three-phase voltage source behind a constant filter impedance and with a control bandwidth smaller than 5 Hz. These characteristics have been demonstrated to have significant benefits against a number of challenges faced by the future power systems. The key benefits can be summarised as follows:

- Contribution to system inertia and provision of synchronising torque to the system, in order to help with the high RoCoF issue;
- No reliance on a stiff voltage source as conventional DQCI converters, and provision of reference voltage to the network;
- Provision of fast (sub-cycle) fault current response and ability to act as a sink to counter unbalance in system voltage;
- Enhancement of system stability, and ability to mitigate the issues associated with high penetration of conventional DQCI converters mainly resulting from the poor performance of PLL and high bandwidth ($\geq$ 50 Hz) of the control system;

- Ability to deal with sub-synchronous oscillations and interactions with conventional synchronous machines[4];
- Potential to mitigate power quality issues such as harmonics, inter-harmonics and unbalance in system voltage[1];
- Reduce the possibility of voltage instability during or post fault, e.g. voltage collapse, blocking or over-voltage, with utilization of the dynamic breaking block (for VSM-type controllers);
- Ability to be modelled in the RMS simulation and so conduct larger electrical system studies.

Additionally, the grid forming converter controls could be added to HVDC, large scale transmission connected or deeply embedded wind/solar power, or energy storage devices. In combination of its abilities stated above, it is considered an ideal candidate for NSG applications in the future power networks. Whilst the results presented are very encouraging, VSM-type and VSM0H techniques are not the only existing solutions to ensure stability of future power networks. Nevertheless, these control strategies point to a solution which is comprehensive in nature and can potentially address multiple issues.

Potential disadvantages associated with grid forming converters should also be considered while implementing such techniques in the power system. These are increased/higher frequency ripple in the converter DC side current resulting from AC voltage unbalance or harmonics, cost of over-rating converters when providing power support, source of energy behind of such converters, and possibility of traditional power system instability.

5.7 Summary

Based on the tipping point studies, NFP analysis and comparative case studies, the effectiveness of alternative converter control techniques in enhancing stability of power networks with high penetration of converters have been quantified. The maximum achievable system tipping points are summarised in Figure 5-31. The systematic

[4] Note that this ability is not within scope of the thesis.

assessment included, but was not limited to, selected parameters of supplementary droop controllers on DQCI converter, SEBIR control, VSM0H control and VSM-type control.

While certain combinations of droop slope and filtering time window settings for variants of the DQCI controller may be beneficial to system stability, uncertainties of such effect are of concern in a real power network. For example, with SEBIR control implemented on DQCI converters, rather than providing expected inertial response, delays in the measurement and control process have practically excluded this type of control from the inertial response category. As proposed in [7, 8], it is better to refer to SEBIR as 'fast frequency response'. Moreover, it has been found in this chapter that contrary to initial expectation implementing SEBIR type control can potentially destabilise the network. On the other hand, the VSM0H and VSM-type control algorithms (as representatives of grid forming converters) have shown positive effects on system stability. Both methods effectively enhance system stability and have the potential of achieving 100% penetration of converters in a network.

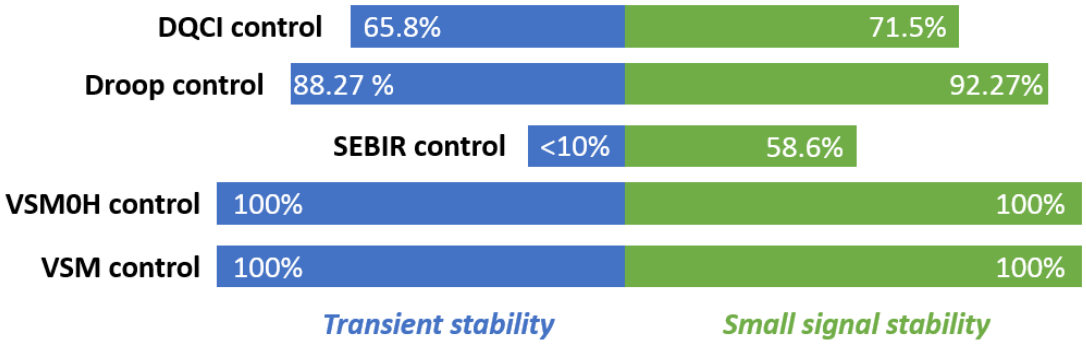

Figure 5-31. Summary of maximum achievable system tipping points in terms of both transient stability and small signal stability with various converter control technologies

References

[1] National Grid (GB), "The Grid Code," 2016. Available: http://www2.nationalgrid.com/UK/Industry-information/Electricity-codes/Grid-Code/, accessed in 2017/5/25.

[2] ENSTO-E, "Network Code for Requirements for Grid Connection Applicable to all Generators," 2016. Available: https://www.entsoe.eu/major-projects/network-code-development/requirements-for-generators/Pages/default.aspx, accessed in 2017/5/25.

[3] EirGrid, "The Grid Code," 2015. Available: http://www.eirgridgroup.com/site-files/library/EirGrid/GridCodeVersion6.pdf, accessed in 2017/5/26.

[4] ENTSO-E, "Network Code on High Voltage Direct Current Connections and DC-connected Power Park Modules," 2016. Available: https://www.entsoe.eu/major-projects/network-code-development/high-voltage-direct-current/Pages/default.aspx, accessed in 2017/2/16.

[5] A. Roscoe, "Measurement, control and protection of microgrids at low frame rates supporting security of supply," Doctoral Thesis, University of Strathclyde, Glasgow, 2009, Available: http://strathprints.strath.ac.uk/39631/, accessed in 2017/10/31.

[6] A. J. Roscoe, I. F. Abdulhadi, and G. M. Burt, "P and M Class Phasor Measurement Unit Algorithms Using Adaptive Cascaded Filters," *IEEE Transactions on Power Delivery,* vol. 28, pp. 1447-1459, 2013.

[7] National Grid (GB), "System Operability Framework," 2016. Available: http://www2.nationalgrid.com/UK/Industry-information/Future-of-Energy/System-Operability-Framework/, accessed in 2017/2/10.

[8] "Implementation Guidance Document (IGD) on High Penetration of Power Electronic Interfaced Power Sources (HPoPEIPS)," 2017 Available: https://www.entsoe.eu/Documents/Network%20codes%20documents/Implementation/CNC/170322_IGD25_HPoPEIPS.pdf, accessed in 2017/8/15.

[9] A. Avras, M. Yu, J. Zafar, A. J. Roscoe, and F. Coffele, "TPE002 Phase 1 Final Report: A Stable Grid with 100% Converter Penetration," Power Network Demonstration Centre (UK), January 2018.

[10] R. Ierna, A. Roscoe, M. Yu, H. Urdal, A. Dyśko, C. Booth, and J. Zhu, "Effects of VSM Convertor Control on Penetration Limits of Non-Synchronous Generation in the GB Power Sytstem," in *15th Wind Integration Workshop*, Vienna, 2016.

[11] "Effects of VSM/Option 1 (Grid Forming) Converter Control on Penetration Limits of Non-Synchronous Generation (NSG) in the GB Power System," June 2017. Available: https://www.nationalgrid.com/sites/default/files/documents/GC0100%20Annex%206%20FFCI%20supporting%20documents.pdf, accessed in 2017/12/15.

Chapter 6

Conclusions and Future Work

6.1 Conclusions

Conventional power networks have been dominated by synchronous generation such as thermal plants that use coal or gas as energy recourse, the very nature of which has raised concerns related to environment, economics and politics in recent years. Future power networks are expected to transform rapidly from the conventional, predictable and controllable synchronous generation portfolio to a non-synchronous and less-predictable energy scenarios with increasing penetration of intermittent renewable energy sources and power transfers via HVDC links. With the majority of countries worldwide signing up to environmental agreements to reduce CO_2 emissions and increase the use of renewable resources, challenges introduced by the dramatic transition which the existing power networks are facing, attract wide attention of system operators, manufacturers and researchers.

Modern converters typically operate on the vector current control principle, referred to as DQCI control in this work, which employs a phase locked loop (PLL) to provide synchronisation with the grid, from which a *dq* frame is established. However, the theoretical justification for the DQCI control algorithm is ultimately rooted in the assumption that the converter is connected to a strong AC system, such that the PLL dynamics can be ignored in the analysis. It has been widely discussed and reported that dynamics of the PLL are largely dependent on system strength; thus the stability of the DQCI controller is also dependent on system strength. As the proportion of DQCI converter capacity rises, the effective grid impedance between the voltage sources (i.e. synchronous generators) and the converters increases. At some point, termed as system tipping point in this thesis, the aggregated transient reactance is so large that, when added to the grid impedance, it causes the DQCI converters to become unstable. This instability is primarily related to the high variability of the voltage at the converter connection point when the converter injects its currents into a large equivalent grid impedance.

In this thesis, based on a RGBT model in DIgSILENT PowerFactory (RMS simulation) and a higher-fidelity APS model in MATLAB Simulink (EMT simulation with significantly reduced number of buses), system instabilities have been detected and assessed in terms of both transient stability and small signal stability under high penetration of conventional DQCI converters as discussed in Chapter 4. In order to study the stability thresholds, i.e. the tipping points, a tipping point search (TPS) method has

been established in this work which iteratively searches for the critical penetration level. At each iteration the method determines whether the system is stable based on a set of assumed detection criteria using the following indices: frequency, RoCoF, voltage magnitude, voltage THD, PLL locking signal in the DQCI controller, and voltage flicker perception level with reference to grid code requirements. Systematic stability quantification in both RMS simulation and EMT simulation is one of the main contributions of this work.

To gain insight into the effects of various parameters on a power network, the tipping points have been investigated under changing system inertia, system impedance, converter capacity factor and load type. The results have shown a strong correlation between system tipping points and system impedance, which echoed the reported stability issues associated with the poor converter control performance when system impedance is high.

As mentioned in Chapter 4, with increasing capacity factor in DQCI converters system tipping points have been found to decrease, mainly as a result of increased system equivalent impedance. At the same time, contrary to some discussions found in technical literature, inertia has been proven to have little effect on the system tipping points, although it is still very important from the point of view of system operation. Moreover, a direct relationship between the tipping points and the steady-state voltage angle difference between the converter terminal(s) and the stiff point in a network has been verified. The higher angle difference could lead to lower tipping points, i.e. negative effect on system stability.

Additionally, with an increasing amount of NLL, such as electric vehicle chargers, harmonics could be introduced into the network, causing a degradation in power quality. While this is not a particularly significant issue in conventional stiff power networks, it cannot not be ignored in networks with high penetration of converters. With introduction of NLLs in the system model, it has been found that the voltage THD level increased significantly. Therefore, the system tipping points could be reduced significantly when there are enough non-linear loads connected and where the power quality could be problematic in Chapter 4.

It should be noted that the absolute value of the tipping points established in this work is subject to specific modelling assumptions and could be different in a different

simulation model or in a real power network. It has been found that the trends of tipping points are affected by interactions between many factors in the model. Learning in detail about the combined effects of various factors in a power network (which could easily include more than a hundred parameters) could lead to very tedious multi-dimensional studies which go beyond the aims of this work. In this thesis, it is of more importance to reveal the instabilities associated with high penetration of converters and potential ranges of stability thresholds that could potentially result in future power networks, and also to provide a coherent analytical framework (the TPS method) which could be applied to any power system model for studying the tipping points.

Another simulation based tool which has been introduced in this work, i.e. the NFP analysis tool, allows a visualisation of the response of a device to variations in network frequency over a range of dynamic frequencies as introduced in Chapter 3. With this tool a clear distinction can be made between devices that provide frequency support through droop-slope type response and devices with inertial-type response. The NFP analysis can be carried out based on either a linearised model or time-domain simulation model. Although this method is not a classical stability assessment technique, it can be used to give a useful graphical insight into the device behaviour during network disturbances, and may offer indication of potential instability with implementation of various types of devices in a power network. Three key trendlines, R_{Droop} (droop asymptote), R_H (inertia trendline) and R_{HD} (trendline of inertia and damping effect), obtained for a synchronous machine plus a number of more subtle details have been established and can be interpreted to give further understanding of the device response in both magnitude and phase. By comparing to the key trendlines and responses of various controllers to a SG (R_{SG}), it has been found that the NFP response of a DQCI converter (R_{DQCI}) is significantly different in both magnitude and phase. As expected, R_{DQCI} does not follow either R_H or R_{HD}; this is because there is no inertia inherently provided by such converters; that being said, a converter may be able to contribute to frequency response by employing frequency droop controller. However, for the phase chart of R_{DQCI}, a significant phase difference between R_{SG} and R_{DQCI} has been found where the DQCI converter could become nearly anti-phase with the SG rotor oscillation; this could imply the stability issues at high penetration of DQCI converters, as discussed in Chapter 4. It also has been noticed that this phase difference could easily be affected by any settings in the DQCI control system and would be rather difficult to predict in any actual power system.

In order to achieve the goal of high (up to 100%) penetration level of converters in a power network, stability issues with the DQCI control need to be overcome. The recent state-of-art of converter techniques that have the potential of resolving system stability issues have been reviewed and discussed. In this thesis, groups of the proposed techniques have been categorised based on whether DQCI control and PLL are used or not. By applying the novel TPS method and NFP analysis tool, the tipping points of networks with various types of converters connected could be studied.

Supplementary control loops and/or modifications can be added within the DQCI control system so that desired features could potentially be built on the basis of existing technology, such as inertia emulation, frequency and voltage controllers, and enhanced PLL algorithms, as discussed and investigated in Chapter 2 and 5.

- In the conventional power systems, system inertia is contributed by synchronous units (both generators and motors). The rotors of those machines are directly coupled with the grid which allows power disturbances to be directly transferred onto mechanical torque. The torque naturally acts on the machine rotor and thus provides a frequency response quoted as inertial response. However, as renewable energy generation or HVDC interconnectors are normally connected to the AC grid via power electronic devices, they are decoupled from the AC grid and do not contribute to system inertia. This can be compared to a roller which slows power transfer between the generator and the network while a change in frequency at one side will not affect the other. Therefore, it has been a rather popular topic to emulate inertia on the converter interface to provide instant frequency support during power imbalance events. Intuitively, with inertia emulation implemented on the DQCI converter, the network is expected to be more stable with higher system tipping points, i.e. higher penetration level of converters should be achievable.

  However, it has been found in this work that the inertia emulation technique implemented on a converter interface, i.e. the SEBIR control, which adjusts converter power output according to the measured RoCoF and with reference to the Swing Equation, requires significant signal filtering. Insufficient SEBIR signal noise reduction could destabilise the system at a much lower tipping point than would otherwise be possible. Furthermore, although frequency nadir following

power disturbances could be reduced with well-filtered SEBIR control applied to the converters, this form of response is distinctly different from the true inertia provided by synchronous machines. Therefore, it is best to refer to SEBIR-type control as "fast frequency response". Examined by the NFP analysis, DQCI converters equipped with SEBIR control does not align with the inertia trendline and it could act antiphase to SG rotor oscillations at particular "unfortunate" combinations of RoCoF measurement window and/or filter lags which may be difficult to predict in any real case.

- Frequency and voltage droop controllers have been applied to the synchronous units in the conventional power networks and found to be effective in facilitating power sharing between generators after any power imbalance events. Such controllers have been widely discussed and utilised in converter-interfaced generation to provide necessary active and reactive power support so that the frequency and voltage could be controlled within desired operating ranges. From the results of system tipping points in terms of both small signal stability and transient stability, it has been found that implementing the droop controllers on DQCI converter could possibly have a negative effect on system stability and it could be worse if the drooped signal is insufficiently filtered. Again, this is due to increased interactions introduced by the droop control signals in the high-bandwidth inner current control loop in the DQCI converter, as well as the disturbed voltages measured at the converter PCC when connected to weak grid. Therefore, to reduce such negative effects as much as possible, especially when applying aggressive droop slopes on DQCI converters, the drooped signals need to be carefully filtered.
- Based on technical literature, improving the performance of the PLL could potentially help in resolving control stability issues associated with the DQCI converters. One of the solutions is to reduce the bandwidth of the PLL so that the stability thresholds can be increased, however, this could result in a slower dynamic response of the converter. Another solution is to synchronise the PLL with a more stiff point in the network. This could be a slack bus, a stiff source in the network, or a virtual stiff point established by estimating an equivalent grid impedance. The key objective is to ensure that the voltages fed into the PLL are less disturbed. However, there are uncertainties about the existence of such stiff

point in a real power network. With increasing penetration of converters, the accuracy of the estimated grid impedance when establishing the virtual remote point cannot be guaranteed. The power network infrastructure/power flow is constantly changing especially with utilisation of less-predictable renewable energy sources such as wind and solar PV. Therefore, these techniques have not been further explored in this work.

Due to the identified unsatisfying grid synchronisation of a PLL and resulting control stability issues, the alternative converter control algorithms that replace the conventional DQCI controller have been reviewed and investigated. Considering the benefits for existing system operation, stability enhancement as well as control and protection systems, it is of great benefit to mimic the operation principles of a traditional synchronous machine on a converter interface. Furthermore, traditional synchronous machines with the speed governor control and excitation control provide favourable features to support system operation in either transmission or distribution networks. This includes the provision of natural inertia and damping of system oscillations, frequency regulation through governor control, control of voltage and reactive power flow, islanding operation, and balanced/unbalanced fault current infeed. Therefore, the VSM concept, or often quoted as the grid forming converter by ENTSO-E and GB National Grid, has been increasingly popular in this field in recent years which enables the converters to operate (to certain extent) in a way similar to synchronous machines.

Among the various VSM techniques proposed by researchers which emulate different features of a synchronous machine, the VSM0H control and a VSM-type control have been selected as representative candidates to be investigated in this work as discussed and investigated in Chapter 2 and 5. Essentially, both techniques (and the majority of the other types of VSM-type converters) behave as a robust balanced three-phase voltage source set behind a filter impedance, forming a similar setup to that found in SGs. This is in stark contrast with the DQCI-controlled converter, whose objectives are such that the converter behaves as a balanced sinusoidal current source. This voltage-source behaviour is important; consequently, the VSM-type converter mitigates power quality and high-frequency oscillations in the voltage waveforms at its connection point, and could provide balanced/unbalanced/non-linear load currents instantaneously as a natural response to system events.

- As a simplified version of the full model of a synchronous machine, the VSM-type control algorithm established in this work emulates the rotor dynamics and damping based on the electrical angle change across the filter impedance, which is considered to be equivalent to a rotor angle. In other words, this VSM-type response contains only "spring" (power output is proportional to virtual rotor angle) and "damper" (power output is proportional to the derivative of virtual rotor angle) terms. Also, this VSM response adds an extra "mass" term via a finite value of virtual inertia constant which changes the device from purely damped response to one with a 2nd order transfer function with an associated natural resonant frequency, i.e. providing virtual inertial response. Under situations where a fault (either balanced/unbalanced) happens in the network, the VSM-type control in this work adopts a dynamic braking technique which sets the virtual inertia constant to an extremely high value when the converter terminal voltages are detected as less than 0.85 p.u. based on the GB Grid Code requirements to prevent the integrator changing the frequency of the converter and advancing the operating angle under such circumstances. Such implementation reduces the post-fault power oscillations and minimises rating requirements for converters. Another advantage of the VSM-type converter is that its parameters could be configured to suit any desired needs such as high damping factor to reduce post-event rotor oscillations, while conventional SGs have many physical constraints. Tipping point results when implementing VSM-type converter into the network were promising: system stability could potentially be improved significantly with a much higher tipping points, in terms of both transient stability and small signal stability, even with 100% penetration level achieved in this specific simulated power system model with a small amount of VSM-type converter contributing to the total converter capacity. This technique has been also tested in the RGBT model in DIgSILENT PowerFactory which has shown a similar effect on system stability. The NFP charts for VSM-type converter showed a great similarity to the SG when the same governor controller is applied to both generators.
- An alternative to the VSM-type is the VSM0H, so termed because it does not emulate inertia. The phase angle synthesised at the swing bridge is purely derived from an integrator which advances at the rate determined from a conventional droop slope of frequency versus measured active power output, and the

magnitude is derived from a conventional voltage droop slope of voltage versus reactive power. With the measurements of active and reactive power averaged over 1 cycle (using adaptive boxcar filter), the derived drive voltages sent to the switching bridge appear to be steady during scenarios with the presence of unbalance and harmonics. Therefore, the VSM0H converter could behave as a stable balanced voltage source to the grid. It should be noted that although there is no inertia emulation in the VSM0H control, in fact, if a VSM0H converter (alone) is feeding a power island and an active power load step occurs, then the frequency would experience a rapid ramp from the initial value to a new frequency over one fundamental cycle as determined by the averaging filter window length and droop slope settings. As a result, this control strategy does not directly mitigate high RoCoF following an event, but the frequency nadir can be well managed by the VSM0H strategy.

Similarly, it has been found in this work that the VSM0H-type converter behaves in a stable manner across the whole frequency range on the NFP charts, and it can provide positive effect on system stability with much higher system tipping points.

The key advantages of the VSM techniques investigated in this work compared to the conventional DQCI controller are briefly summarised below.

- As VSM converter behaves as a voltage source to the grid with much limited control bandwidth, compared with DQCI converter which operates as a current source, it could potentially reduce the risk of instability, controller interaction and the effects of imbalance and harmonics on the measurements. It could also potentially provide synchronising power and a reference voltage for other VSMs, SG and DQCI based generation.
- While still limited to the maximum instantaneous currents allowed through the converter hardware, VSM techniques allow faster and more appropriate fault infeeds in a similar way as the traditional synchronous machines. With mechanism of the dynamic braking applied (such as in the VSM-type control demonstrated in this thesis), a possibility of voltage instability during or post fault could be reduced.

- Unlike conventional SG where many of the parameters are determined by the physical design of the machine, for VSM converters, variables are defined in software and could be changed in real time with no additional hardware cost.
- Compared to the conventional high-bandwidth DQCI controller (mostly analysed using EMT simulation), it is easier to model the VSM0H and VSM-type controllers using RMS simulation which makes it possible to conduct large system studies using software packages such as DIgSILENT PowerFactory.

Both techniques (VSM0H and VSM-type) can be both implemented in the future power networks, along with other promising control techniques, which point to solutions that are comprehensive in nature and resolving multiple issues. However, it should also be noted that as the majority of VSM techniques drive the converter as a voltage source, it is important to implement current limitation (even during short-term current overloads) in the control system to avoid damage to converter hardware, especially with the presence of fault events.

The TPS method for detection of system stability threshold has a generic nature and can be used to any system model, with the set of criteria easily to be modified based on different network requirements. Moreover, with the assistance of NFP analysis tool, generation responses when exposed to various network frequency perturbations can be visualised and compared to gain deeper understanding of how they behave, interact and potentially reveal useful information on reasons for certain instabilities. Such studies could become increasingly relevant in the future power networks as more and more converter-interfaced devices are expected to be implemented with various control techniques. It is vital to fully study such control techniques on system dynamics and more importantly their effect on the network stability.

6.2 Future work

The work presented in this thesis proposed tools, TPS method and NFP analysis tool, to study the instabilities and tipping points associated with conventional converter-interfaced devices with various control techniques in the future power networks. In the light of the direction that this work took, the following research avenues may be of interest to both academia and industry:

- Since the focus of this work was on the connection of converters to the power system, a constant voltage source has been used at the DC side of the converters; thus, it was assumed that an infinite amount of energy can be generated from/absorbed by the DC side. A more detailed model of the energy source, such as wind farm or PV array, should be modelled in the future, coupled with which should be an investigation into the effects of finite energy supplies on system stability. And the converter control algorithms discussed in this work can be applied to the rectifier of the HVDC link or converter connected by generation to explore their impacts and interactions with the control system for the energy sources.
- Effects of various types of converter connected in parallel in the same power network can be investigated in terms of their interactions with each other and system dynamics under disturbances such as power imbalance, faults and islanding operation.
- Representative converter control techniques have been selected and investigated in this work. More converter control algorithms that have the potential of assisting system stability under high penetration of converters could be proposed by researchers which can be tested in terms of their impact on system tipping points and dynamic responses utilising the TPS method and NFP analysis tool introduced in this work.
- Stability limits and performance of various types of converters could be tested in a more complicated power network model and/or the converter hardware-in-loop (CHIL) environment to more realistically establish their impact.
- The NFP analysis tool is based on network frequency perturbation which mainly reveals the dynamic active power responses of different generator. On the other hand, network voltage perturbation (NVP) method, which can be used as a companion of the NFP method, could be established to enable a study of the coupling between the frequency and voltage responses of the power system, to further improve insight and understating of the potential for instability in power systems with high penetration of converters.

Appendices

Appendix A Settings for APS model in MATLAB

TABLE I

SETTINGS FOR EVENTS

Parameter	Value
Load step size	0.01 p.u.
Fault duration	100 ms
Fault resistance	0.002 Ω

TABLE II

SETTINGS FOR DQCI CONVERTER (BASE CASE)

Parameter	Value
Rated AC voltage V_{acnom}	100 kV
Nominal DC link voltage V_{dcnom}	200 kV
Phase reactor resistance R_{PR} and inductance L_{PR}	0.002 p.u., 0.2 p.u.
Switching frequency $f_{switching}$	4000 Hz
Capacity factor CF_{DQCI}	60%
Frequency droop slope $D_{f,DQCI}$ and LPF $\tau_{f,DQCI}$ time constant	4%, 0.5s
Voltage droop slope $D_{v,DQCI}$ and LPF $\tau_{v,DQCI}$ time constant	8%, 0.5s

TABLE III

SETTINGS FOR SG

Parameter	Value
Rated terminal voltage V_{acnom}	33 kV
Inertia constant H_{SG}	5s
X_d , $X_d^{'}$, $X_d^{''}$	1.65 p.u., 0.25 p.u., 0.2 p.u.
X_q , $X_q^{'}$, $X_q^{''}$, X_l	1.59 p.u., 0.46pu , 0.2 p.u., 0.14 p.u.
$T_d^{'}$, $T_d^{''}$, $T_q^{'}$	4.5s, 0.04s, 0.67s
Capacity factor CF_{SG}	60%
Governor model	IEEEG1 Steam turbine and governor model
Frequency droop slope $D_{f,SG}$	4%
Excitation system	AC1A Excitation system
Voltage droop slope $D_{v,SG}$	8%

TABLE IV

SETTINGS FOR AC NETWORK

Parameter	Value
Total system rating S_{System}	60 GVA
Rated network voltage V_{nom}	275 kV
Line resistance R_{Line} and inductance L_{Line} (each line)	0.005 p.u., 0.04 p.u.
Load model	RLC series circuit
Load power factor PF_{Load}	0.95 lagging

Appendix B Clarke and Park transformation

For electric machines, their behaviours are usually described by three-phase voltage and current which are time-varying, and their mathematical modelling and analysis of such device are often complex. Normally, mathematical techniques will be employed to reduce three time-varying AC quantities to two DC quantities and therefore simplify the analysis process. This is often applied to the power converter control system as well.

In order to simplify the analysis and control of the three-phase sinusoidal signals, it is common for the VSC to be controlled in the two-dimensional stationary *αβ*-frame or rotational *dq*-frame. While they have the same benefit of reducing the control efforts, analysis under the rotational *dq*-frame have additional merits such that a sinusoidal command tracking problem can be transferred to an equivalent DC command tracking problem to enable the PI control, and the time-varying inductances under *abc*-frame can be transformed to equivalent constant parameters [1]. Moreover, it is more unified as components in the large power systems are formulated and analysed in *dq*-frame [2]. This means that the control system should only act on perturbations off the nominal values.

The Clarke transform converts the three-phase signal (*abc*) to a two-phase signal where the two components (*αβ*) are orthogonal. The Park transform then converts the *αβ* signal to a *dq* signal. Relationships between the three types of coordination frames are shown in Figure B-1 and Table B-1, where the position of *d*-axis with respect to a-axis or *α*-axis is determined by $\theta=\omega t$ and ω is the rotational speed of the *dq* reference frame.

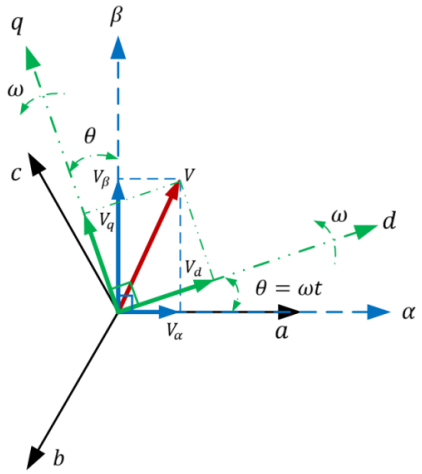

Figure B-1.Vector diagram defining the SRF and voltage vector orientations

Table B-1. Transformations between *abc*-frame, *dq*-frame and *αβ*- frame (with voltage vector V used as an example)

Transformation	Equations	
Clarke Transform ***abc* to *αβ***	$\begin{bmatrix} V_\alpha \\ V_\beta \end{bmatrix} = \frac{2}{3}\begin{bmatrix} 1 & -1/2 & -1/2 \\ 0 & \sqrt{3}/2 & -\sqrt{3}/2 \end{bmatrix}\begin{bmatrix} V_a \\ V_b \\ V_c \end{bmatrix}$	(B-1)
Inverse Clarke Transform ***αβ* to *abc***	$\begin{bmatrix} V_a \\ V_b \\ V_c \end{bmatrix} = \begin{bmatrix} 1 & 0 \\ -1/2 & \sqrt{3}/2 \\ -1/2 & -\sqrt{3}/2 \end{bmatrix}\begin{bmatrix} V_\alpha \\ V_\beta \end{bmatrix}$	(B-2)
Park Transform ***αβ* to *dq***	$\begin{bmatrix} V_d \\ V_q \end{bmatrix} = \begin{bmatrix} \cos\theta & \sin\theta \\ -\sin\theta & \cos\theta \end{bmatrix}\begin{bmatrix} V_\alpha \\ V_\beta \end{bmatrix}$	(B-3)
Inverse Park Transform ***dq* to *αβ***	$\begin{bmatrix} V_\alpha \\ V_\beta \end{bmatrix} = \begin{bmatrix} \cos\theta & -\sin\theta \\ \sin\theta & \cos\theta \end{bmatrix}\begin{bmatrix} V_d \\ V_q \end{bmatrix}$	(B-4)
From *abc* to *dq*	$\begin{bmatrix} V_d \\ V_q \end{bmatrix} = \frac{2}{3}\begin{bmatrix} \cos\theta & \cos(\theta-\frac{2}{3}\pi) & \cos(\theta+\frac{2}{3}\pi) \\ -\sin\theta & -\sin(\theta-\frac{2}{3}\pi) & -\sin(\theta+\frac{2}{3}\pi) \end{bmatrix}\begin{bmatrix} V_a \\ V_b \\ V_c \end{bmatrix}$ (B-5)	
From *dq* to *abc*	$\begin{bmatrix} V_a \\ V_b \\ V_c \end{bmatrix} = \begin{bmatrix} \cos\theta & -\sin\theta \\ \cos(\theta-\frac{2}{3}\pi) & -\sin(\theta-\frac{2}{3}\pi) \\ \cos(\theta+\frac{2}{3}\pi) & -\sin(\theta+\frac{2}{3}\pi) \end{bmatrix}\begin{bmatrix} V_d \\ V_q \end{bmatrix}$	(B-6)

Appendix C Operation of VSC

Figure C-1 shows a schematic diagram of a typical three-phase, two-level VSC. The most basic form of VSC, i.e. the half-bridge, single-phase, two-level VSC [1], is shown in Figure C-2. Three half-bridge VSCs connected in parallel form the three-phase configuration where each half-bridge converter is interfaced with one phase of a three-phase AC system. This arrangement is called 'two-level' VSC as each of its AC-side terminals can assume either of the voltage levels. The two-level VSC can provide a bidirectional power flow path between the DC system and the three-phase AC system. In this section, the basic half-bridge converter configuration as shown in Figure C-2 will be used to understand the operation principles of a VSC.

The half-bridge VSC consists of an upper switch cell and a lower switch cell, while each cell contains a fully controllable, unidirectional switch in parallel with a diode, i.e. Q_1 and D_1, Q_4 and D_4 shown in Figure C-2. The net voltage on the DC side is maintained with DC sources, battery units, or more elaborate configuration such as the DC side of an AC/DC converter. In Figure C-2, two DC voltage sources have been used to represent the DC system, each with voltage magnitude of $V_{DC}/2$. For the AC side, an AC voltage source is used to represent the AC network that the VSC is interfaced with. A phase reactor (a series RL branch) is included to provide filtering of harmonics whilst ensuring a low-ripple AC-side current. It is called a two-level converter as the switched AC-side voltage, at any instant, is either voltage at node *p* or at node *n*, according to which switch cell is on. The fundamental component of the AC-side voltage is usually controlled using a PWM technique [3, 4].

The PWM can be carried out by various types of techniques, such as sinusoidal PWM [5, 6], space vector PWM [5-7], and selected-harmonic-elimination PWM [8, 9]. The most common PWM technique used for VSC is to compare a high-frequency periodic triangular waveform, the carrier signal, with a slow-varying waveform known as the modulating signal, as shown in Figure C-3. The carrier signal is a periodic triangular waveform (often used for high-power converters) with period of T_s and changing its magnitude between -1 and 1. Figure C-4 presents an example of PWM waveforms for a three-level converter.

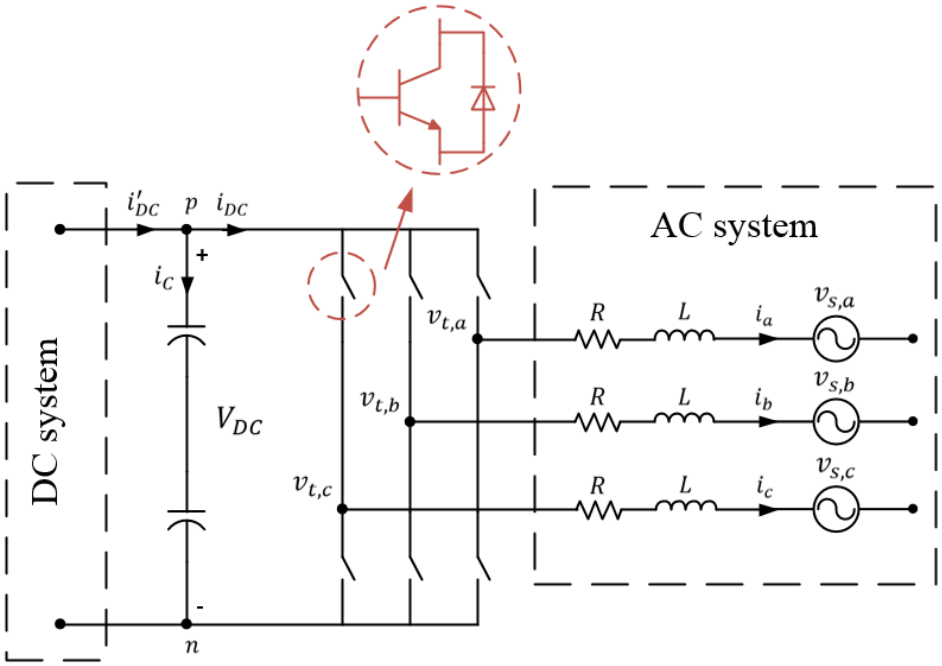

Figure C-1. Schematic diagram of a three-phase, two-level VSC

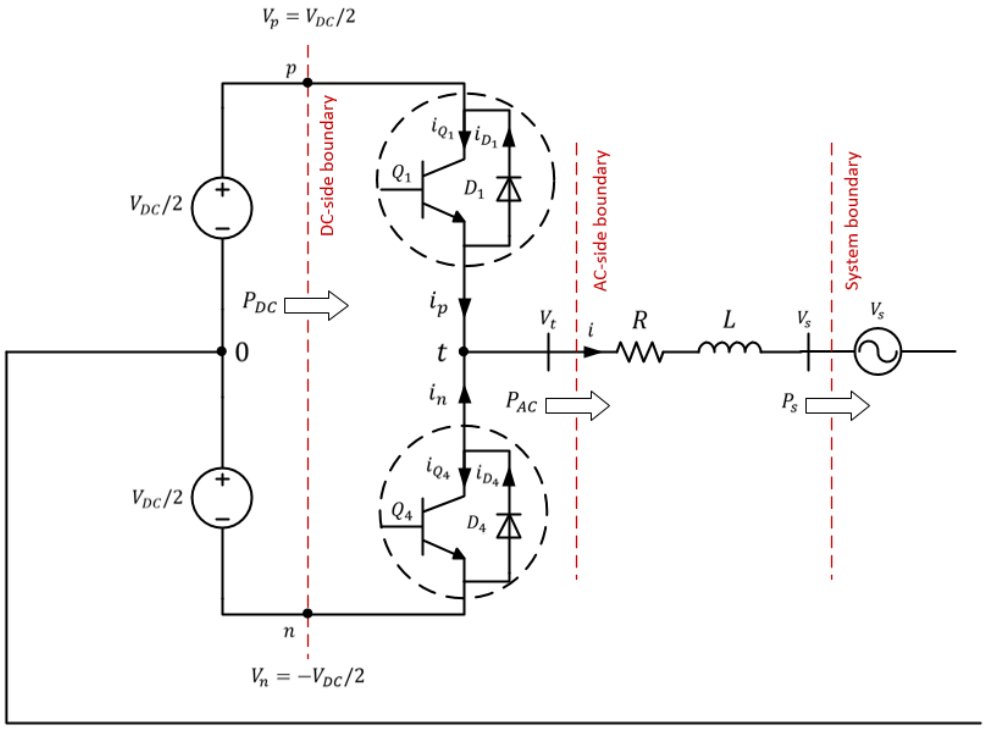

Figure C-2. Simplified circuit of a half-bridge converter

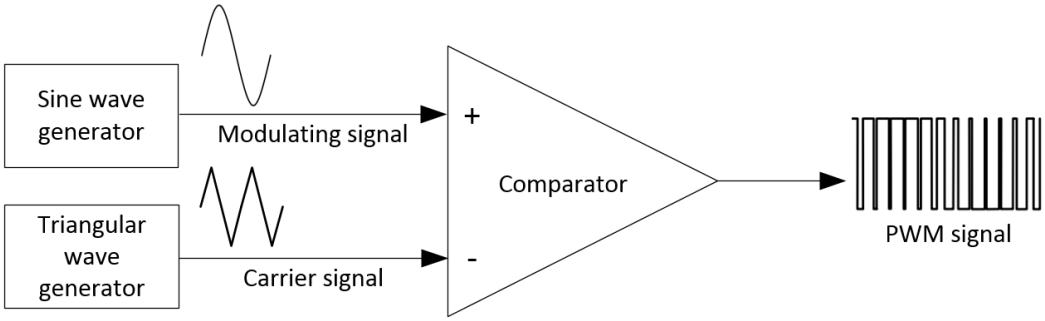

Figure C-3. Schematic diagram of the mechanism to generate PWM gate signal

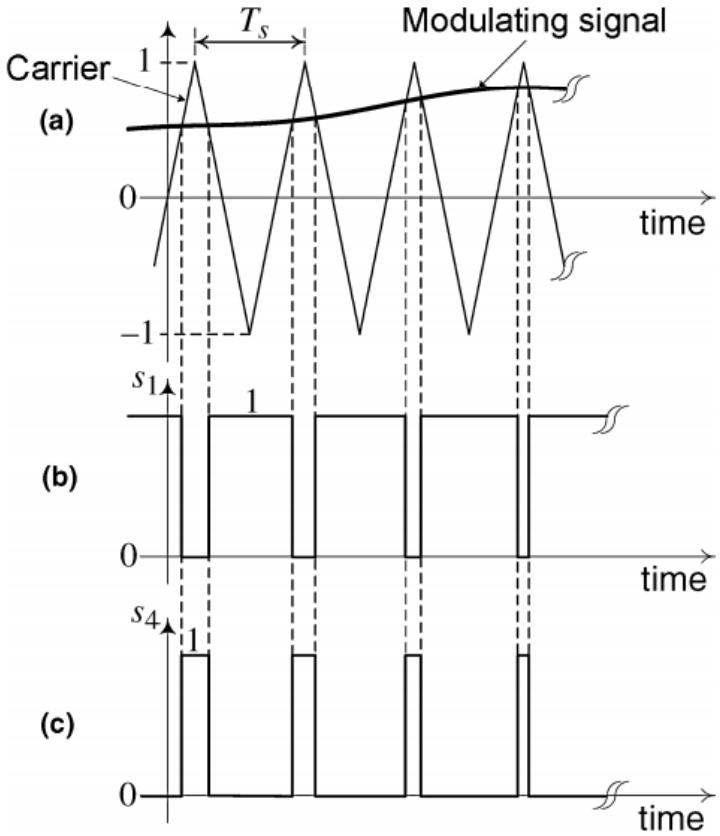

Figure C-4. Signals based on PWM switching strategy: (a) carrier and modulating signals; (b) switching function of the switch; and (c) switching function of the switch [1]

References

[1] A. Yazdani and R. Iravani, *Voltage-Sourced Converters in Power Systems : Modeling, Control, and Applications*: Wiley-IEEE Press, 2010.

[2] P. Kundur, N. J. Balu, and M. G. Lauby, *Power system stability and control* vol. 7: McGraw-hill New York, 1994.

[3] N. Mohan, T. M. Undeland, and W. P. Robbins, *Power Electronics: Converters, Applications, and Design (Third Edition)*: Wiley, 2003.

[4] D. G. Holmes and T. A. Lipo, *Pulse Width Modulation for Power Converters: Principles and Practice*: Wiley-IEEE Press, 2003.

[5] L. Yushan, A. R. Haitham, G. Baoming, B. Frede, E. Omar, and L. Poh Chiang, "Modulation Methods and Comparison," in *Impedance Source Power Electronic Converters*, ISBN 9781119037088: Wiley-IEEE Press, 2016, p. 424in 2017/5/15.

[6] W. Liuping, C. Shan, Y. Dae, G. Lu, and N. Ki, "Control of Semiconductor Switches via PWM Technologies," in *PID and Predictive Control of Electrical Drives and Power Converters using MATLAB / Simulink*, ISBN 9781118339459: Wiley-IEEE Press, 2015, p. 360.

[7] S. Xiaofang, R. Binbin, L. Shijie, and Z. Ruilan, "Optimal Space Vector Modulation Control for Three-Phase Inverter," in *Communication Systems and Information Technology: Selected Papers from the 2011 International Conference on Electric and Electronics (EEIC 2011) in Nanchang, China on June 20-22, 2011, Volume 4*, ISBN 978-3-642-21762-3, M. Ma, Ed. Berlin, Heidelberg: Springer Berlin Heidelberg, 2011, pp. 609-616.

[8] M. S. A. Dahidah and V. G. Agelidis, "Selective Harmonic Elimination PWM Control for Cascaded Multilevel Voltage Source Converters: A Generalized Formula," *IEEE Transactions on Power Electronics,* vol. 23, pp. 1620-1630, 2008.

[9] Y. Zhang, D. Xu, C. Yan, and S. Zou, "Hybrid PWM Scheme for the Grid Inverter," *IEEE Journal of Emerging and Selected Topics in Power Electronics,* vol. 3, pp. 1151-1159, 2015.